



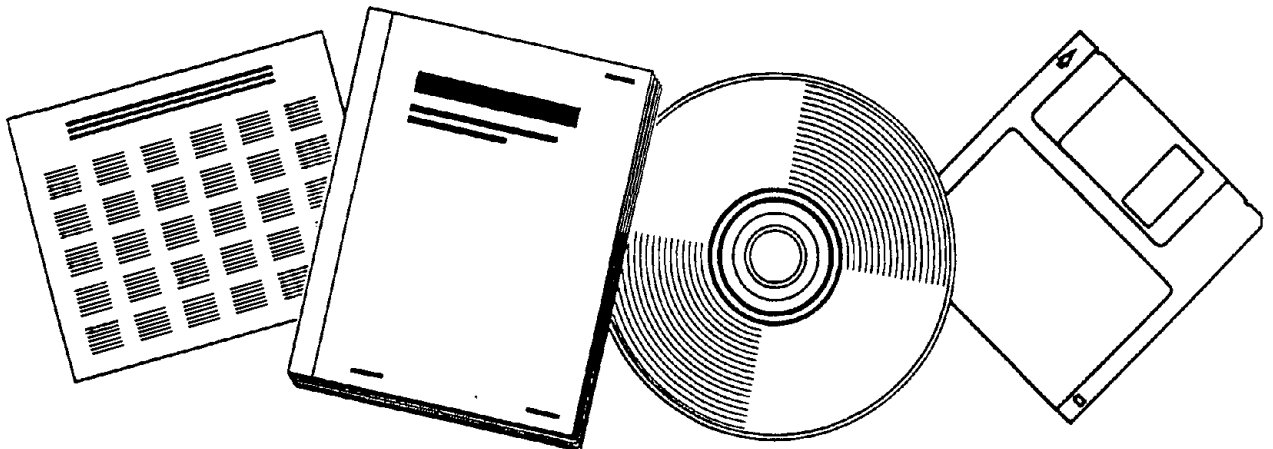
PB97-179444

NTIS[®]
Information is our business.

DEVELOPMENT OF A NEW SACRIFICIAL CATHODIC PROTECTION SYSTEM FOR STEEL EMBEDDED IN CONCRETE

(U.S.) CORRPRO COMPANIES, INC., MEDINA, OH

MAY 97



U.S. DEPARTMENT OF COMMERCE
National Technical Information Service

Development of a New Sacrificial Cathodic Protection System for Steel Embedded in Concrete



PB97-179444

PUBLICATION NO. FHWA-RD-96-171

MAY 1997



U.S. Department of Transportation
Federal Highway Administration

Research and Development
Turner-Fairbank Highway Research Center
6300 Georgetown Pike
McLean, VA 22101-2296

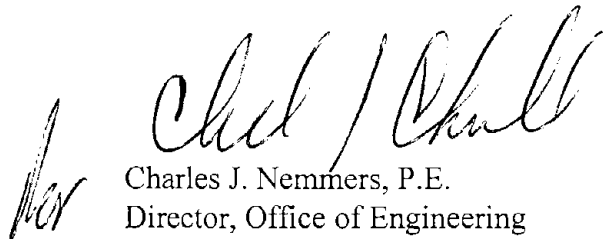


REPRODUCED BY:
U.S. Department of Commerce
National Technical Information Service
Springfield, Virginia 22161

FOREWORD

This report documents a study to develop metal alloys that could be used as sacrificial anodes to cathodically protect steel embedded in reinforced or prestressed concrete.

This is an interim report that describes the laboratory evaluation of the performance of existing sacrificial zinc anodes used on concrete structures and the applicability of existing sacrificial alloy compositions to cathodic protection of steel embedded in concrete. This report describes laboratory studies performed to develop improved sacrificial alloys for the cathodic protection of steel in concrete. This report will be of interest to bridge engineers, owners, and designers of prestressed structures. This work will also be of interest to owners, inspectors, design firms, and construction contractors of reinforced and concrete buildings and other structures.


Charles J. Nemmers, P.E.
Director, Office of Engineering
Research and Development

NOTICE

This document is disseminated under the sponsorship of the Department of Transportation in the interest of information exchange. The United States Government assumes no liability for its contents or use thereof. This report does not constitute a standard, specification, or regulation.

The United States Government does not endorse products or manufacturers. Trade or manufacturers' names appear herein only because they are considered essential to the object of this document.



1. REPORT NO. FHWA-RD-96-171		3. RECIPIENT'S CATALOG NO.	
4. TITLE AND SUBTITLE DEVELOPMENT OF A NEW SACRIFICIAL CATHODIC PROTECTION SYSTEM FOR STEEL EMBEDDED IN CONCRETE		5. REPORT DATE May 1997	
7. AUTHOR(S) M. Funahashi and W.T. Young		6. PERFORMING ORGANIZATION CODE	
9. PERFORMING ORGANIZATION NAME AND ADDRESS Corpro Companies, Inc. 610 Brandywine Parkway West Chester, PA 19380		8. PERFORMING ORGANIZATION REPORT NO.	
12. SPONSORING AGENCY NAME AND ADDRESS Office of Engineering Research and Development Federal Highway Administration, HNR-10 6300 Georgetown Pike McLean, VA 22101-2296		10. WORK UNIT NO. (TRAIS) 3D4b	
15. SUPPLEMENTARY NOTES Contracting Officer's Technical Representative (COTR): Y.P. Virmani, HNR-10 Subcontractors involved in the development of new alloys were Sumitomo Metal Mining Co. and Drexel University Materials Engineering Department, Dr. Alan Lawley.		11. CONTRACT OR GRANT NO. DTFH61-92-C-00079	
16. ABSTRACT <p>This is the interim report for a study to evaluate the use of sacrificial cathodic protection for reinforced and prestressed concrete bridge members. Cathodic protection (CP) using impressed current is an accepted and common method used to provide corrosion protection to steel in concrete. Sacrificial cathodic protection, however, is relatively easy to apply, does not require that the anode be electrically isolated from the steel, and does not require an external power supply. Attempts to apply sacrificial anode CP to bridge structures have met with limited success because conventional sacrificial anode alloys operate at a low fixed potential and the conductivity of concrete often does not permit satisfactory current output. The Florida Department of Transportation has applied arc-sprayed zinc to several bridges in the marine environment. This study examined the performance of existing sacrificial alloys in different environments for sacrificial CP, and developed new sacrificial alloys for protecting steel in concrete. The study consisted of both laboratory and field tasks. The first task consisted of tests to identify suitable environments for sacrificial alloys. In this task, test blocks with and without a sprayed zinc coating were exposed to northern marine, northern semi-rural, and southern marine environments; a laboratory environment; and seawater splash zone exposure. The results indicate that a sprayed zinc anode can reduce the corrosion of embedded steel in concrete. In the second task, two bridges with a zinc sacrificial anode in the Florida Keys were inspected and tested. Data on anode current output, anode and cathode potential, and anode and cathode depolarization were recorded. The results indicate that pure zinc does not provide long-term protection because of eventual passivation in non-wet areas. The third task tested existing sacrificial alloys for their performance when applied to concrete. The laboratory studies into existing commercial sacrificial alloys did not produce favorable results and so further laboratory work to develop new alloys was conducted. The above studies indicated the need to identify a sacrificial alloy or alloys that could provide adequate CP current for the long term. The fourth task consisted of this developmental study. The result was a series of aluminum-zinc-indium alloys that are capable of maintaining reasonably high potentials and current output under a range of concrete conditions for longer than pure zinc or aluminum. Field testing on a bridge structure is scheduled.</p>		13. TYPE OF REPORT AND PERIOD COVERED Interim Report October 1992 to April 1995	
17. KEY WORDS Cathodic Protection, Corrosion, Prestressed Concrete, Post-Tensioned Concrete, Pre-Tensioned Concrete, Cathodic Protection, Bridges, Sacrificial Anodes		14. SPONSORING AGENCY CODE	
18. DISTRIBUTION STATEMENT No restrictions. This document is available to the public through the National Technical Information Service, Springfield, VA 22161.		15. SUPPLEMENTARY NOTES	
19. SECURITY CLASSIF. (OF THIS REPORT) Unclassified	20. SECURITY CLASSIF. (OF THIS PAGE) Unclassified	21. NO. OF PAGES 160	22. PRICE

SI* (MODERN METRIC) CONVERSION FACTORS

APPROXIMATE CONVERSIONS TO SI UNITS

APPROXIMATE CONVERSIONS FROM SI UNITS

Symbol	When You Know	Multiply By	To Find	Symbol	Symbol	When You Know	Multiply By	To Find	Symbol
LENGTH					LENGTH				
in	inches	25.4	millimeters	mm	mm	millimeters	0.039	inches	in
ft	feet	0.305	meters	m	m	meters	3.28	feet	ft
yd	yards	0.914	meters	m	m	meters	1.09	yards	yd
mi	miles	1.61	kilometers	km	km	kilometers	0.621	miles	mi
AREA					AREA				
in ²	square inches	645.2	square millimeters	mm ²	mm ²	square millimeters	0.0016	square inches	in ²
ft ²	square feet	0.093	square meters	m ²	m ²	square meters	10.764	square feet	ft ²
yd ²	square yards	0.836	square meters	m ²	m ²	square meters	1.195	square yards	yd ²
ac	acres	0.405	hectares	ha	ha	hectares	2.47	acres	ac
mi ²	square miles	2.59	square kilometers	km ²	km ²	square kilometers	0.386	square miles	mi ²
VOLUME					VOLUME				
fl oz	fluid ounces	29.57	milliliters	mL	mL	milliliters	0.034	fluid ounces	fl oz
gal	gallons	3.785	liters	L	L	liters	0.264	gallons	gal
ft ³	cubic feet	0.028	cubic meters	m ³	m ³	cubic meters	35.71	cubic feet	ft ³
yd ³	cubic yards	0.765	cubic meters	m ³	m ³	cubic meters	1.307	cubic yards	yd ³
MASS					MASS				
oz	ounces	28.35	grams	g	g	grams	0.035	ounces	oz
lb	pounds	0.454	kilograms	kg	kg	kilograms	2.202	pounds	lb
T	short tons (2000 lb)	0.907	megagrams (or "metric ton")	Mg (or "t")	Mg (or "t")	megagrams (or "metric ton")	1.103	short tons (2000 lb)	T
TEMPERATURE (exact)					TEMPERATURE (exact)				
°F	Fahrenheit temperature	5(F-32)/9 or (F-32)/1.8	Celcius temperature	°C	°C	Celcius temperature	1.8C + 32	Fahrenheit temperature	°F
ILLUMINATION					ILLUMINATION				
fc	foot-candles	10.76	lux	lx	lx	lux	0.0929	foot-candles	fc
fl	foot-Lamberts	3.426	candela/m ²	cd/m ²	cd/m ²	candela/m ²	0.2919	foot-Lamberts	fl
FORCE and PRESSURE or STRESS					FORCE and PRESSURE or STRESS				
lbf	poundforce	4.45	newtons	N	N	newtons	0.225	poundforce	lbf
lbf/in ²	poundforce per square inch	6.89	kilopascals	kPa	kPa	kilopascals	0.145	poundforce per square inch	lbf/in ²

NOTE: Volumes greater than 1000 l shall be shown in m³.

* SI is the symbol for the International System of Units. Appropriate rounding should be made to comply with Section 4 of ASTM E380.

TABLE OF CONTENTS

<u>Chapter</u>		<u>Page</u>
	INTRODUCTION	1
1	EFFECT OF ENVIRONMENT ON GALVANIC CATHODIC PROTECTION	5
	Test Specimen Construction	5
	Test Conditions and Results	6
	Summary	17
2	STUDY OF EXISTING SACRIFICIAL ZINC ANODE CATHODIC PROTECTION SYSTEMS	19
	Bahia Honda Bridge.....	19
	Niles Channel Bridge	28
	Conclusions From Study of Existing Sacrificial Anode Cathodic Protection Systems	34
3	STUDY OF EXISTING METALS AND ALLOYS AS SACRIFICIAL ANODES.....	35
	Concrete Block Construction.....	36
	Environmental Test.....	36
	Anode Efficiency Tests.....	42
	Atmospheric Corrosion.....	45
	Anode Capacity Tests	46
	Cyclic Polarization Tests	46
	Effect of pH on Alloy Behavior.....	50
	Conclusions on Study of Existing Alloys.....	53
4	DEVELOPMENT OF NEW ANODE ALLOYS	55
	Phase I. Screening Tests	55
	Phase II. Tests With Sprayed Alloys	64
	Phase III. Application of Alloys to a Bridge Substructure	73
	CONCLUSIONS.....	77
	APPENDIX. ADDITIONAL TEST DATA	79
	REFERENCES	147

LIST OF FIGURES

<u>Figure No.</u>		<u>Page</u>
1.	Arrangement of wires and plate cathodes in test block.	6
2.	Test block showing wedges used for chloride-contaminated mortar .	7
3.	Test blocks mounted beneath a shelter.	9
4.	Test blocks mounted in exposed location.	10
5.	Schematic diagram of mortar test blocks mounted on seawall.	10
6.	Condition of north-facing cathodes with and without zinc anode.....	12
7.	Condition of south-facing cathodes with and without zinc anode	12
8.	Steel plate cathodes located on seawall at Ocean City, with and without zinc anode	16
9.	Niles Channel Bridge.....	20
10.	Bahia Honda Bridge.....	20
11.	Zinc anode coating on one bent of Niles Channel Bridge.....	21
12.	Zinc anode coating on one bent of Bahia Honda Bridge.....	21
13.	Zinc anode coating applied to exposed rebar on Bahia Honda Bridge	22
14.	Rebar probe and anode window locations for pile tested at Bahia Honda Bridge	23
15.	Zinc anode window depolarization tests — Bahia Honda Bridge	27
16.	The x-ray diffraction pattern from zinc-concrete interface of adhesion dolly #1 from the Bahia Honda Bridge	28
17.	Zinc coating applied to exposed rebar of Niles Channel Bridge	29
18.	Schematic of rebar probes on Niles Channel Bridge	30
19.	Rebar probes on Niles Channel Bridge.....	30

20.	Anode windows on Niles Channel Bridge	31
21.	Schematic of anode window identification on Niles Channel Bridge	31
22.	Electrical continuity band on Niles Channel Bridge	32
23.	Concrete blocks in the environmental chamber	37
24.	Schematic of test block wiring	38
25.	Key to potential and polarization diagrams, figures 50 through 70 ...	39
26.	Anode capacity test set-up	47
27.	Test set-up for pH tests.	51
28.	Anode-to-cathode current densities with decreasing pH.	52
29.	Instant-off potentials of anodes vs. solution pH.....	53
30.	Anode capacity vs. zinc content of aluminum alloy	56
31.	Static potential vs. zinc content of aluminum alloy, before capacity tests	57
32.	Static potential vs. zinc content of aluminum alloys, after capacity tests	57
33.	Weight loss vs. zinc content	59
34.	Current capacity vs. indium content	61
35.	Static potentials after capacity tests vs. indium content.	61
36.	Current output vs. indium content for Al-10Zn alloy.....	62
37.	Instant-off potentials vs. indium content for Al-10Zn alloy.....	62
38.	Current output vs. indium content for Al-20Zn alloy.....	66
39.	Instant-off potentials vs. indium content for Al-20Zn alloy.....	66
40.	Current output vs. indium content for Al-30Zn alloy.....	67

41.	Instant-off potentials vs. indium content for Al-30Zn alloy.....	67
42.	Current output for Zn-55Al alloy.....	68
43.	Instant-off potentials for Zn-55Al alloy.....	68
44.	Galvanic current vs. pH in simulated concrete pore solution.....	69
45.	Instant-off potentials vs. pH in simulated concrete pore solution.....	69
46.	Arc-spraying of Al-10Zn-0.2In wire.....	70
47.	Flame-spraying of Al-20Zn-0.2In wire.....	70
48.	Cross section of Al-10Zn-0.2In alloy-to-concrete interface.....	71
49.	Cross section of Al-10Zn-0.2In alloy-to-concrete interface.....	72
50.	Environmental test results for experimental alloys and pure zinc and aluminum at 90°F (32°C).....	74
51.	Environmental test results for experimental alloys and pure zinc and aluminum at 70°F (21°C).....	75
52.	Environmental test results for experimental alloys and pure zinc and aluminum at 40°F (4°C).....	76
53.	Environmental tests - galvanic current, instant-off potential, potential, and polarization data, 90°F (32°C), 90% RH (1300 ppm Cl).....	79
54.	Environmental tests - galvanic current, instant-off potential, potential, and polarization data, 90°F (32°C), 90% RH (3800 ppm Cl).....	80
55.	Environmental tests - galvanic current, instant-off potential, potential, and polarization data, 90°F (32°C), 70% RH (1300 ppm Cl).....	81
56.	Environmental tests - galvanic current, instant-off potential, potential, and polarization data, 90°F (32°C), 70% RH (3800 ppm Cl).....	82

57.	Environmental tests - galvanic current, instant-off potential, potential, and polarization data, 90°F (32°C), 40% RH (1300 ppm Cl)	83
58.	Environmental tests - galvanic current, instant-off potential, potential, and polarization data, 90°F (32°C), 40% RH (3800 ppm Cl)	84
59.	Environmental tests - galvanic current, instant-off potential, potential, and polarization data, 70°F (21°C), 90% RH (1300 ppm Cl)	85
60.	Environmental tests - galvanic current, instant-off potential, potential, and polarization data, 70°F (21°C), 90% RH (3800 ppm Cl)	86
61.	Environmental tests - galvanic current, instant-off potential, potential, and polarization data, 70°F (21°C), 70% RH (1300 ppm Cl)	87
62.	Environmental tests - galvanic current, instant-off potential, potential, and polarization data, 70°F (21°C), 70% RH (3800 ppm Cl)	88
63.	Environmental tests - galvanic current, instant-off potential, potential, and polarization data, 70°F (21°C), 40% RH (1300 ppm Cl)	89
64.	Environmental tests - galvanic current, instant-off potential, potential, and polarization data, 70°F (21°C), 40% RH (3800 ppm Cl)	90
65.	Environmental tests - galvanic current, instant-off potential, potential, and polarization data, 40°F (4°C), 90% RH (1300 ppm Cl)	91
66.	Environmental tests - galvanic current, instant-off potential, potential, and polarization data, 40°F (4°C), 90% RH (3800 ppm Cl)	92
67.	Environmental tests - galvanic current, instant-off potential, potential, and polarization data, 40°F (4°C), 70% RH (1300 ppm Cl)	93

68.	Environmental tests - galvanic current, instant-off potential, potential, and polarization data, 40°F (4°C), 70% RH (3800 ppm Cl)	94
69.	Environmental tests - galvanic current, instant-off potential, potential, and polarization data, 40°F (4°C), 40% RH (1300 ppm Cl)	95
70.	Environmental tests - galvanic current, instant-off potential, potential, and polarization data, 40°F (4°C), 40% RH (3800 ppm Cl)	96
71.	Galvanic, self-corrosion, and anode efficiency data for pure zinc	97
72.	Galvanic, self-corrosion, and anode efficiency data for zinc alloy 1	98
73.	Galvanic, self-corrosion, and anode efficiency data for zinc-5% Al	99
74.	Galvanic, self-corrosion, and anode efficiency data for zinc-15% Al	100
75.	Galvanic, self-corrosion, and anode efficiency data for zinc-55% Al	101
76.	Galvanic, self-corrosion, and anode efficiency data for pure aluminum	102
77.	Galvanic, self-corrosion, and anode efficiency data for aluminum alloy 1	103
78.	Galvanic, self-corrosion, and anode efficiency data for aluminum alloy 2	104
79.	Galvanic, self-corrosion, and anode efficiency data for aluminum-5% Zn	105
80.	Galvanic, self-corrosion, and anode efficiency data for aluminum-10% Zn	106
81.	Galvanic, self-corrosion, and anode efficiency data for aluminum-1% Mg	107
82.	Galvanic, self-corrosion, and anode efficiency data for aluminum-10% Mg	108

83.	Galvanic, self-corrosion, and anode efficiency data for aluminum-5% Zn-3.5% Mg	109
84.	Galvanic, self-corrosion, and anode efficiency data for aluminum-5% Zn-0.1% Sn	110
85.	Cyclic polarization curves on pure zinc before galvanic coupling, at high current, and at low current (3800 ppm Cl).....	111
86.	Cyclic polarization curves on pure zinc after galvanic coupling, at high current, and at low current (1300 ppm Cl).....	112
87.	Cyclic polarization curves on zinc alloy before galvanic coupling, at high current, and at low current (3800 ppm Cl).....	113
88.	Cyclic polarization curves on zinc alloy after galvanic coupling, at high current, and at low current (1300 ppm Cl).....	114
89.	Cyclic polarization curves on zinc-5% Al alloy before galvanic coupling, at high current, and at low current (3800 ppm Cl).....	115
90.	Cyclic polarization curves on zinc-5% Al alloy after galvanic coupling, at high current, and at low current (1300 ppm Cl).....	116
91.	Cyclic polarization curves on zinc-15% Al alloy before galvanic coupling, at high current, and at low current (3800 ppm Cl).....	117
92.	Cyclic polarization curves on zinc-15% Al alloy after galvanic coupling, at high current, and at low current (1300 ppm Cl).....	118
93.	Cyclic polarization curves on zinc-55% Al alloy before galvanic coupling, at high current, and at low current (3800 ppm Cl).....	119
94.	Cyclic polarization curves on zinc-55% Al alloy after galvanic coupling, at high current, and at low current (1300 ppm Cl).....	120
95.	Cyclic polarization curves on pure aluminum before galvanic coupling, at high current, and at low current (3800 ppm Cl).....	121
96.	Cyclic polarization curves on pure aluminum after galvanic coupling, at high current, and at low current (1300 ppm Cl).....	122
97.	Cyclic polarization curves on aluminum alloy 1 before galvanic coupling, at high current, and at low current (3800 ppm Cl).....	123

98.	Cyclic polarization curves on aluminum alloy 1 after galvanic coupling, at high current, and at low current (1300 ppm Cl).....	124
99.	Cyclic polarization curves on aluminum alloy 2 before galvanic coupling, at high current, and at low current (3800 ppm Cl).....	125
100.	Cyclic polarization curves on aluminum alloy 2 after galvanic coupling, at high current, and at low current (1300 ppm Cl).....	126
101.	Cyclic polarization curves on aluminum-5% Zn alloy before galvanic coupling, at high current, and at low current (3800 ppm Cl).....	127
102.	Cyclic polarization curves on aluminum-5% Zn alloy after galvanic coupling, at high current, and at low current (1300 ppm Cl).....	128
103.	Cyclic polarization curves on aluminum-10% Zn alloy before galvanic coupling, at high current, and at low current (3800 ppm Cl).....	129
104.	Cyclic polarization curves on aluminum-10% Zn alloy after galvanic coupling, at high current, and at low current (1300 ppm Cl).....	130
105.	Cyclic polarization curves on aluminum-1% Mg alloy before galvanic coupling, at high current, and at low current (3800 ppm Cl).....	131
106.	Cyclic polarization curves on aluminum-1% Mg alloy after galvanic coupling, at high current, and at low current (1300 ppm Cl).....	132
107.	Cyclic polarization curves on aluminum-10% Mg alloy before galvanic coupling, at high current, and at low current (3800 ppm Cl).....	133
108.	Cyclic polarization curves on aluminum-10% Mg alloy after galvanic coupling, at high current, and at low current (1300 ppm Cl).....	134
109.	Cyclic polarization curves on aluminum-5% Zn-3.5% Mg alloy before galvanic coupling and at low current (3800 ppm Cl)	135

110.	Cyclic polarization curves on aluminum-5% Zn-3.5% Mg alloy after galvanic coupling, at high current, and at low current (1300 ppm Cl).....	136
111.	Cyclic polarization curves on aluminum-5% Zn-0.1% Sn alloy before galvanic coupling, at high current, and at low current (3800 ppm Cl).....	137
112.	Cyclic polarization curves on aluminum-5% Zn-0.1% Sn alloy after galvanic coupling, at high current, and at low current (1300 ppm Cl).....	138
113.	Anodic polarization of pure aluminum and aluminum-zinc alloys (10 to 30 percent zinc) in simulated porewater solution	139
114.	Anodic polarization of aluminum-zinc alloys (40 to 70 percent zinc) in simulated porewater solution	140
115.	Anodic polarization of aluminum-zinc alloys (80 to 100 percent zinc) in simulated porewater solution	141
116.	Anodic polarization of aluminum-10% zinc alloys vs. indium in simulated porewater solution	142
117.	Anodic polarization of aluminum-20% zinc alloys vs. indium in simulated porewater solution	143
118.	Anodic polarization of aluminum-30% zinc alloys vs. indium in simulated porewater solution	144
119.	Anodic polarization of aluminum-50% zinc alloys vs. indium in simulated porewater solution	145

LIST OF TABLES

<u>Table No.</u>		<u>Page</u>
1.	Test results of concrete blocks located in the laboratory	14
2.	Test results on marine and non-marine exposed concrete blocks with and without zinc sacrificial anode	15
3.	Results from blocks exposed to seawater	16
4.	Test results of rebar probes at the Bahia Honda Bridge	24
5.	Test results on zinc test windows at the Bahia Honda Bridge	25
6.	Test results of rebar probes at the Niles Channel Bridge.....	33
7.	Test results on zinc test windows at the Niles Channel Bridge	33
8.	Results of atmospheric exposure tests on the anode materials	45
9.	Compositions of aluminum-zinc-indium alloys tested	59

INTRODUCTION

Many structures have been built to support our nation's highway system in the last several decades. Since the late 1960's, the infrastructure has been facing major problems regarding significant corrosion of conventional reinforcing steel. Both conventional and prestressed reinforced concrete bridges, which were once thought to be virtually maintenance-free, are deteriorating as a result of extensive use of deicing salt. In addition, numerous reinforced and prestressed concrete structures located in marine environments are also experiencing corrosion caused by seawater or chloride-laden air. Maintenance costs for concrete structures that are exposed to such corrosive environments have become large expenditures for many owners.

In order to extend the service lives of existing structures, various protection methods have been evaluated on those structures. In the late 1970's, the Federal Highway Administration (FHWA) expended considerable effort to assess the effectiveness of various repair methods as applied primarily to reinforced concrete bridge decks. The conclusion was that "only cathodic protection (CP), either alone or in combination with other repair methods, is capable of completely stopping the corrosion of the reinforcing steel in chloride-contaminated concrete."⁽¹⁾ Recently, the FHWA further encouraged states to protect existing bridges before they reach the stage where replacement is necessary. The FHWA strongly suggested that CP systems should be used more frequently as a cost-effective means to extend the useful life of chloride-contaminated bridges.⁽²⁾

Since the first impressed current CP system was installed on a bridge deck in California in 1973, the technology has advanced significantly. The majority of CP systems for reinforced concrete structures are of the impressed current type. With impressed current CP, an external direct current (dc) power supply, or rectifier, is used to force cathodic protection current from the anode through the concrete to the reinforcing steel.

The sacrificial CP system does not require a rectifier because the source of the dc current is the anode. All metals have their own oxidation potential (emf) in a particular environment. When two different metals are electrically connected to each other, and both are embedded or immersed in an electrolyte (e.g., water, soil, and concrete), a galvanic cell is established.⁽³⁾ As a result, electrical current flows naturally from the more active (anodic) metal to the less active (cathodic) metal through the electrolyte. When the potentials of two metals in a galvanic cell are greatly different, more current is generated. Therefore, when a metal or an alloy is more anodic than steel embedded in concrete, the more active metal or alloy can be used as a sacrificial anode.

Sacrificial metals commonly used for CP in soil and seawater environments are zinc, aluminum, magnesium, and their alloys. The potential difference of the sacrificial anode with respect to steel is dependent upon the surrounding environment. The effectiveness of an anode is not only determined by the potential of the anode, but also by the magnitude of its anodic polarization. Polarization is the change in the effective potential of the anode (or cathode) resulting from current between the anode and the cathode. The essential requirement for an anode is that it be able to provide adequate current density to polarize the steel sufficiently where the steel will either not corrode at all, or will corrode at an acceptable rate in a cost-effective manner.

Important considerations in selecting an anode are:

- Material composition.
- Potential (oxidation).
- Current output.
- Anode efficiency.
- Polarization characteristics with time.

The external factors that have to be taken into consideration in relation to anode performance are:

1. Surface area of steel requiring protection.
2. Electrolyte:
 - Chemical composition.
 - Temperature.
 - Electrical resistivity.
 - pH.
3. Electrical contact of the anode with the electrolyte.

Thus, the performance of a sacrificial anode is a complex interaction between the electrochemical properties of the anode and the environmental factors affecting it.

In 1977, two types of galvanic cathodic protection systems were installed and tested in Illinois by the Portland Cement Association under the National Cooperative Highway Research Program (NCHRP).(4,5) Sacrificial alloys used in this study were zinc ribbon and perforated zinc sheet. The zinc ribbon was placed in saw-cut slots in the bridge deck. The perforated zinc sheet was placed on the concrete deck surface and covered with an open-graded asphalt. Environmental factors, such as temperature, moisture, and salt content, appeared to play an important role in the functioning of the above field-applied systems. The CP systems were not very successful because of the poor distribution of cathodic protection current to the rebars and the relatively high cost of the systems. This limited success in sacrificial (galvanic) anode cathodic protection systems prevented further development even though they had inherent simplicity and low maintenance costs. Thus, in the last two decades, much of the work on application of cathodic protection to reinforced concrete structures has centered on impressed current techniques.

Recently, the Florida Department of Transportation (DOT) studied the concept of using a thermally sprayed zinc coating as a sacrificial anode for atmospherically exposed concrete bridge components in marine environments. Using the concrete metallizing technique developed by the California Department of Transportation (Caltrans), zinc was applied and tested as a sacrificial anode for bridge substructures in 1983.(6,7) In addition, detailed laboratory tests were conducted on the sprayed zinc sacrificial anode. The results indicated that the cathodic protection current produced by the zinc anodes decreased with time in areas of dryer concrete above the splash zone. However, anodes installed in the splash zone of marine structures appeared to perform well. Thus, the use of thermally sprayed zinc is somewhat limited to wet concrete.

To develop a new sacrificial anode material for sacrificial cathodic protection of reinforced and prestressed concrete substructures of bridges, an intensive research and development program evolved. The program consisted of four tasks:

1. Study the effect of the environment on sacrificial anode cathodic protection.
2. Study existing sacrificial anodes applied to reinforced concrete structures in the field.
3. Evaluate suitable materials for their use as sacrificial anodes and determine the limitations of those materials.
4. Develop and test new sacrificial anode materials by thermally spraying them on concrete specimens.

A sprayed-type sacrificial anode is most suitable for bridge substructures. Bridge substructures consist of vertical and overhead surfaces, as well as irregularly shaped concrete surfaces. In addition, since many substructures are highly visible, the sacrificial anode must not only work properly, it may also have to satisfy aesthetic requirements.(9)

To spray metal onto concrete surfaces, two types of techniques (flame spray and arc spray) are generally used for field structures.(8) The flame-spray process uses a hand-held gun. A single zinc wire is fed through the back of the gun using air-driven mortar inside the gun and is melted by the mix of oxygen and acetylene gases. The resultant molten metal is propelled out of the gun nozzle by compressed air.

The arc-spray process is basically similar, but uses high-voltage direct current (dc) instead of flame. Two metal wires of the alloy being deposited are fed to the spray gun through a power supply unit through hoses to the gun, along with high-pressure air. Each wire is charged with a high dc voltage. At the tip of the arc-spray gun, the arc melts the wires. At the same time, a jet of compressed air passes through the arc and sprays the molten metal onto the concrete surface as a coating.

This report discusses the research work leading to the development of successful sacrificial anode alloys that can be used on both wet and dry concrete surfaces to protect the corroding embedded steel in chloride-contaminated bridge members.

CHAPTER 1

EFFECT OF ENVIRONMENT ON GALVANIC CATHODIC PROTECTION

Some bridge member surfaces are exposed to wind and rain, while others are sheltered from the elements by their position beneath the bridge. Portions of these members are exposed to wetting by rain, some are exposed to splash and mist from passing traffic or ocean waves, and some are exposed to saltwater leakage from the deck expansion joints. When saltwater evaporates, the salt residue remains on the concrete surfaces of the members. Continued wetting and drying builds up the salt concentration over time. The wet-dry cycles also tend to draw the salts into small cracks and pores in the concrete, which affects corrosion. Other environmental variables that impact corrosion and the performance of sacrificial anode cathodic protection are temperature cycling and ambient relative humidity (RH). Corrosion rate and cathodic protection current density demand vary from negligible to significant as these parameters change. The current output of galvanic (sacrificial) anodes might also be influenced by these parameters.

The purpose of this work was to examine the effect of these variables on the performance of pure zinc as a sacrificial anode to cathodically protect steel reinforcing. Electrochemical parameters are usually used to evaluate the effectiveness of cathodic protection. However, for constantly changing variables, traditional electrochemical tests become impractical. Thus, a test method that cumulatively integrates corrosion over time was used.

Test Specimen Construction

These tests employed thin steel wires, 0.025 in (0.6 mm) in diameter, embedded in mortar blocks. The mortar was Type I portland cement mixed with sand (1:3), with a water-to-cement ratio of 0.45. The dimensions of each block were 14 in x 8 in x 3 in (35.6 cm x 20.3 cm x 7.6 cm). Twenty 6-in- (15.2-cm-) long wires were arranged in parallel in each block, as shown in figure 1. All wires were embedded in chloride-free mortar except for two small segments of each wire that were to be exposed to chloride-contaminated mortar. Figure 2 shows the specimen set-up. After the mortar cured for 30 days, the two narrow slots that exposed the small wire segments were filled with mortar (the same mix as above) containing 0.5 percent chloride (as total weight). The two junctions between the chloride-contaminated and uncontaminated mortar were perpendicular to each wire axis, thus creating strong galvanic corrosion cells on the wires. One block was also produced with chloride-free mortar in the slot as a control. To simulate the steel-to-concrete surface area ratio of concrete bridge substructures, a perforated steel sheet, 3 in x 12 in x 0.125 in thick (7.6 cm x 30.5 cm x 0.3 cm thick) with a 40 percent opening, was also embedded below the layer of wires in the block. A total of 64 blocks were produced for the test. The blocks were moist-cured for 3 days and were exposed to laboratory air for 27 days. Pure zinc was then applied to the top of half of the blocks (32) using the arc-spray technique. The zinc anode was connected to the steel wires and plate cathodes using an external connection to allow potential measurements.

The blocks were exposed in controlled laboratory and in exterior environments as described below. The laboratory environments included different temperature and humidity conditions.

The exterior environments exposed the blocks to marine and non-marine conditions. The expectation was that corrosion would initiate at the two junction points on the wire and result in a relatively rapid loss in electrical continuity from one end to the other end. The continuity of the steel wires was tested periodically.

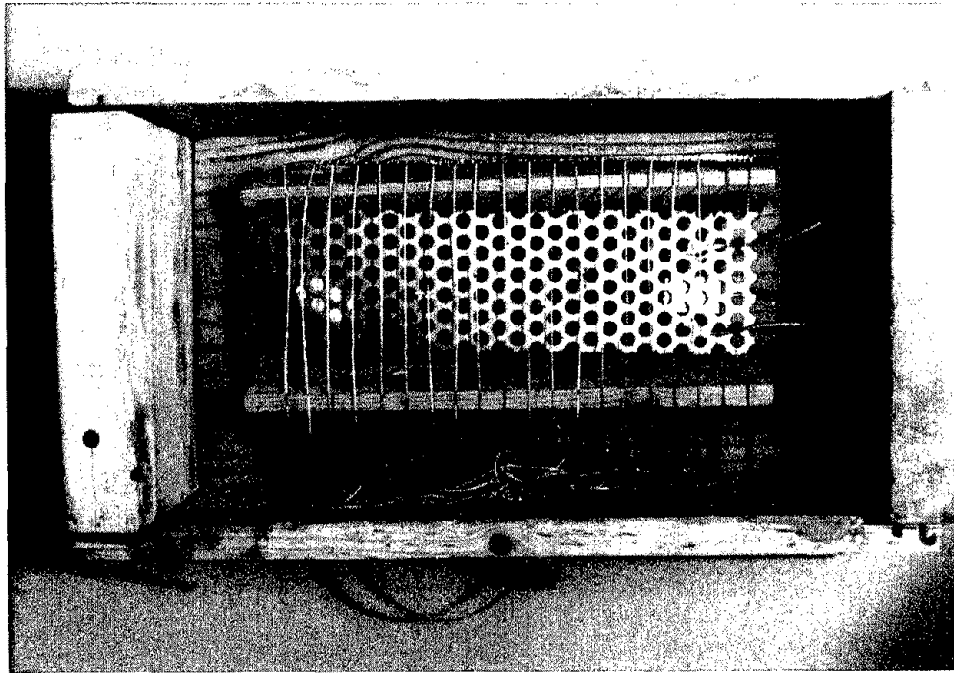


Figure 1. Arrangement of wires and plate cathodes in test block.

Test Conditions and Results

Controlled Laboratory Environments

Test Conditions

A total of 10 blocks with and without a zinc anode were exposed to each of the following laboratory conditions:

1. Two blocks exposed at a room temperature of 60° to 80°F (15° to 27°C) and a relative humidity between 40 and 60 percent. In this test, the slot was filled with chloride-free cement mortar. This specimen was used as a control.
2. Two blocks exposed at a room temperature of 60° to 80°F (15° to 27°C) and a relative humidity between 40 and 60 percent.

3. Two blocks exposed the same as condition 1, but freshwater spray was applied to the anode surface for approximately 30 s twice a day, 5 days a week.
4. Two blocks exposed the same as condition 1, but 3 percent saltwater spray was applied to the anode surface for approximately 30 s twice a day, 5 days a week.
5. Two blocks exposed in a 100 percent relative humidity enclosure.

All test blocks were exposed to their respective environments for approximately 20 months. The continuity of the wires was tested periodically using an electrical continuity tester. After the exposure tests were completed, the blocks were dismantled and the wires and plates were visually examined. The existence of corrosion of all wires exposed in the slots was determined, and the remaining diameter of each wire embedded in the slots was measured using a toolmaker's microscope. In addition, the following information was collected from the test blocks:

- Corroded surface area of the perforated steel plate cathode, if any.
- Open circuit corrosion potential of the perforated steel plate cathode using a copper-copper sulfate (CSE) reference electrode.
- Open circuit potential of the sprayed zinc anode using a copper-copper sulfate reference electrode.
- Total chloride concentration in the mortar located near the steel plate-mortar interface.

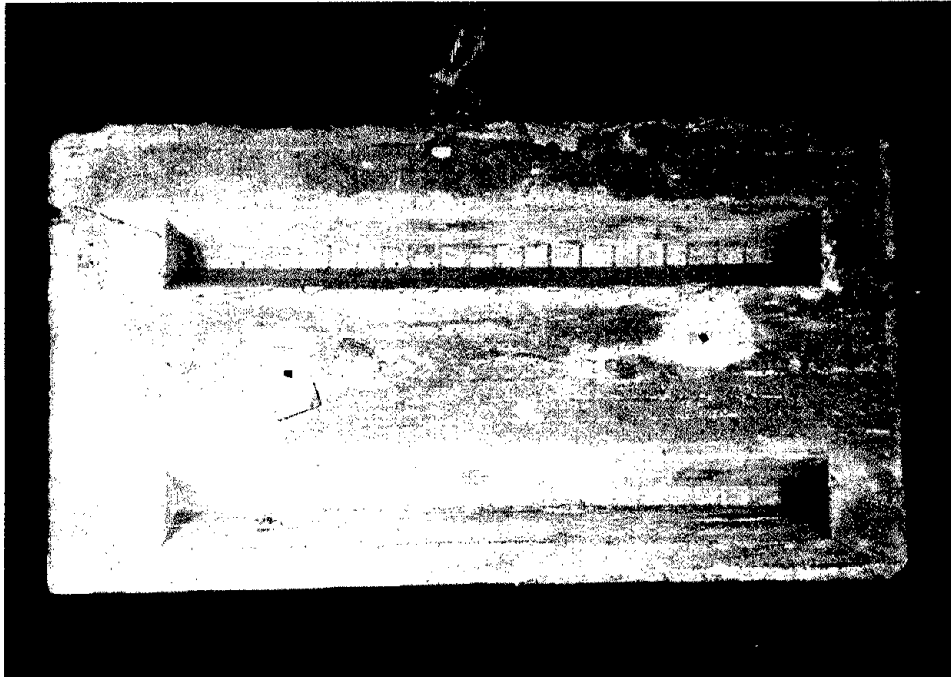


Figure 2. Test block showing wedges used for chloride-contaminated mortar.

Results

Table 1 summarizes the conditions of the test blocks exposed in the laboratory. The wires exposed to chloride-free cement mortar did not show corrosion. The average diameters of the wires in the control blocks with and without the zinc anode are 25.2 mils* (638 μm) and 26.1 mils (662 μm), respectively.

The average diameters of the wires in chloride-containing mortar (with and without the zinc anode) that had not been exposed to water during the test period were approximately the same as the control blocks. However, 8 of the 20 wires in the block without the zinc anode showed corrosion on the wire, but no corrosion was observed on the wires with the zinc anode. It appears that the zinc sacrificial anode prevented the initiation of corrosion caused by chlorides in the mortar before the blocks became dry.

The test blocks with the zinc anode exposed to freshwater spray had superficial corrosion on five wires, whereas in the block without the anode, nine wires had corrosion. Since the environment for the embedded wires appeared not to be so corrosive, the effect of the zinc anode was negligible.

On the other hand, the blocks that had received the 3 percent salt spray showed more effect from the zinc anode cathodic protection. Although, the number of wires that experienced corrosion were similar in the blocks with and without the anode, the corrosion losses on the wires in the block without the anode were much greater than those in the block with the anode. Thus, the 3 percent salt water appeared to improve zinc anode performance during the test period, probably by increasing the conductivity of the environment.

The wires in the block without zinc anode that were exposed to 100 percent humidity had significant cross-section loss in 9 of the 20 wires. The reduction of the average diameter was approximately 3 mils (0.118 μm), or about 12 percent of the original thickness. The reduction of the wires in the specimen with zinc anode was negligible, indicating the effectiveness of cathodic protection by the zinc anode.

Marine and Non-Marine Environments

Test Conditions

Eight test blocks were vertically mounted on wooden frames, as shown in figure 3. The blocks were mounted in the wooden frames with two blocks (one with an anode and one without an anode) facing north, east, south, and west. Two frame types were used, as follows:

- Sheltered (figure 3). These frames had a roof that prevented direct rain and sun exposure with the blocks.

* 1 mil = 0.001 inch

- Boldly exposed (figure 4). These frames had no protective roof and were exposed to direct rain and sun exposure.

The frames with their test blocks were exposed in three climactic areas to analyze the benefits of the zinc-coating sacrificial anode in various environments. The three areas were:

1. Sea Isle City, NJ, a northern marine atmosphere located about 300 ft (91 m) from the Atlantic Ocean (eight blocks).
2. Daytona Beach, FL, a southern marine atmosphere located about 575 ft (175 m) from the Atlantic Ocean (eight blocks).
3. West Chester, PA (northern semi-rural environment) (eight blocks).

In addition, six test blocks (three with and three without zinc anode) were exposed to a seawater environment in Ocean City, NJ. These blocks were mounted on a seawall such that two were exposed to an atmospheric marine environment directly above the water line, two were exposed in the splash zone, and two were mounted at the high-tide line. Figure 5 shows schematically the test block arrangement at Ocean City. As shown in figure 5, the bottom set of blocks was exposed to complete immersion at high tide. The middle set of blocks was exposed to seawater splash when water conditions were rough. The top set was relatively dry during most of the exposure period.



Figure 3. Test blocks mounted beneath a shelter.

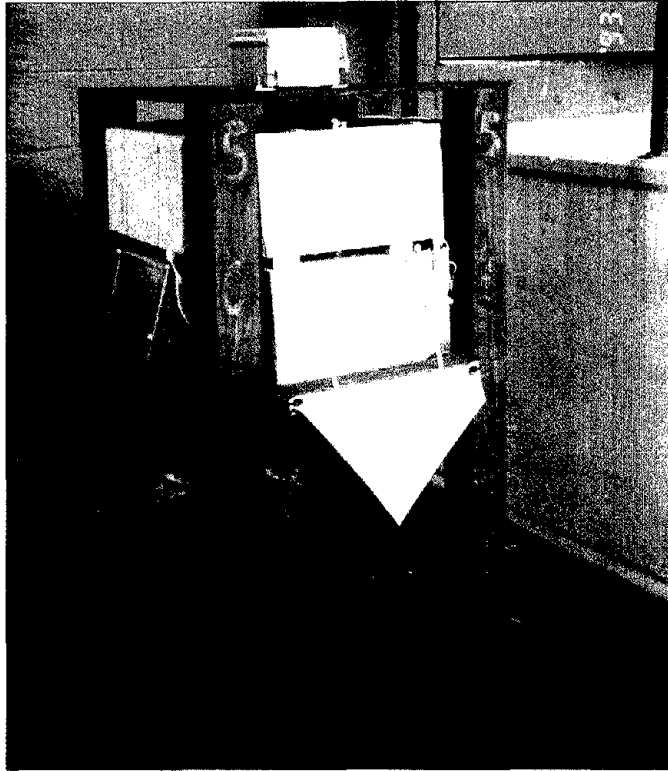


Figure 4. Test blocks mounted in exposed location.

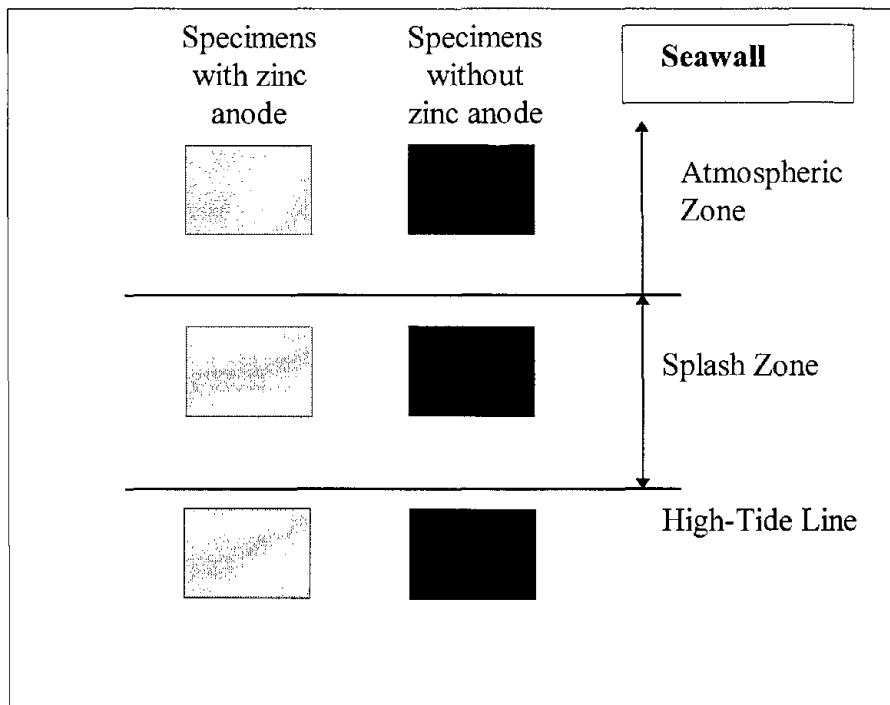


Figure 5. Schematic diagram of mortar test blocks mounted on seawall.

Results

The test blocks that had been exposed at the Ocean City and Daytona Beach atmospheric test sites gained additional chlorides during the exposure period. The mortar cover over the perforated steel plate in the non-anode side of the block was approximately 1 in (2.5 cm) thick. Chlorides deposited on the surface from the marine atmosphere diffused into the blocks. Some of the chlorides reached the steel plate and passed through the holes in the plate, resulting in corrosion on both sides of the plate.

A different condition was found in the specimens exposed at the West Chester test site. Since the test site was not in a marine or deicing salt area, additional chlorides were not introduced into the test blocks. However, the sides of the perforated steel plate showed corrosion in small areas when the blocks were opened for visual examination (figure 6). This corrosion was caused by the chlorides that diffused from the salt-contaminated mortar in the slots.

The findings from the specimens exposed to the marine and non-marine environments are shown in table 2 and are summarized below:

SEA ISLE CITY, NEW JERSEY, SITE

The zinc anode seemed to prevent the initiation of corrosion on some wires. However, the zinc anode considerably reduced the corrosion on the steel plate despite the high chloride concentrations found (approx. 900 to 1500 ppm) near the steel-mortar interface (figure 7). In addition, lower chloride concentrations were detected near the steel-mortar interface embedded in the blocks with the zinc anode. It is thought that this was caused by chloride migration from the cathode in the presence of the cathodic protection. The open circuit potentials of the zinc anode ranged from -429 mV (copper-copper sulfate reference) to -640 mV, indicating passivation of the zinc. The corrosion (open circuit) potentials of the steel plates embedded in the blocks with the zinc anode were more noble than the plates in the blocks without an anode, resulting in less probability of active corrosion. In spite of the relatively low negative potential of the zinc anode at the end of the test period, the zinc anode apparently reduced corrosion on the steel plates. The effects of test block orientation at the test site and sheltering of the anodes were not significant to either the anode performance or condition of the steel embedded in the test blocks in these tests.

DAYTONA BEACH, FLORIDA, SITE

The zinc anode seemed to prevent the initiation of corrosion on some wires. In particular, almost all wires in the blocks with the zinc anode that had been boldly exposed to the environment did not show corrosion. On the other hand, the majority of the wires in the block without the zinc anode and facing south showed significant corrosion. The corrosion surface areas on the steel plates with the anode were much less than those without the anode, except for the block facing south under the shelter. Moderate amounts of chloride (approx. 138 to 413 ppm) were detected near the steel plate-concrete interface embedded in the blocks. The chloride concentrations were not significantly different despite the existence of the zinc anode. The open circuit potentials of

the zinc anode were widely scattered, ranging from -484 mV to -838 mV (CSE). The corrosion (open circuit) potentials of the steel plates embedded in the blocks with the zinc anode were more noble than the blocks without the anode, resulting in less probability of active corrosion.

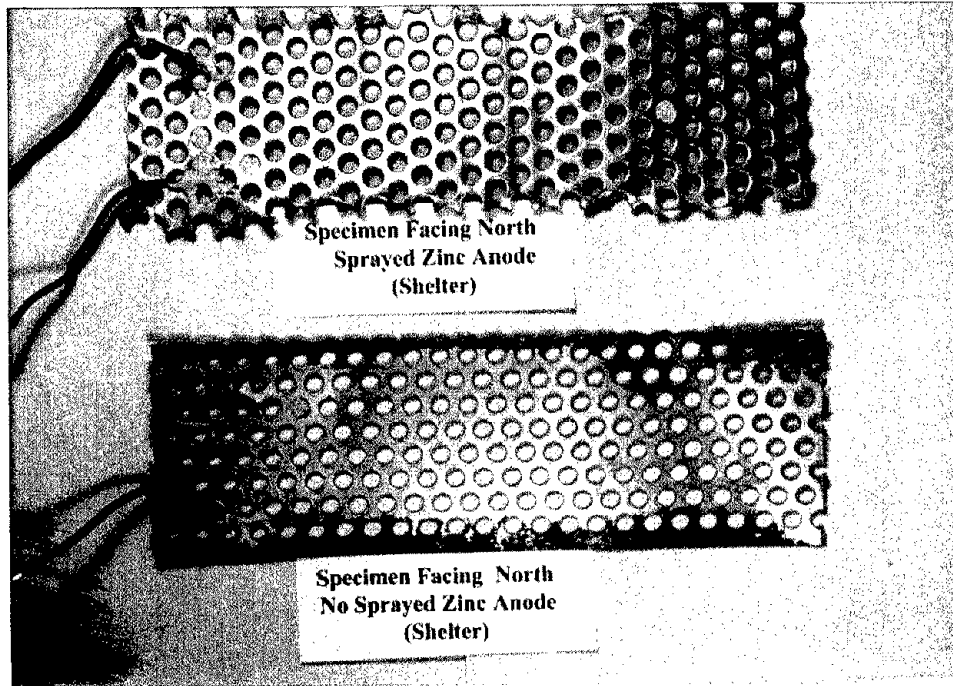


Figure 6. Condition of north-facing cathodes with and without zinc anode (West Chester site).

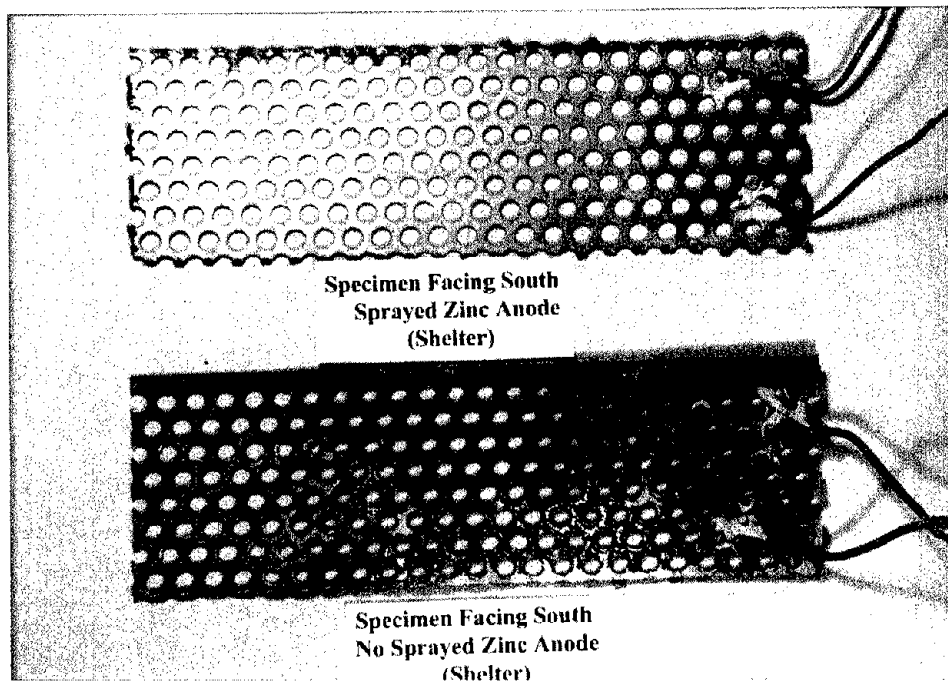


Figure 7. Condition of south-facing cathodes with and without zinc anode (Ocean City site).

WEST CHESTER, PENNSYLVANIA, SITE

Corrosion of the steel wire embedded in the blocks with the zinc anode was negligible. The zinc anode seemed to prevent the initiation of corrosion on some wires. In particular, the zinc anode performed well enough to prevent the initiation of corrosion of wires embedded in chloride-contaminated mortar. The steel plate cathodes in the blocks that had the zinc anode and that were not sheltered were much less corroded than in the blocks without zinc anodes. On the other hand, the condition of the steel plates in the blocks located under the shelter was not significantly different whether or not a zinc anode was used. The open circuit potentials of the zinc anode were widely scattered and ranged from -427 mV to -936 mV (CSE). The zinc open circuit potentials were more active on the blocks that were not sheltered. The corrosion (open circuit) potentials of the steel plates embedded in the boldly exposed blocks with the zinc anode were more noble than the blocks without the anode. The cathodic protection appears to have either maintained the passive film on the steel plate or prevented chlorides from the chloride-contaminated mortar from reaching the steel surface.

SEAWATER ENVIRONMENT

Table 3 shows the findings from the specimens exposed to the seawater environment in Ocean City, NJ. The zinc anodes considerably reduced corrosion of the wires embedded in the cement mortar. In particular, the zinc anode on the blocks located in the atmospheric zone greatly reduced the corrosion loss (figure 8). However, the visual examination and the corrosion potentials of the steel plates in all test blocks indicate that significant amounts of corrosion affected the steel plates despite the existence of the zinc anode. The chloride concentrations near the steel plates ranged from approximately 6300 ppm to 11,000 ppm. The zinc anode evidently could not totally prevent corrosion of the steel plates embedded in these high chloride concentration environments. The open circuit potentials of the zinc anodes indicated that the zinc that was occasionally exposed to direct seawater contact maintained more active potentials [-973 mV (CSE)]. However, the potential of the zinc exposed in the atmospheric zone was less active [-675 mV (CSE)]. The block located in the tidal zone lost the majority of the zinc coating from corrosion of the zinc on the outside of the coating.

Table 1. Test results of concrete blocks located in the laboratory.

	Exposure Condition*	Avg. Wire Diameter (mil)	Standard Deviation	No. of Corroding Wires
Dry Condition (control - no chloride in slot mortar)				
No zinc anode	Condition 1	26.1	1.21	0
Zinc anode	Condition 1	25.2	0.49	0
Dry Condition (chloride in slot mortar)				
No zinc anode	Condition 1	24.6	1.29	8
Zinc anode	Condition 1	25.0	0.38	0
Freshwater Spray (chloride in slot mortar)				
No zinc anode	Condition 2	24.4	2.29	9
Zinc anode	Condition 2	24.7	1.89	5
3% Saltwater Spray (chloride in slot mortar)				
No zinc anode	Condition 3	23.0	2.48	11
Zinc anode	Condition 3	24.3	0.98	10
100% Relative Humidity (chloride in slot mortar)				
No zinc anode	Condition 4	22.2	4.04	9
Zinc anode	Condition 4	25.1	1.22	4

1 mil = 0.001 inch = 25.4 μ m

* NOTES:

- Condition 1: Room temperature of 60 deg. to 80 deg. F (15 deg. to 27 deg. C) and relative humidity between 40 and 60%.
- Condition 2: Same as Condition 1, but freshwater spray was applied to the anode surface for approx. 30 s twice a day during weekdays.
- Condition 3: Same as Condition 1, but 3% saltwater spray was applied to the anode surface for approx. 30 s twice a day during weekdays.
- Condition 4: Specimens were maintained in 100% relative humidity enclosure.

Table 2. Test results on marine and non-marine exposed concrete blocks with and without zinc sacrificial anode.

A. SPECIMENS EXPOSED UNDER SHELTER

Location	Avg. diameter of wires, mils (Std. Dev.)		# Corroding Wires		% Corrosion on Plate		Steel Plate				O.C. Zinc Potential (mV/CSE)
	Anode Exposure Direction		No CP	CP	No CP	CP	Potential (mV/CSE)		Chloride (ppm)*		
	No CP	CP	No CP	CP	No CP	CP	No CP	CP	No CP	CP	
Ocean City											
South	24.9 (0.50)	24.7 (0.43)	1	1	85	5	-375	-97	n/a	n/a	-640
East (facing ocean)	24.0 (2.92)	25.7 (0.62)	3	1	27	13	-289	-145	1417	1076	-473
North	25.1 (1.49)	25.5 (1.81)	3	1	84	4	-413	-183	n/a	n/a	-469
West	23.9 (1.77)	24.3 (1.58)	6	4	72	13	-358	-157	n/a	n/a	-617
Daytona Beach											
South	25.7 (0.48)	25.7 (0.61)	15	4	75	63	n/a	n/a	n/a	n/a	n/a
East (facing ocean)	24.2 (1.28)	25.2 (0.57)	9	3	92	10	-357	-136	138	413	-667
North	23.8 (2.55)	25.6 (1.77)	2	2	95	9	-367	-131	n/a	387	-484
West	23.4 (2.58)	24.7 (2.10)	1	2	23	7	-287	-183	n/a	n/a	-515
West Chester											
South	23.3 (1.78)	23.8 (1.83)	13	5	17	7	-84	-133	n/a	n/a	-427
East (facing building)	25.3 (0.58)	24.8 (0.69)	2	2	15	15	-145	-123	n/a	n/a	-433
North	24.9 (1.50)	25.5 (0.51)	5	1	27	3	-57	-137	n/a	n/a	-691
West	24.2 (1.14)	25.1 (1.01)	7	2	29	13	-82	-47	n/a	n/a	-409

B. SPECIMENS EXPOSED WITHOUT SHELTER

Location	Avg. diameter of wires, mils (Std. Dev.)		# Corroding Wires		% Corrosion on Plate		Steel Plate				O.C. Zinc Potential (mV/CSE)
	Anode Exposure Direction		No CP	CP	No CP	CP	Potential (mV/CSE)		Chloride (ppm)*		
	No CP	CP	No CP	CP	No CP	CP	No CP	CP	No CP	CP	
Ocean City											
South	25.7 (0.39)	25.6 (0.56)	1	2	25	3	-223	-142	n/a	n/a	-429
East (facing ocean)	23.8 (1.43)	24.7 (0.36)	9	1	33	17	-290	-177	1395	980	-499
North	n/a	24.9 (1.93)	4	n/a	n/a	7	-325	n/a	n/a	n/a	n/a
West	25.3 (1.39)	25.5 (0.98)	6	1	80	3	-359	-177	n/a	n/a	-585
Daytona Beach											
South	21.5 (2.87)	25.1 (0.33)	15	0	60	11	-368	n/a	n/a	n/a	n/a
East (facing ocean)	24.7 (2.07)	25.9 (0.92)	7	2	15	17	n/a	-45	n/a	413	-838
North	23.1 (3.24)	24.8 (0.93)	4	0	33	9	-229	-154	249	387	-485
West	25.9 (0.23)	25.7 (0.90)	1	0	60	13	n/a	n/a	265	n/a	n/a
West Chester											
South	23.1 (3.39)	23.9 (1.06)	15	0	73	3	-342	-131	n/a	n/a	-936
East (facing building)	23.7 (2.15)	25.6 (0.75)	7	3	43	2	-213	-206	n/a	n/a	-911
North	25.0 (1.33)	25.3 (1.08)	4	2	33	6	-145	-223	n/a	n/a	-733
West	22.3 (2.86)	25.1 (2.32)	1	0	46	1	-283	-104	n/a	n/a	-465

O.C. = Open Circuit
1 mil = 0.001 in = 25.4 μm

n/a = not available
* Laboratory analysis

Table 3. Results from blocks exposed to seawater.

Specimen ID	A1 (Zinc)	B1 (No Zinc)	A2 (Zinc)	B2 (No Zinc)	A3 (Zinc)	B3 (No Zinc)
Exposure Condition	Atmos.	Atmos.	Splash	Splash	Tide	Tide
Avg. diameter of wire (mil)*	24.8	16.2	23.9	20.0	24.8	21.8
Standard Deviation	2.03	7.70	2.78	7.01	1.87	5.21
No. of Wires Corroding*	5	15	9	13	6	20
% of Corrosion on Plate*	65	98	85	93	40	93
Steel Plate Static Potential (mV/CSE)	-458	-535	-555	-562	-576	-524
Zinc Anode Static Potential (mV/CSE)*	-675		-973		-785	
Chloride Conc. (ppm)**	6,547	9,325	6,349	9,232	9,595	10,669

* After 20 months exposure. ** Chloride sample taken near steel plate. 1 mil = 0.001 in = 25.4 μ m

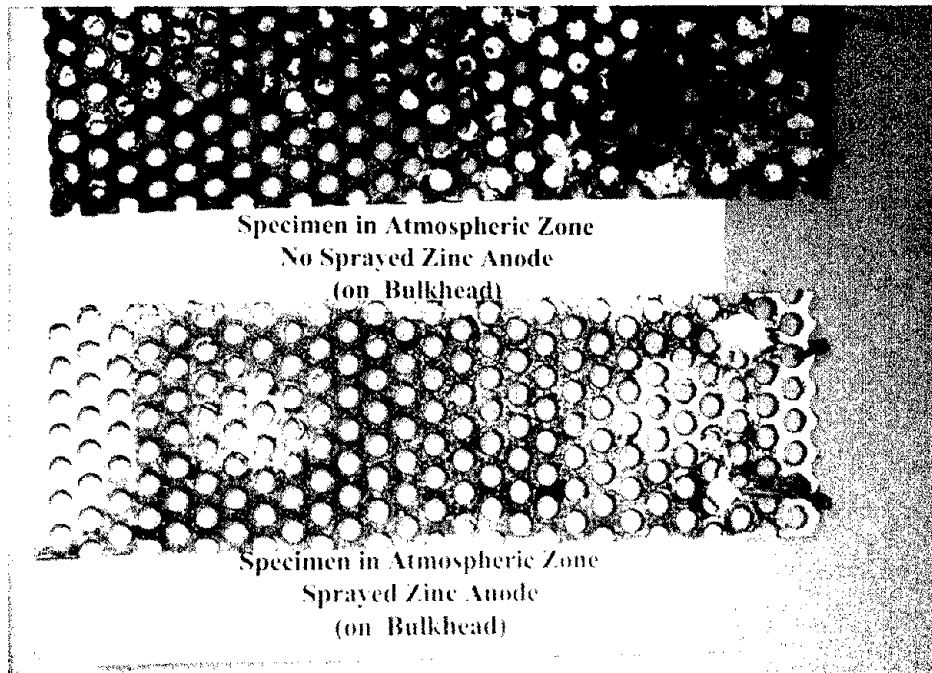


Figure 8. Steel plate cathodes located on seawall at Ocean City, with and without zinc anode.

Summary

The tests discussed in this chapter indicate that the direction of exposure does not affect the performance of a zinc sacrificial anode. An exception to this would be if the exposure direction resulted in increased moisture or salt on the surface. In that case, the anode might continue to display active potentials and would be expected to perform better than a similar anode located in the drier environment. The zinc anode cathodic protection did reduce the amount of corrosion on the cathodes, although it did not completely prevent corrosion. The zinc anodes that were exposed to highly corrosive conditions, such as direct seawater contact, displayed more active potentials (i.e., > -800 mV) and did not passivate. While the zinc anode did reduce the amount of corrosion, it did not completely prevent corrosion of the steel. Where the test blocks were exposed in the atmosphere, the open circuit potential of the zinc anode approached that of corroding steel (passivated) in most of the test blocks, which will result in less current between the anode and the cathode. This might result in a reduction in the amount of cathodic protection for the embedded steel. The observed passivation of the zinc and the incomplete cathodic protection indicated the need to identify an alloy that might provide more effective cathodic protection.

CHAPTER 2

STUDY OF EXISTING SACRIFICIAL ZINC ANODE CATHODIC PROTECTION SYSTEMS

The investigation team visited two bridges in Florida in November 1992 in order to evaluate existing sacrificial sprayed zinc cathodic protection systems on bridge structures. The Niles Channel Bridge (figure 9) and the Bahia Honda Bridge (figure 10), located in the Florida Keys, were selected for this study. Sprayed zinc was applied to five piles of the Niles Channel Bridge (figure 11) and one pile of the Bahia Honda Bridge (figure 12). The piles of the Niles Channel Bridge contain epoxy-coated reinforcing steel, and the piles of the Bahia Honda Bridge contain bare reinforcing steel. Both bridges had experienced severe corrosion of the reinforcing steel, resulting in concrete spalls. Florida DOT applied the sprayed zinc coatings to selected Niles Channel Bridge members in November 1988 and to selected Bahia Honda Bridge members in April 1991.

Bahia Honda Bridge

Sprayed zinc was applied to one pile of the Bahia Honda Bridge. The concrete and exposed steel reinforcing was first abrasive blasted, then the zinc coating was applied directly to exposed reinforcing steel and concrete (figure 13). Twelve rebar probes were installed in the pile tested. Ten probes were installed in two vertical rows of five probes each at approximately 2-ft (60-cm) intervals in the column, and two probes were installed in the footing, as shown in figure 14. Six probes were connected to the CP system, and the other six probes had not been connected as controls. Since the zinc was sprayed directly onto exposed rebar, the anode could not be separated from the rebar to conduct tests. However, anode tests could be conducted at “windows” cut into the anode. A total of six 1-ft x 1-ft (30-cm x 30-cm) windows of zinc coating were isolated from the bulk zinc coating by saw-cutting. Four of the six windows are located on the column in one vertical row separated by approximately 1.5 ft (45.7 cm), as shown in figure 20. One window was located on the vertical surface of the footing, and another window was located on the top surface of the footing. A 0.75-in- (2-cm-) wide stainless steel band was used to provide electrical continuity between the window and the surrounding zinc coating.

Rebar Probe (Cathode) Measurements

All cathode testing was performed on the rebar probes, since it was not possible to electrically isolate the rebar in the pile from the anode. The following tests were conducted on the rebar probes:

- Current.
- Instant-off potential.
- Depolarization over 24 h.
- Static potential after depolarization.
- Resistance between rebar probe and anode window.



Figure 9. Niles Channel Bridge.



Figure 10. Bahia Honda Bridge.

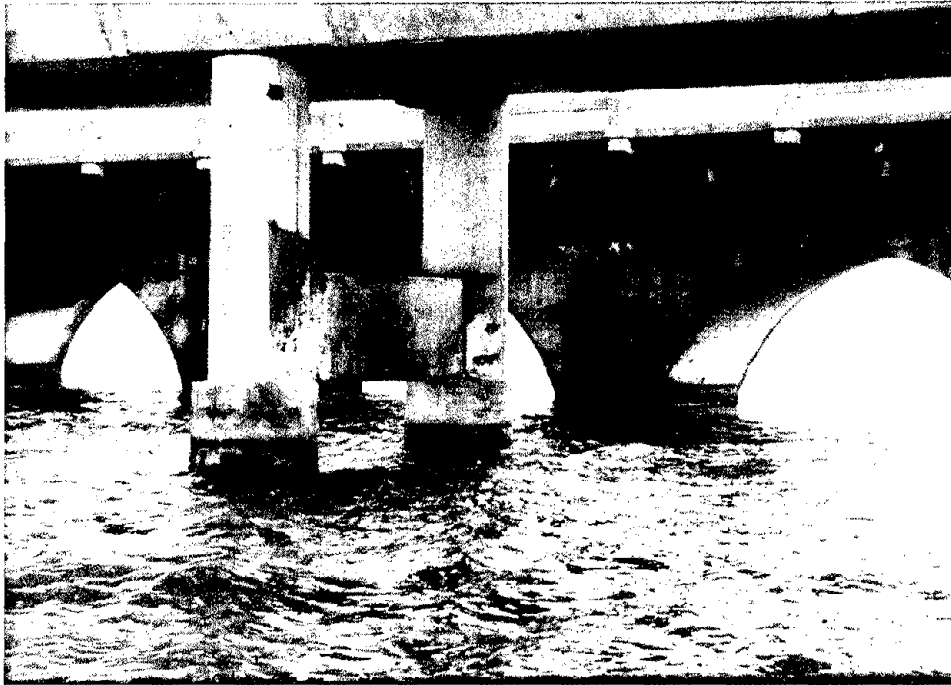


Figure 11. Zinc anode coating on one bent of Niles Channel Bridge.

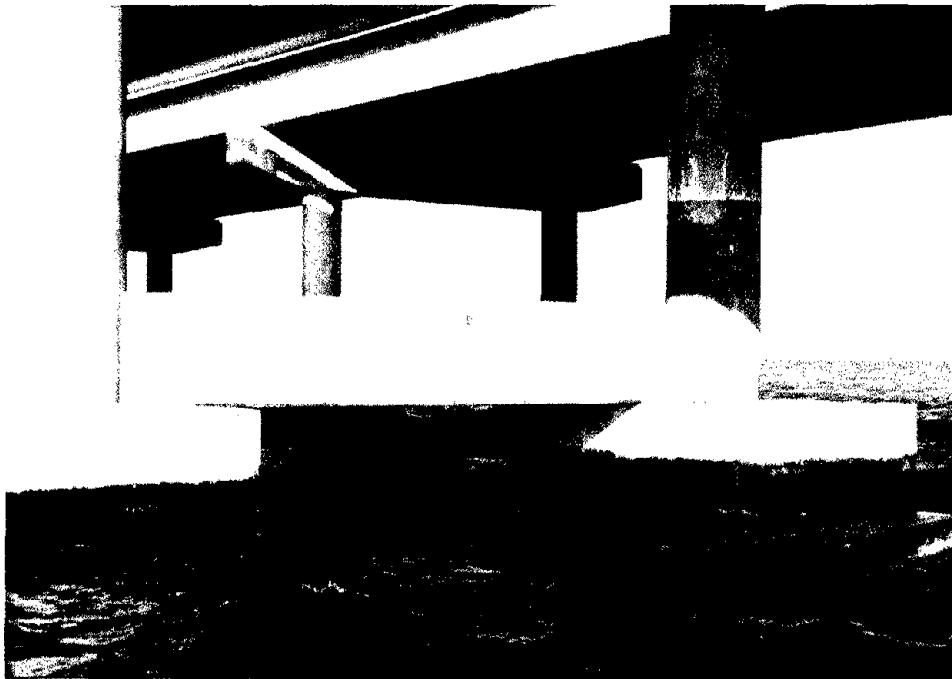


Figure 12. Zinc anode coating on one bent of Bahia Honda Bridge.

Cathodic protection current received by each rebar probe was measured using a low-resistance ammeter. The current was measured by connecting an ammeter between the rebar probe and the zinc anode. “Instant-off” potential of each rebar probe was measured using a pencil-size copper-copper sulfate reference electrode and a high-impedance voltmeter. After a small amount of concrete surface area was exposed by removing the zinc coating at the rebar probe locations, the reference electrode was fixed on the exposed concrete surface. A conductive gel provided the bridge between the electrode and the concrete. Immediately after the rebar probe was disconnected from the zinc anode, the potential of the rebar probe was measured. Depolarization tests were performed on the rebar probes at the time of the depolarization measurements for the windows. The depolarizing potentials of the rebar probes were recorded every 5 min using a voltmeter/data logger and copper-copper sulfate reference electrodes for approximately 24 h. After the depolarization tests were completed, the static potential of the rebar probes was measured using a voltmeter. The resistance between the probe and the zinc coating was measured using an alternating current (ac) resistance meter at the end of the depolarization tests. Table 4 summarizes the electrical test results obtained from the rebar probes.



Figure 13. Zinc anode coating applied to exposed rebar on Bahia Honda Bridge (bands were used to hold reference cells onto the column).

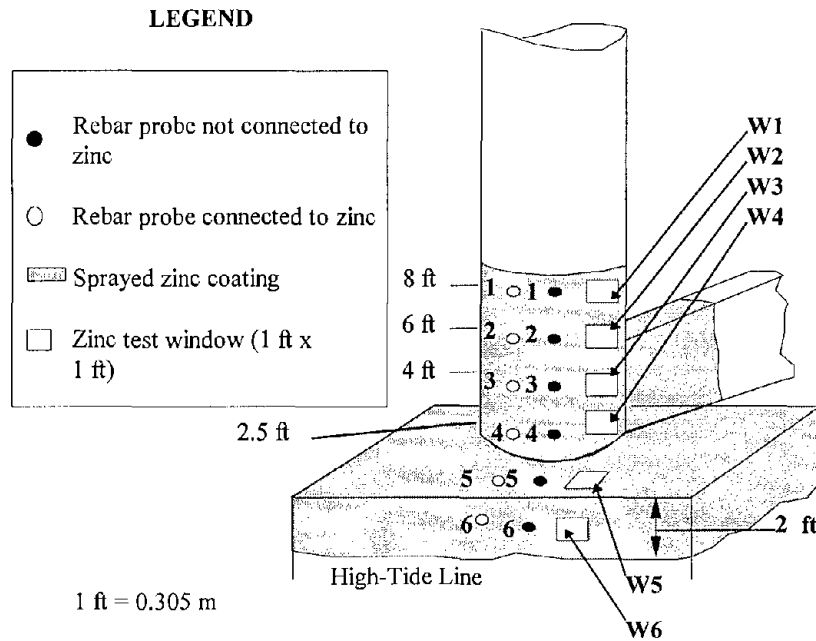


Figure 14. Rebar probe and anode window locations for pile tested at Bahia Honda Bridge.

The depolarization tests indicate that the amount of depolarization decreased with increased distance from the water. The static potentials of the rebar probes embedded in the column, including the probes that had not been connected to the zinc anode, exhibited passive potentials. It is suspected that the cement mortar used to embed the rebar probes did not contain chlorides. If the probes were not corroding, the amount of current received and the amount of depolarization on the probes might not be representative of the corroding reinforcing steel in the concrete. Therefore, it is likely that depolarization on the non-corroding probes was not only caused by the current from the zinc anode, but also by current from the surrounding corroding reinforcing steel. When non-corroding rebar is cast in chloride-free concrete, it has a passive potential. The passive rebar can be polarized by the surrounding corroding rebar embedded in chloride-contaminated concrete that is at a more active potential.(11,17,18) When a rebar probe is not corroding, the potential difference between the probe and the zinc anode is greater because of the more positive (passive) potential of the probe. Furthermore, when the steel is embedded in chloride-free concrete, the steel polarizes more with less cathodic protection current density.(12) As a result, the rebar probe receives more current from the zinc anode and polarizes more readily than corroding steel. Thus, it is difficult to determine the effectiveness of the sacrificial anode cathodic protection system using the rebar probes installed. However, the amount of cathodic protection current received from the zinc may be sufficient to protect the rebar up to 2.5 ft (76 cm) from the water line, based on the current density to the probe.

The resistance between Probe A6 and the zinc anode was low because of frequent exposure to seawater. The potential difference between the “instant-off” potentials of the rebar probe and the zinc, which is the driving voltage of the anode to the steel, is greater than those found in the Niles Channel Bridge system (as will be discussed). These two factors — the low resistance and the higher driving voltage — appear to contribute to the better performance of the sprayed zinc cathodic protection system on the Bahia Honda Bridge.

Table 4. Test results of rebar probes at the Bahia Honda Bridge.
(Note: CP installed April 1991, tests conducted November 1992.)

Probe ID	Height From High-Tide Line (ft)	Current Density on Probe (mA/ft ²)	Potential Difference Between Anode & Probe* (mV)	Instant-Off Potential of Probe (mV/CSE)	Static Potential of Probe** (mV/CSE)	Probe Depol. at 1 h [at 24 h] (mV)	Resistance Between Zinc & Rebar Probe (ohm)
A1	8	0.29	73	-315	-206	53 [109]	2200
A2	6	0.55	12	-408	-194	153 [214]	1400
A3	4	0.70	62	-423	-182	180 [241]	4900
A4	2.5	3.30	35	-537	-180	254 [354]	670
A5	2 ***	1.15	20	-593	-	-	1200
A6	1	7.80	59	-668	-441	[227]	550
B1	8	not	-	-	-124	-	-
B2	6	connected	-	-	-178	-	-
B3	4	to	-	-	-185	-	-
B4	2.5	anode	-	-	-245	-	-
B5	2 ***		-	-	-406	-	-
B6	1		-	-	-434	-	-

* Potential difference between the “instant-off” potentials of the rebar probe and the zinc.

** Potential at 24 h of the depolarization test.

*** Top of footing.

1 ft = 0.305 m

1 mA/ft² = 10.75 mA/m²

CSE = copper-copper sulfate reference electrode

Anode Measurements

As stated previously, the electrical characteristics of the anode could be measured at the windows cut into the anode. The measurements on the anode included:

- Current.
- Instant-off potential.
- Depolarization.
- Adhesion between the zinc and concrete.
- pH of the concrete immediately beneath the zinc.
- Surface analysis of the zinc at the concrete interface.

Anode current output from each zinc test window was measured using a low-resistance ammeter. Before disconnecting the stainless steel band crossing the zinc window and the surrounding zinc,

the ammeter was connected between the window and the surrounding zinc. After the stainless steel band was disconnected from the window, the current output was measured. “Instant-off” anode potential of each zinc window was measured using a pencil-size copper-copper sulfate reference electrode and a high-impedance voltmeter. After a small amount of concrete surface area was exposed by removing the zinc coating at the center of the window, the reference electrode was fixed on the exposed concrete surface. To avoid activating the zinc coating and to prevent changing the anode potential by using water or a wet sponge, thick conductive gel was used at the reference electrode-to-concrete interface. Immediately after the zinc window was disconnected from the surrounding zinc, the potential of the window was measured. Using the reference electrodes and a high-impedance voltmeter/data logger, the depolarization of the zinc anode windows was measured for approximately 24 h. The depolarizing potentials were recorded every 5 min. After the depolarization tests were completed, the static potentials of the zinc windows were measured using a voltmeter. Table 5 summarizes the results of the electrical tests on the zinc windows.

Table 5. Test results on zinc test windows at the Bahia Honda Bridge.

Test Window ID	Height From High-Tide Line (ft)	Anode Current Density at Window (mA/ft ²)	“On” Potential (mV/CSE)	“Instant-Off” Potential (mV/CSE)	“Inst.-off” – “On” Potential (mV)	Static Potential at 1 h [at 24 h] (mV/CSE)	Depolarization at 1 h [at 24 h] (mV)
W1	8	0.35	-428	-379	49	-491 [-516]	112 [137]
W2	6	0.56	-553	-524	29	-500 [-500]	24 [24]
W3	4	0.62	-466	-422	44	-526 [-529]	104 [107]
W4	2.5	1.4	-660	-527	133	-581 [-553]	54 [26]
W5	2	n/a*	n/a*	n/a*	n/a*	n/a*	n/a*
W6	1	n/a*	n/a*	n/a*	n/a*	n/a*	n/a*

* Due to the poor electrical connection of stainless steel band to window or the surrounding zinc, the window was electrically isolated, resulting in no current output.
 1 ft = 0.305 m
 1 mA/ft² = 10.75 mA/m²
 n/a = not available

Figure 15 graphically shows the results of depolarization tests conducted at the zinc windows. After the test windows were disconnected from the surrounding zinc, most of the zinc depolarized in the active direction, as would be expected. However, the zinc of window W2 polarized in the passive direction, indicating that it had received current when connected to the CP system. This polarization behavior was probably caused by current reversal. If the potential of the reinforcing steel embedded in the concrete is more negative than that of zinc, the reinforcing steel becomes an anode, resulting in acceleration of the corrosion of the steel. This is confirmed by the instant-off potentials of the anode and rebar probe (see tables 4 and 5). The depolarization behavior of the zinc in figure 15 shows that the zinc reached equilibrium conditions after approximately 1 h of the depolarization test. This short period of depolarization may be caused by the small amount of zinc polarization in the environment.

The cathodic protection current density on the zinc window decreased with increasing distance from the high-tide line. The current densities on the Bahia Honda Bridge windows are greater than those on the Niles Channel system (as will be discussed). This may be the result of the bare reinforcing steel in the structure causing the circuit resistance between the zinc window and the reinforcing steel to be lower on the Bahia Honda Bridge. The resistance of the steel reinforcing in the pile could not be measured directly. The resistance data between the zinc window and rebar probes do not reflect the differences between the coated and uncoated rebar. The static potentials of the zinc windows (after the windows were disconnected from the surrounding zinc for 24 h) are sufficiently noble, indicating passivation of the zinc.

Both the relatively large rebar probe depolarization and high cathodic protection current generated by the zinc anode of window W4 in the splash zone indicate that the zinc-steel galvanic cell appears to be under cathodic control, suggesting an efficient cathodic protection system at that location.

Zinc coating adhesion strength was measured at five locations at the column and footing, using an Elcometer Model 106 coating adhesion gauge per American Society for Testing and Materials (ASTM) D4541. The results are summarized as follows:

Dolly No.	Test Locations	Bond Strength (lbf/in²)
1	Approx. 2 ft above the high-tide line	10
2	Top of footing	n/a*
3	Approx. 4 ft above the high-tide line	n/a*
4	Approx. 4.5 ft above the high-tide line	<10
5	Approx. 5 ft above the high-tide line	100

* n/a = not available. Due to the epoxy adhesive failure on the dollies, the bond strengths could not be measured.

1ft = 0.305 m 1 lbf/in² = 6.89 kPa

The zinc-to-concrete interface pH at each adhesion test location was measured using pH paper. The pH of the concrete under the zinc coating ranged from 10.5 to 11.5.

The x-ray diffraction analysis of the zinc-to-concrete interface on one of the adhesion-strength pull specimens (dolly #1) indicates that negligible amounts of zinc corrosion products exist at the zinc-concrete interface. Figure 16 shows the x-ray diffraction graph for the Bahia Honda Bridge. The red trace shows the pattern for zinc oxide and the blue trace shows the pattern for zinc. The magnitude of the peaks is very small for the zinc oxide, suggesting few corrosion products present. This, in turn, suggests that little corrosion of the zinc has occurred, implying that this portion of the anode has discharged little current.

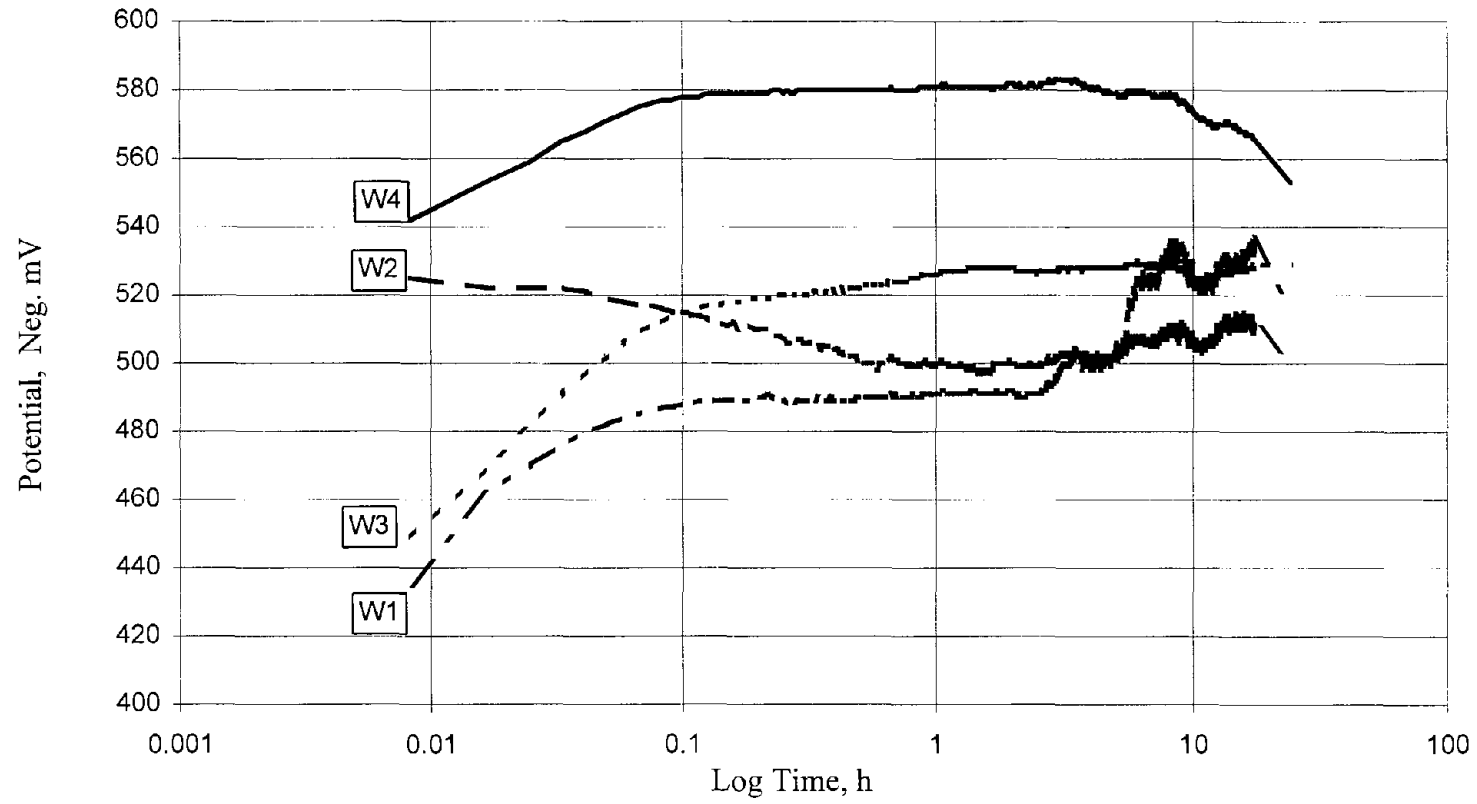


Figure 15. Zinc anode window depolarization tests – Bahia Honda Bridge.

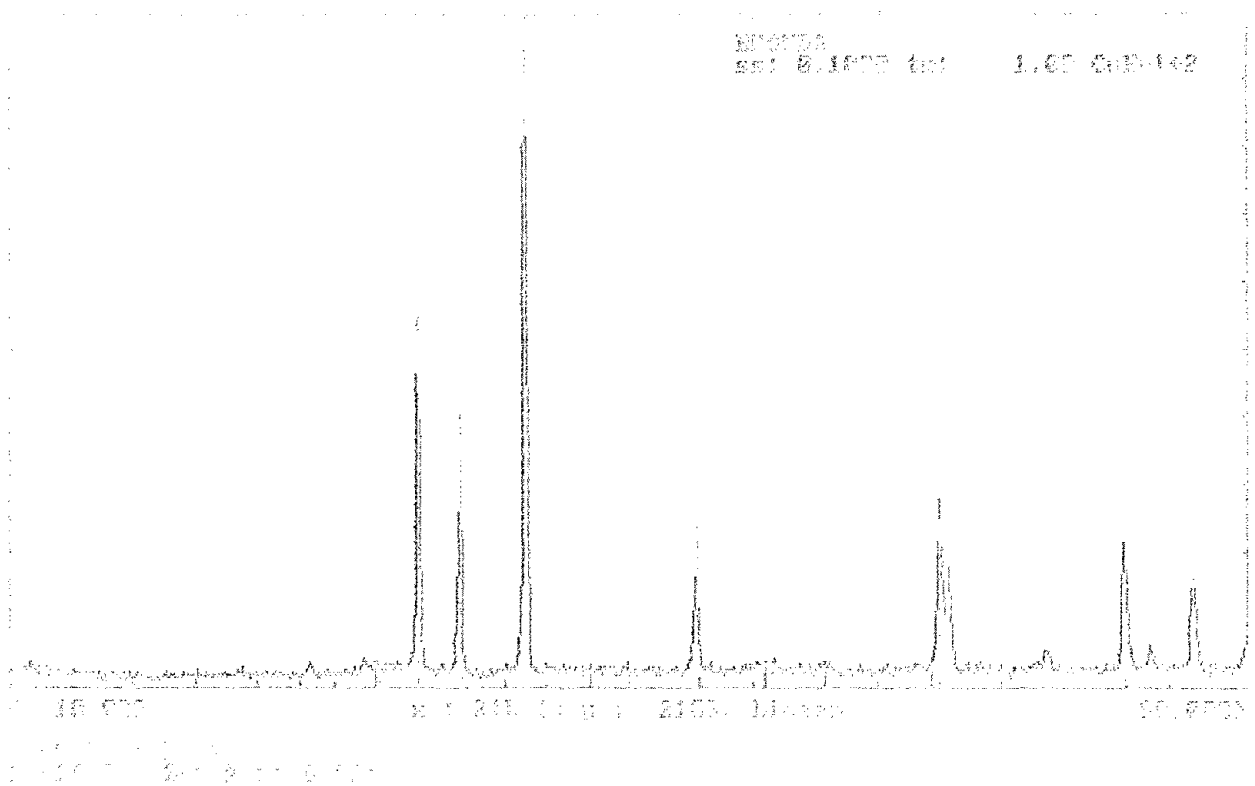


Figure 16. The x-ray diffraction pattern from zinc-concrete interface of adhesion dolly #1 from the Bahia Honda Bridge.

Niles Channel Bridge

The zinc coating was applied to the piles from the top of the footer to 6 ft (1.8 m) above the footer (see figure 11). In addition, the zinc coating was applied to the strut beginning at the strut-column intersection and extending 1 ft (0.3 m) on both sides and at the top of the strut.(10) As on the Bahia Honda Bridge, the zinc coating was applied not only to the concrete surface, but also to directly exposed reinforcing steel after the epoxy coating and corrosion products had been removed by sandblasting (see figure 17). Thus, the zinc coating was permanently bonded to the steel structure. Furthermore, to prevent atmospheric corrosion of the zinc coating, a mastic coating was applied over the zinc coating on half of each pile surface.

A total of eight rebar probes were installed in one of the columns. The reported exposed surface area of each rebar probe is 2 in² (12.9 cm²). The probes were installed in a total of eight core holes in two vertical rows of four probes each at approximately 1-ft (0.3-m) intervals to span the zinc-coated areas from top to bottom. The core holes were filled with cementitious mortar. Four probes (Probes A1 through A4) in one row were connected to the CP system, and the other four probes (Probes B1 through B4) were not connected to act as controls (see figure 18). The lowest probes were located approximately 2 to 3 ft (0.6 to 0.9 m) above the high-tide line (figures 18 and 19).

As in the Bahia Honda Bridge, windows had been cut into the anode to allow data collection on the anode. Six 1-ft x 1-ft (30-cm x 30-cm) areas (“windows”) of zinc coating were isolated from the bulk of the zinc coating by saw-cutting at various elevations (figure 20). The test windows are located in two vertical rows of three windows each at approximately 1-ft (0.3-m) separations (figure 21). The lower half of the column was coated with a mastic coating so that one row of windows was covered with the paint. A 0.75-in- (2-cm-) wide stainless steel band was installed across each window and surrounding zinc coating to provide electrical continuity, as shown in figure 22. The lowest windows were located approximately 5 ft (1.5 m) above the high-tide line.

The following tests were used to evaluate the zinc sacrificial anode cathodic protection systems on the Niles Channel Bridge:

Rebar Probe (Cathode) Measurements

Similar tests to those at the Bahia Honda Bridge were conducted at the Niles Channel Bridge, except that a data logger was not used to record depolarization.

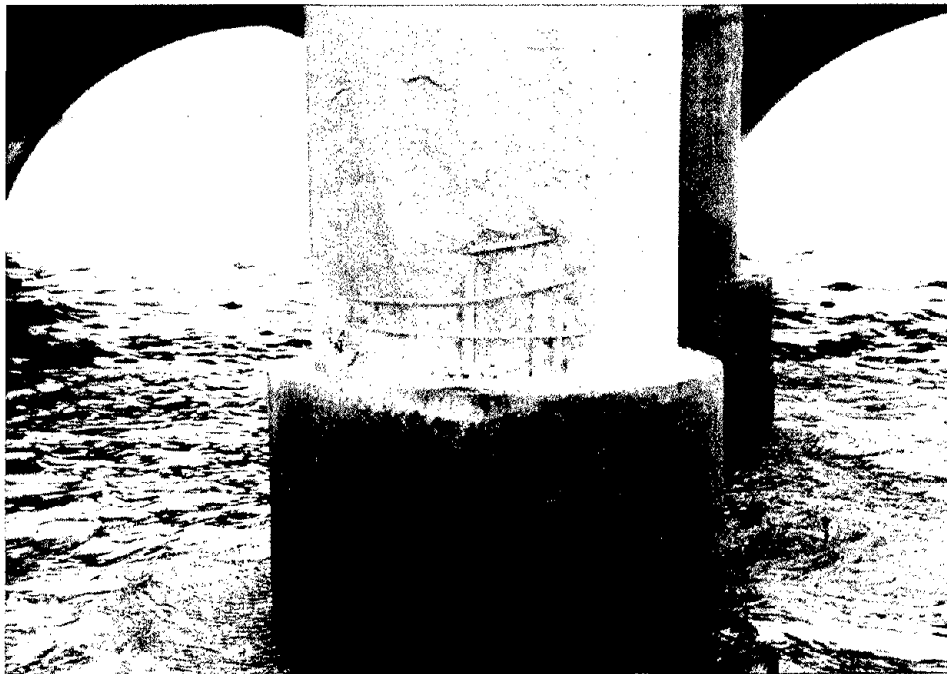


Figure 17. Zinc coating applied to exposed rebar of Niles Channel Bridge.

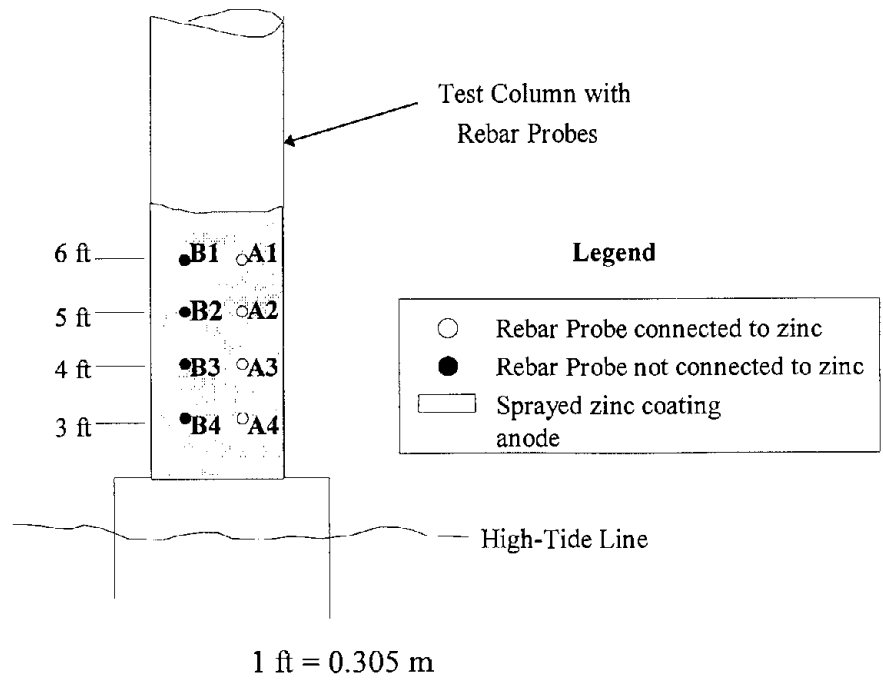


Figure 18. Schematic of rebar probes on Niles Channel Bridge.

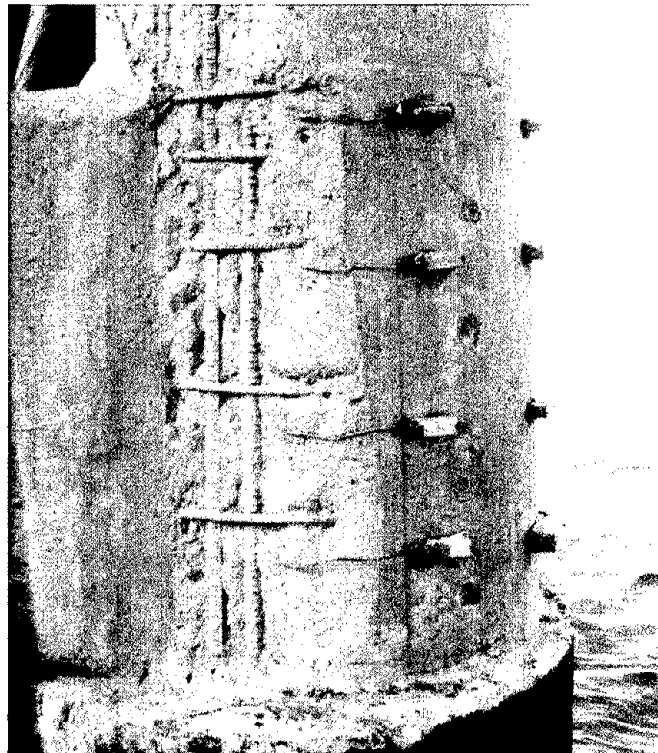


Figure 19. Rebar probes on Niles Channel Bridge.



Figure 20. Anode windows on Niles Channel Bridge.

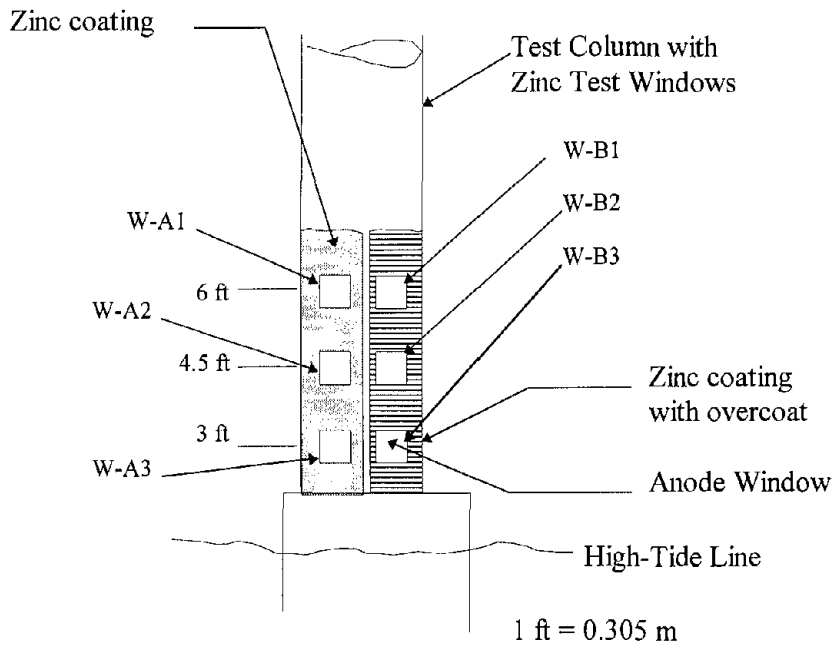


Figure 21. Schematic of anode window identification on Niles Channel Bridge.

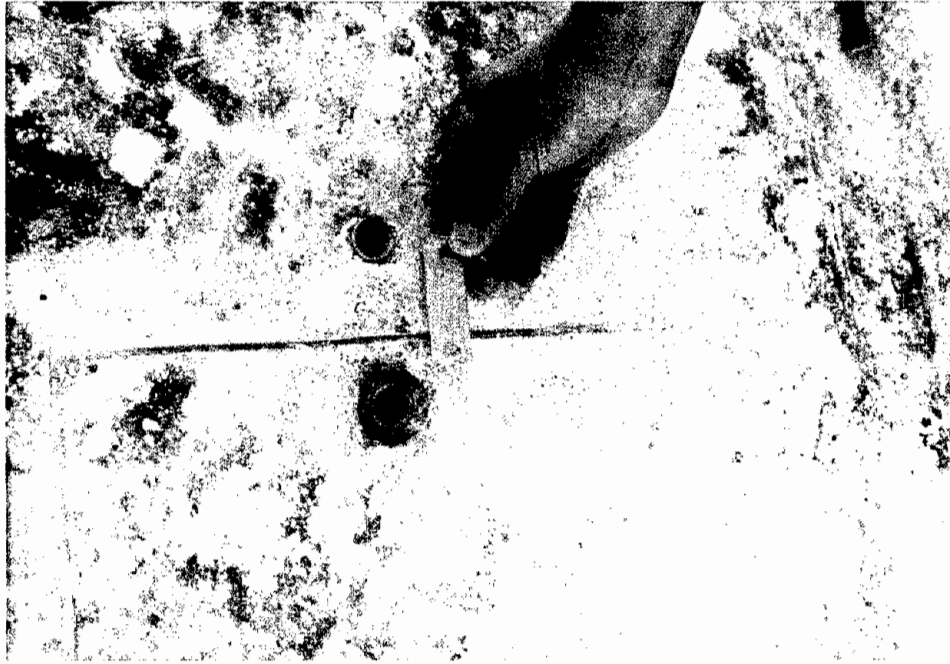


Figure 22. Electrical continuity band on Niles Channel Bridge.

Depolarization tests were performed on the rebar probes at the time of the depolarization measurements for the windows. The potentials of the rebar probes were recorded initially and after approximately 24 h. After the depolarization tests were completed, the static potential of the rebar probes was measured using a voltmeter. Table 6 shows the summary of the electrical test results obtained from the rebar probes.

The depolarization tests indicated that the rebar probes that were located up to 5 ft (1.52 m) from the high-tide line met the “100-mV depolarization” criterion despite the low cathodic protection current densities received by the probes. However, note that the static potentials of all rebar probes, including the probes that had not been connected to the zinc anode, indicate passivity of the rebar probes. It is suspected that the cement mortar used to embed the rebar probes did not contain chlorides. As a result, the rebar probes have not corroded, except for Probe B3.

Table 6. Test results on rebar probes at the Niles Channel Bridge.
(Note: CP installed November 1988, tests conducted November 1992.)

Probe ID	Height From High-Tide Line (ft)	Current Density on Probe (mA/ft ²)	Potential Difference Between Anode & Probe* (mV)	Instant-Off Potential of Probe (mV/CSE)	Static Potential of Probe** (mV/CSE)	Probe Depol. at 24 h (mV)	Resistance Between Zinc & Rebar Probe (ohm)
A1	6	0.07	2	-213	-132	81	2800
A2	5	0.14	3	-293	-140	153	1800
A3	4	0.31	18	-274	-146	123	1700
A4	3	0.54	9	-408	-185	223	1000
B1	6	control	-	-	-177	-	2100
B2	5	control	-	-	-162	-	1500
B3	4	control	-	-	-345	-	4100
B4	3	control	-	-	-219	-	1200

* Potential difference between the "instant-off" potentials of the rebar probe and the zinc.

** Potential at 24 h of the depolarization test.

1 ft = 0.305 m

1 mA/ft² = 10.75 mA/m²

CSE = copper-copper sulfate reference electrode

Anode Measurements

Similar measurements to those at the Bahia Honda Bridge were obtained at the Niles Channel Bridge. The testing was conducted in a similar manner, except that zinc-to-concrete interface potentials and anode window static and depolarization after 24 h were not measured. Table 7 summarizes the results of the electrical tests on the zinc windows.

Table 7. Test results on zinc test windows at the Niles Channel Bridge.

Test Window ID	Height From High-Tide Line (ft)	Anode Current Density at Window (mA/ft ²)	"On" Potential (mV/CSE)	"Instant-Off" Potential (mV/CSE)	"Inst.-Off" - "On" Potential (mV)	Static Potential at 24 h (mV/CSE)	Depolarization at 24 h (mV)
W-A1	6	n/a*	n/a*	n/a*	n/a*	n/a	n/a
W-A2	4.5	0.009	-618	-618	0		
W-A3	3	0.024	-569	-572	+3		
W-B1**	6	n/a*	n/a*	n/a*	n/a*	n/a	n/a
W-B2**	4.5	0.008	-502	-506	+4		
W-B3**	3	0.018	-570	-568	-2		

* Due to the poor electrical connection of stainless steel band to window or the surrounding zinc, the window was electrically isolated, resulting in no current output.

** Uncoated section.

1 ft = 0.305 m

1 mA/ft² = 10.75 mA/m²

n/a = not available

The cathodic protection current density on the zinc window decreased with increased distance from the high-tide line. The mastic overcoating did not appear to affect the current output from the windows based on this limited data.

Adhesion strengths of the zinc coating to the concrete were measured using an Elcometer coating adhesion gauge. Aluminum dollies were epoxied to the coating. After the epoxy cured, the dollies were pulled with the Elcometer, and the force needed to pull the dolly (and coating) from the surface was measured. Zinc coating adhesion strength was measured at four locations on the column, and the results are summarized as follows:

Dolly No.	Test Locations	Bond Strength (lbf/in²)
1	Approx. 6 ft above high-tide line on SE face	75
2	Approx. 5 ft above high-tide line on SE face	100
3	Approx. 4 ft above high-tide line on SE face	150
4	Approx. 5 ft above high-tide line on NE face	25

1 ft = 0.305 m 1 lbf/in² = 6.89 kPa

The zinc bond strength does not appear to be related to the distance from the water line. Dolly no. 4 indicated low bond strength; however, it is unknown whether the low bond strength was caused by zinc corrosion products or poor surface preparation.

Samples of the zinc-concrete interface were obtained from the structure using the adhesion test dollies. The x-ray diffraction analysis was used to analyze the corrosion products at the zinc-concrete interface on one of the adhesion dollies from the 5-ft (1.5-m) level. The x-ray diffraction analysis indicated that negligible amounts of zinc corrosion products existed at the zinc-concrete interface on the samples tested. This is a similar finding to that from the Bahia Honda Bridge. As in the Bahia Honda Bridge, this suggests that little current discharged from the anode at this location.

Conclusions From Study of Existing Sacrificial Anode Cathodic Protection Systems

1. The tests conducted at the Bahia Honda and Niles Channel Bridges in the Florida Keys indicated that zinc as a sacrificial galvanic anode material is capable of protecting embedded steel reinforcing in areas that are wetted by saltwater.
2. Locations above direct water contact are not as well cathodically protected.
3. The degree of protection on the relatively dry areas of these bridges is difficult to gauge because of the inability to isolate the anode from the embedded steel and the question about whether or not the rebar probes were initially embedded in salted mortar backfill.
4. These tests did indicate that further testing of alternate anode alloys should be pursued.

CHAPTER 3

STUDY OF EXISTING METALS AND ALLOYS AS SACRIFICIAL ANODES

Fifteen different alloys were tested for use as sacrificial anodes on steel-reinforced concrete structures. Most of the metals and alloys have been used either as sacrificial anodes in underground and aqueous environments, or as metallic coatings for steel.(13-16) However, these alloys, except pure zinc, have not been tested on concrete structures. Conventional anode materials and additional alloys selected on the basis of alloy phase diagrams were tested. The following alloys were tested:

1. Pure zinc.
2. Conventional zinc alloy anode for underground application, provided by Sumitomo Metal Mining (0.3% Al, 0.12% Si, 0.01% Sn, and other trace elements).
3. Zinc-5% Aluminum.
4. Zinc-15% Aluminum.
5. Zinc-55% Aluminum.
6. Pure aluminum.
7. Conventional aluminum alloy anode for underwater application, provided by Sumitomo Metal Mining (3% Zn, 0.1% Si, 0.02% Zr, and 0.2% In).
8. Proprietary high-efficiency aluminum alloy anode for underwater application, provided by Sumitomo Metal Mining, containing 0.022% indium.
9. Aluminum-5% Zinc.
10. Aluminum-10% Zinc.
11. Aluminum-1% Magnesium.
12. Aluminum-10% Magnesium.
13. Aluminum-5% Zinc-3.5% Magnesium.
14. Aluminum-5% Zinc-0.1% Tin.
15. Pseudo Zinc-Aluminum.

These alloys were produced in the laboratory using pure metals, cast into concrete test blocks, connected to an embedded cathode in the test block, and subjected to six different test procedures. The tests were:

1. **Environmental Tests** - In these tests, the alloys were tested at various temperature and humidity conditions.
2. **Anode Efficiency Tests** - In these tests, the local action corrosion rate and galvanic corrosion rate of the alloys were measured.
3. **Atmospheric Corrosion** - These tests measured the corrosion rate of the alloys, in the form of plates, in a marine environment.

4. **Anode Capacity** — The current capacity of the alloys was tested using a modified ASTM procedure.
5. **Cyclic Polarization** — The anodic behavior of each alloy was studied before and after connection to a cathode.
6. **Effect of pH on Anode Performance** — The pH of a porewater solution was reduced and the effect on anode potential and current was measured.

The details of each of these tests are presented in this chapter.

Concrete Block Construction

A total of 57 concrete blocks were produced using Type I portland cement. Aggregate size was about 0.5 in (1.28 cm). The blocks were 6 in (15.2 cm) wide x 18 in (45.7 cm) long x 2 in (5.1 cm) high. The water/cement ratio of the concrete was 0.42. Approximately 1300 ppm (5 lb/yd³ or 3 kg/m³) of chloride was mixed in the fresh concrete in half of the blocks. In the other blocks, approximately 3800 ppm (15 lb/yd³ or 9 kg/m³) of chloride was mixed into the concrete. Each concrete block contained a perforated mild steel sheet, 4 in x 15 in x 0.13 in (10 cm x 38 cm x 0.3 cm), which had a 40 percent opening to simulate the reinforcing steel surface area ratio in concrete. The ratio of the steel-to-concrete surface area (0.6) was used as it is typical for a reinforced concrete substructure. The concrete blocks were cured in a 100 percent humidity environment for 7 days and then cured in laboratory air for about 30 days. The type and number of concrete blocks used can be summarized as follows:

Test	No. of Concrete Blocks Used	
	Chloride, lb/yd ³	
	5	15
Environmental Tests	15	14
Anode Efficiency	-	14
Cyclic Polarization	-	14

$$1 \text{ lb/yd}^3 = 16.02 \text{ kg/m}^3$$

Environmental Test

Procedure

The anodes were either rolled into sheets or sprayed onto the blocks using thermal spray. The commercial alloy sheets were produced in the laboratory using pure metals, then rolled into thin sheets, 4 in x 15 in x 0.02 in (10.2 cm x 38.1 cm x 0.5 mm). The pure aluminum and pure zinc were purchased commercially and then arc-sprayed onto the concrete blocks using a Metco gun. The pseudo-zinc aluminum alloy (No. 15) was obtained by simultaneously feeding pure aluminum and zinc wires into the arc-spray gun and coating the concrete test block.

After the concrete cured, each anode sheet was embedded in mortar overlay, 0.75 in to 1 in (1.9 cm to 2.5 cm) thick, containing the same chloride concentration as the concrete block. The sprayed metal was not overlaid. A hole was drilled into the center of the top surface, which contained the anode, approximately 1 in (2.5 cm) deep using a 0.5-in- (1.3-cm-) diameter drill bit in order to place a pencil-type copper-copper sulfate reference electrode. This reference electrode enabled continuous measurement of anode and cathode potentials.

The 15 alloys were tested in concrete at various temperature and humidity conditions. The specimens were placed in a large environmental chamber, which was built for this project (figure 23). The anodes, steel plates, and reference electrodes were connected to electrical wires, which were brought to the outside of the environmental chamber and connected to a terminal board so that current and potential values could be monitored (figure 24). The amount of galvanic current for each specimen was measured every 120 min using a data logger that monitored the potential across a 10-ohm shunt located between the anode and cathode terminals.

A total of nine different temperature and humidity conditions were generated. The ambient temperature in the environmental chamber was set at 40°, 70°, or 90°F (4°, 21°, or 32°C), and the relative humidity at each temperature was controlled at 40, 70, and 90 percent. The specimens were exposed continuously to each environment for 10 days. At the end of the 10th day, depolarization tests were run on both the steel cathode and anode of each concrete specimen. A digital oscilloscope was used to measure “instant-off” potentials of the cathodes and anodes. Prior to conducting the depolarization tests, the magnitude of current between the anode and steel for each specimen was measured through the 10-ohm resistor. The depolarization potentials were monitored up to 4 h.



Figure 23. Concrete blocks in the environmental chamber.

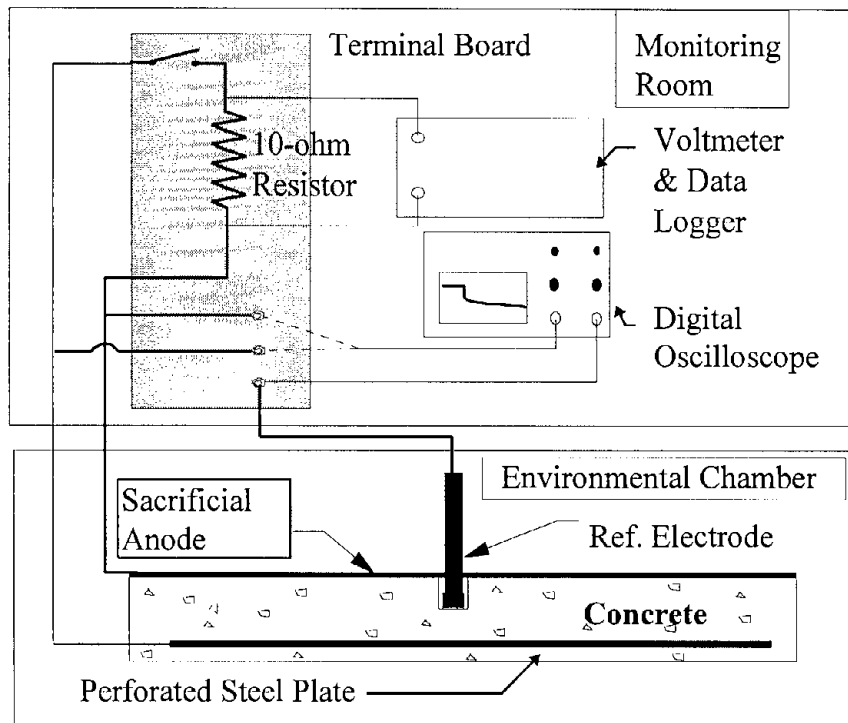


Figure 24. Schematic of test block wiring.

Results

The environmental test data are presented in figures 53 through 70 in the appendix. Figure 25 shows the interpretation of figures 50 through 70. These data are plotted graphically to allow a comparison between the alloys. The numbers in parentheses indicate the amount of depolarization that occurred on the anode and cathode. The top and bottom sides of the lower black rectangle show the “instant-off” and “static” potentials of the anode, respectively. The bottom and top sides of the top black rectangle show the “instant-off” and “static” potentials of the cathode. The space between the two rectangles is the driving voltage between the anode and cathode when they were electrically connected to each other.

Figures 53 through 70 in the appendix show the performance and the effectiveness of the cathodic protection for each of the alloys. It is interesting to note that sacrificial alloys that produced sufficient current density at the beginning of the testing period appeared to cause passivation of the steel plates and to reduce corrosion activity in chloride-contaminated concrete. This condition is shown by the noble static potentials of the steel plates at the end of the depolarization tests. As a result, small cathodic protection current densities were able to sufficiently polarize the steel in the later portions of the test period. Therefore, to evaluate the

performance of the alloys using cathode depolarization was difficult because the corrosion condition of the cathodes had changed from the initial conditions by the time of the final testing.

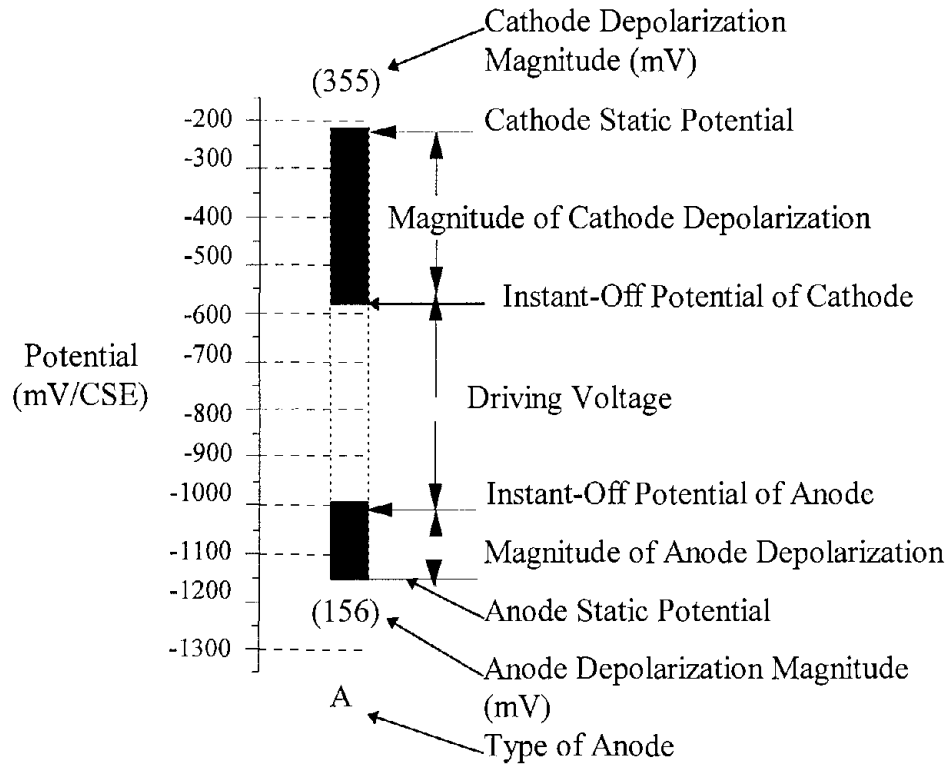


Figure 25. Key to potential and polarization diagrams, figures 50 through 70.

The results of the tests are summarized as follows:

1. 90°F (32°C) and 90 percent relative humidity (RH) environment (figures 53 and 54).

All aluminum-based anodes produced sufficient current density in concrete. The anodes in the higher chloride-containing concrete (3800 ppm - figure 54) generated considerably higher current densities because of the higher driving voltages than those in lower chloride-containing concrete (1300 ppm - figure 53). When the aluminum-based anodes embedded in the low chloride-containing concrete were connected to the steel plates, the alloys provided more polarization (larger positive instant-off potential) and more depolarization (larger negative static potential) than those in the high chloride-containing mixed concrete, except the Al-5Zn-3.5Mg alloy.

Zinc-based anodes behaved similarly to the aluminum alloys. However, the driving voltages were generally less than those of the aluminum-based anodes because of the lower open circuit potentials of the zinc-based anodes.

2. 90°F (32°C) and 70 percent RH environment (figures 55 and 56).

Significant changes occurred in the current densities of all the anodes compared with those tested at 90°F (32°C) and 90 percent RH. Generally, chloride levels did not significantly affect current densities from the anodes. The Al-5Zn, Al-10Zn, Al-10Mg, and Al-5Zn-0.1Sn alloys exhibited high driving voltages; however, the currents were considerably reduced. This might have been caused by the high circuit resistance of drier concrete. Some of the anodes had more noble potentials than those in 90 percent relative humidity. Pure zinc produced negligible current. The direction of galvanic current flow from pure aluminum, Al-1Mg, and Al-5Zn-3.5Mg in the high chloride-containing concrete reversed because of the high negative static potentials of the steel plates. Aluminum-based alloys embedded in the low chloride-containing concrete exhibited more polarization and depolarization than those in high chloride-containing concrete. All of the alloys in the high chloride-containing concrete appeared to produce insufficient cathodic protection current density to the steel.

3. 90°F (32°C) and 40 percent RH environment (figures 57 and 58).

This environment appears to be difficult for the anodes due to the high circuit resistance caused by drier concrete. The current densities produced by all the aluminum-based alloys were not adequate in the high chloride-containing concrete despite some anodes having relatively high driving voltages. All the steel plates in the low chloride-containing concrete exhibited passivity, resulting in large amounts of polarization at low current densities. Since the steel embedded in the high chloride-containing concrete exhibited various amounts of depolarization, it was difficult to evaluate anode performance with the steel depolarization test results. It appears that conventional aluminum alloy, Al-5Zn, Al-10Zn, and Al-5Zn-0.1Sn alloys performed better than the other alloys in this environment.

4. 70°F (21°C) and 90 percent RH environment (figures 59 and 60).

The results were similar to those in the 90°F (32°C) and 90 percent RH environment, except for the pure zinc, Zn-15Al, Zn-55Al, conventional and high-efficiency aluminum anodes, and Al-5Zn-3.5Mg alloys. In this environment, pure zinc and Al-5Zn, Al-10Zn, and Al-1Mg appeared to perform better than the other anodes in low and high chloride-containing concrete.

5. 70°F (21°C) and 70 percent RH environment (figures 61 and 62).

This moderate environment appears to be favorable to all the alloys, particularly the aluminum-based alloys embedded in low chloride-containing concrete. The static potentials of all the zinc-based anodes showed passivation. In general, higher current densities were produced by the anodes embedded in the concrete containing the high chloride concentrations.

6. 70°F (21°C) and 40 percent RH environment (figures 63 and 64).

The potentials of the steel plates embedded in low chloride-containing concrete displayed passivation [-100 to -250 mV (CSE)]. As a result, the depolarization on the steel plates was greater than 100 mV, with a current density as low as 0.05 mA/ft² (0.00045 mA/m²). The potentials of the aluminum-based alloys, except pure aluminum, were considerably more active than those of the zinc-based anodes.

7. 40°F (4°C) and 90 percent RH environment (figures 65 and 66).

The zinc, aluminum, and Zn-55Al anodes performed similarly in both the high and low chloride-containing concrete. Some of the aluminum-based anodes (i.e., high-efficiency aluminum anode, Al-5Zn, Al-10Zn, Al-10Mg, Al-5Zn-3.5Mg) had high negative static potentials in the concrete containing both the high and low chloride concentrations. However, when those anodes were connected to the steel plates, large amounts of anode polarization occurred.

8. 40°F (4°C) and 70 percent RH environment (figures 67 and 68).

The results were similar to those obtained in the 40°F (4°C) and 90 percent RH environment. Zinc-based anodes showed passivation, indicated by low negative potentials. With the aluminum-based anodes, except pure aluminum and the conventional aluminum alloy, the chloride concentration affected the polarization behavior.

9. 40°F (4°C) and 40 percent RH environment (figures 69 and 70).

The performance of the anodes embedded in high chloride-containing concrete varied considerably. In particular, the zinc-based anode performances were not consistent in this environment. The Al-5Zn, Al-10Zn, and Al-5Zn-0.1Sn maintained relatively high negative static potentials despite the chloride concentration in the concrete.

Summary

Both aluminum and zinc alloy anodes produced higher potentials and currents in the high-temperature (90°F/32°C), high-relative-humidity (90 percent) environment; however, the zinc-based alloys produced lower currents and lower voltages. The effect of humidity was to decrease current output and produce more noble alloy potentials. Some current reversals were even observed at the 70 percent RH level with some of the aluminum alloys. The current between the anodes and cathodes was particularly poor at the 40 percent RH condition. The behavior of the alloys at 70°F (21°C) was similar to that at 90°F (32°C) at corresponding relative humidity values. The aluminum alloys remained more active than the zinc alloys, even at the 40 percent RH condition. At the 40°F (4°C) condition, both the zinc and aluminum alloys performed similarly at 90 percent RH, but the aluminum alloys outperformed the zinc alloys at the lower relative humidity levels.

Anode Efficiency Tests

Procedure

Anode life is dependent not only on metal dissolution due to galvanic corrosion between the anode and the cathode, but also on corrosion of the anode itself in the concrete environment. The amount of metal available for useful cathodic protection determines the efficiency. The efficiency of each alloy was evaluated by measuring both the galvanic current and the self-corrosion current of the anode.

Self-corrosion current of the alloy at the concrete-anode interface was measured using the linear polarization resistance (LPR) technique. Concrete blocks were produced for these tests as were previously described (the pseudo-zinc-aluminum alloy was not tested). Each anode was embedded in concrete that contained approximately 3800 ppm (15 lb/yd³ or 9 kg/m³) of chloride. The concrete blocks were stored in a 100 percent humidity chamber at room temperature. A 10-ohm shunt was connected between the zinc and steel plates to measure the amount of galvanic current using a voltmeter (see figure 24). After the anode was disconnected from the steel, the potentials of the anode and the steel were monitored until the potentials became steady. Using a pencil-type copper-copper sulfate reference electrode that was fixed in the drilled hole and the steel plate as the counter electrode, the self-corrosion current of the anode was measured. The computerized potentiostat was used to measure IR-drop free potentials of the anode and steel. After the linear polarization resistance measurements were completed, the anode and steel plates were electrically connected until the next measurements were taken. A total of 19 measurements were made during the 46-day test period.

Results

The results of the self-corrosion and galvanic current measurements were plotted for each anode material and are shown in figures 71 through 84 in the appendix. Based on the amounts of both the self-corrosion and galvanic corrosion currents for each alloy, the efficiencies of the alloys were calculated and plotted. The results are summarized as follows:

Pure Zinc (figure 71)

The galvanic current reached approximately 2.5 mA in 2 days, then the magnitude of current gradually decreased with time, resulting in negligible amounts of galvanic current at the end of the test period. The magnitude of the self-corrosion current was considerably greater than that of the galvanic current during the test period. The efficiency of the anode was originally 28 percent and it decreased with time.

Conventional Zinc Anode (figure 72)

The behavior of galvanic current output with time was similar to that of the pure zinc. The magnitude of the self-corrosion current was considerably greater than that of the galvanic current

and it varied with time. The efficiency was initially approximately 30 percent and it decreased with time, reaching approximately 5 percent at the end of the test.

Zinc-5% Aluminum (figure 73)

The galvanic current output behaved similarly to that of pure zinc; however, the initial current was greater (approximately 7 mA). The magnitude of the self-corrosion current was significantly greater than that of the galvanic current during the test period. After the self-corrosion current reached approximately 17 mA after 12 days, the current rapidly decreased to as low as 2 mA. The efficiency of this material was relatively high (40 percent) initially, but dropped to approximately 10 percent.

Zinc-15% Aluminum (figure 74)

The galvanic current output varied up to 17 days of the test period; however, it became steady at approximately 1 mA. The self-corrosion current of this material varied during the 46-day test period, ranging from 15 mA to 4 mA. The efficiency was somewhat higher than that of the previous materials.

Zinc-55% Aluminum (figure 75)

The behavior of the galvanic current output with time was similar to that of the pure zinc. The self-corrosion current was considerably higher and varied with time, ranging from 25 mA to 2 mA. The efficiency also varied with time, ranging from 18 percent to 2 percent.

Pure Aluminum (figure 76)

The magnitude of the self-corrosion current was slightly higher than that of the galvanic current during the test period. The galvanic current output increased with time and reached a peak on the second day of testing. Then the current output gradually decreased with time. The efficiency of the pure aluminum ranged from 60 percent to 40 percent.

Conventional Aluminum Anode (figure 77)

The behavior of the galvanic current output with time was also similar to that of the pure zinc. However, the reduction of the current was gradual, and the magnitude of the current was approximately 2 mA at the end of the test. The self-corrosion current also decreased with time. The efficiency was relatively consistent and was approximately 30 percent to 40 percent during the test period.

High-Efficiency Aluminum Anode (figure 78)

Self-corrosion and galvanic corrosion were similar in this alloy. After they reached peaks at 7 days into the testing, they decreased with time. The reduction rate was more gradual with the

galvanic current than with the self-corrosion current. The efficiency varied with time early in the testing; however, it became steady at 30 percent to 40 percent after 20 days.

Aluminum-5% Zinc (figure 79)

The galvanic and self-corrosion currents gradually decreased with time. The efficiency varied with time, ranging from 20 percent to 60 percent.

Aluminum-10% Zinc (figure 80)

The amount of initial self-corrosion current was 30 mA, but rapidly decreased until 22 days into the testing. Thereafter, the self-corrosion current appeared to be steady at approximately 3 mA. The behavior of the galvanic current output with time was also similar to that of the pure zinc. The efficiency was initially as low as 20 percent; however, it gradually increased to 40 percent to 50 percent later in the testing.

Aluminum-1% Magnesium (figure 81)

The amount of galvanic current was greater than the self-corrosion current during the early half of the testing. The galvanic current gradually decreased with time; however, the reduction in the current was not significant. The efficiency of the anode was as high as 80 percent at the beginning of the testing; however, it decreased to about 30 to 40 percent.

Aluminum-10% Magnesium (figure 82)

Initial self-corrosion was 18 mA, but rapidly decreased until 8 days into the test. Thereafter, the self-corrosion current became steady at approximately 5 mA. The behavior of the galvanic current output with time was also similar to that of pure zinc. The efficiency was relatively consistent at around 20 percent during the test period.

Aluminum-5% Zinc-3.5% Magnesium (figure 83)

Initial self-corrosion was 20 mA, but it rapidly decreased until 8 days into the test. Thereafter, the self-corrosion current gradually decreased with time. The behavior of the galvanic current output with time was also similar to that of pure zinc. The efficiency varied with time, ranging between 18 to 40 percent.

Aluminum-5% Zinc-0.1% Tin (figure 84)

The amount of self-corrosion current consistently decreased with time. The behavior of the galvanic current output with time was also similar to that of pure zinc. The efficiency was relatively steady at approximately 20 percent during the test period.

Summary

It was noted that after a few days of exposure to the 100 percent relative humidity environment, the galvanic current from almost all anodes started to decrease with time and became relatively steady by the end of the 46-day test period. The cause of this behavior was investigated during this project and the results are discussed later in this report.

Atmospheric Corrosion

Procedure

Atmospheric corrosion of the air side of the anode, if it is not protected with a barrier coating, can reduce the life of the anode. The atmospheric corrosion loss for 14 alloys was measured using a 2.5-in x 4-in x 0.02-in (6.4-cm x 10.2-cm x 0.5-mm) rolled plate of the alloy. Each anode specimen was weighed prior to the exposure testing. The test panels were then exposed to a marine atmosphere about 300 ft (91 m) from the Atlantic Ocean in Sea Isle City, NJ, for approximately 4 months. Following the removal of the corrosion products on the panels with a stiff bristle brush, the panels were reweighed to determine the weight loss.

Results

Table 8 shows the results of the 4-month atmospheric exposure tests on the anode materials.

Table 8. Results of atmospheric exposure tests on the anode materials.

Anode Material	Initial weight (g)	Weight after exposure (g)	Weight loss (g)	Weight loss (%)
Pure zinc	25.1700	25.0939	0.0761	0.3
Conventional Zn anode	20.0700	20.0586	0.0114	0.6
Zn-5%Al	16.4800	16.4126	0.0695	0.4
Zn-15%Al	16.0147	15.9478	0.0669	0.4
Zn-55%Al	11.5582	10.5765	0.9817	8.5
Pure Al	5.2025	5.1381	0.0644	1.2
Conventional Al anode	8.6274	8.5777	0.0497	0.6
High-Efficiency Al anode	7.8375	7.7755	0.0620	0.8
Al-5%Zn	7.9296	7.8740	0.0556	0.7
Al-10%Zn	8.6020	8.5598	0.0422	0.5
Al-1%Mg	8.7108	8.6400	0.0708	0.8
A-10%Mg	21.9009	21.9084	0.0075	0.03
Al-5%Zn-3.5%Mg	7.8230	7.7601	0.0629	0.8
Al-5%Zn-0.1%Sn	7.5753	7.5219	0.0534	0.7

Summary

All of the alloys exhibited some corrosion during the test period, but none exhibited excessive corrosion loss. The weight losses of all materials except Zn-55Al are negligible and are corrosion-resistant to the marine atmosphere.

Anode Capacity Tests

Procedure

Anode capacity is the number of ampere-hours per unit weight of metal expected from a sacrificial alloy. Each of the 14 alloys (see table 8) were tested to measure anode capacity using an impressed current of 1 mA/cm² of anode surface. The test set-up is described in figure 26 and is similar to ASTM G97 (“Test Method for Laboratory Evaluation of Magnesium Sacrificial Anode Test Specimens for Underground Applications”) used to measure the anode capacity of magnesium alloys for underground use. A simulated concrete porewater solution with chloride (3.2 wt. % KCl + 2.45 wt. % NaOH + 0.1 wt. % Ca(OH)₂) was used for the test solution. After the exposure time, the anode materials were removed from the solution. The anodes were washed with fresh water and a stiff bristle brush and then reweighed to determine the weight loss. The anode capacity of each anode material was calculated by the following equation:

$$\text{Anode capacity (A-h/kg)} = \text{Total current (A-h)} / \text{Weight loss (kg)}$$

Results

When the anode specimens were immersed in simulated concrete pore solution, chemical reactions occurred immediately and dissolved the specimens at rapid rates. It is believed that this rapid chemical reaction between the specimen and the solution was caused by the metallurgical characteristics of the rolled-sheet anodes. The sheets were in the as-rolled condition; therefore, the grain structure was in a highly distorted and segregated condition. As a result, excessive weight losses occurred due to the self-corrosion of the anodes, which would not be indicative of a thermally sprayed material. Therefore, the data are not presented in this report.

Cyclic Polarization Tests

Procedure

In order to test the pitting and passivation tendencies of the alloys, cyclic polarization was used. In this test, the alloy is immersed in an electrolyte and anodically polarized to a point beyond the transpassive region, then the scan is reversed until the original potential is reached. The curves are analyzed for the characteristics of the reverse scan and hysteresis effects. The general technique is described in ASTM G61 (“Test Method for Conducting Cyclic Potentiodynamic Polarization Measurements for Localized Corrosion Susceptibility of Iron-, Nickel-, or Cobalt-Based Alloys”).

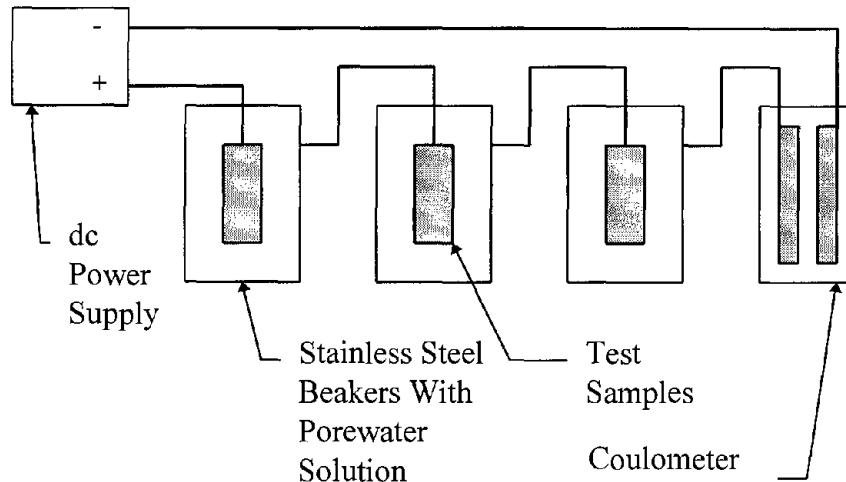


Figure 26. Anode capacity test set-up.

Concrete blocks containing a steel cathode similar to those previously described were made. Six alloy samples, 2 in x 3 in x 0.02 in (5.1 cm x 7.7 cm x 0.5 mm), were embedded in a mortar overlay, 0.75 in to 1 in (1.91 cm to 2.54 cm) thick, containing 3800 ppm of chloride. Three of the six anode samples were electrically connected to a steel cathode embedded in the concrete, and the other three anodes were isolated. The purpose of casting multiple samples of each alloy was that the test procedure would induce pitting on the sample tested and thus prevent its use in future tests, so a fresh sample was used each time a new test was conducted. The concrete blocks were stored in a 100 percent humidity chamber for 46 days.

Using a computerized potentiostat, cyclic polarization measurements were conducted on each of the six anode samples at the following times:

- Prior to exposure in the 100 percent humidity chamber.
- At the point of maximum galvanic current from the alloy in the anode efficiency tests.
- After reduction of galvanic current from the alloy in the anode efficiency tests (near the end of the tests).

Results

Figures 85 through 112 show the cyclic polarization curves obtained in this test. The cyclic polarization curves obtained from the alloy specimens that were never connected to the steel cathode provided the information on the corrosion behavior of the alloy in the chloride-contaminated concrete environment. The curve obtained from an anode that had been connected to the steel cathode prior to the polarization test provides information on the corrosion behavior of the alloy coupled with steel (cathode). The cyclic polarization curves were compared to the self-corrosion and galvanic corrosion data obtained in the efficiency tests.

Pure Zinc

Figure 85 shows the cyclic polarization curves before connecting the alloy to the cathode, and figure 86 shows the polarization curves after connecting the anode alloy to the cathode. When the sample was not connected to a cathode, the zinc showed uniform corrosion at both the higher and lower corrosion currents. However, the zinc showed passive behavior during both the low- and high-current periods when the steel was electrically connected.

Conventional Zinc Anode

Figures 87 and 88 show the results of this test. When the sample was not connected to a cathode, the conventional zinc alloy showed uniform corrosion at both the higher and lower corrosion currents. The alloy showed passive behavior during both the low- and high-current periods when the steel cathode was electrically connected.

Zinc-5% Aluminum

Figures 89 and 90 show the results of this test. For the sample not connected to a cathode, the zinc-5% aluminum alloy showed uniform corrosion at both the higher and lower corrosion currents. The alloy showed passive behavior during both the low- and high-current periods.

Zinc-15% Aluminum

Figures 91 and 92 show the results of this test. For the sample not connected to a cathode, the zinc-15% aluminum alloy showed passivity at more noble potentials and uniform behavior at more active potentials. The alloy showed passive behavior during both the low- and high-current periods.

Zinc-55% Aluminum

For the sample not connected to a cathode, the alloy showed uniform corrosion at both the higher and lower corrosion currents. The alloy showed passive behavior during both the low- and high-current periods. Figures 93 and 94 show the results of this test.

Pure Aluminum

Figures 95 and 96 show the results of this test. For the sample not connected to a cathode, the alloy showed passive behavior at both active and noble potentials. The alloy showed passive behavior during both the low- and high-current periods.

Conventional Aluminum Anode

For the sample not connected to a cathode, the conventional aluminum anode alloy showed uniform corrosion at both the higher and lower corrosion currents. The alloy showed passive

behavior during both the low- and high-current periods. Figures 97 and 98 show the results of this test.

High-Efficiency Aluminum Anode

For the sample not connected to a cathode, the high-efficiency aluminum alloy showed uniform corrosion at both the higher and lower corrosion currents. The alloy showed passive behavior during the high-current period and showed pitting behavior at the low-current period. Figures 99 and 100 show the results of this test.

Aluminum-5% Zinc

Figures 101 and 102 show the results of this test. For the sample not connected to a cathode, the alloy showed uniform corrosion at the higher corrosion current and passive behavior at the lower corrosion current. The alloy connected to the cathode showed pitting behavior during the high-current period and passive behavior during the low-current period.

Aluminum-10% Zinc

Figures 103 and 104 show the results of this test. For the sample not connected to a cathode, the alloy showed uniform corrosion at both the higher and lower corrosion currents. The alloy connected to the cathode showed pitting tendencies during the high-current period and passive behavior during the low-current period.

Aluminum-1% Magnesium

For the sample not connected to a cathode, the alloy showed uniform corrosion at both the higher and lower corrosion currents. The alloy connected to the cathode showed passive tendencies during both high- and low-current periods. Figures 105 and 106 show the results of this test.

Aluminum-10% Magnesium

For the sample not connected to a cathode, the aluminum-10% magnesium alloy showed uniform corrosion at both the higher and lower corrosion currents. The alloy connected to the cathode showed passive tendencies during the high-current period and uniform behavior during the low-current period. Figures 107 and 108 show the results of this test.

Aluminum-5% Zinc-3.5% Magnesium

Figures 109 and 110 show the results of this test. For the sample not connected to a cathode, the alloy showed passive tendencies at both the higher and lower corrosion currents. The anode connected to the cathode showed passive tendencies during both high- and low-current periods.

Aluminum-5% Zinc-0.1% Tin

Figures 111 and 112 show the results of this test. For the sample not connected to a cathode, the alloy showed uniform corrosion at both the higher and lower corrosion currents. The anode connected to the cathode showed passive tendencies during both high- and low-current periods.

Summary

The cyclic polarization studies indicate that all the alloys except Al-5Zn, Al-10Zn, and Al-10Mg were in the passive condition when electrically connected to a steel cathode. The reduction in galvanic current output from those anodes appeared to be caused by shifting the passive region of the anodic curves in the direction of lower current density. The shift in the anode polarization curves may be caused by corrosion products. After the tests were completed, the pH at the anode-to-concrete interface was measured on several specimens, including pure zinc, Zn-15Al, pure aluminum, and Al-1Mg. The pH ranged from 8 to 10.5.

Al-5Zn and Al-10Zn appeared to initially corrode by pitting when connected to the steel cathodes. However, the pitting tendency in the passive films disappeared later. Consequently, the galvanic current outputs appeared to decrease with time.

The Al-10Mg displayed unique behavior. Passivation was indicated when the steel cathode was connected to the anode. However, the passive behavior later disappeared in the polarization curve, and the anode appeared to corrode uniformly.

Effect of pH on Alloy Behavior

Procedure

Since low pH was suspected of causing the passivation of the zinc anode on the bridge members examined, as described in chapter 2, laboratory tests were devised to examine this phenomenon. A total of 14 galvanic cells, each consisting of an anode alloy and a steel cathode, were prepared. The anode samples were 3 in x 4 in x 0.02 in (7.6 cm x 10.2 cm x 0.5 mm). The steel cathodes were 6 in x 4 in x 0.02 in (15.3 cm x 10.2 cm x 0.5 mm). The anodes and steel plates were held to a fixed separation of 4 in (10.2 cm) using a fiberglass spacer. Each anode was connected to the corresponding steel cathode through a 10-ohm shunt. The galvanic cells were then immersed in a simulated concrete pore solution (pH = 13.2). The solution was slowly purged with carbon dioxide gas to reduce the pH of the solution. During the purging process, the "instant-off" potential of the anode and the amount of current flowing through the shunt were measured while recording the pH of the solution. A schematic of the test set-up is shown in figure 27.

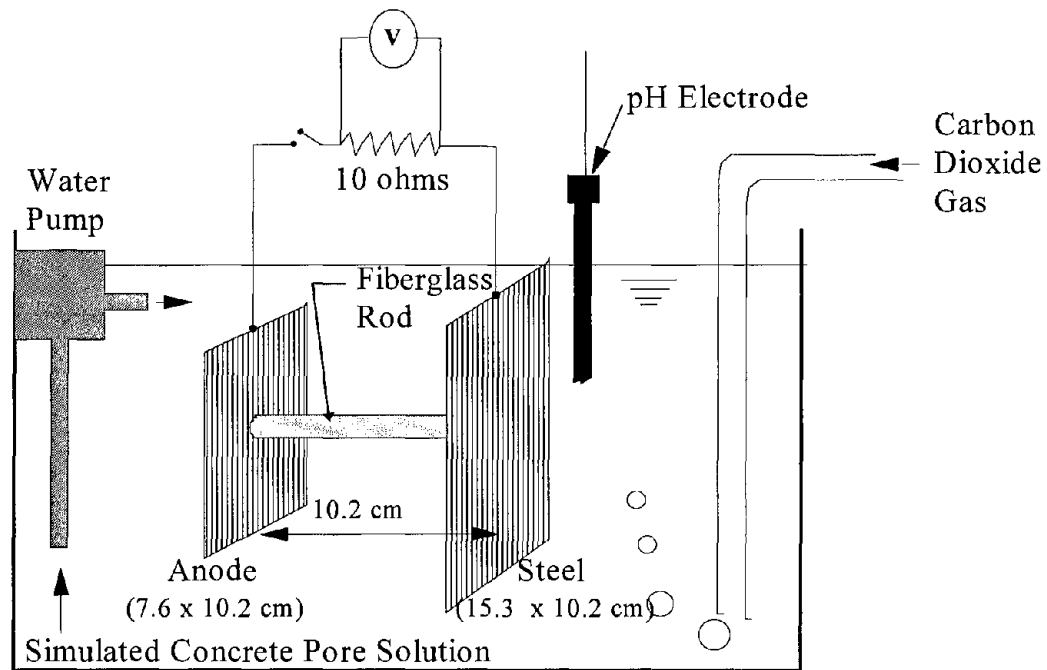


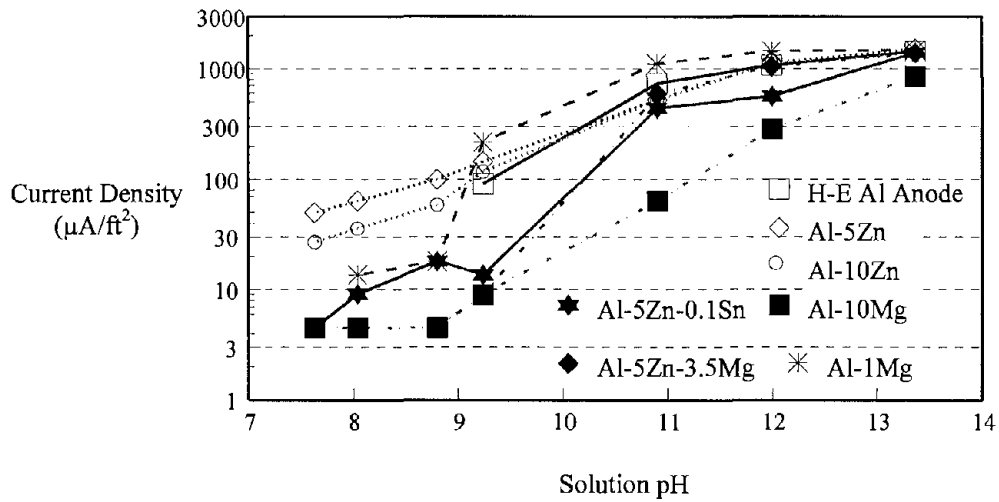
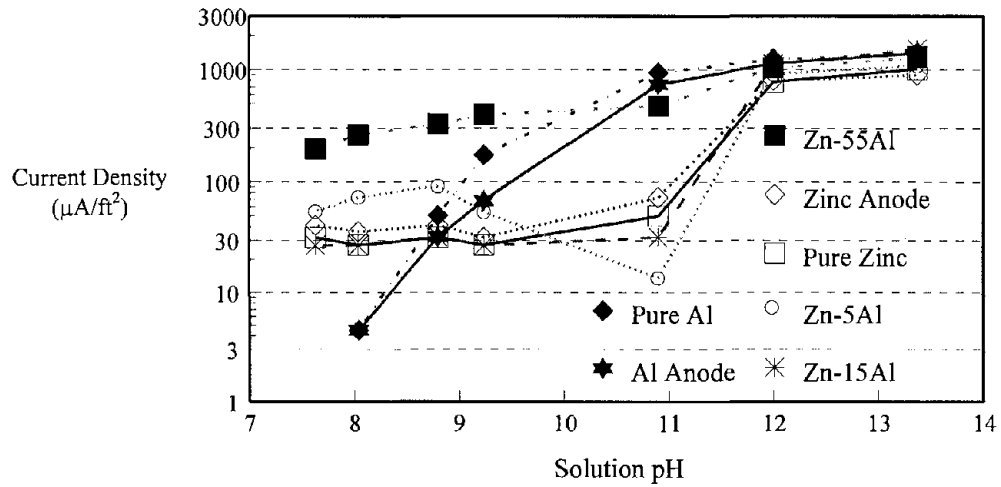
Figure 27. Test set-up for pH tests.

Results

Figure 28 shows the current densities between the anodes and steel plates while decreasing solution pH. The amount of current on all the anodes, except the Zn-55Al anode, was considerably reduced below a pH of 12.

Figure 29 shows the relationship between the “instant-off” potentials of the anodes and the pH of the solution. The potentials of all the anodes, except the Zn-55Al anode, were rapidly shifted to a more positive (noble) direction below a pH of 12.

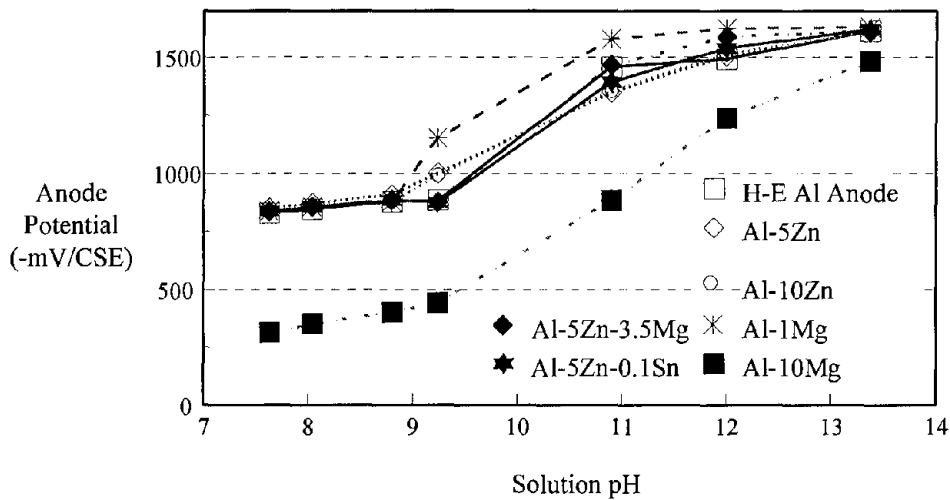
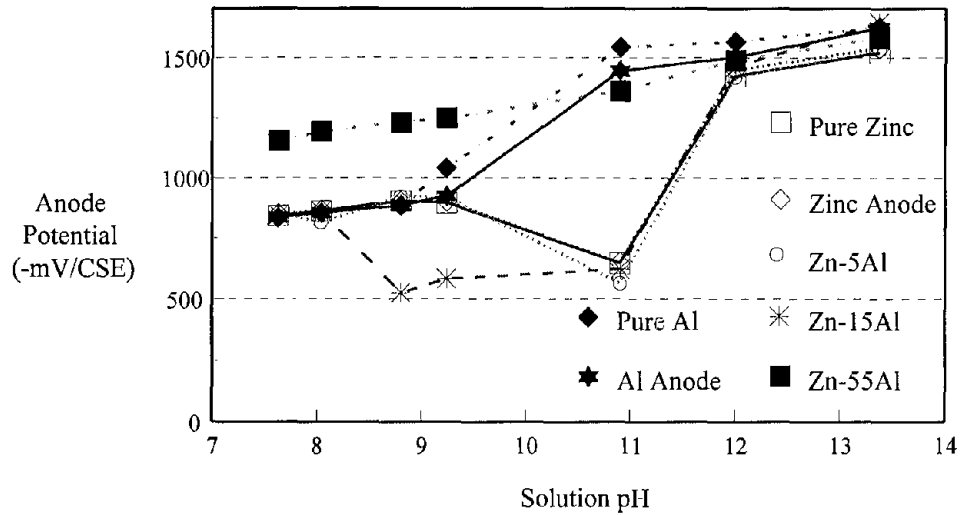
The electrochemical behavior of the anodes in various pH environments was consistent with the galvanic current outputs observed during the efficiency testing.



$$1 \mu\text{A}/\text{ft}^2 = 1 \mu\text{A}/\text{m}^2$$

H-E Al = High-Efficiency Aluminum Alloy

Figure 28. Anode-to-cathode current densities with decreasing pH.



H-E Al = High-Efficiency Aluminum Alloy

Figure 29. Instant-off potentials of anodes vs. solution pH.

Conclusions on Study of Existing Alloys

1. Both aluminum alloys and zinc alloys produce sufficient galvanic current under higher ambient temperature and humidity conditions; however, both temperature and particularly

humidity play a key role in the amount of current produced and the driving potentials of the alloys.

2. The zinc alloys and most of the aluminum alloys were ineffective in producing sufficient current to protect steel embedded in the concrete at low temperatures and low relative humidity conditions.
3. The exception was the zinc-55% aluminum alloy, which also shifted to more noble potentials, but the potentials were more active than the other alloys. The current output of this alloy also remained higher than the other alloys at a low pH. The performance of this alloy suggested that further work was needed on the aluminum-zinc alloy system. This work is discussed in chapter 4.
4. The pH of the concrete environment plays a critical role in the current output and driving potential of the alloys tested. As the pH drops below 12, the current decreases and the potential becomes more noble (closer to that of steel).
5. The cyclic polarization studies indicate that all the alloys, except Al-5Zn, Al-10Zn, and Al-10Mg, were in the passive condition when electrically connected to a steel cathode. The reduction in galvanic current output from those anodes appeared to be caused by shifting the passive region of the anodic curves in the direction of lower current density. The shift in the anode polarization curves may be caused by corrosion products.
6. All of the alloys exhibited some atmospheric corrosion during the test period, but none exhibited excessive corrosion loss. The weight losses of all materials, except Zn-55Al, are negligible and are considered corrosion-resistant to the marine atmosphere.

CHAPTER 4

DEVELOPMENT OF NEW ANODE ALLOYS

The existing pure and binary aluminum and zinc alloys and tertiary aluminum-zinc alloys evaluated in chapter 3 in simulated porewater and concrete environments exhibited passivation as the pH of the simulated concrete porewater solution decreased. However, several did show a lesser tendency toward passivation and these might be useful as sacrificial alloys to protect embedded steel in concrete. Alloys consisting of aluminum and zinc with a third alloying element to inhibit passivation were tested to overcome the observed deficiencies in existing alloys. Both Sumitomo Metal Mining Company and Drexel University participated as subcontractors in the development of new alloys. The objective of this task was to screen a large number of compositions to find one that provided the best current and potential characteristics under conditions of low pH. Following the screening tests, detailed testing of the alloy(s) applied to concrete samples was conducted.

One of the major goals in developing new alloys for sacrificial anodes was that alloys need to perform relatively well in lower pH (<12) electrolytes. The use of carbon dioxide to purge simulated porewater was found to be effective in identifying the effect of pH on reducing the galvanic current from sacrificial alloys tested in chapter 3. This test was used to screen the new alloys.

Phase I. Screening Tests

Binary Aluminum-Zinc Alloy Tests

Aluminum-zinc was selected as the major alloy group for further development because of its better overall performance compared to the other alloys tested as discussed in chapter 3. In order to evaluate aluminum-zinc alloy performance at various zinc contents, nine binary alloys were produced by adding zinc from 10 to 90 percent in increments of 10 percent. Cylindrical specimens (2 cm in diameter x 15 cm long) were cast for each alloy. Pure zinc and pure aluminum were also tested at the same time as controls. Anodic potentiodynamic polarization, corrosion and instant-off potentials, electrical capacities, and weight loss were measured in order to evaluate the effect of zinc.

The potentiodynamic polarization curves were constructed in a simulated concrete pore solution. In this test, the potential of the alloy under test is adjusted by a computer-controlled potentiostat and the resulting curve of potential vs. applied current is plotted. Two samples of each alloy were tested. For aluminum-zinc alloys containing 80 percent zinc or more, the anodic polarization curves indicated strong passivation behavior with low current density when the alloys polarized approximately -1100 mV to a silver-silver chloride (SSC) reference electrode. The current density decreased with increasing zinc content, and the passivation tendency appeared to increase. In particular, alloys containing less than 40 percent zinc indicated higher current densities (approx. 10 to 20 $\mu\text{A}/\text{cm}^2$) in the range between -900 mV and -700 mV vs. an

SSC reference electrode, which are expected to be near or in the operating potential range of the anode when it is connected to a steel cathode.

The electrical capacity of aluminum-zinc alloys with various zinc contents was measured using the test technique previously described in chapter 2. Figure 30 shows the results of the electrical capacity tests for the aluminum-zinc alloys. The capacities of the alloys containing 10 to 50 percent zinc were approximately 500 A-h/kg and appeared to increase with increasing zinc content. Figure 31 shows the static potential of the alloy with different zinc contents measured with the alloy immersed in simulated concrete porewater. These potentials were obtained prior to the capacity tests, and two samples were tested for each composition. The potentials of the alloys containing 0 to 30 percent zinc were approximately -1500 mV vs. an SSC reference electrode. The potentials shifted to -1600 to -1700 mV vs. SSC with 40 to 70 percent zinc content. The potentials of the alloys containing more than 70 percent zinc were approximately -1500 mV vs. SSC. However, the static potentials measured after the capacity tests varied significantly with zinc content, as shown in figure 32. The static potentials of the two alloys containing 50 and 60 percent zinc were not similar. The potentials of the alloy containing 80 percent zinc and pure zinc were positive with respect to the reference electrode (see figure 32).

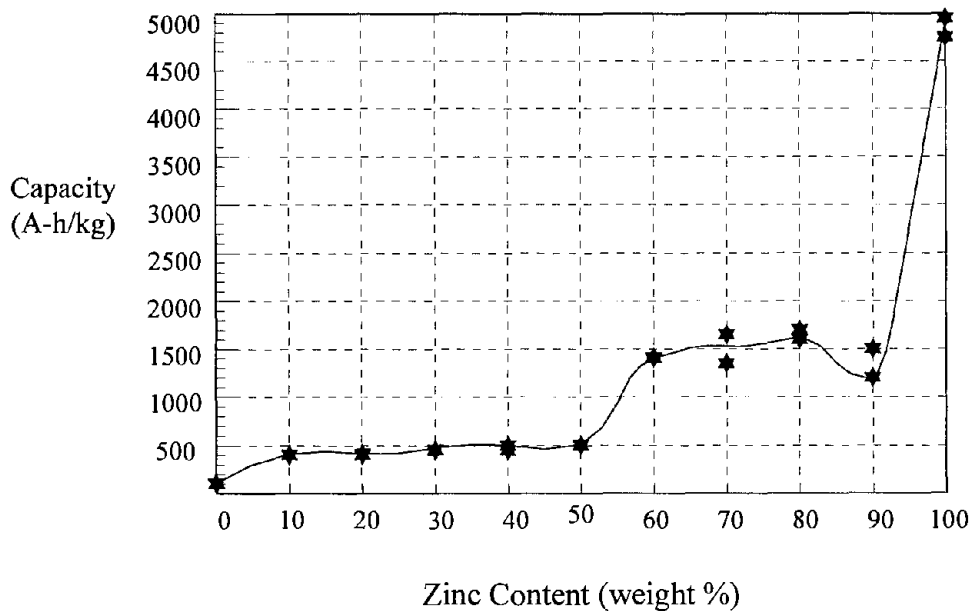


Figure 30. Anode capacity vs. zinc content of aluminum alloy.

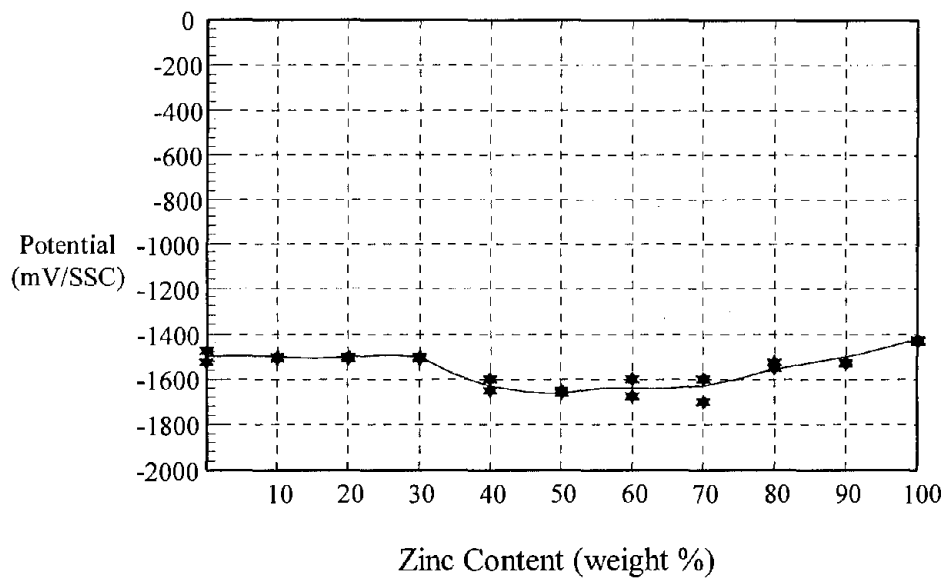


Figure 31. Static potential vs. zinc content of aluminum alloy, before capacity tests.

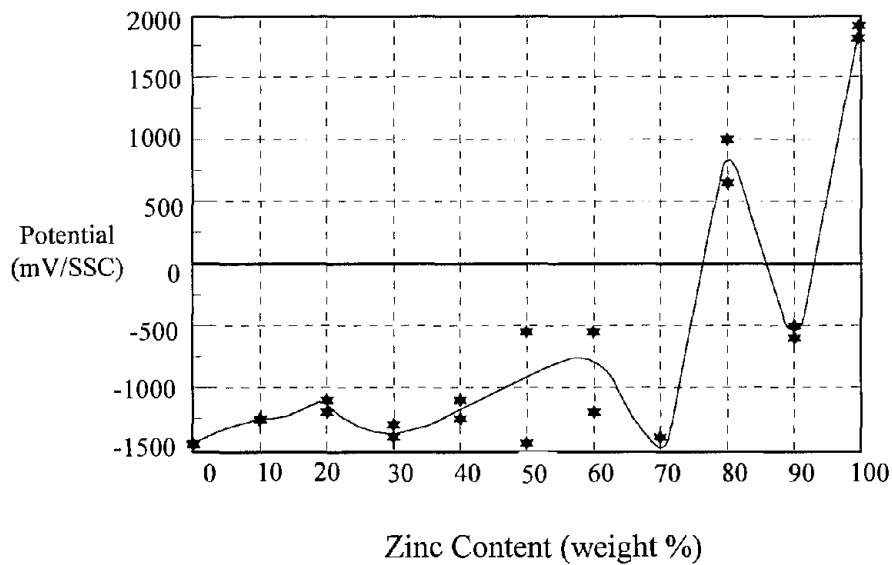


Figure 32. Static potential vs. zinc content of aluminum alloy, after capacity tests.

Figure 33 shows the results of weight loss testing for the alloys after immersion in simulated concrete porewater solution for 10 days at 25°C. Figure 33 also shows the weight losses of the

specimens used for the capacity tests. The weight losses measured in the immersion tests resulted from self-corrosion, and the weight losses that occurred during the capacity tests were caused by both self-corrosion and the impressed current. The trends in weight loss with respect to zinc content caused by both immersion testing and capacity tests were similar to each other, although the weight loss caused by the capacity test was larger as might be expected. Pure aluminum had the largest weight loss (1.5 g/cm^2 and 2 g/cm^2) caused by self-corrosion and impressed current, respectively. The weight loss of the aluminum alloy containing 10 percent zinc was approximately 0.5 g/cm^2 . The weight loss of the alloys decreased with increasing zinc content.

Summary of Binary Alloy Tests

Zinc contents above 60 percent will yield higher current capacity; however, the tests suggest that a high zinc content could result in the type of passive behavior observed in the laboratory and in the field. The zinc should be held to less than about 70 percent. The potentials of the alloys with 50 and 60 percent zinc indicated some instability. Therefore, further testing was carried out with the zinc content held to below 50 percent.

Tertiary Alloy Tests

Various amounts of indium, ranging from 0.05 to 0.57 percent, were added to the aluminum-zinc alloys to determine if this element could inhibit passivation in lower pH (<12) concrete pore solutions. The optimum amounts of indium were based on the results obtained by potentiodynamic polarization, potential, and electrical capacity measurements in simulated concrete pore solution. Further tests evaluated the electrochemical performance of the alloys in simulated concrete pore solutions at various pH levels by purging the solution with carbon dioxide, as described in chapter 3. As in the binary alloy tests, the specimens were cast into cylindrical shapes for testing. Table 9 shows the detailed composition of the alloys. In addition to the indium, the electrochemical effect of titanium and zirconium in Al-55Zn alloys was also evaluated. Al-55Zn-0.04Ti, Al-55Zn-0.08Ti, Al-55Zn-0.04Zr, and Al-55Zn-0.08Zr alloys were prepared to test in various pH simulated concrete pore solutions.

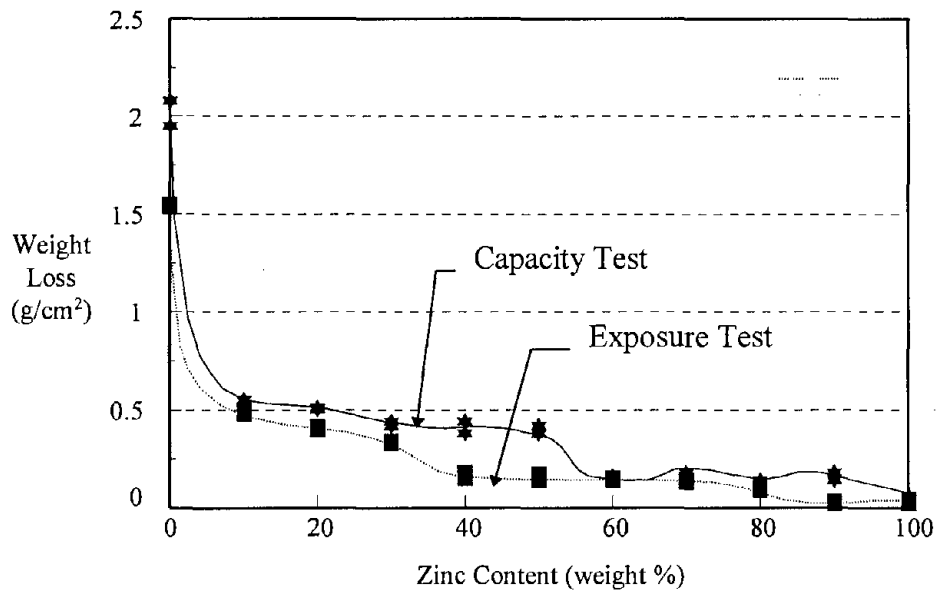


Figure 33. Weight loss vs. zinc content.

Table 9. Compositions of aluminum-zinc-indium alloys tested.

Sample No.	Nominal Alloy Composition (weight percent)		
	Aluminum	Zinc	Indium
1	Bal.	10	0.05
2	Bal.	10	0.10
3	Bal.	10	0.20
4	Bal.	10	0.50
5	Bal.	20	0.05
6	Bal.	20	0.10
7	Bal.	20	0.20
8	Bal.	20	0.50
9	Bal.	30	0.05
10	Bal.	30	0.10
11	Bal.	30	0.25
12	Bal.	30	0.50
13	Bal.	50	0.05
14	Bal.	50	0.10
15	Bal.	50	0.25
16	Bal.	50	0.50

Anodic polarization curves were obtained for the aluminum-zinc-indium alloys listed in table 9 in simulated concrete porewater solution (see figures 114 to 119). The Al-10Zn alloy containing 0.05 percent indium displayed passivation in the range of -1400 to -900 mV to an SSC reference electrode (figure 116). However, when the indium content increased to 0.1 percent or greater, the passive behavior became less noticeable in that potential range.

Similar behavior was observed in the polarization curves for Al-20Zn with indium (figure 117). Increasing the indium content of the Al-20Zn alloy caused the polarization current density to increase in the potential range between -1400 mV and -900 mV SSC. For potentials more noble than -900 mV SSC, the effect of the indium content became less noticeable.

With the Al-30Zn alloy, the effect of increasing the indium content is to cause the polarization current density to increase in the potential range between -1400 mV and -1100 mV SSC (figure 118). For potentials more positive than -1100 mV SSC, the effect of the indium content became less noticeable.

The polarization current density for Al-50Zn with various indium contents is relatively high compared to the previous alloys (figure 119). The effect of the indium content, however, was not significant with regard to the current density.

Figure 34 shows the results of the electrical capacities of the Al-10Zn, Al-20Zn, Al-30Zn, and Al-50Zn alloys with various indium contents. The capacities of the alloys containing indium were more than 1500 A-h/kg, and were considerably higher than those without indium (approx. 500 A-h/kg). For Al-10Zn and Al-20Zn, the capacity of the alloys appeared to increase with increasing indium content. For the Al-30Zn alloy, the higher indium contents do not appear to influence the capacity, which was relatively consistent at approximately 1600 A-h/kg. The capacity of the Al-50Zn alloy increased up to 0.1 percent indium; however, the capacity decreased when the indium content was increased more than 0.1 percent.

Figure 35 shows the static potentials measured after the capacity tests of those alloys with various indium contents. For the Al-10Zn and Al-20Zn alloys, the potentials shifted more negative with increasing indium content up to 0.1 percent. The potentials were relatively constant at approximately -1600 mV SSC when the indium content was more than 0.1 percent. For the Al-30Zn, indium contents up to 0.25 percent did not appear to influence the potential. When indium was added to more than 0.3 percent to Al-30Zn, the potential shifted to more positive values. For the Al-50Zn alloy, the potentials appeared to be independent of the indium content. The potentials were largely scattered from -1600 mV to -1300 mV SSC.

Figures 36 and 37 show the current outputs and the “instant-off” potentials of the Al-10Zn alloy with various indium contents in various pH solutions, respectively. By increasing the indium content from 0.05 to 0.34 percent, the amount of current increased, and the potential tended to shift in a more negative direction in the pH range between 10 and 13. However, the effect of the indium content was negligible on the current and potential in the pH range between 8 and 10.

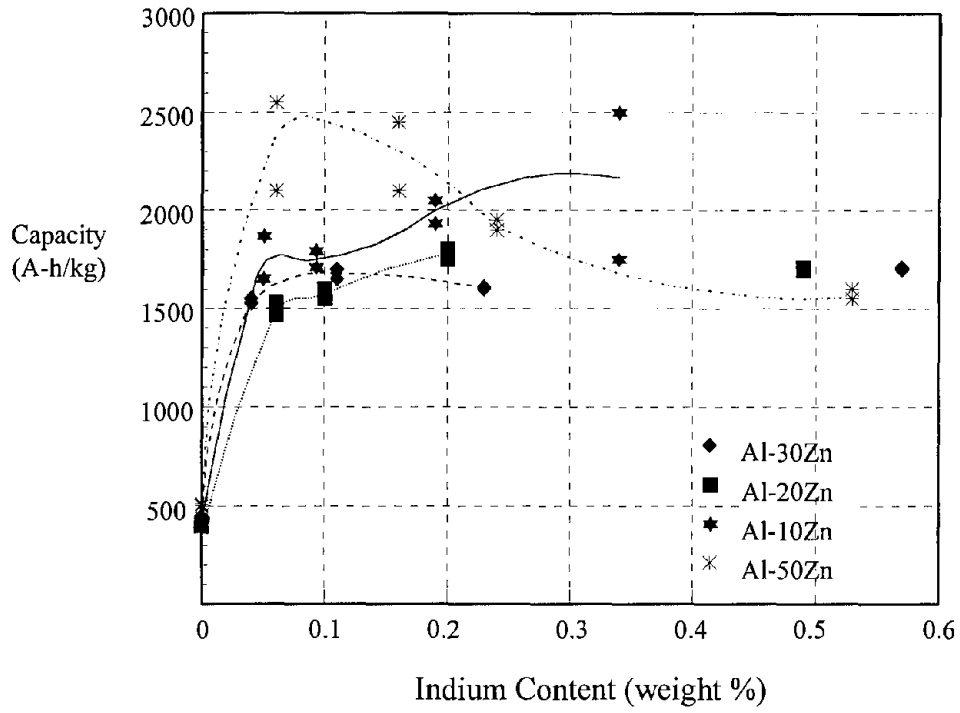


Figure 34. Current capacity vs. indium content.

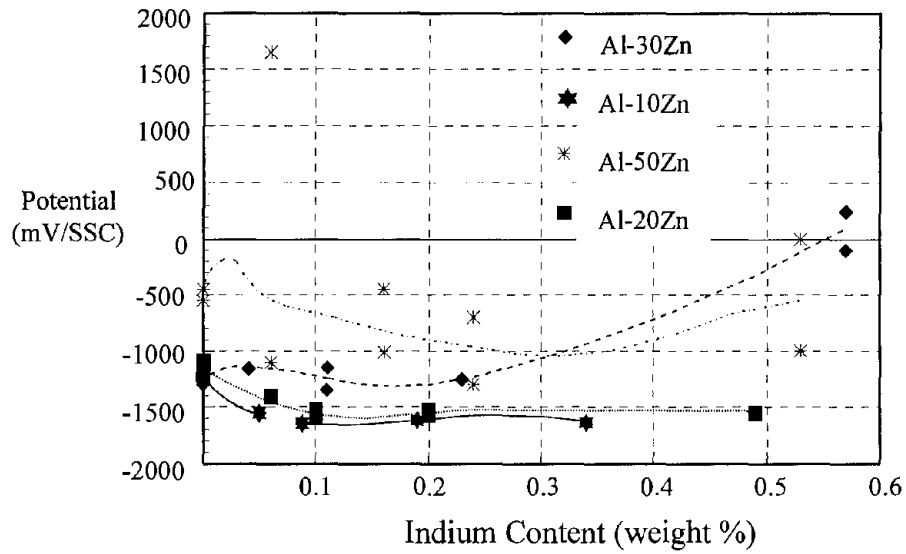


Figure 35. Static potentials after capacity tests vs. indium content.

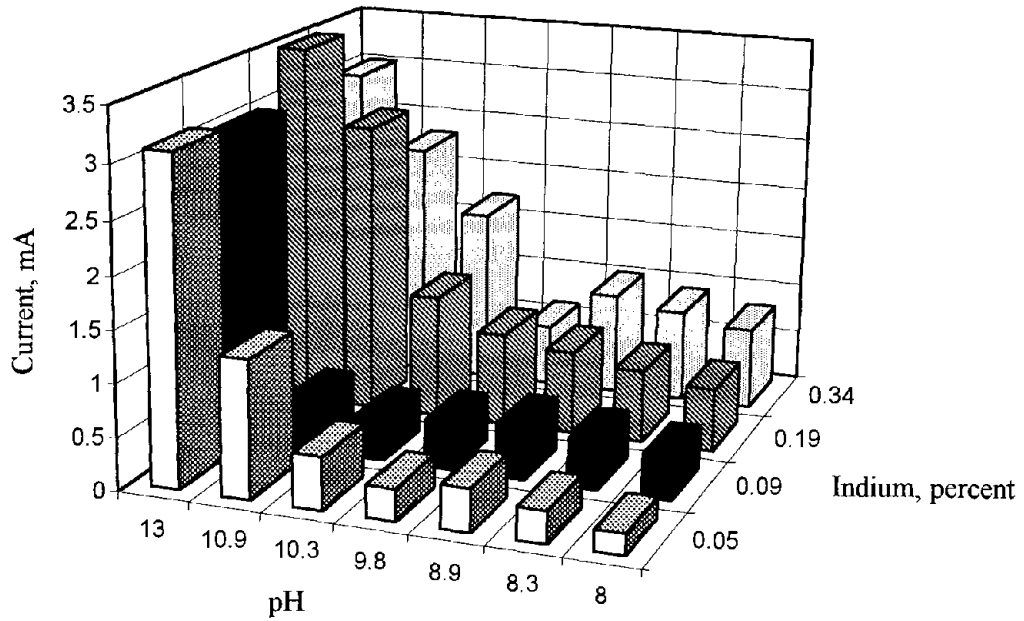


Figure 36. Current output vs. indium content for Al-10Zn alloy.

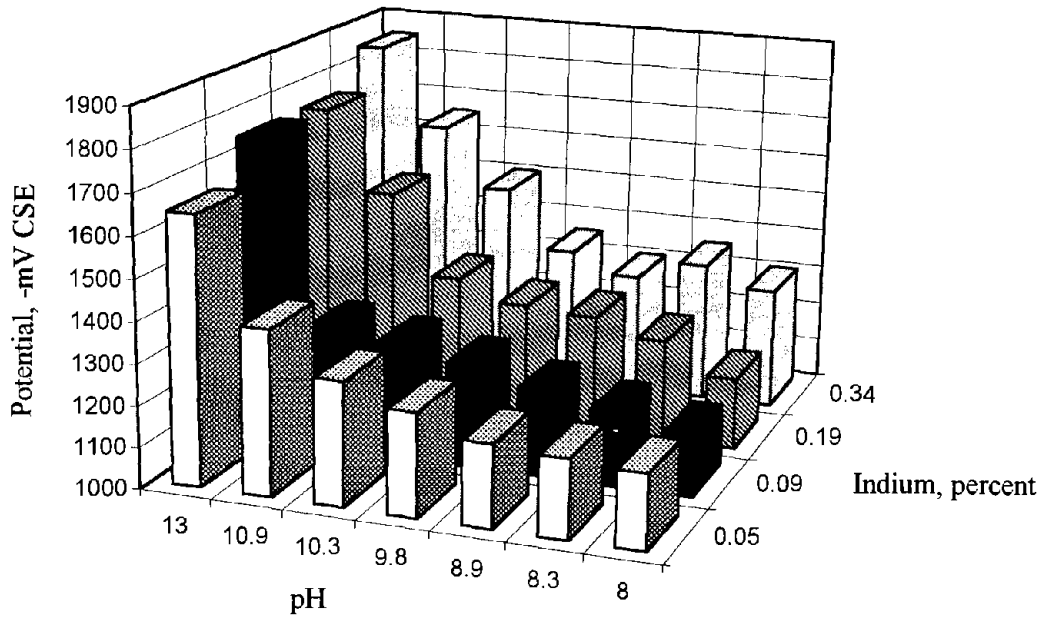


Figure 37. Instant-off potentials vs. indium content for Al-10Zn alloy.

Figures 38 and 39 show the current outputs and “instant-off” potentials of the Al-20Zn alloy with various indium contents in the porewater solutions. In the pH range between 13 and 10.3, the amount of current increased with increasing indium content. However, there was also no effect on the current output below a pH of 10.3. An indium content greater than 0.06 percent in Al-20Zn appeared to have less effect on the potential in the pH range between 8 and 13. With increasing indium content, the potentials shifted slightly in a more negative direction above a pH of 10.3; however, there was no potential shift below a pH of 10.3.

Figures 40 and 41 show the current outputs and the “instant-off” potentials for the Al-30Zn alloy with various indium contents in the various solutions. The trends of the current output and the potential with respect to solution pH were similar to those of the Zn-20Al alloy with indium. In the pH range between 10.3 and 13, the amount of current increased with increasing indium content. However, there was no effect on the current output below a pH of 10.3. An indium content greater than 0.06 percent in Al-30Zn had less effect on the potential in the pH range between 8 and 13. Increasing the indium content from 0.04 to 0.57 percent caused the potentials to shift slightly in a more negative direction above a pH of 10.3; however, there was no potential shift below a pH of 10.3.

Figures 42 and 43 show the current outputs and the “instant-off” potentials of the Zn-55Al alloys with various titanium or zirconium contents in the porewater solutions. By comparing the potentials and the current outputs of the Zn-55Al without titanium or zirconium, it appears that titanium and zirconium did not improve the performance of the alloys in the lower pH (< 12) concrete pore solutions.

Alloys containing 0.2 percent indium and 10, 20, or 30 percent zinc were selected for further testing. To confirm the suitability of the selected alloys, the three alloys, along with pure zinc and pure aluminum, were immersed in a simulated concrete pore solution and the pH was adjusted with carbon dioxide. The “instant-off” potentials and galvanic current were measured at various pH levels. The results are shown in figures 44 and 45. The potential of the zinc rapidly shifted to a more positive direction below a pH of 12, as expected from previous tests. The potentials of all three alloys showed gradual shifts in a more positive direction with decreasing pH. The amount of the zinc galvanic current was significantly reduced below a pH of 12 and reduced to approximately 1/40 of the original current. On the other hand, the reduction of the current in the three new alloys was only approximately 1/5 of the original current below a pH of 12.

Summary of Tertiary Alloy Tests

The work in this phase tested aluminum-zinc alloys containing a tertiary phase. Indium, titanium, and zirconium were selected for the tertiary phase on the basis of previous use of these alloying elements in sacrificial anode alloys. The tests showed that aluminum-zinc-indium alloys produced the best combination of steady current and high potentials, even in lower pH simulated concrete porewater solutions. It was decided to select three of these alloys for further evaluation as thermally sprayed coatings on concrete.

Phase II. Tests With Sprayed Alloys

Based on the test results from the aluminum-zinc and tertiary alloy tests, the above three alloys were produced in wire form to spray onto concrete using the thermal spray technique. Test blocks using Type I portland cement concrete, 6 in x 18 in x 2 in (15 cm x 46 cm x 5 cm), were prepared. The water/cement ratio of the concrete was 0.42, and approximately 2500 ppm (10 lb/yd³ or 6 kg/m³) of chloride were mixed into the fresh concrete prior to casting. The concrete blocks contained a perforated carbon steel sheet, 4 in x 15 in (10 cm x 38 cm), with a 40 percent opening to simulate the anode-cathode area ratio in the reinforcing steel. Prior to spraying the aluminum alloys, a 0.5-in- (1.3-cm-) wide x 0.04-in- (1-mm-) thick bare titanium strip was attached on the top surface of each concrete block as an anode connector using epoxy resin and plastic fasteners. Pure zinc and pure aluminum were also thermally sprayed onto other concrete blocks for comparison with the new alloys. A total of five concrete test blocks were prepared for testing.

A 0.5-in (1.3-cm) hole was drilled into the center of the top (anode side) surface of the block, approximately 0.75 in (1.9 cm) deep in order to place a pencil-type CSE reference electrode. This reference electrode enabled the measurement of the potentials of the anode and the steel.

The concrete specimens were then placed in an environmental chamber. The anode, the steel, and the reference electrode were connected via electrical wires to a terminal board located outside of the environmental chamber. The galvanic current produced by each specimen was determined by measuring the voltage across a 10-ohm shunt connected in the circuit between the anode and the steel cathode. A data logger was used for the current measurement, with data taken every 120 min.

Testing at various temperatures and humidity levels was conducted as described in chapter 3. A total of nine different environments were generated. The ambient temperature in the environmental chamber was set at 40°, 70°, or 90°F (4°, 21°, or 32°C), and the relative humidity at each temperature was controlled at 40, 70, or 90 percent. The specimens were exposed continuously to each environment for 10 days. At the end of the 10th day, depolarization tests were conducted on both the steel cathode and the anode of each concrete specimen to determine cathodic protection effectiveness and anode performance.

Based on the above test results, Al-10Zn-0.2In, Al-20Zn-0.2In, and Al-30Zn-0.2In were selected for further testing as thermally sprayed coatings. Sumitomo produced several billets of the three alloys. The analyzed composition of the billet alloys were Al-10Zn-0.25In, Al-20Zn-0.23In, and Al-30Zn-0.26In, respectively. In order to produce wires from the billets, a drawing technique was used initially. To thermally spray the alloys, a maximum wire diameter of 0.19 in (4.6 mm) was required. However, it was found that the higher zinc contents in the aluminum alloys made them too brittle to draw into wire. The extrusion method was tried and found to be successful for all three alloys. However, wires of the alloy containing 30 percent zinc could not be coiled due to brittleness.

Arc-spray parameters were investigated for applying the alloys to concrete. The National Research Council (NRC) in Canada was contracted to perform this work, which included determining the appropriate application voltage and current, bond strength, and microstructure. NRC attempted to spray the Al-10Zn-0.2In and Al-20Zn-0.2In onto concrete blocks using an arc-spray machine. Since the wires of Al-30Zn-0.2In were not flexible enough to be coiled, the arc-spray method was not feasible. Furthermore, the brittleness of the 0.19-in (4.6-mm) wires of Al-10Zn-0.2In and Al-20Zn-0.2In prevented the wire from being pulled into the arc-spray machine. The diameter of the Al-10Zn-0.2In wire was reduced to 0.13 in (3.2 mm) by drawing it through dies. In so doing, the flexibility of the wires was improved sufficiently to allow it to be arc-sprayed. However, it was not possible to reduce the wire size of the Al-20Zn-0.2In alloy wire by drawing because the wire continued to break during the drawing process. Therefore, only the Al-10Zn-0.2In was sprayed onto the concrete blocks using the arc-spray technique, as shown in figure 46. This alloy was the only alloy tested by NRC.

Two arc voltages, 25 and 30 V, and two arc amperages, 150 and 200 A, were tried in four combinations for spraying the Al-10Zn-0.2In alloy. The test results indicated that there was no difference in the coating structure or bond between any of the voltage and current settings tested.

One of the findings of previous researchers has been that indium, when added in too large a concentration, will not alloy with the aluminum-zinc alloy, but will segregate instead. The benefits of larger than about 0.02 percent indium have been questioned for normal underground and water use of sacrificial anodes.(19-21) The data previously discussed indicate that, on concrete surfaces at least, higher indium contents do provide a measurable benefit. Some of the work done by NRC Canada was to analyze the wire and sprayed coating for segregation using x-ray diffraction techniques. Small third phase particles consisting of large and variable concentrations of indium were found (16In-11Zn-73Al, 90In-7Al-3Zn, and 48In-39Al-13Zn), while the concentrations of aluminum and zinc outside of these particles followed the bulk concentrations in the alloy. Limited tests on the sprayed coating, while finding some segregation of the aluminum and zinc, were inconclusive as to segregation of the indium. Further work needs to be done to resolve this question should it become an issue.

The Al-20Zn-0.2In and Al-30Zn-0.2In alloy wires were applied to concrete test blocks by a local shop using the flame-spray technique. Figure 47 shows one of the alloys being applied to a block. In addition, pure zinc and pure aluminum were also sprayed onto concrete blocks for comparison. These blocks, along with the Al-10Zn-0.2In-coated block were used for performance testing.

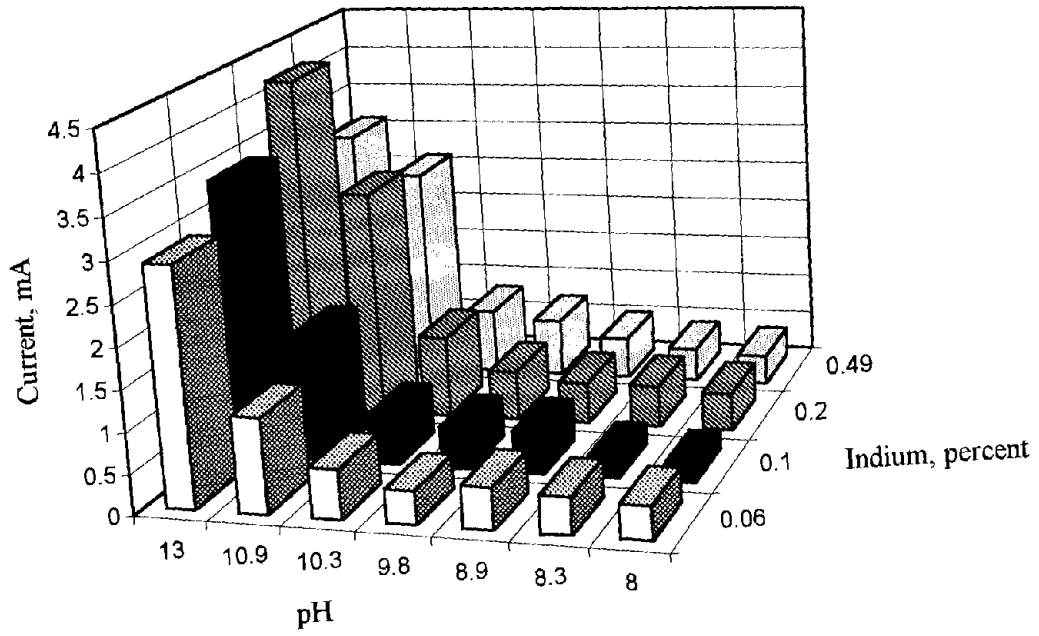


Figure 38. Current output vs. indium content for Al-20Zn alloy.

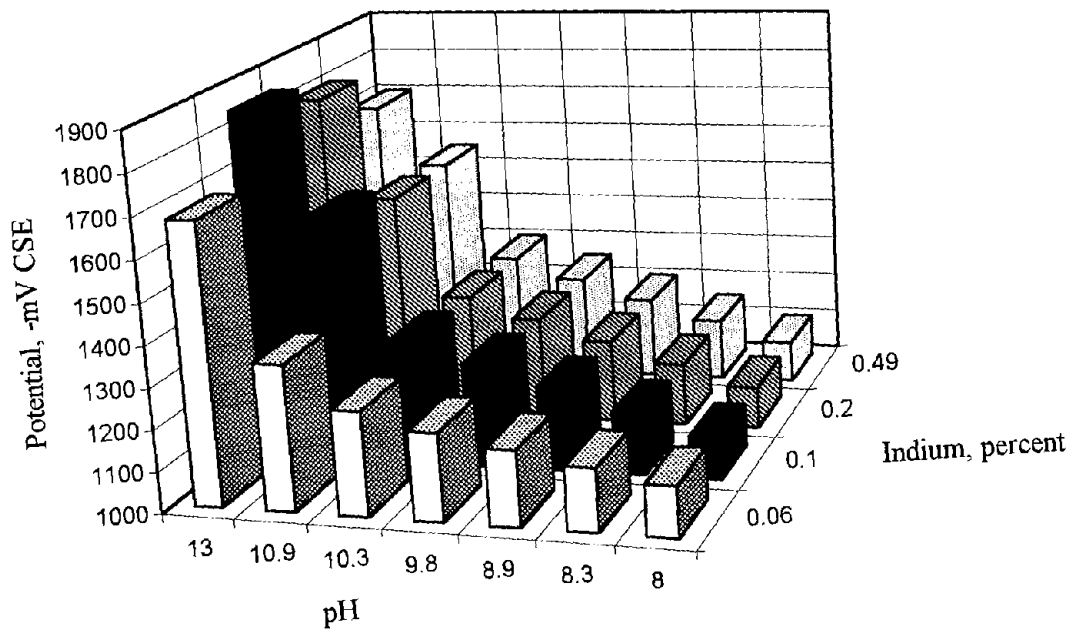


Figure 39. Instant-off potentials vs. indium content for Al-20Zn alloy.

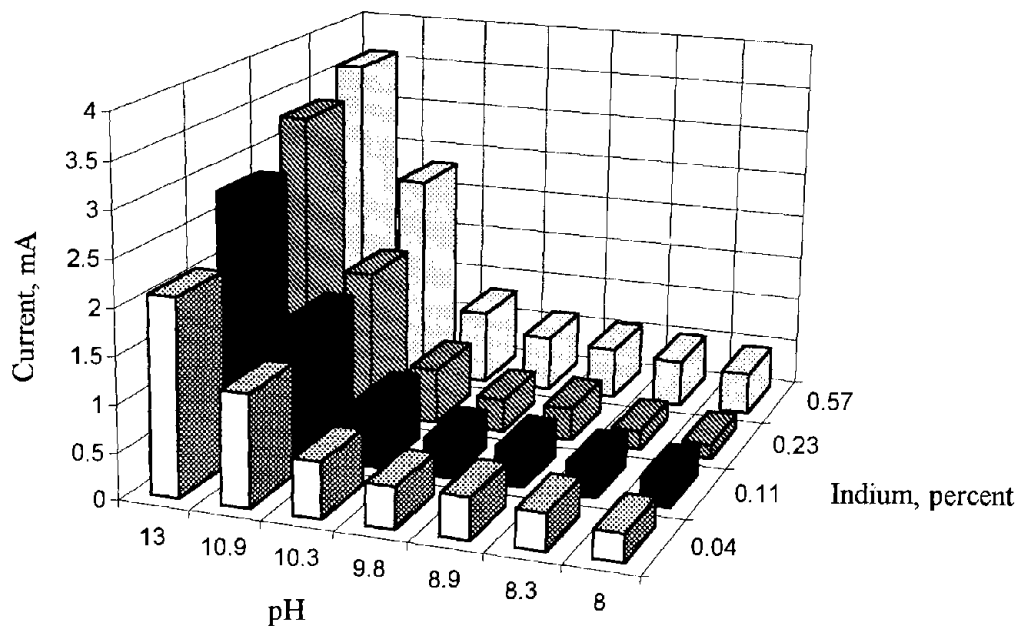


Figure 40. Current output vs. indium content for Al-30Zn alloy.

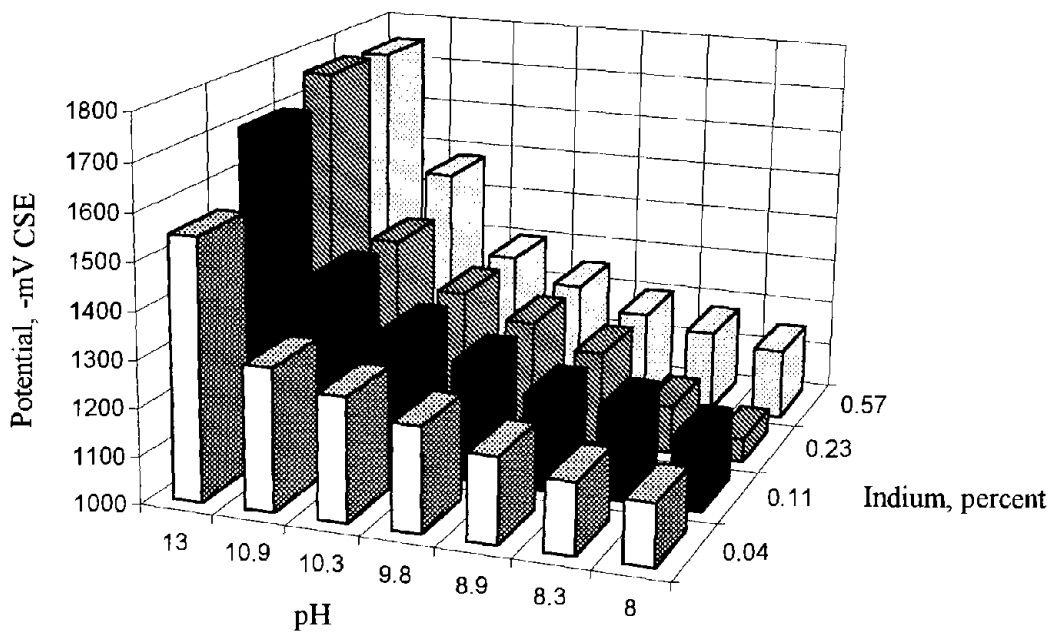


Figure 41. Instant-off potentials vs. indium content for Al-30Zn alloy.

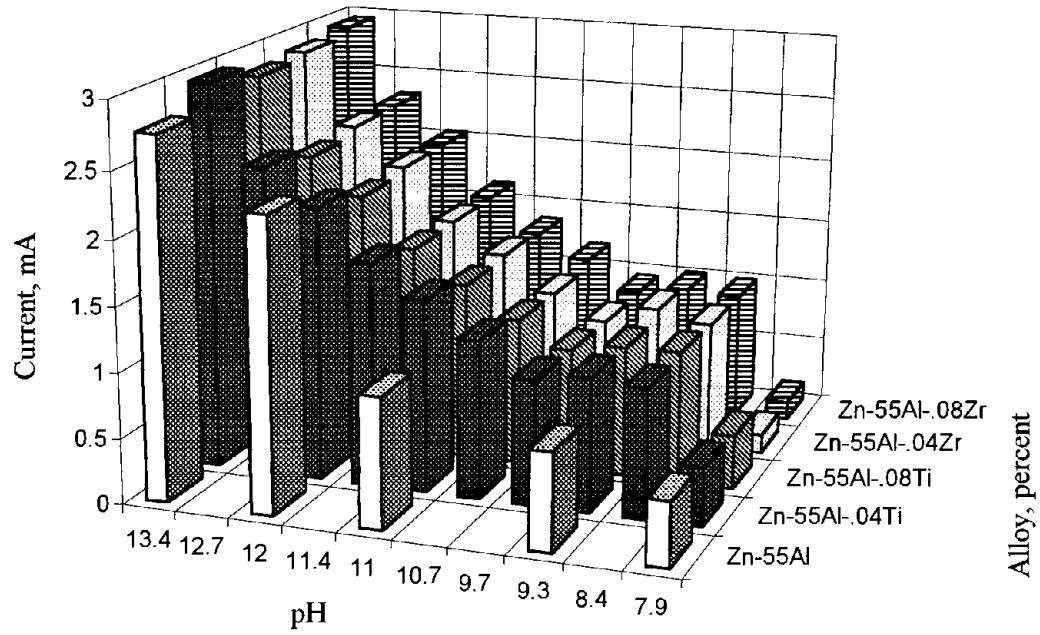


Figure 42. Current output for Zn-55Al alloy.

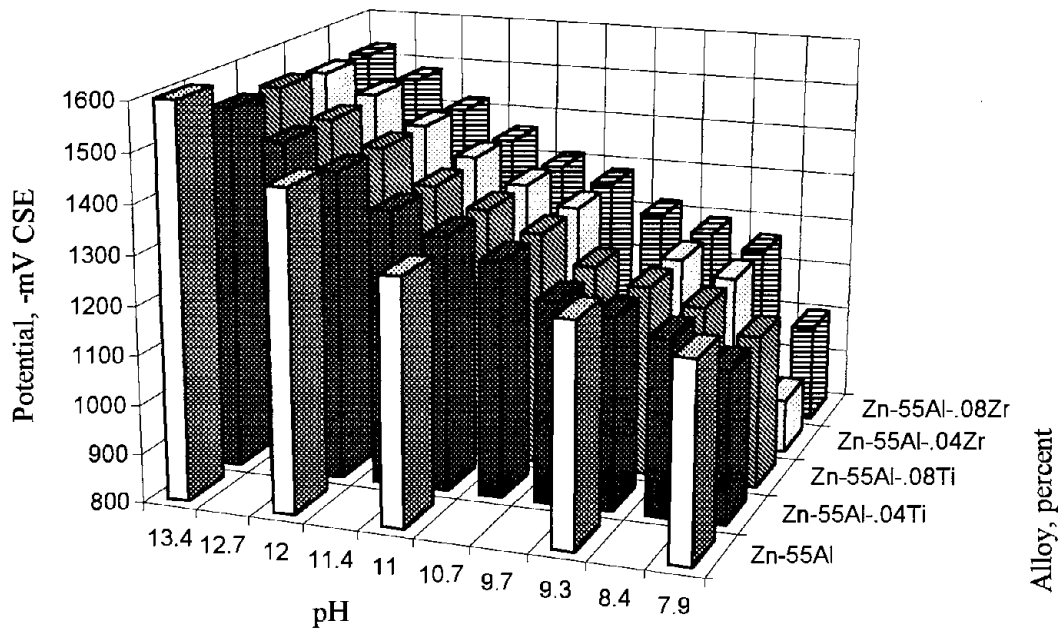


Figure 43. Instant-off potentials for Zn-55Al alloy.

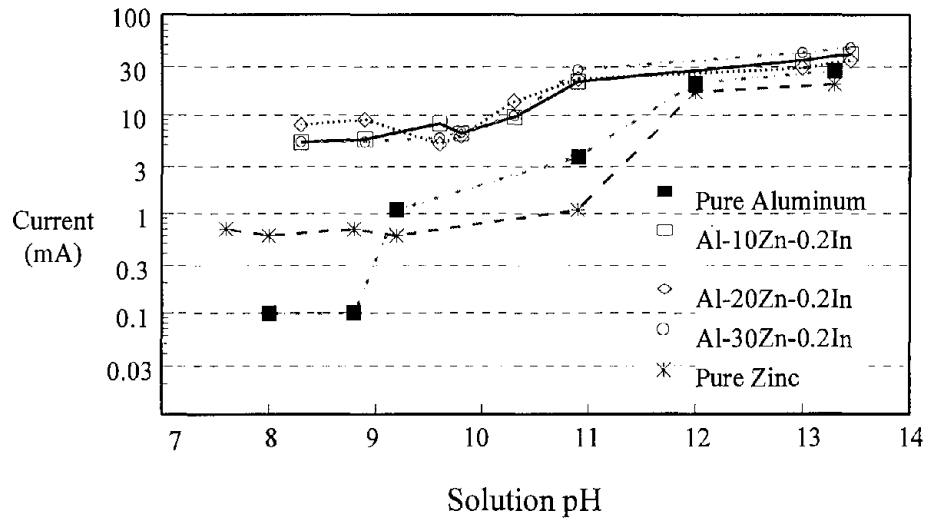


Figure 44. Galvanic current vs. pH in simulated concrete pore solution.

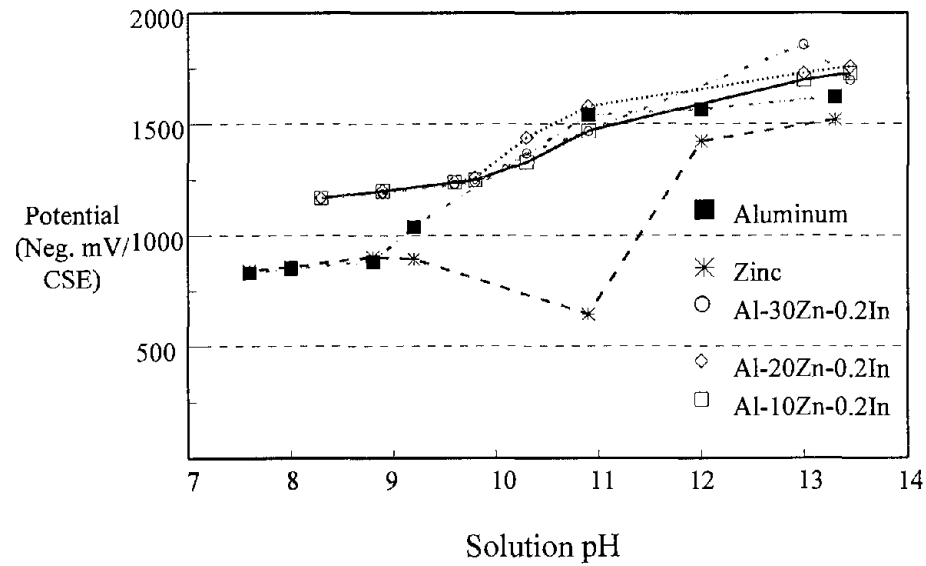


Figure 45. Instant-off potentials vs. pH in simulated concrete pore solution.

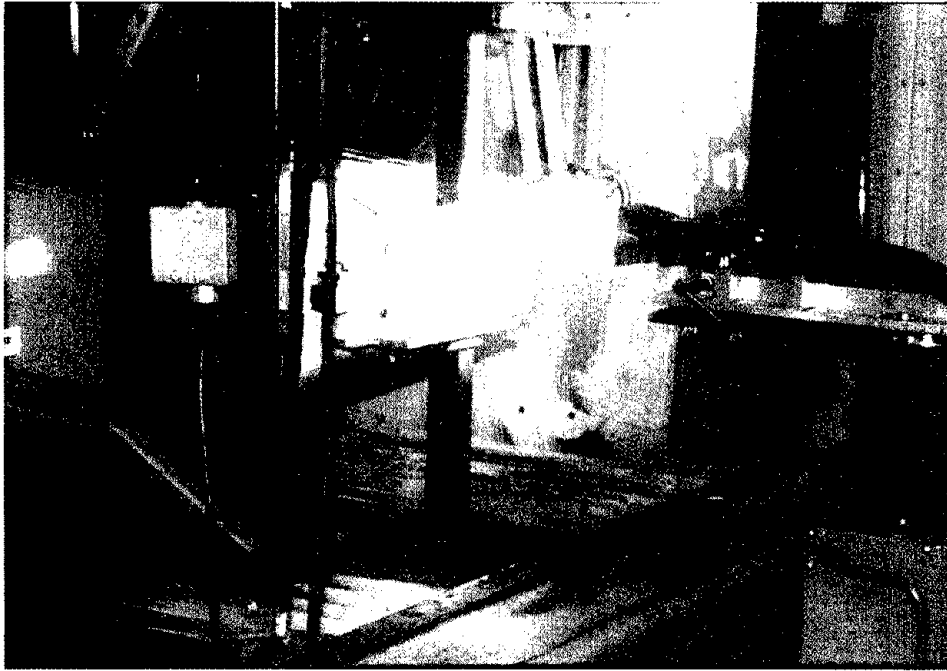


Figure 46. Arc-spraying of Al-10Zn-0.2In wire.

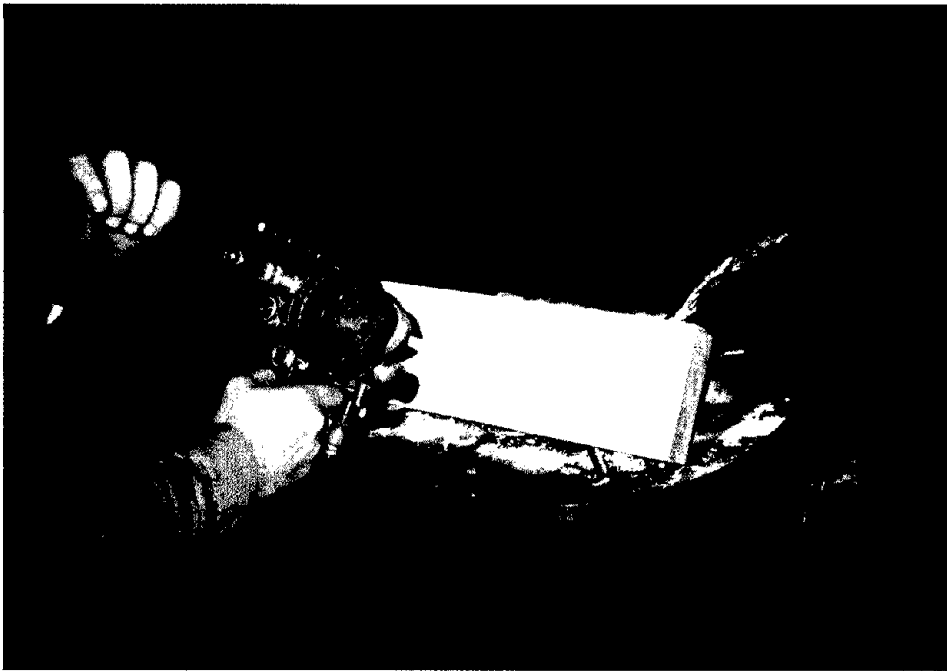


Figure 47. Flame-spraying of Al-20Zn-0.2In wire.

Figures 48 and 49 show cross sections of the Al-10Zn-0.2In alloy-concrete interface obtained by a scanning electron microscope immediately after the alloy was sprayed. The photographs of the concrete-alloy interface show that the new alloy penetrated into almost all concrete pores during the spray application. The average bond strength of this alloy was approximately 235 lbf/in² (1.62 MPa). The range was 180.3 to 294.1 lbf/in² (1.24 to 2.03 MPa). The strong bond strength of the new alloy may result from the low surface tension of the alloy. Note that the separation between the coating and concrete in the photographs occurred during the specimen preparation process for the microscopic examination, not at the concrete-alloy interface. This indicates that the bond strength of the alloy to the concrete exceeded the tensile strength of the concrete.

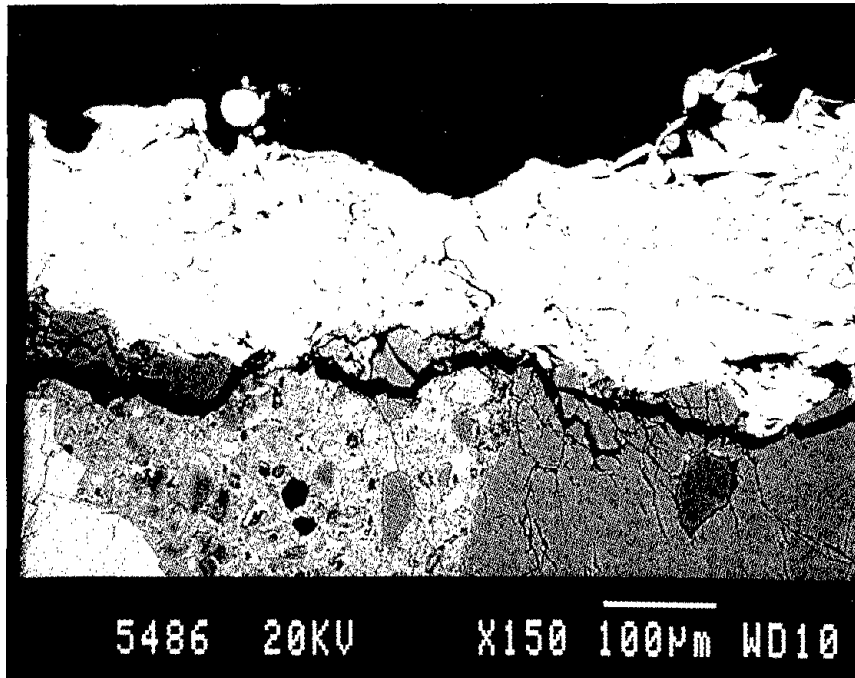


Figure 48. Cross section of Al-10Zn-0.2In alloy-to-concrete interface.

Figures 50 through 52 show the environmental test results on the five sprayed sacrificial anodes, Al-10Zn-0.2In, Al-20Zn-0.2In, Al-30Zn-0.2In, pure zinc, and pure aluminum (see figure 27 for the key to figures 50 through 52). The concrete blocks were exposed to nine different environments — three temperatures, 40°F, 70°F, and 90°F (4°C, 21°C, and 32°C), and three relative humidity levels (40, 70, and 90 percent). The bottom portions of the figures show the depolarization test results on the anodes and steel plates. The numbers in parentheses indicate the amount of depolarization that occurred on each anode and steel plate. The top and bottom edges of the light shaded rectangles show the “instant-off” and “static” potentials of the anode, respectively. The bottom and top edges of the dark shaded rectangles show the “instant-off” and “static” potentials of the steel (cathode), respectively. The opening between the two shaded rectangles is the driving voltage between the anode and cathode when they were electrically connected to each other. The top portions of the graphs show the galvanic (cathodic protection) current densities for the corresponding anodes.

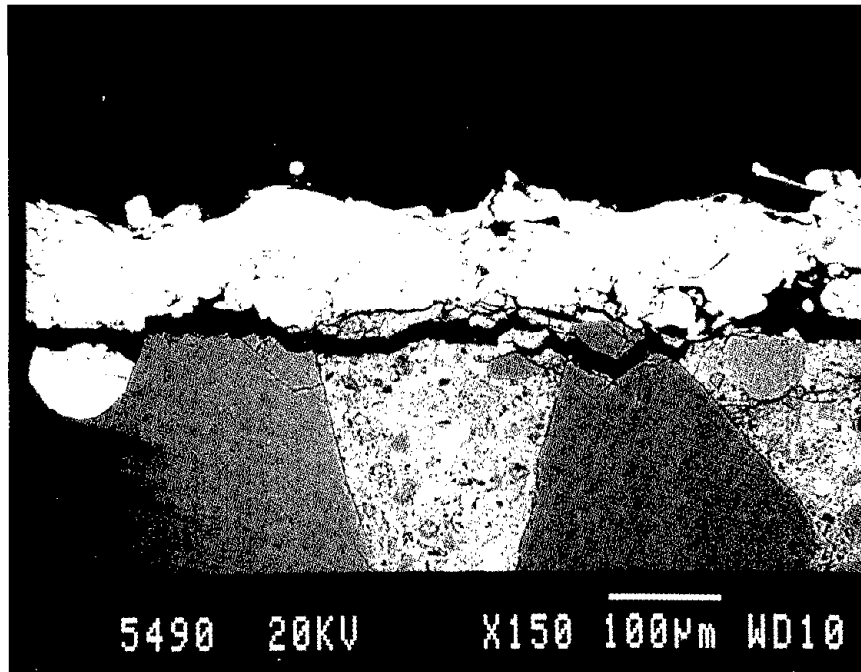


Figure 49. Cross section of Al-10Zn-0.2In alloy-to-concrete interface. (Note break across metal at left and coverage in concrete irregularities.)

Summary

All three new alloys outperformed pure zinc and pure aluminum anodes in all of the environments tested. As stated before in the environmental tests in chapter 3, passive potentials were measured on the steel embedded in some of the chloride-contaminated concrete blocks at the end of the depolarization tests. This tendency was more noticeable on the steel plates that had received higher current densities during the early period of the testing. Thus, applications of low current density [0.03 mA/ft^2 (0.32 mA/m^2)] by the new anode alloys depolarized the steel more than 100 mV in the dry environment (40 percent RH) and low temperature. The Al-20Zn-0.2In alloy appeared to perform the best because it had the smallest anode polarization and maintained relatively active static potentials in all the environments.

Phase III. Application of Alloys to a Bridge Substructure

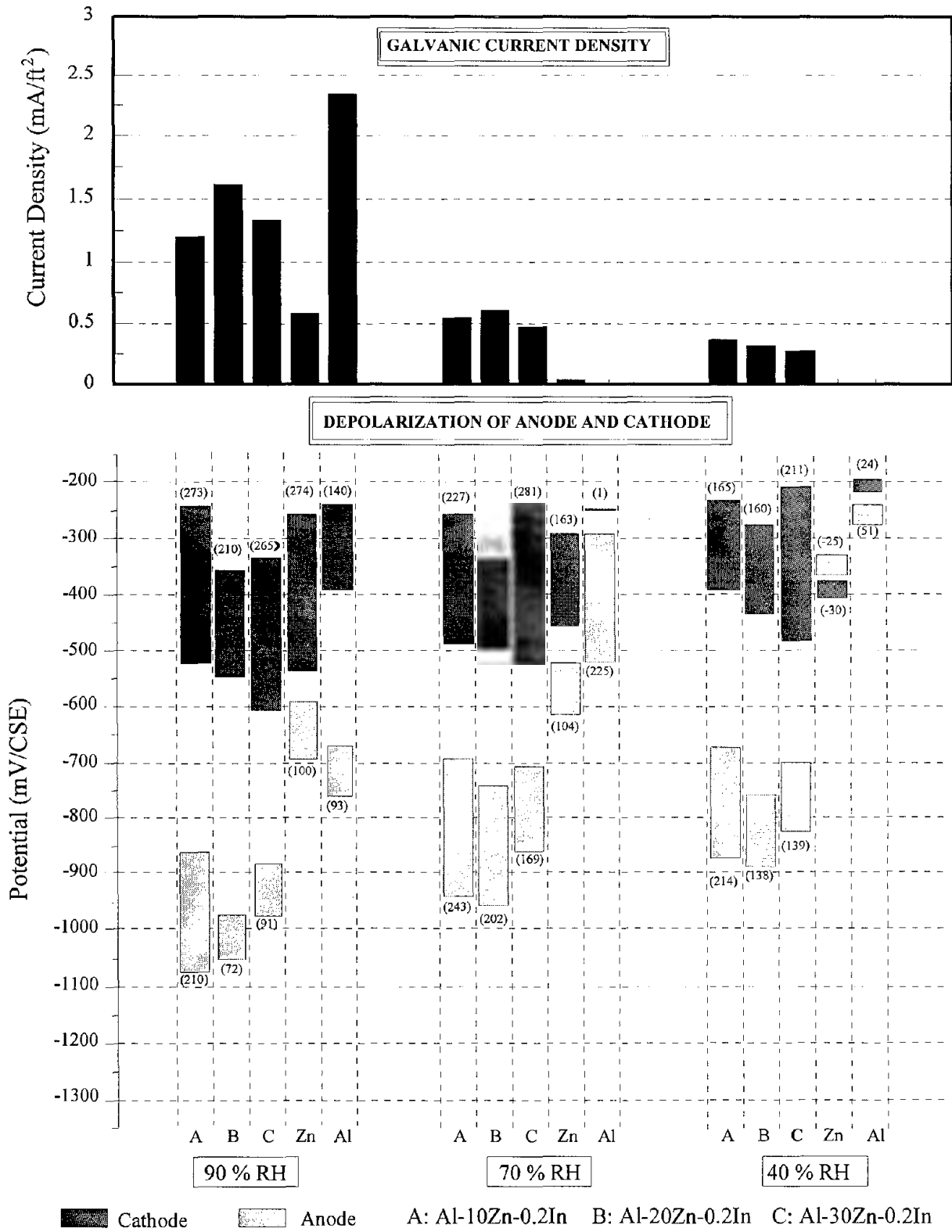
The laboratory work presented in this report shows that the aluminum-zinc-indium alloys developed under this program provide suitable cathodic protection to steel embedded in concrete. The objectives of the project call for this technology to be applied to a bridge structure. Specifically, plans call for installation of the anode material to the substructure of a corroding bridge, and monitoring of the performance of the anode for the remainder of the contract period. Installation began in June 1995, with the system activated in July 1995. The final testing will be conducted in July 1997.

The anode was applied with Florida DOT's assistance to selected columns of the Bryant Patton Bridge, located between Eastpoint and St. George Island in Florida. This bridge is the subject of development work by the Florida DOT that includes the installation of a pure zinc metallized anode in atmospheric corrosion zones and zinc sheet anode material in splash zones.

The developed aluminum alloy anode system was applied to four piles. The surface area covered by the aluminum alloy on each pile is approximately 30 ft² (2.8 m²). Two piles on the Eastpoint side of the bridge were coated with the aluminum alloy anode and the connection to the embedded steel was made through a channel cut into the top of the pile to expose the steel. No attempt was made to isolate any surface steel from the anode. One pile was similarly coated with pure zinc. All three piles were overcoated; one aluminum pile was coated with a moisture-cured polyurethane and one zinc and one aluminum pile were coated with an acrylic paint. These piles were not instrumented.

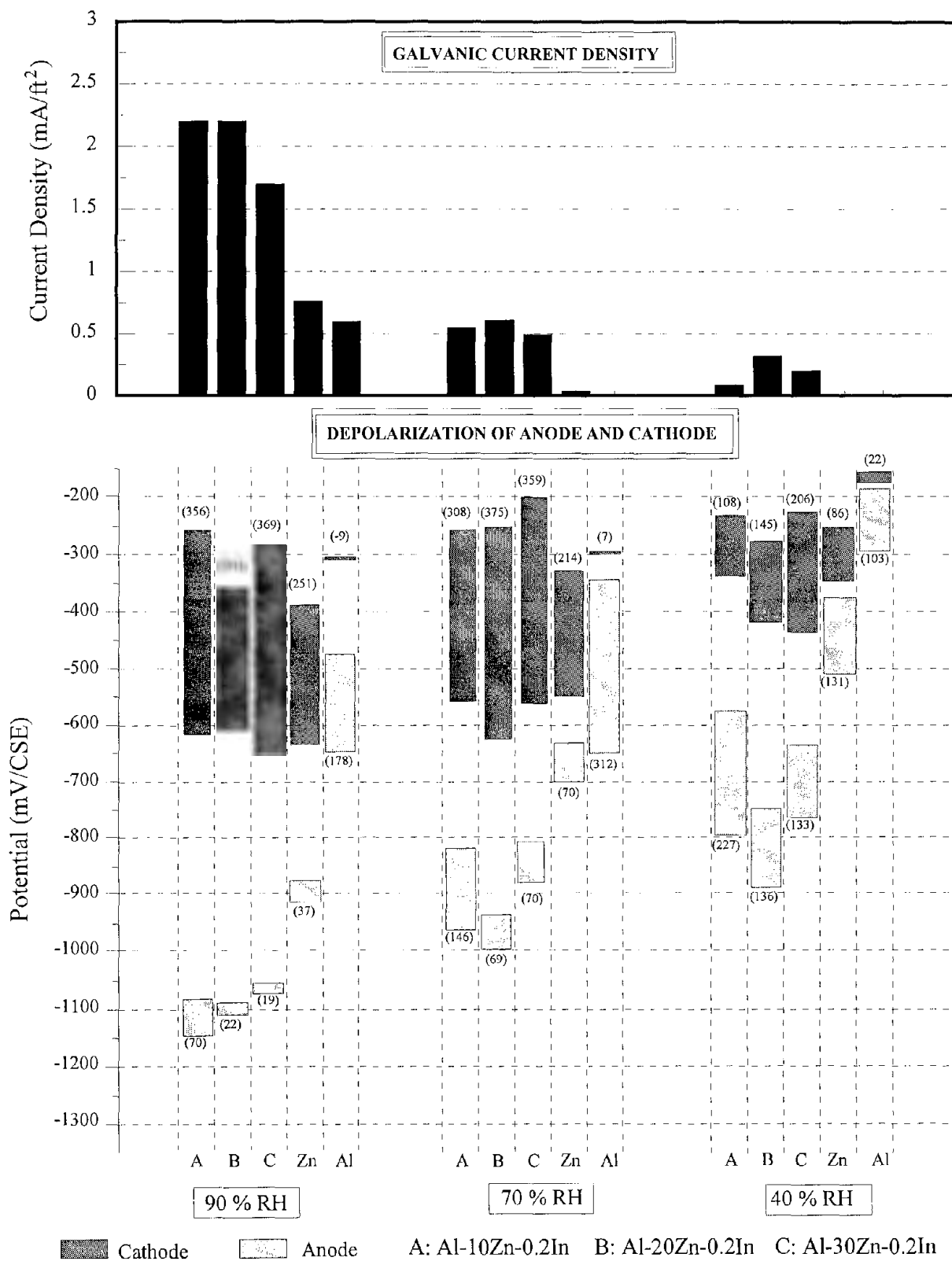
On one bent on the St. George Island side of the bridge, consisting of four piles, two piles were coated with pure zinc and two piles were coated with the aluminum alloy anode. These piles were instrumented in order to measure cathodic protection parameters on a periodic basis. The anodes were applied to these piles such that the anode is electrically isolated from the rebar. Each of the piles was instrumented with the following: an SSC reference electrode, a rebar probe cast into chloride-contaminated concrete [15 lb/yd³ (415 kg/m³)], and wiring. The system was wired into a junction box and connected to a data logger. The purpose of the data logger is to allow close monitoring of operating parameters and frequent tests because the current outputs from the anodes are influenced by the varying environment. Data collected include potentials between the SSC reference electrodes and rebar or rebar probes, CP current in each pile between the anode and rebar or probe, and depolarization of the probes or rebar. The data logger is connected to a modem and cellular telephone to allow remote monitoring and testing. Two trips to the bridge are anticipated — one during anode application and one at the end of the program to perform the final inspection.

The anode on two piles (one aluminum alloy and one zinc) was overcoated with a moisture-cured polyurethane sealer. The anodes on the other two piles were left uncoated. The purpose of the overcoating is to evaluate the need to protect the anode from atmospheric corrosion and water intrusion. The overcoat selected is permeable to moisture, as compared to other traditional barrier coatings for concrete in marine environments.



$$1 \text{ mA/ft}^2 = 10.75 \text{ mA/m}^2$$

Figure 50. Environmental test results for experimental alloys and pure zinc and aluminum at 90°F (32°C).



$$1 \text{ mA/ft}^2 = 10.75 \text{ mA/m}^2$$

Figure 51. Environmental test results for experimental alloys and pure zinc and aluminum at 70°F (21°C).

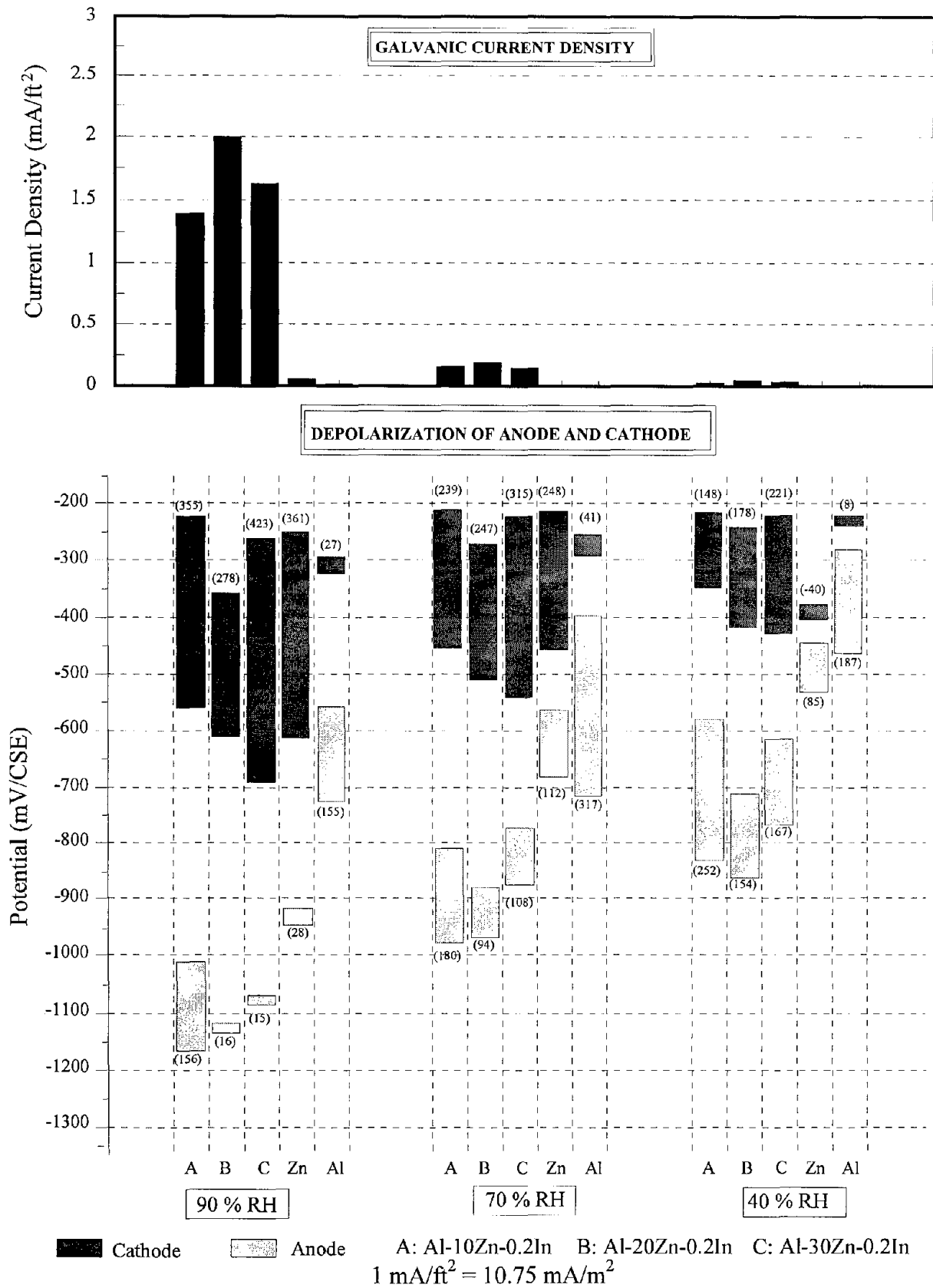


Figure 52. Environmental test results for experimental alloys and pure zinc and aluminum at 40°F (4°C).

CONCLUSIONS

1. The new aluminum alloys developed for use as a sacrificial anode produced sufficient current to cathodically protect steel embedded in chloride-contaminated concrete specimens in the laboratory. The new alloys outperform pure zinc as anodes on concrete.
2. The new aluminum alloy sacrificial anodes were superior to zinc in various environments and in lower pH (<12) simulated concrete pore solution.
3. If a sacrificial anode can produce sufficient cathodic protection current to steel embedded in chloride-contaminated concrete for a relatively short period of time, the sacrificial anode current appears to result in the passivation of the steel by removing chlorides from the immediate vicinity of the steel. As a result, a low galvanic (cathodic protection) current density is adequate to maintain the cathodic polarization of steel.
4. The performance of sprayed zinc as a sacrificial anode on concrete is greatly influenced by the presence of moisture at the anode-concrete interface. The zinc anodes that were exposed to moderately corrosive environments appear to perform well for a relatively short period of time. The zinc anodes that were exposed to highly corrosive environments, such as direct seawater exposure areas, could reduce the corrosion rate of steel; however, the zinc anode could not completely prevent the corrosion of the steel embedded in concrete.
5. The sprayed zinc sacrificial anode installed on field structures appears to produce moderate amounts of cathodic protection current in the areas where concrete resistivity is relatively low due to high moisture levels.
6. The current output from pure zinc and aluminum, as well as commercial sacrificial alloys, significantly decreased at low values of pH. The cause of current reduction in the 15 anode materials that were initially selected for testing appears to be the result of the reduction in pH at the anode-to-concrete interface, caused by corrosion products or carbonation of the concrete.
7. The new aluminum alloy, applied by the arc- or flame-spray process, was readily applied to concrete and penetrated well into concrete pores, resulting in strong adhesion to the concrete surface.

APPENDIX. ADDITIONAL TEST DATA

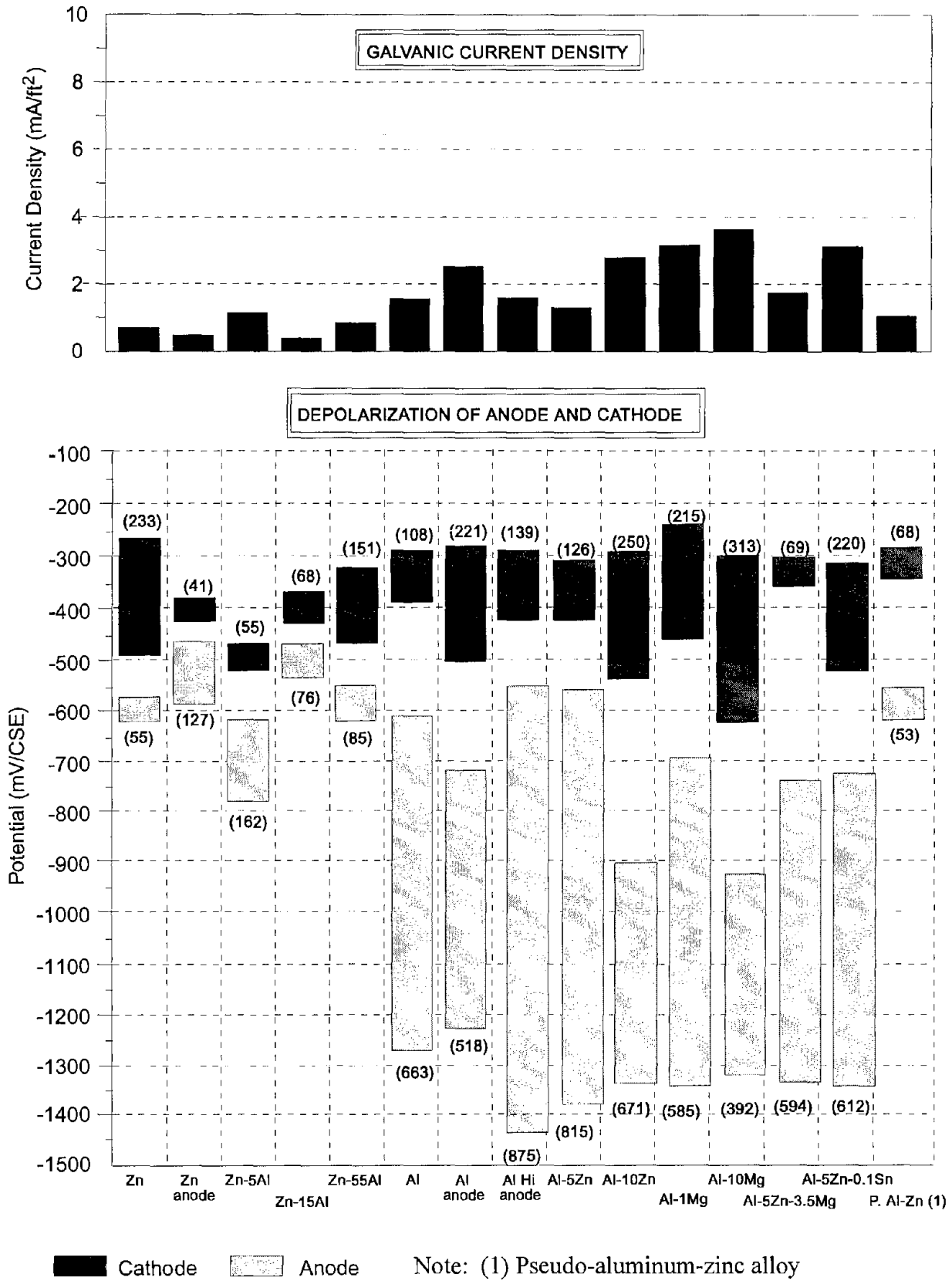
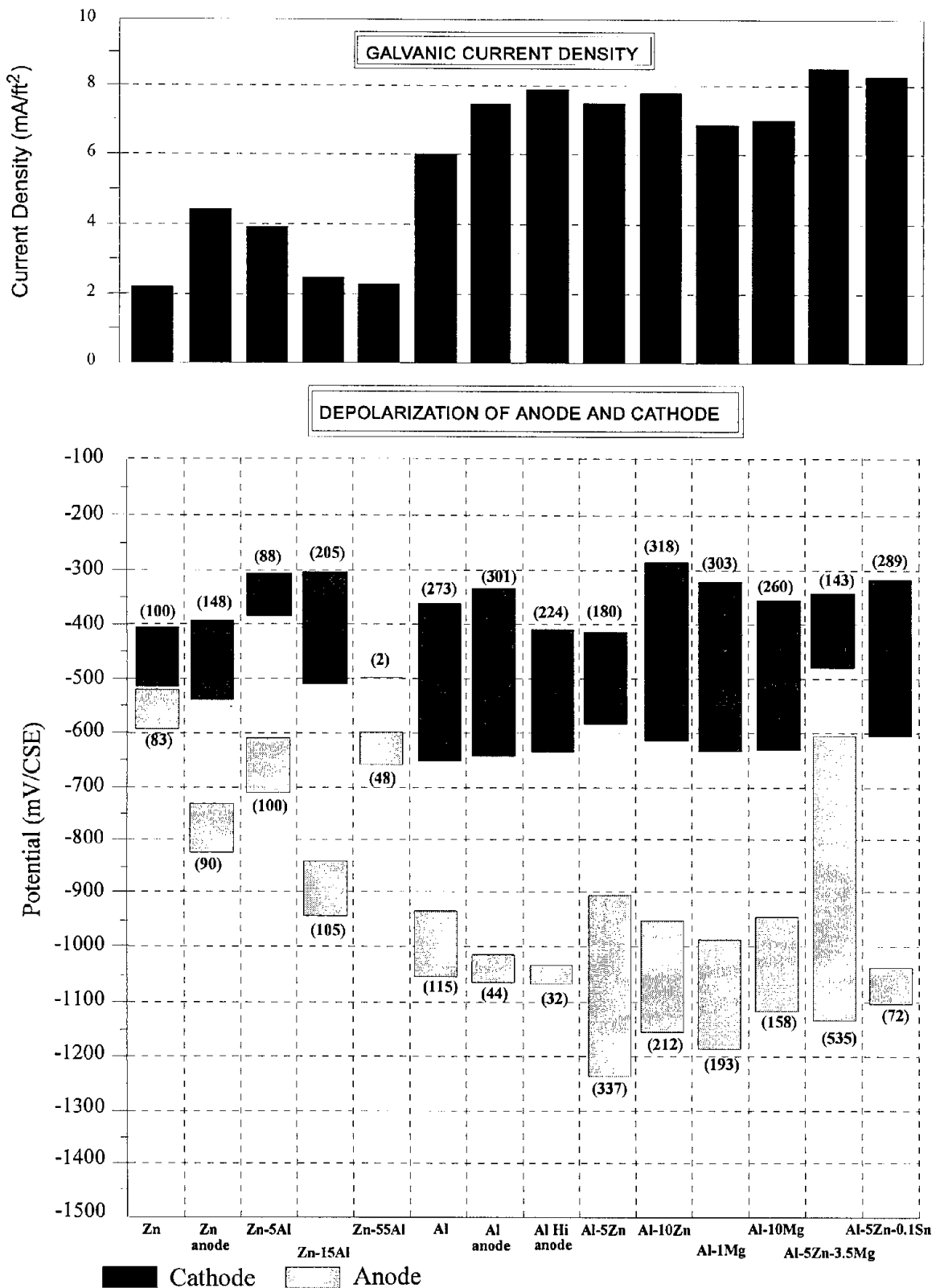
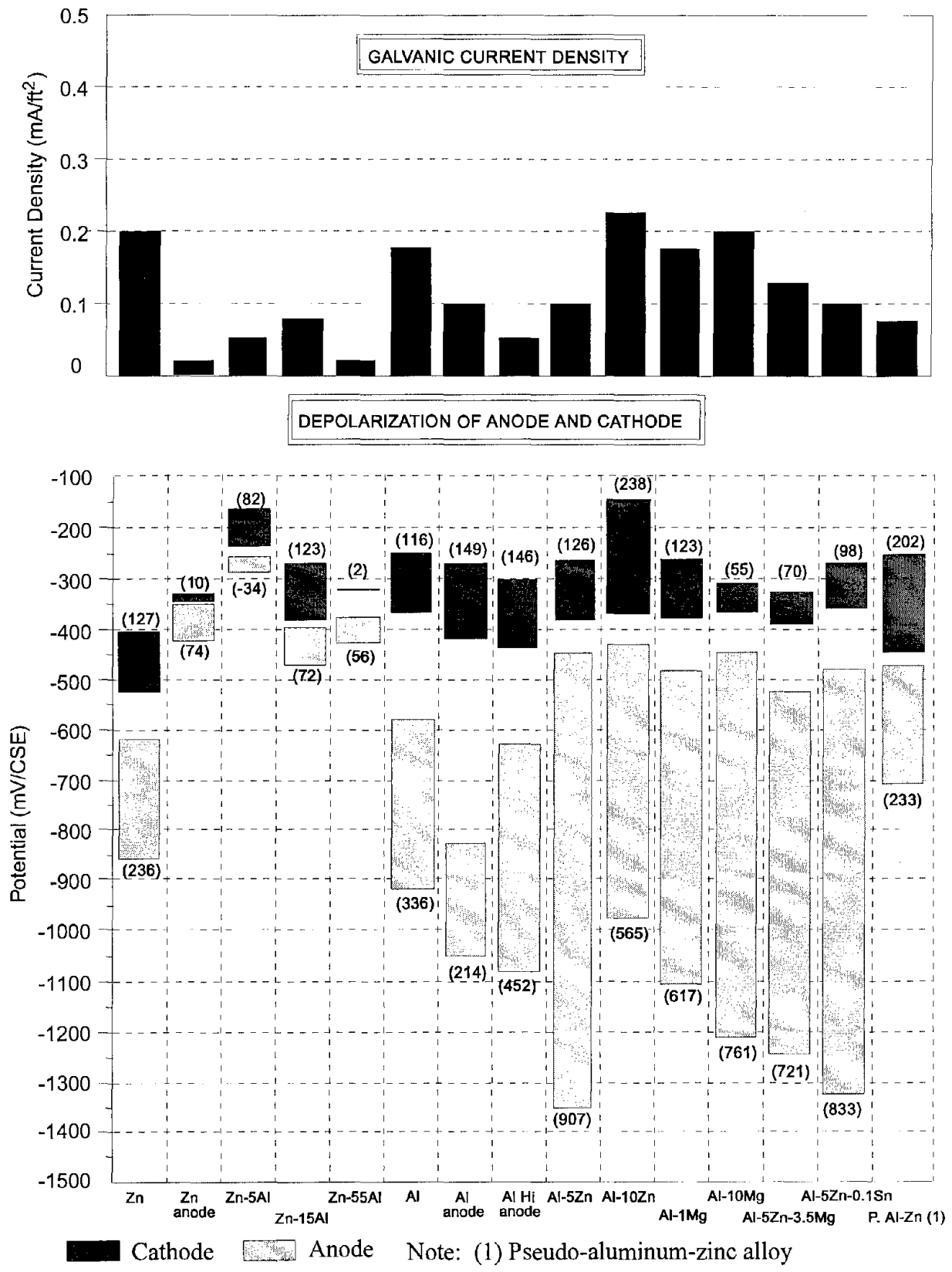


Figure 53. Environmental tests - galvanic current, instant-off potential, potential, and polarization data, 90°F (32°C), 90% RH (1300 ppm Cl).



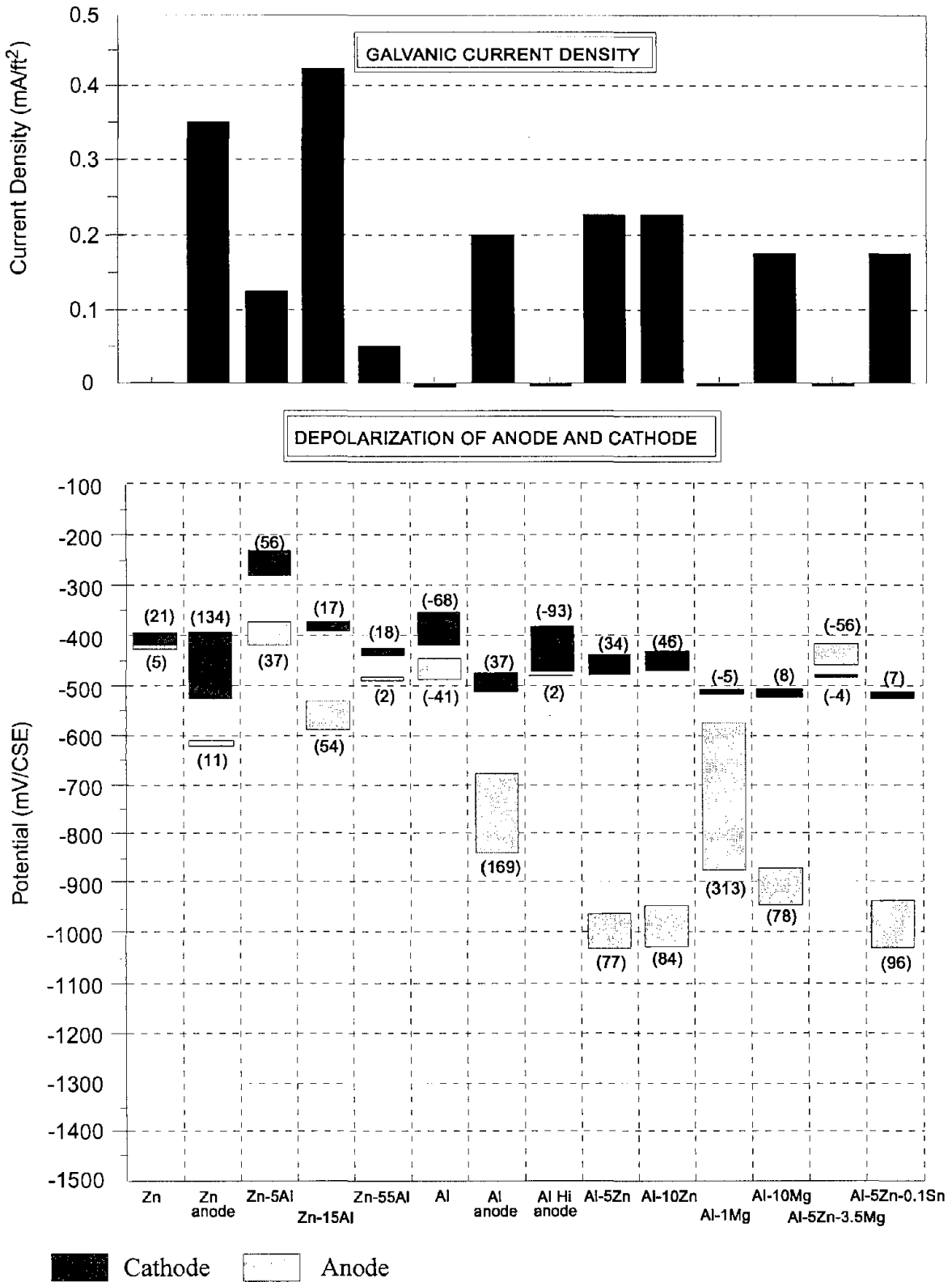
$$1 \text{ mA/ft}^2 = 10.75 \text{ mA/m}^2$$

Figure 54. Environmental tests - galvanic current, instant-off potential, potential, and polarization data, 90°F (32°C), 90% RH (3800 ppm Cl).



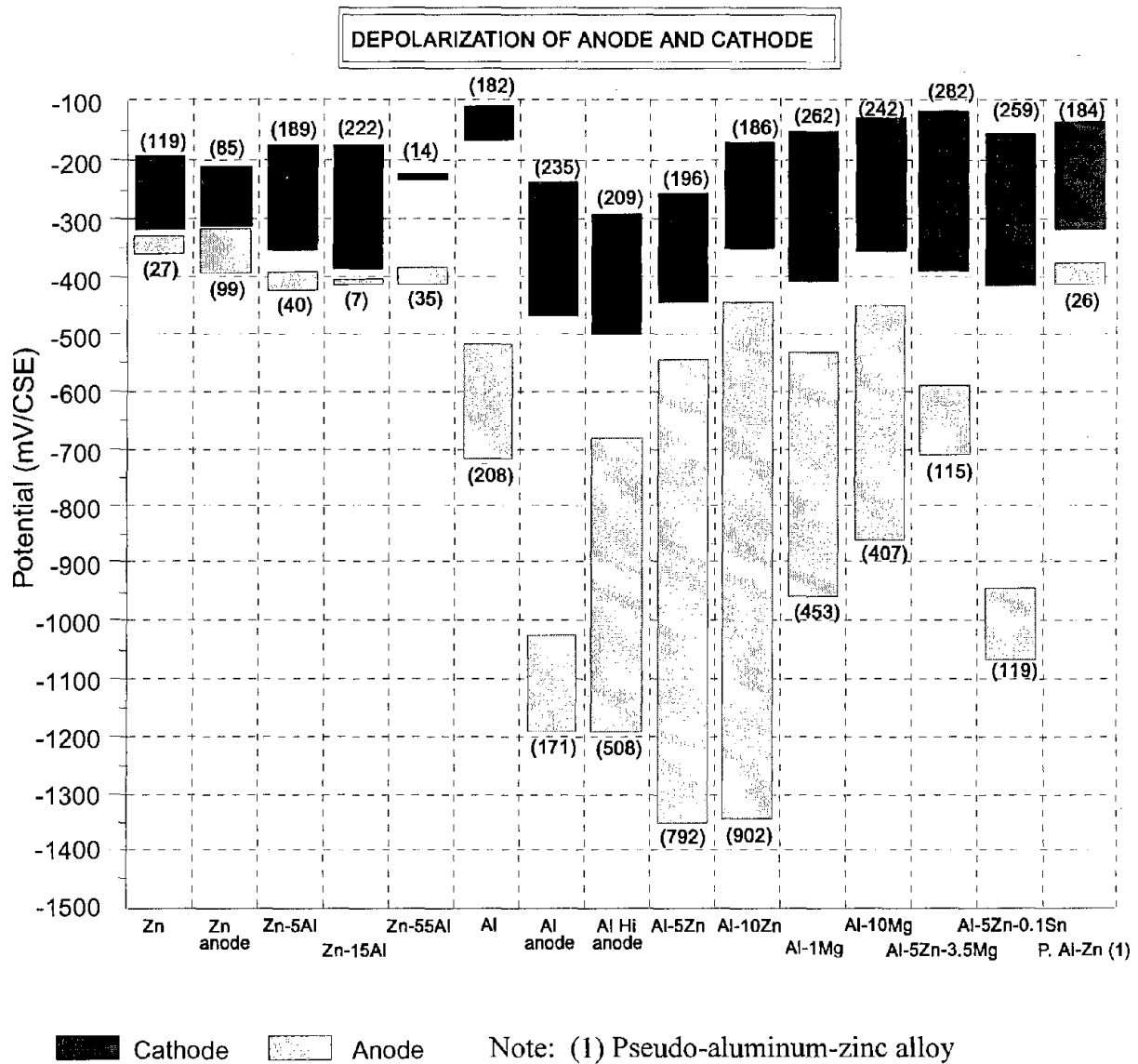
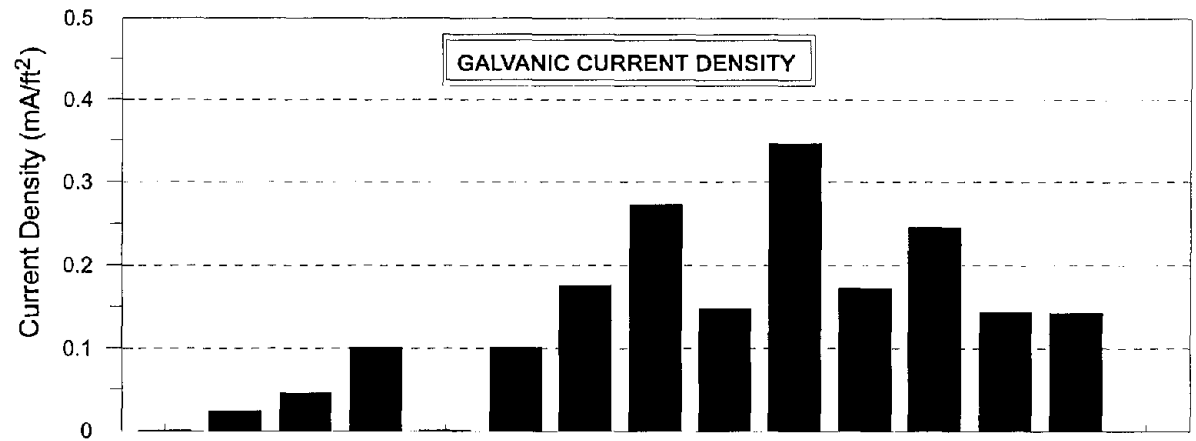
1 mA/ft² = 10.75 mA/m²

Figure 55. Environmental tests - galvanic current, instant-off potential, potential, and polarization data, 90°F (32°C), 70% RH (1300 ppm Cl).



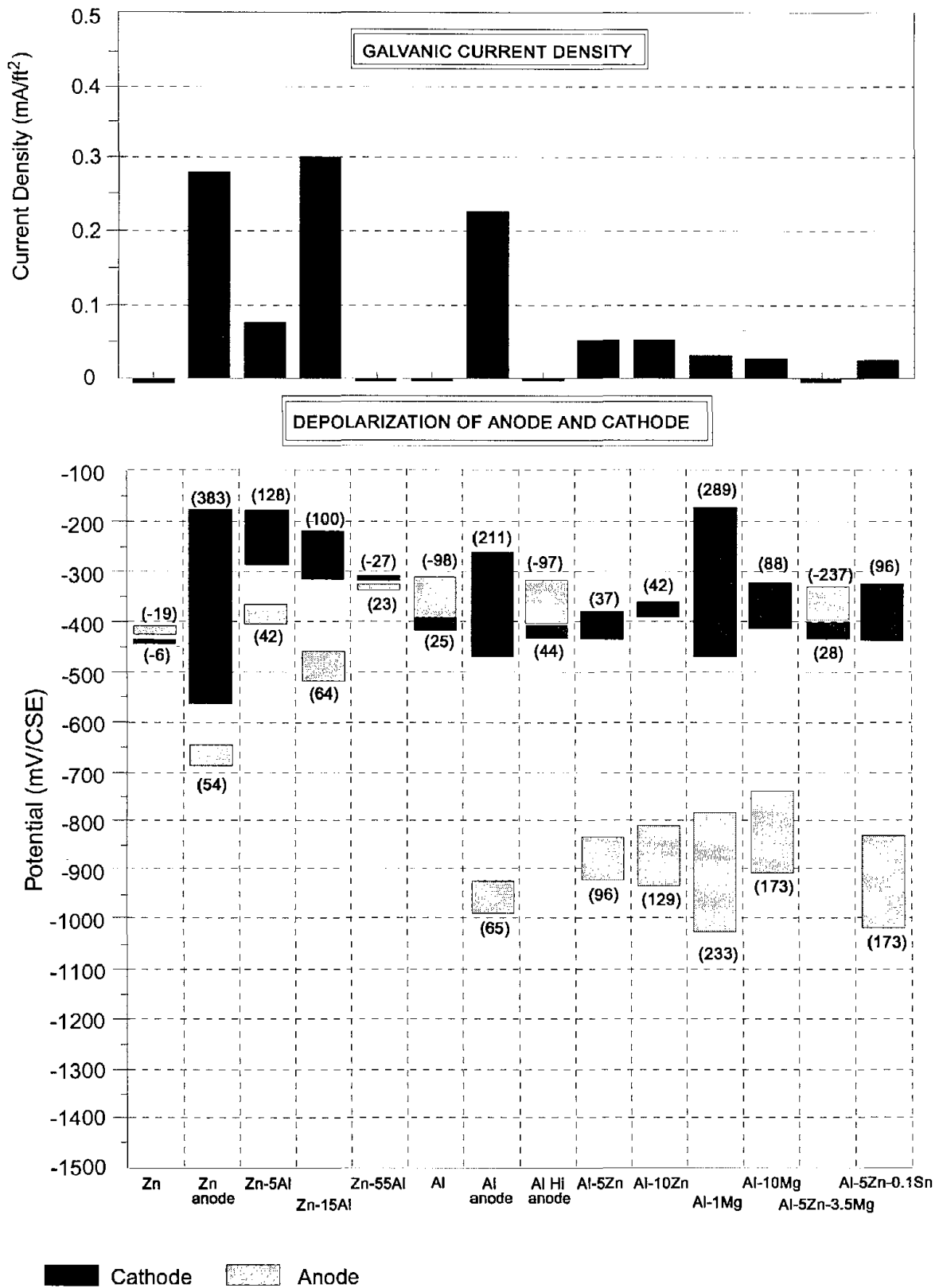
$$1 \text{ mA/ft}^2 = 10.75 \text{ mA/m}^2$$

Figure 56. Environmental tests - galvanic current, instant-off potential, potential, and polarization data, 90°F (32°C), 70% RH (3800 ppm Cl).



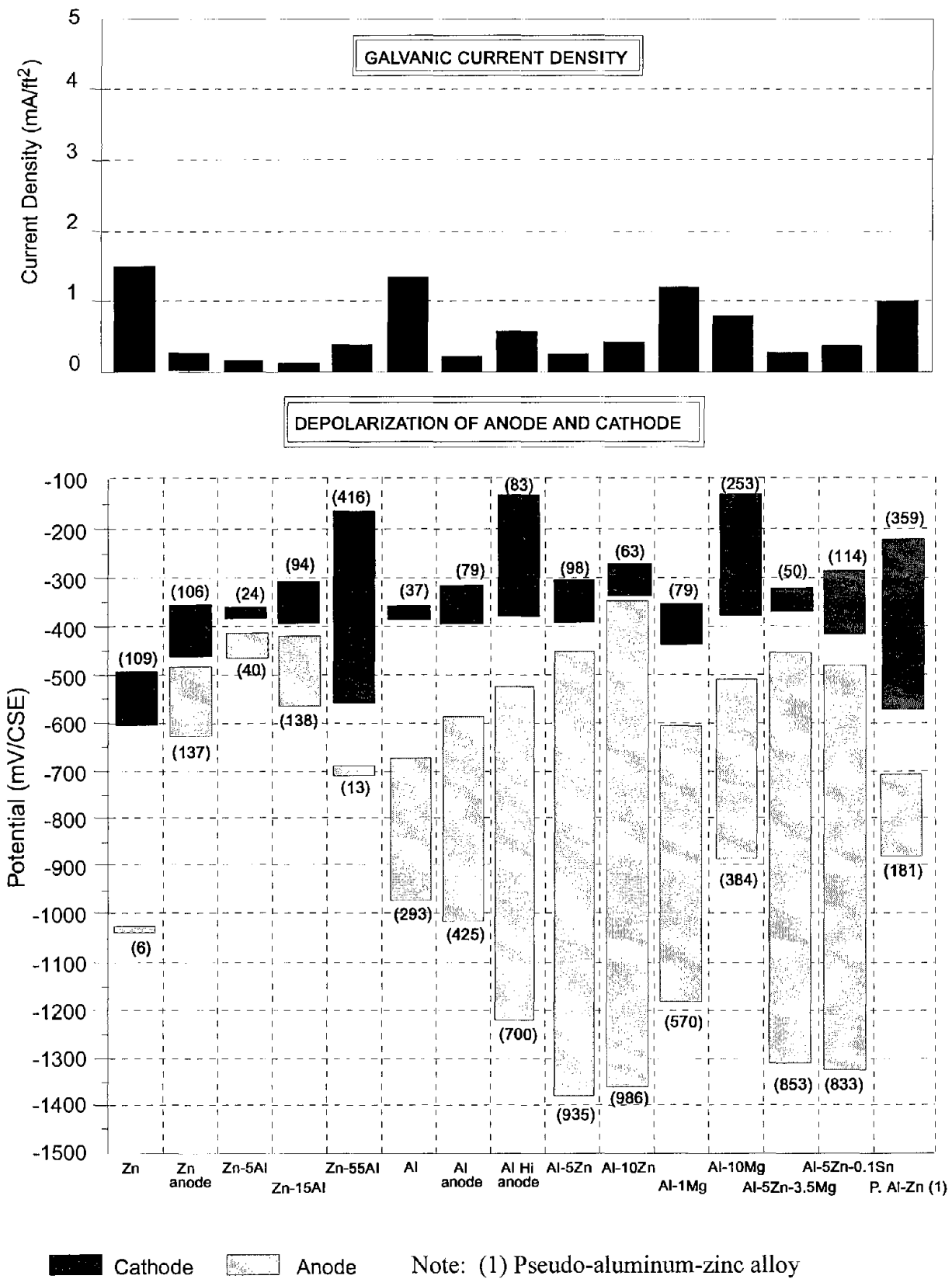
$$1 \text{ mA/ft}^2 = 10.75 \text{ mA/m}^2$$

Figure 57. Environmental tests - galvanic current, instant-off potential, potential, and polarization data, 90°F (32°C), 40% RH (1300 ppm Cl).



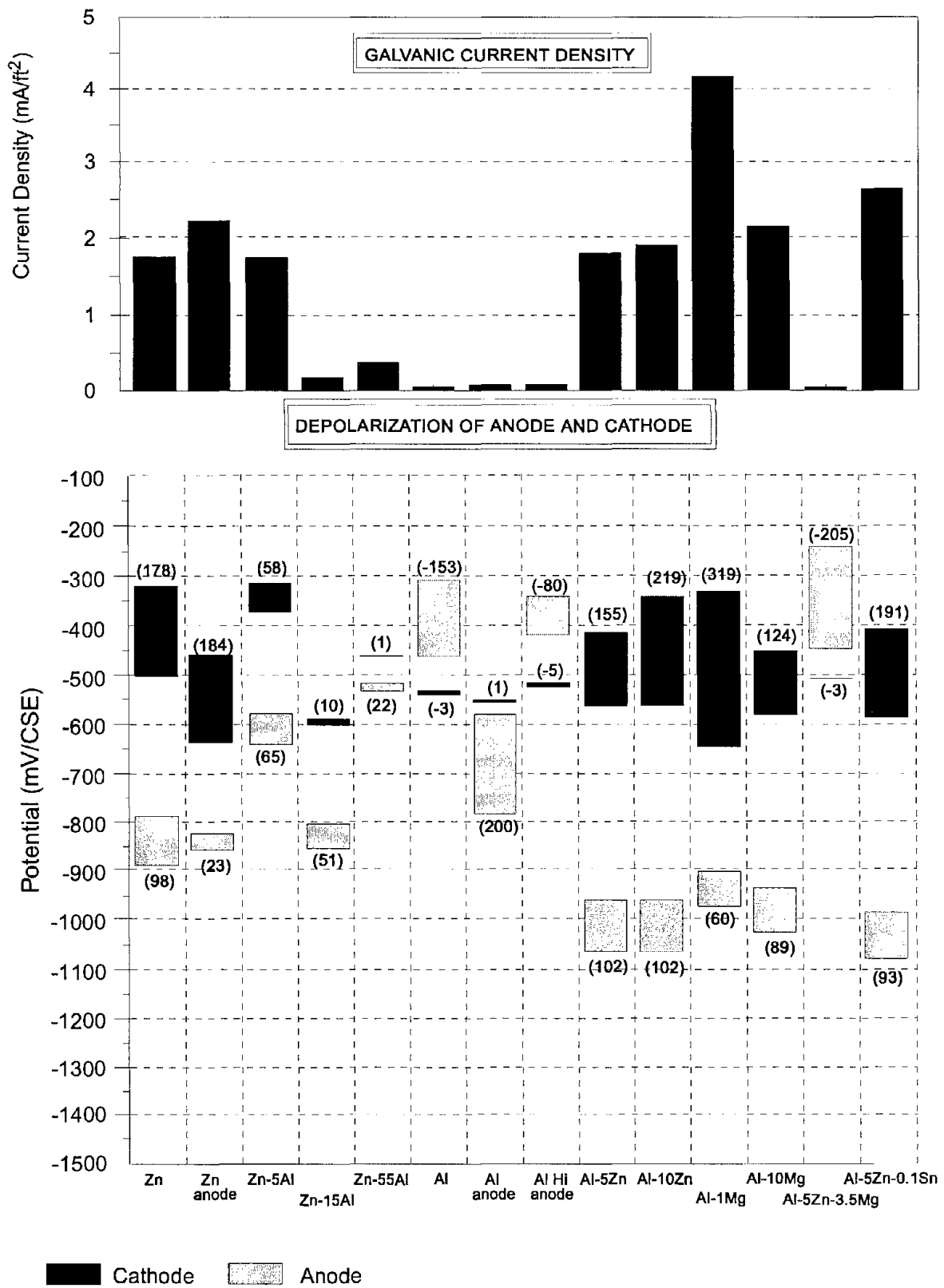
$$1 \text{ mA/ft}^2 = 10.75 \text{ mA/m}^2$$

Figure 58. Environmental tests - galvanic current, instant-off potential, potential, and polarization data, 90°F (32°C), 40% RH (3800 ppm Cl).



$1 \text{ mA/ft}^2 = 10.75 \text{ mA/m}^2$

Figure 59. Environmental tests - galvanic current, instant-off potential, potential, and polarization data, 70°F (21°C), 90% RH (1300 ppm Cl).



$$1 \text{ mA/ft}^2 = 10.75 \text{ mA/m}^2$$

Figure 60. Environmental tests - galvanic current, instant-off potential, potential, and polarization data, 70°F (21°C), 90% RH (3800 ppm Cl).

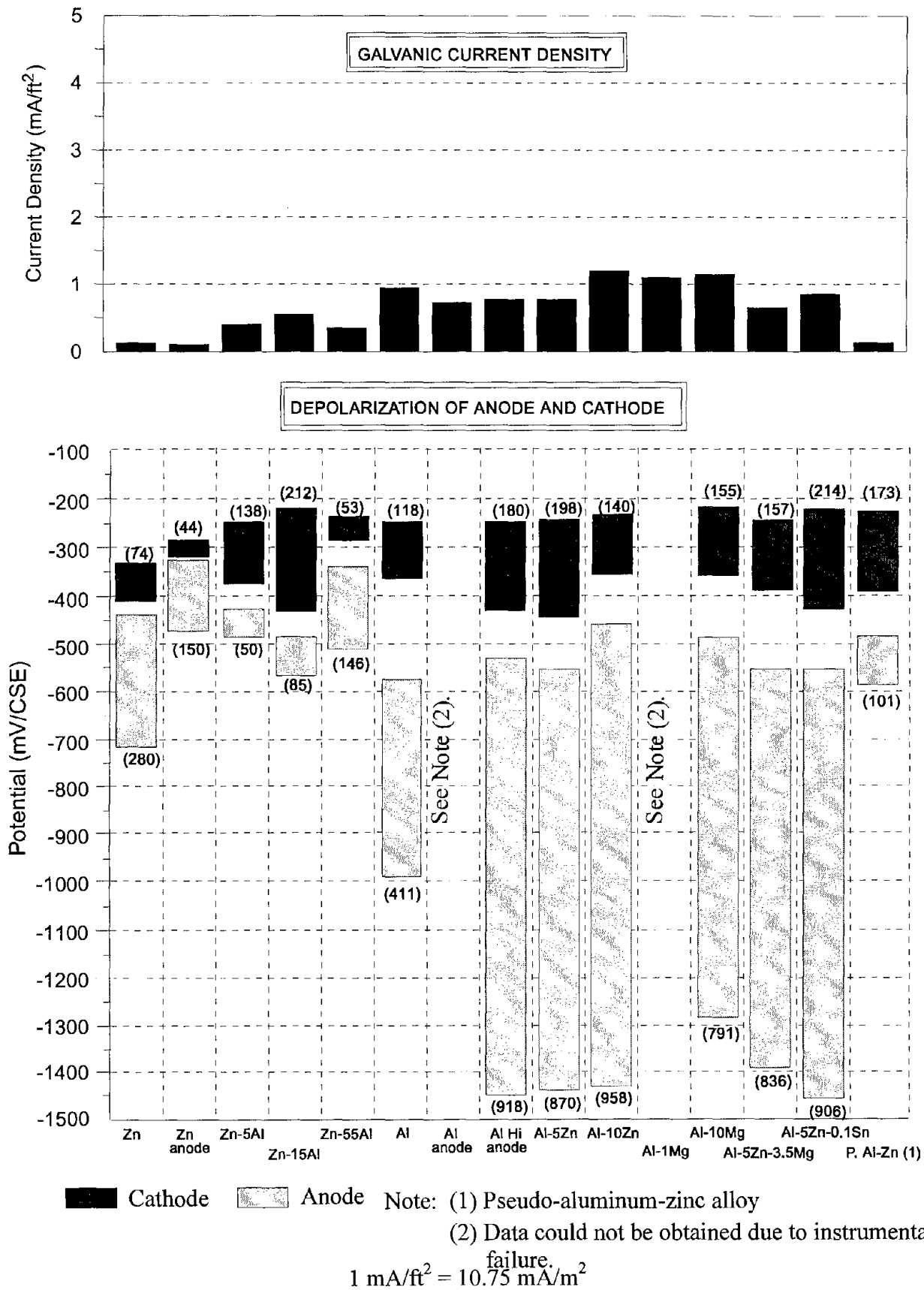


Figure 61. Environmental tests - galvanic current, instant-off potential, potential, and polarization data, 70°F (21°C), 70% RH (1300 ppm Cl).

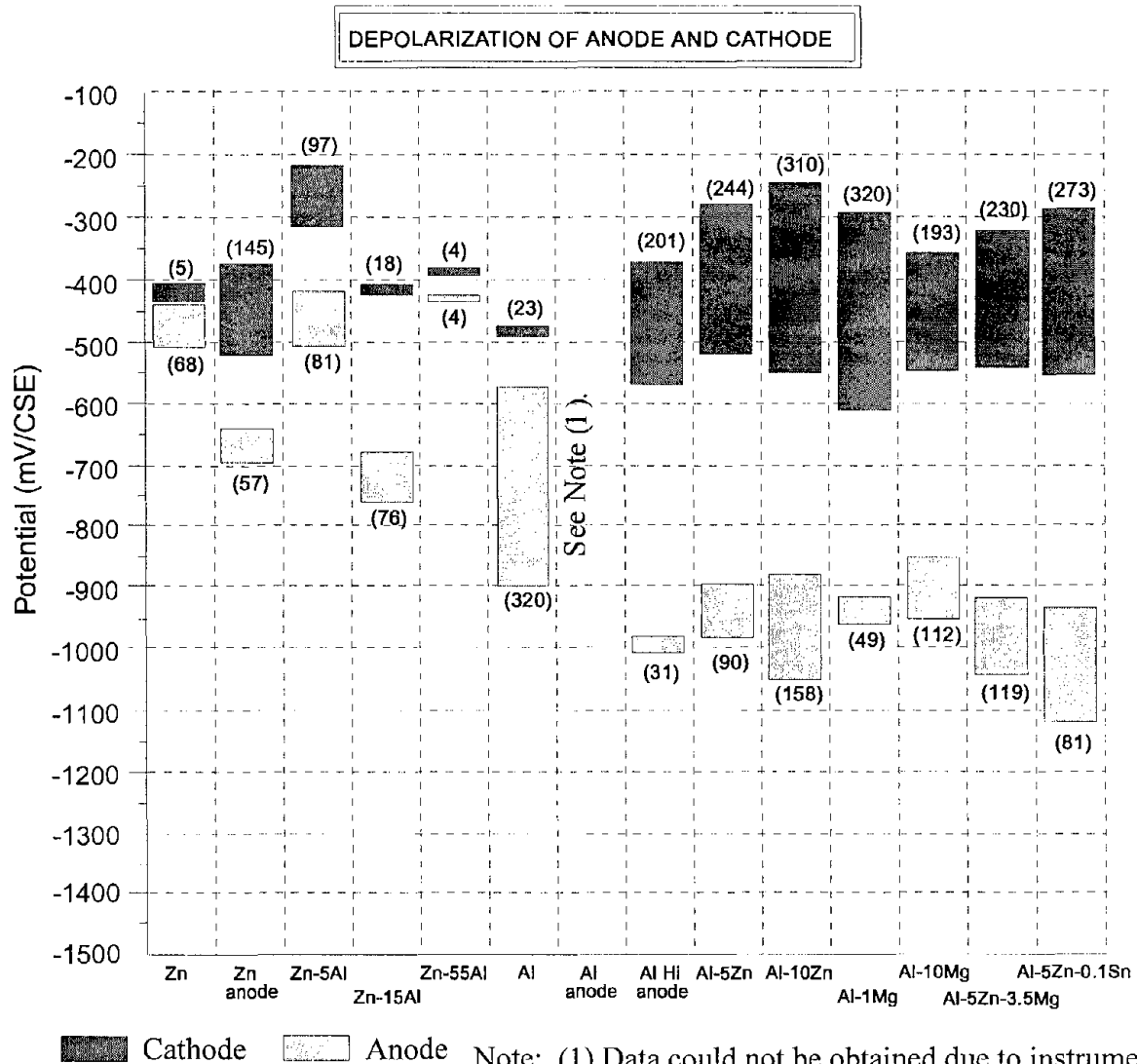
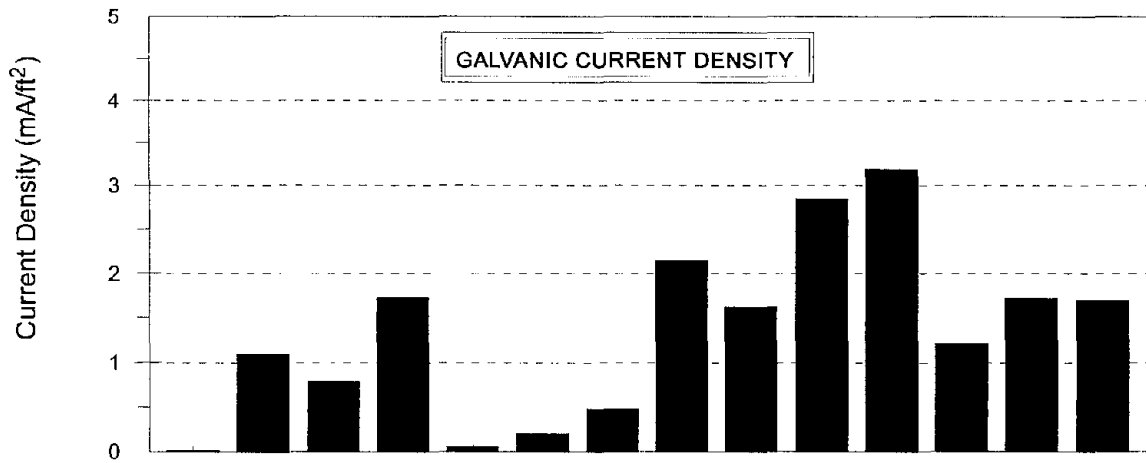


Figure 62. Environmental tests - galvanic current, instant-off potential, potential, and polarization data, 70°F (21°C), 70% RH (3800 ppm Cl).

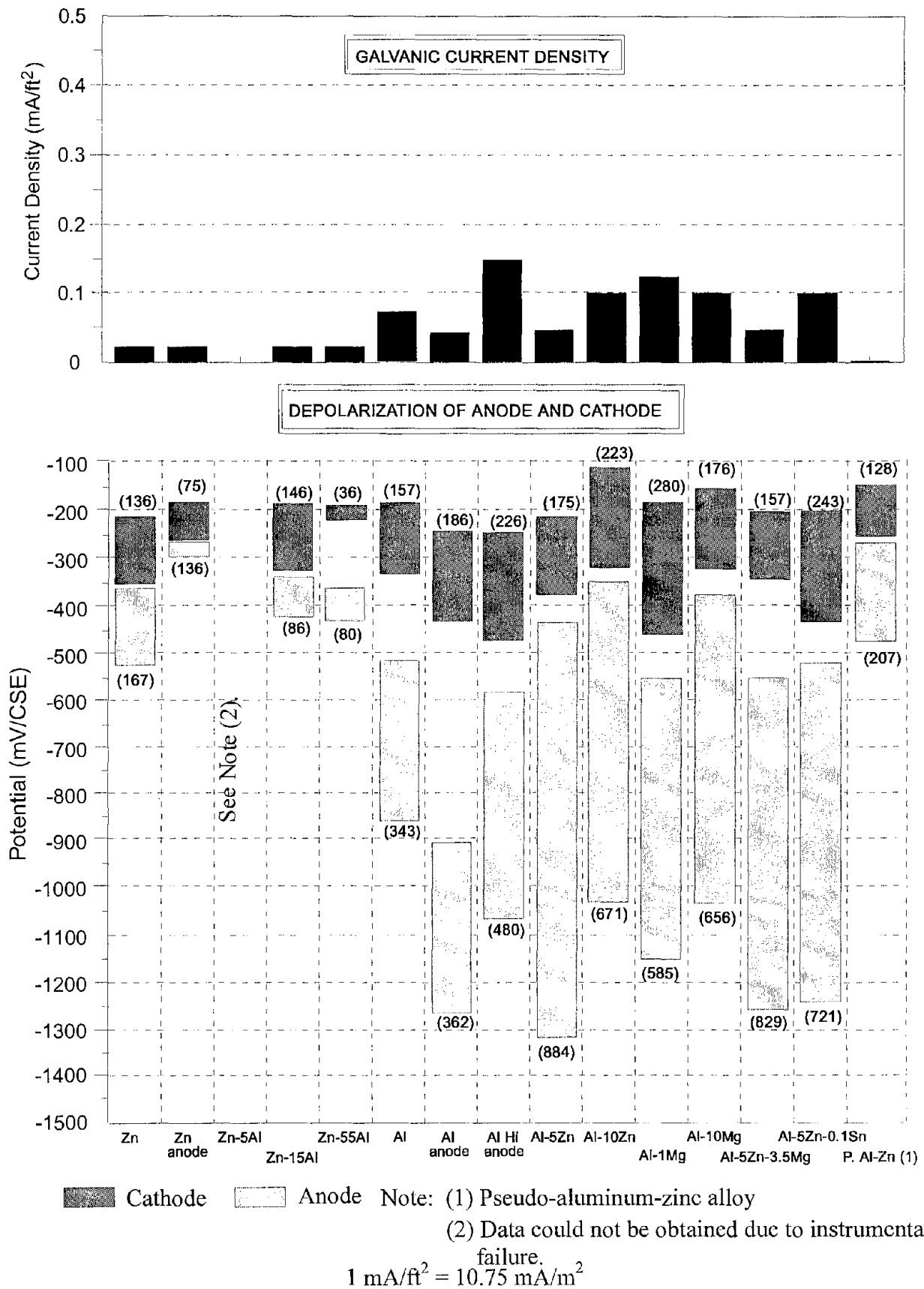
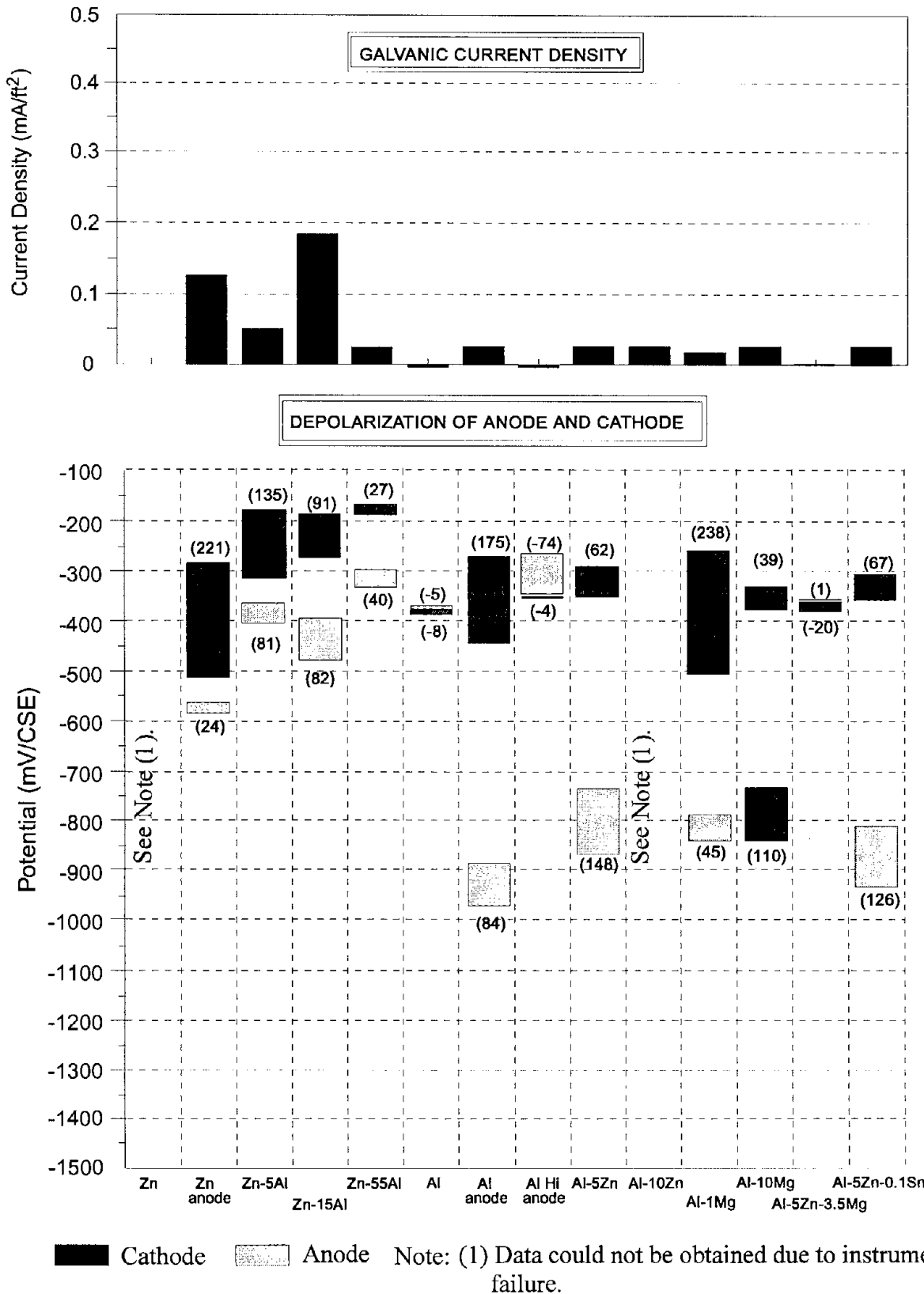
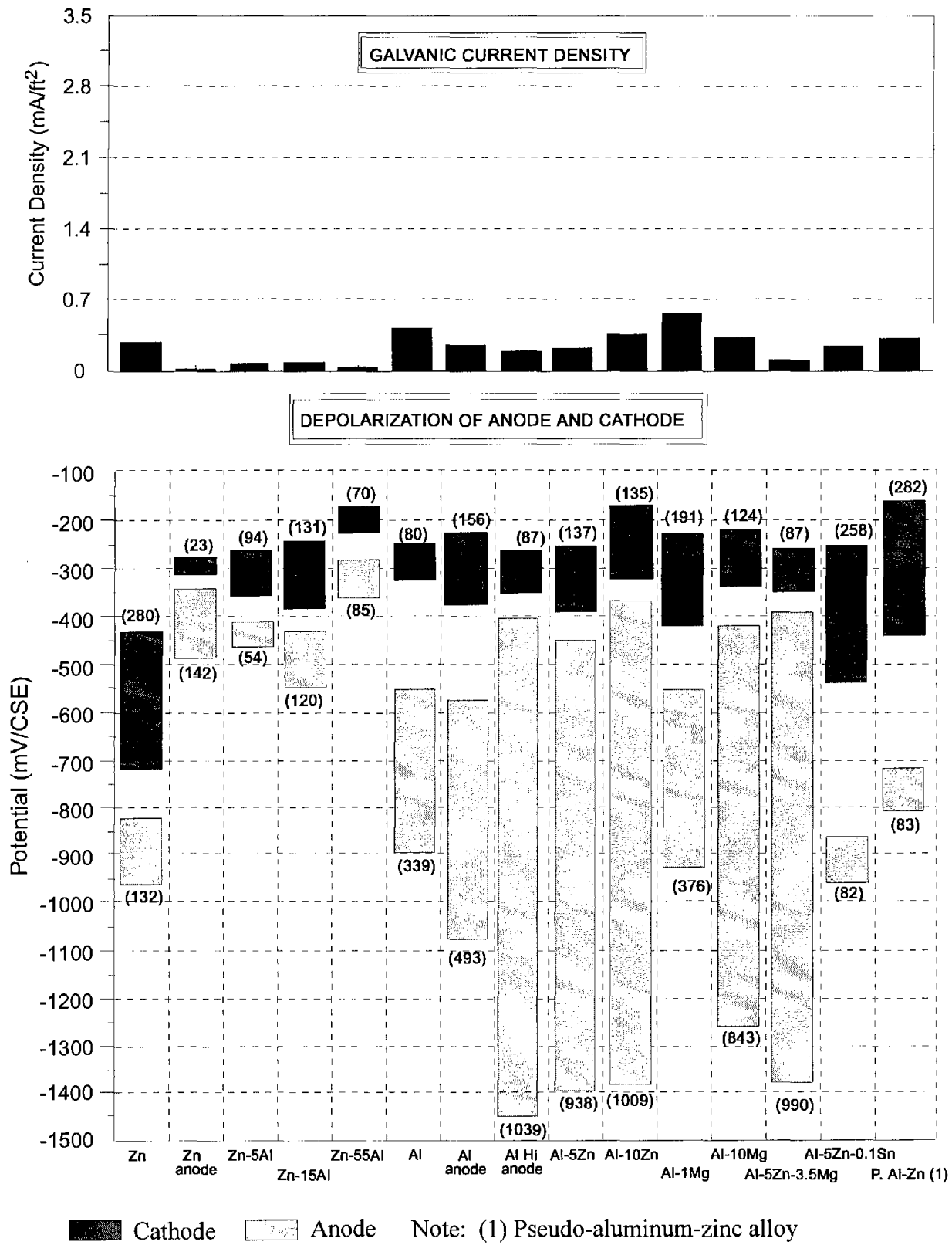


Figure 63. Environmental tests - galvanic current, instant-off potential, potential, and polarization data, 70°F (21°C), 40% RH (1300 ppm Cl).



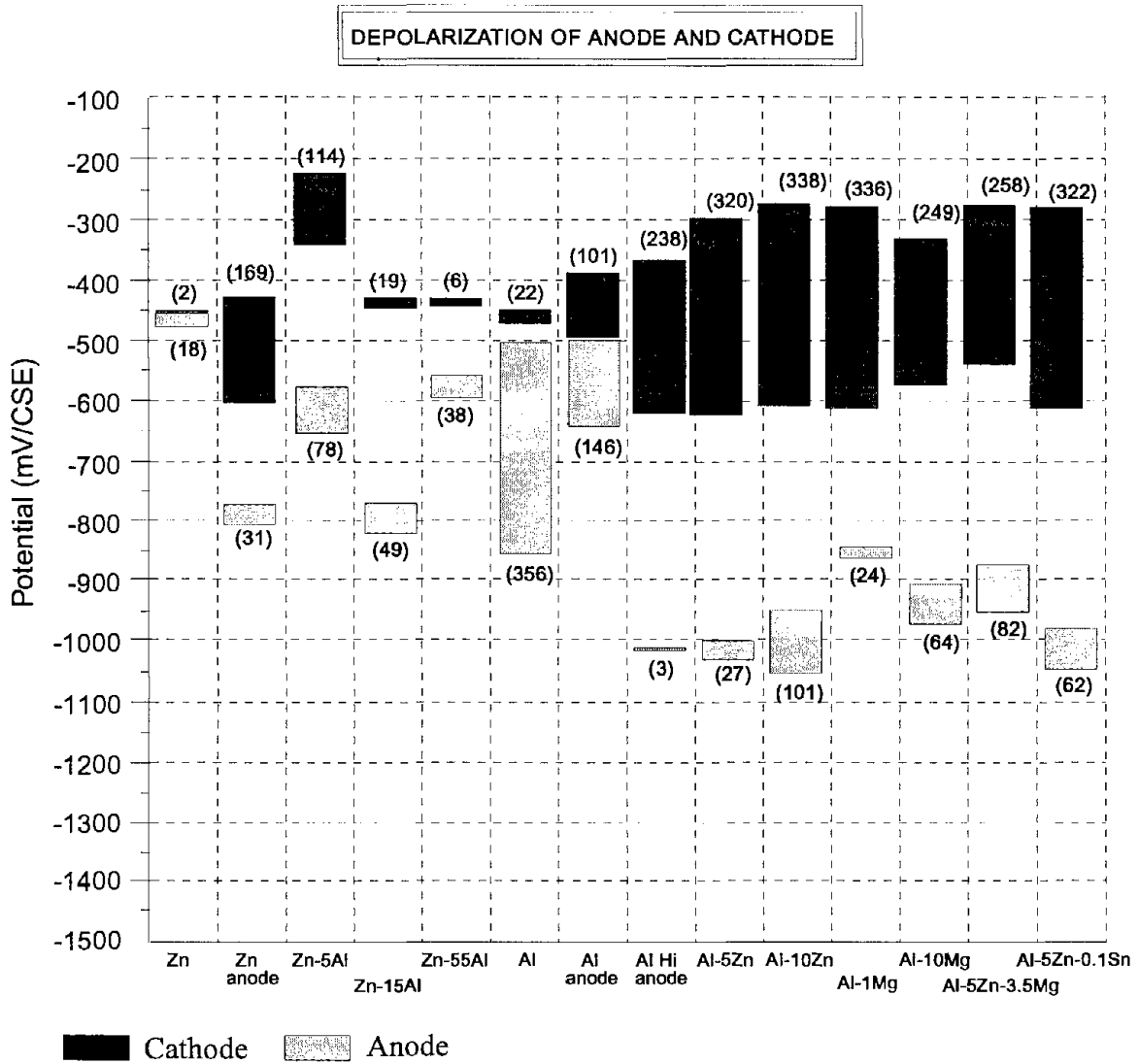
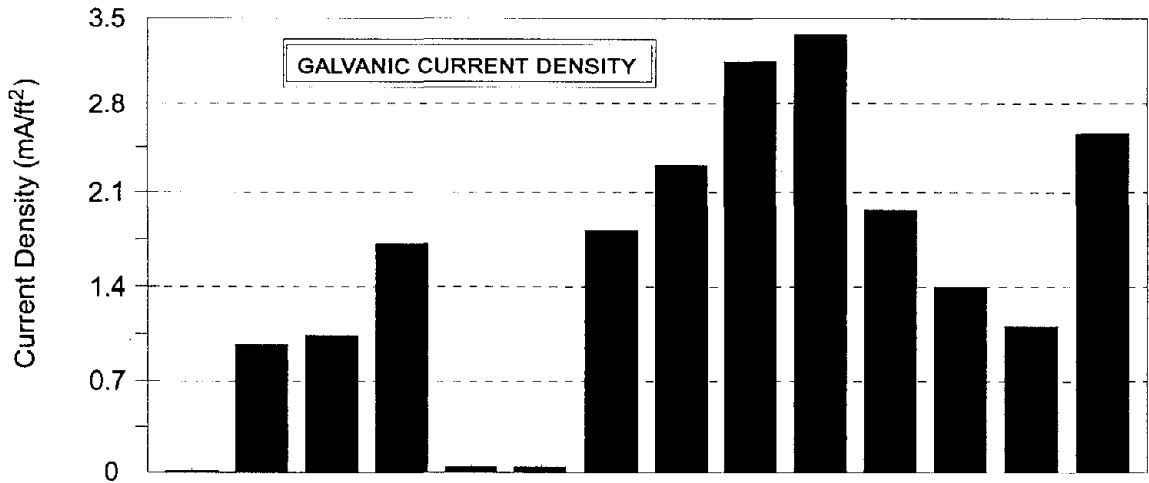
$$1 \text{ mA/ft}^2 = 10.75 \text{ mA/m}^2$$

Figure 64. Environmental tests - galvanic current, instant-off potential, potential, and polarization data, 70°F (21°C), 40% RH (3800 ppm Cl).



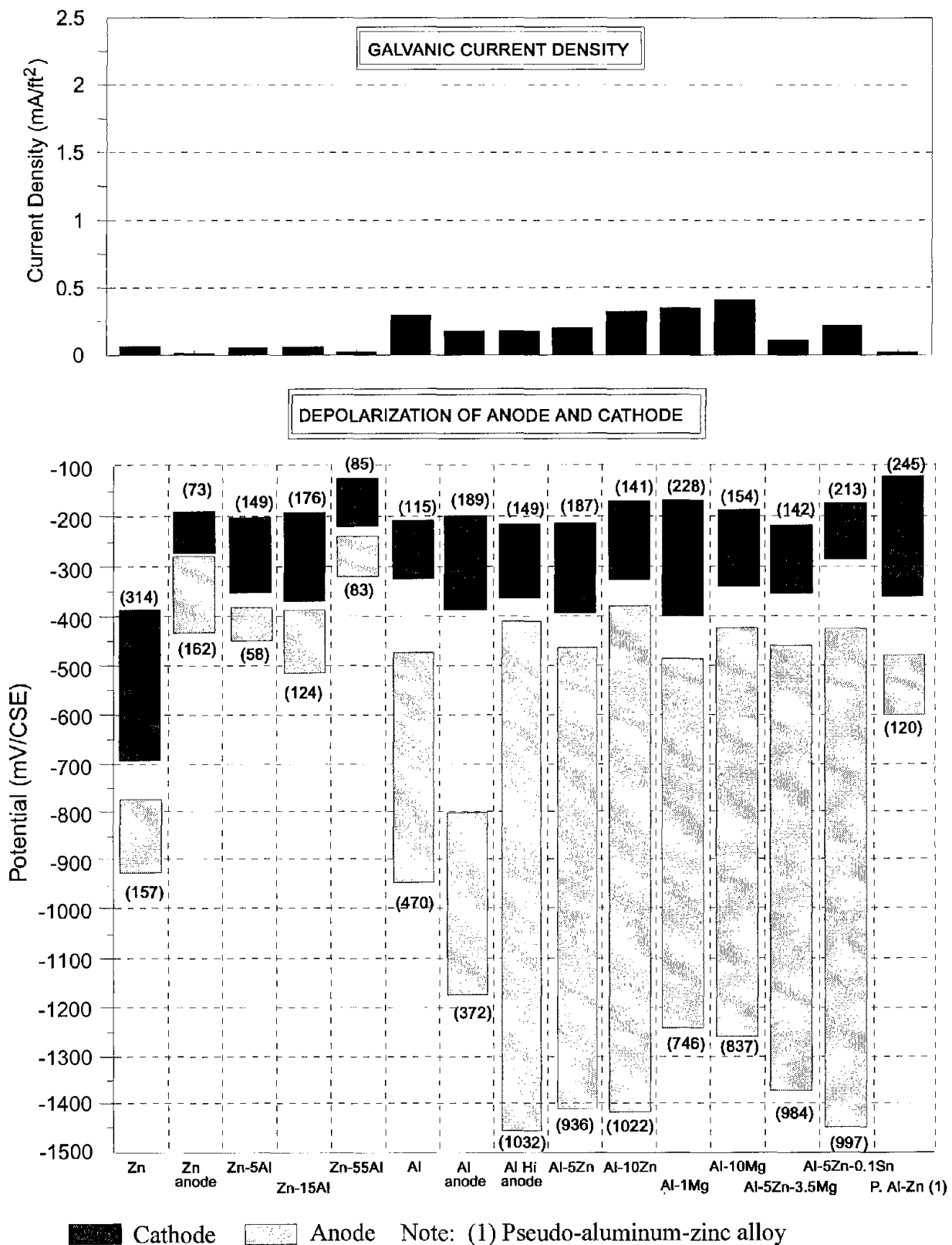
$$1 \text{ mA/ft}^2 = 10.75 \text{ mA/m}^2$$

Figure 65. Environmental tests - galvanic current, instant-off potential, potential, and polarization data, 40°F (4°C), 90% RH (1300 ppm Cl).



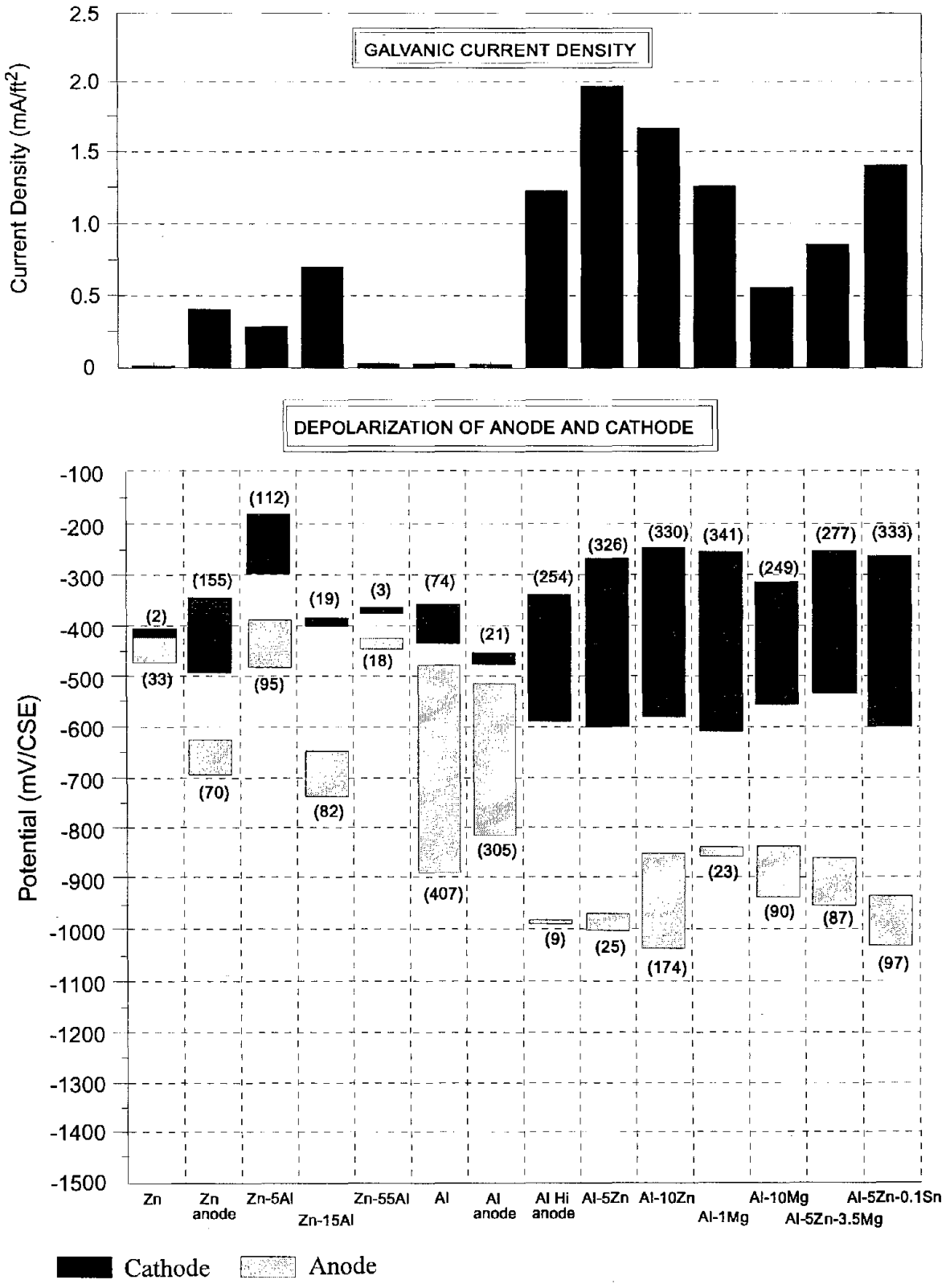
$$1 \text{ mA/ft}^2 = 10.75 \text{ mA/m}^2$$

Figure 66. Environmental tests - galvanic current, instant-off potential, potential, and polarization data, 40°F (4°C), 90% RH (3800 ppm Cl).



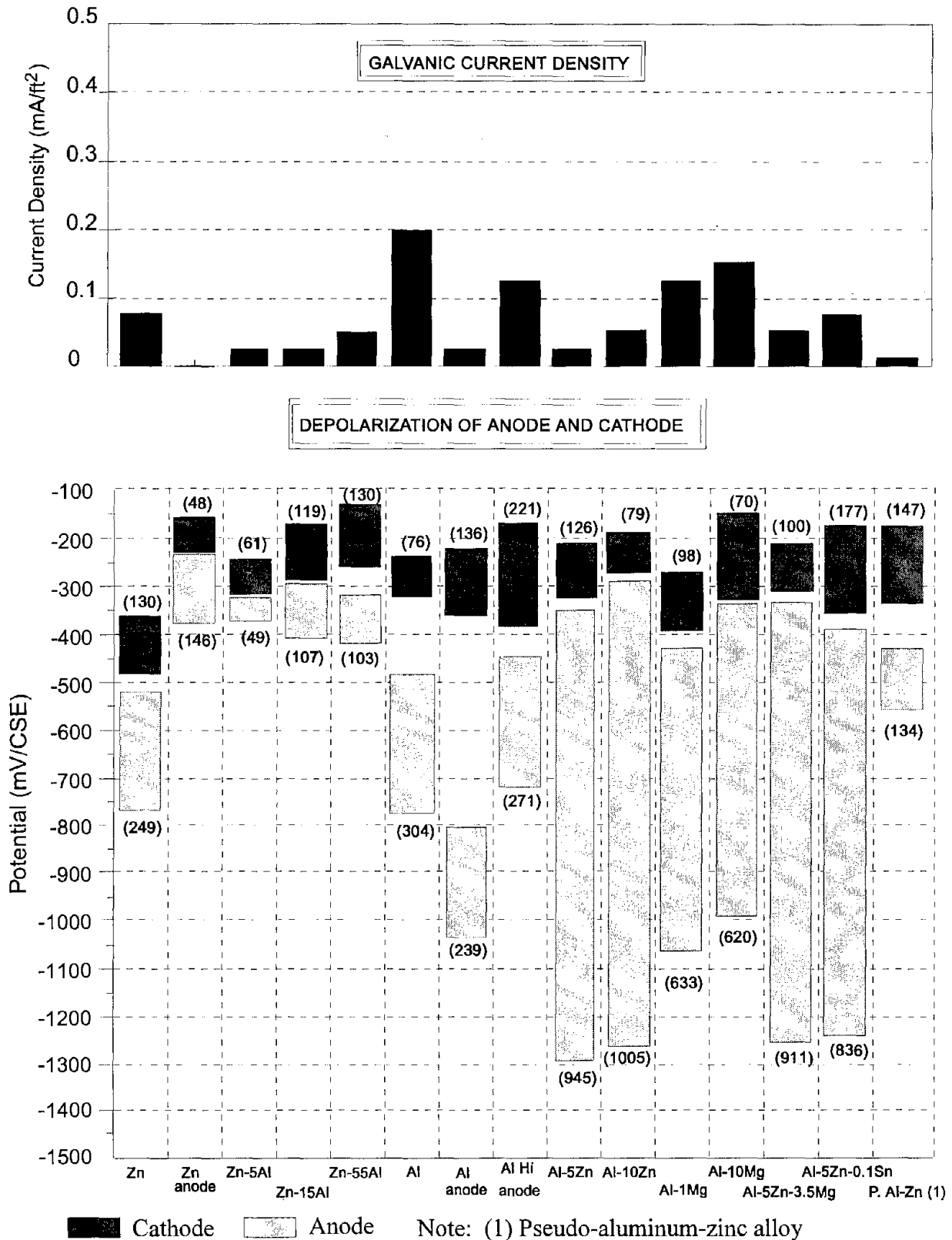
$$1 \text{ mA/ft}^2 = 10.75 \text{ mA/m}^2$$

Figure 67. Environmental tests - galvanic current, instant-off potential, potential, and polarization data, 40°F (4°C), 70% RH (1300 ppm Cl).



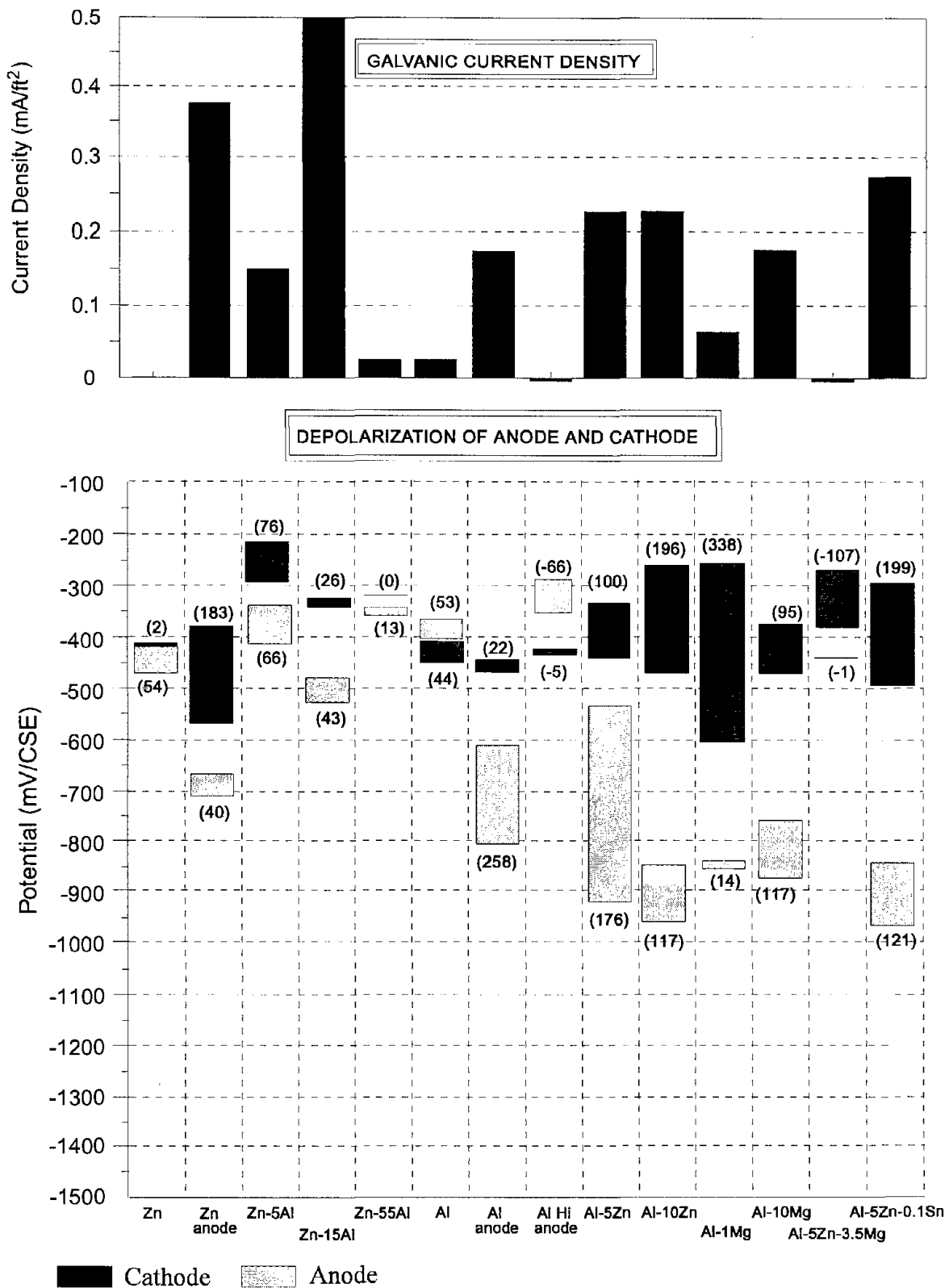
1 mA/ft² = 10.75 mA/m²

Figure 68. Environmental tests - galvanic current, instant-off potential, potential, and polarization data, 40°F (4°C), 70% RH (3800 ppm Cl).



$$1 \text{ mA/ft}^2 = 10.75 \text{ mA/m}^2$$

Figure 69. Environmental tests - galvanic current, instant-off potential, potential, and polarization data, 40°F (4°C), 40% RH (1300 ppm Cl).



$$1 \text{ mA/ft}^2 = 10.75 \text{ mA/m}^2$$

Figure 70. Environmental tests - galvanic current, instant-off potential, potential, and polarization data, 40°F (4°C), 40% RH (3800 ppm Cl).

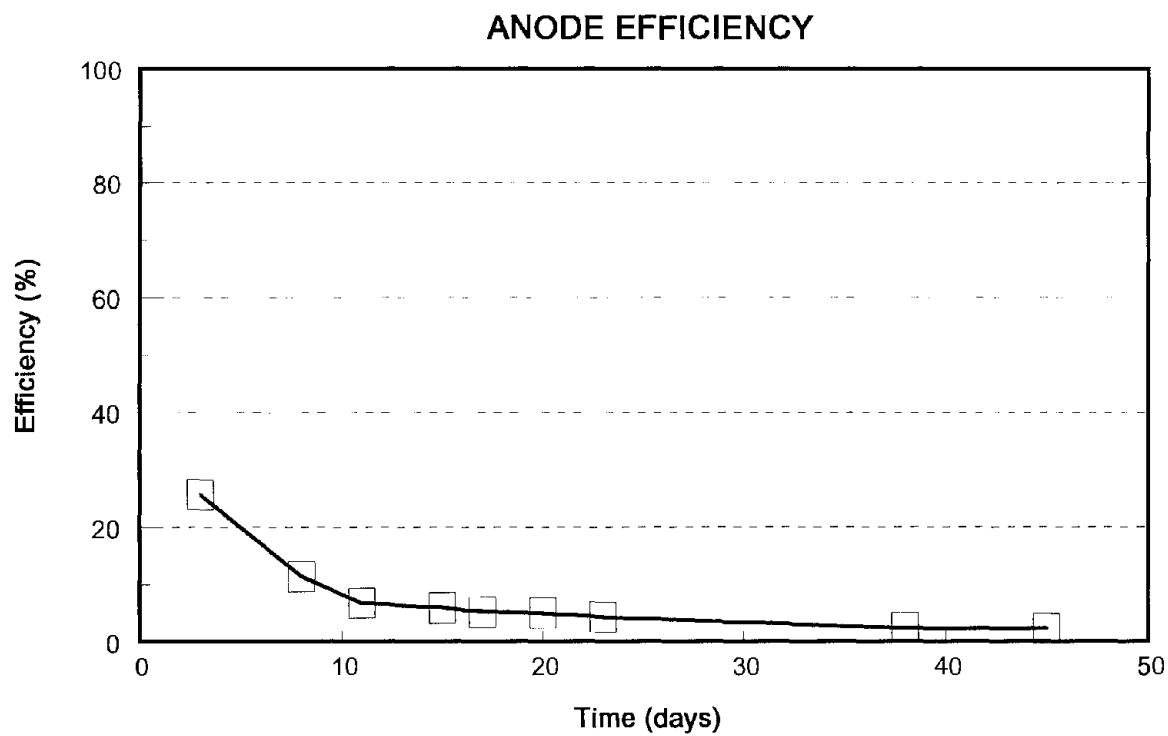
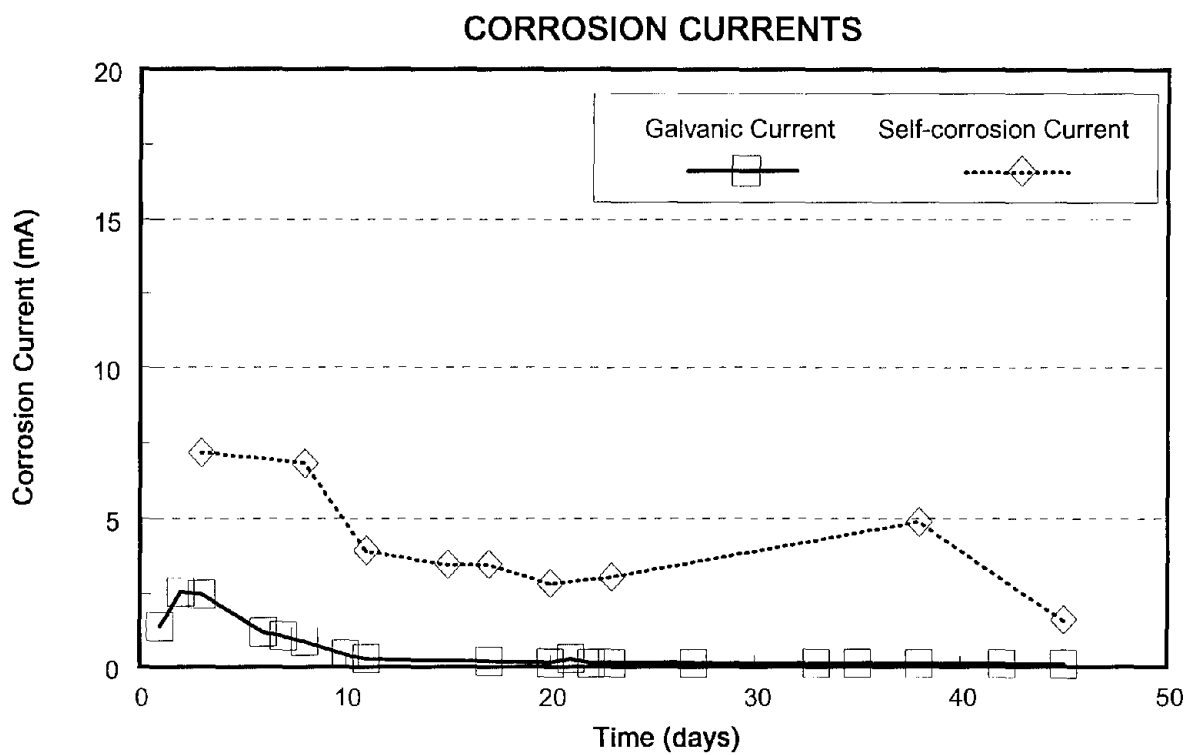


Figure 71. Galvanic, self-corrosion, and anode efficiency data for pure zinc.

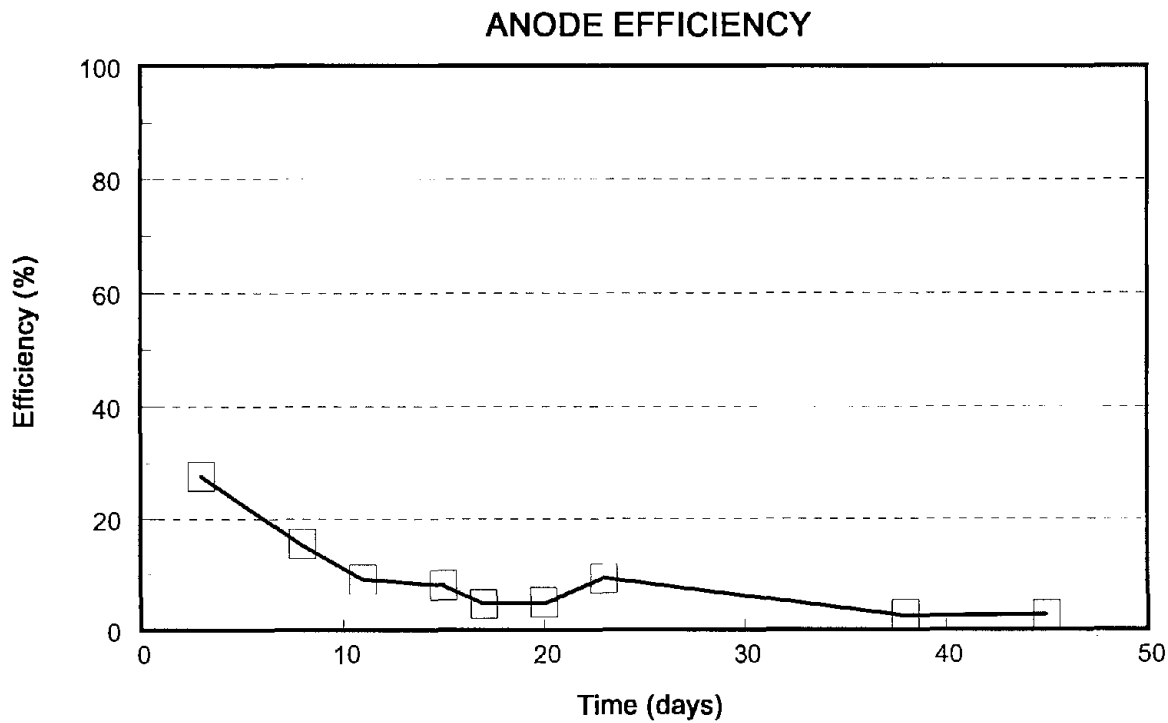
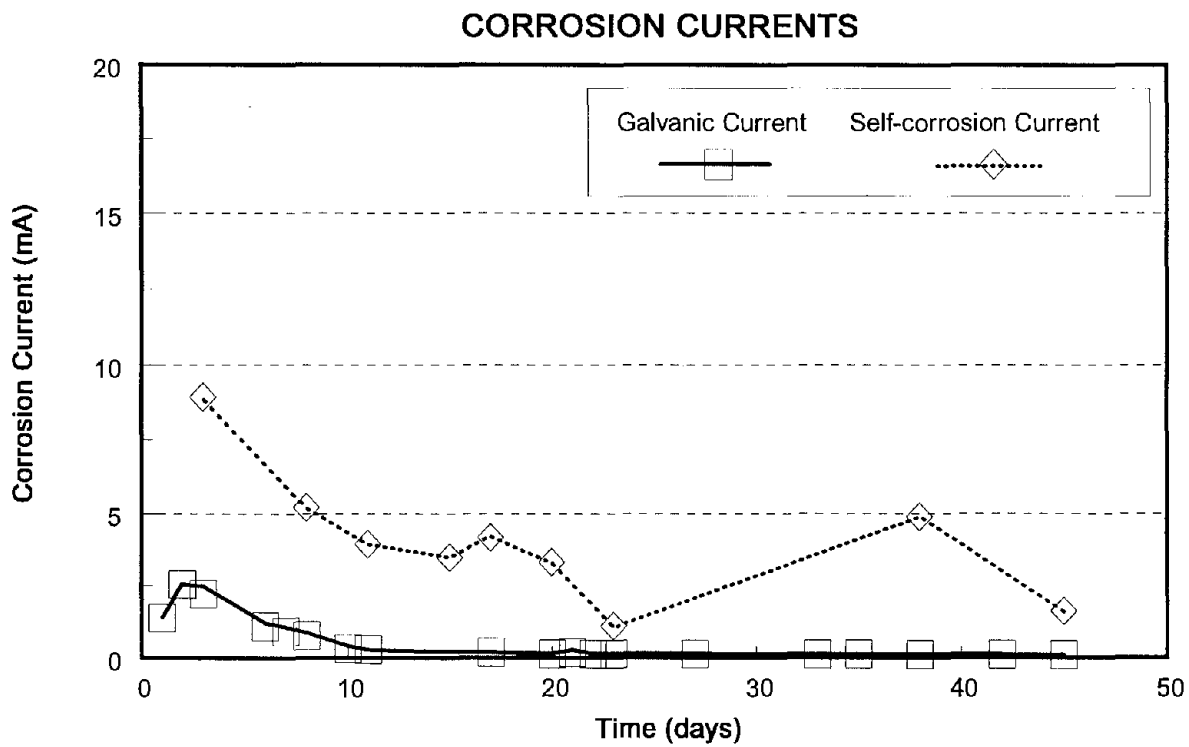


Figure 72. Galvanic, self-corrosion, and anode efficiency data for zinc alloy 1.

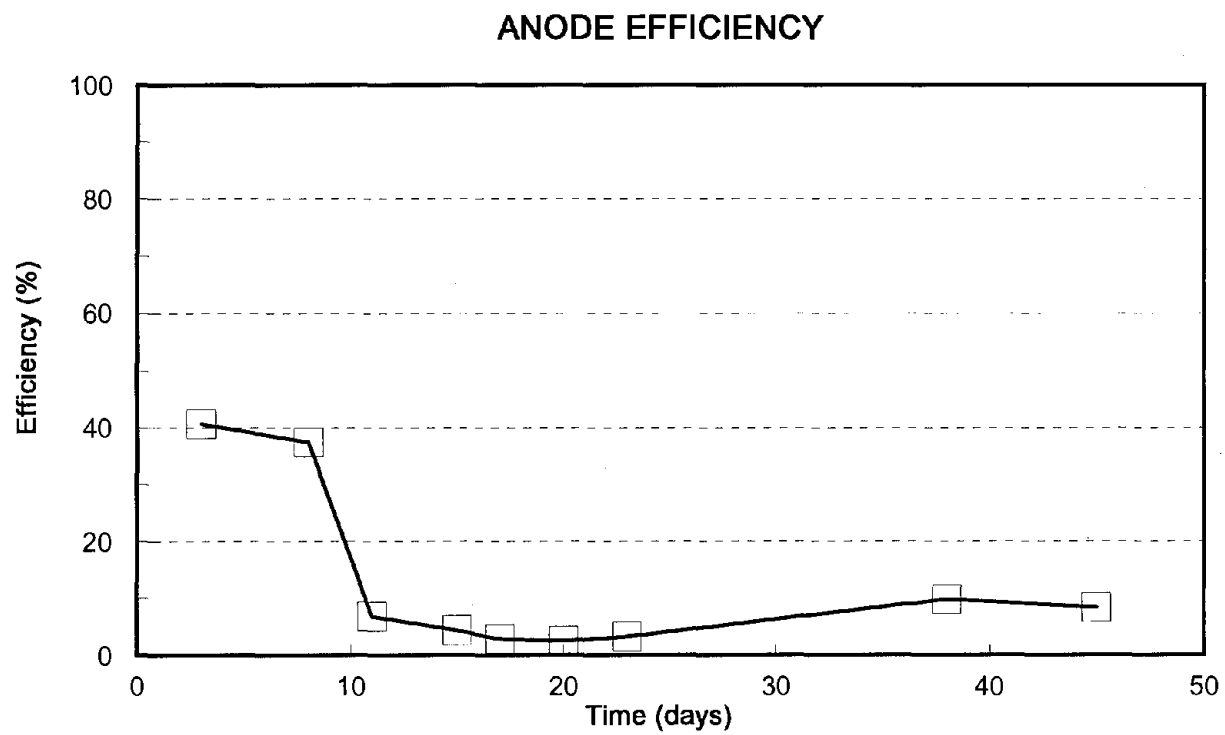
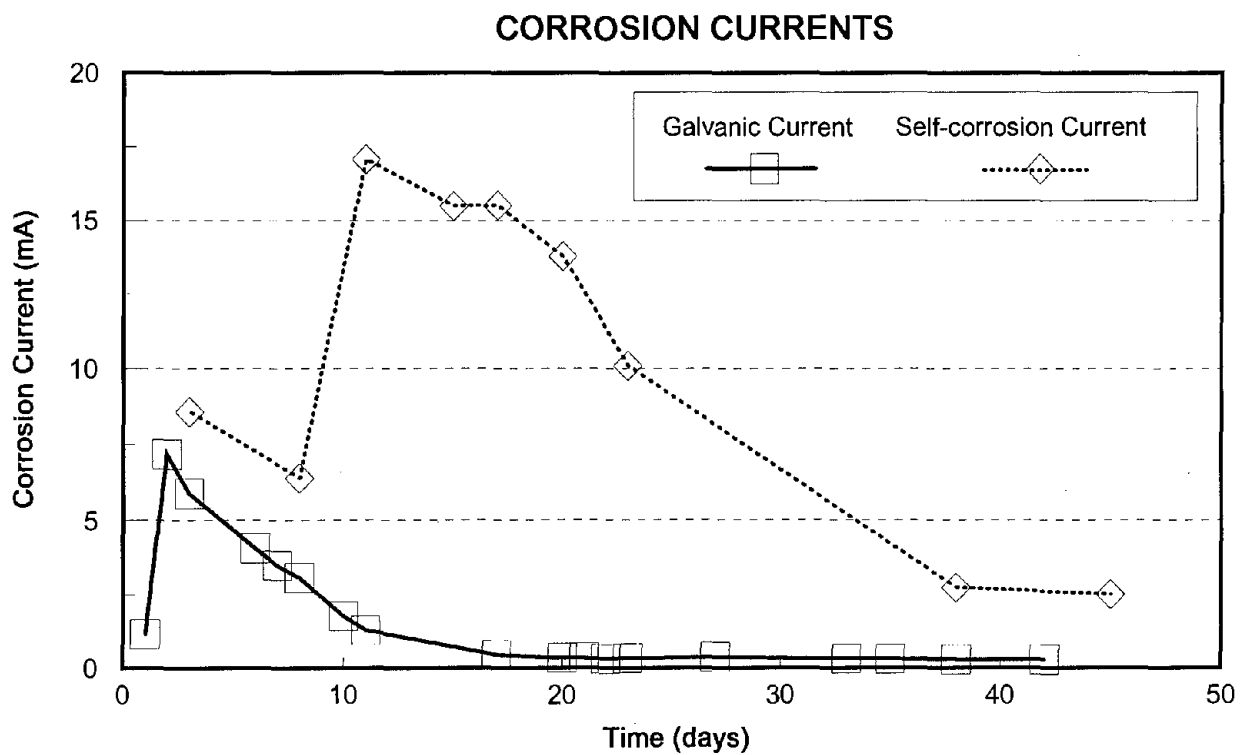


Figure 73. Galvanic, self-corrosion, and anode efficiency data for zinc-5% Al.

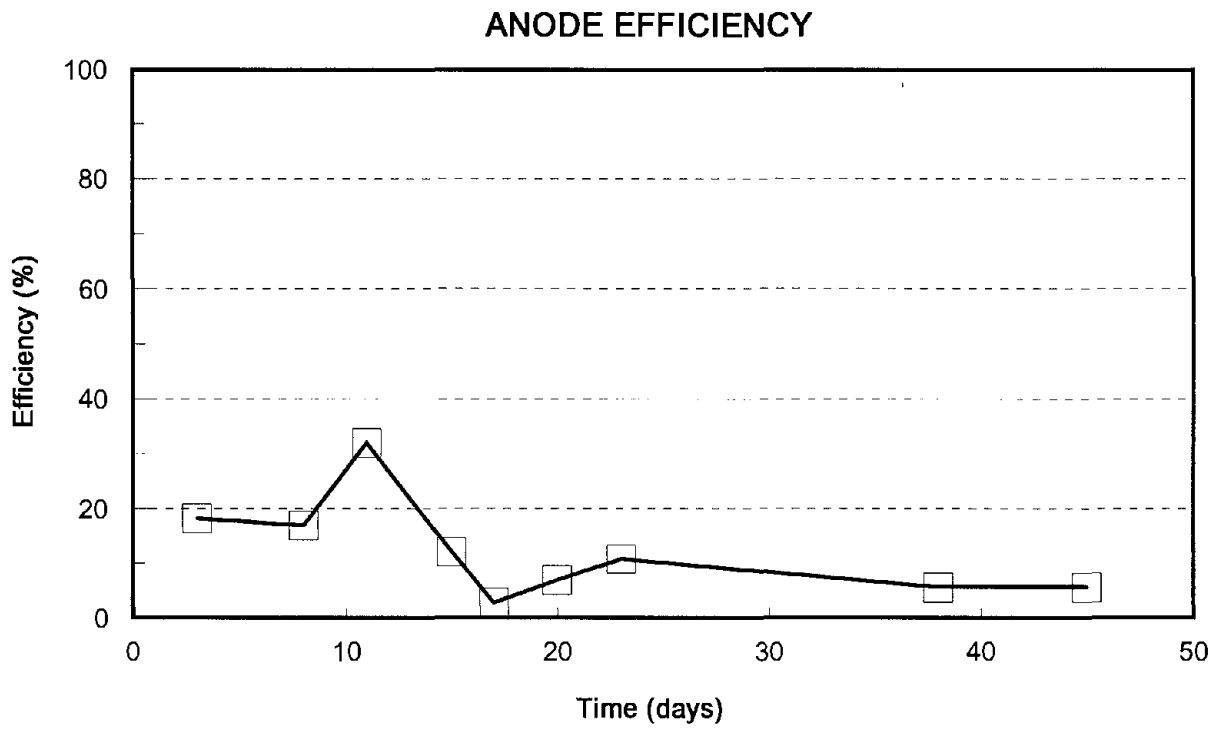
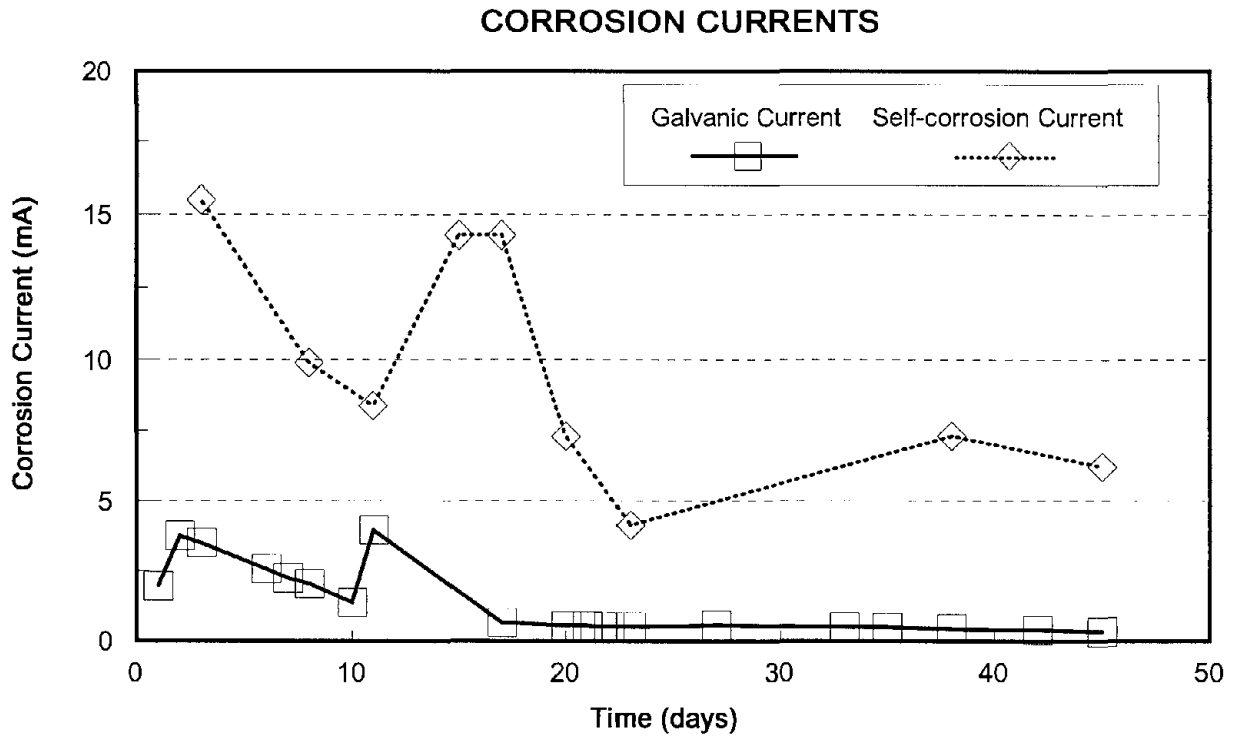


Figure 74. Galvanic, self-corrosion, and anode efficiency data for zinc-15% Al.

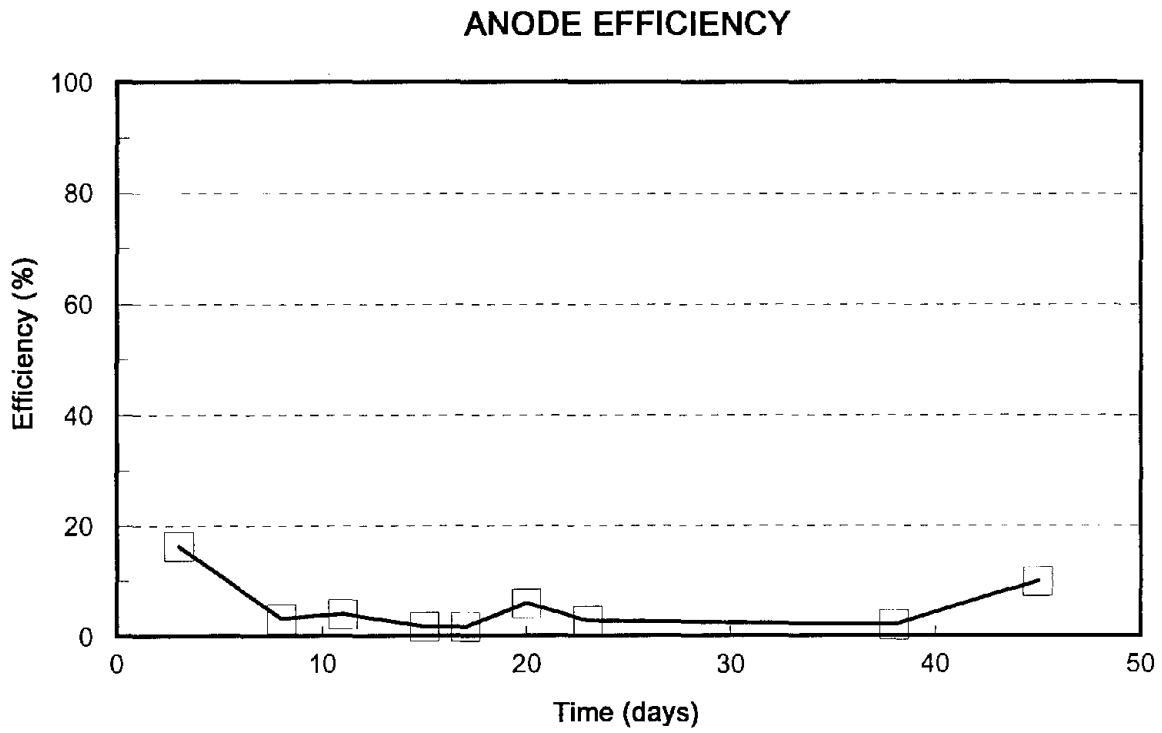
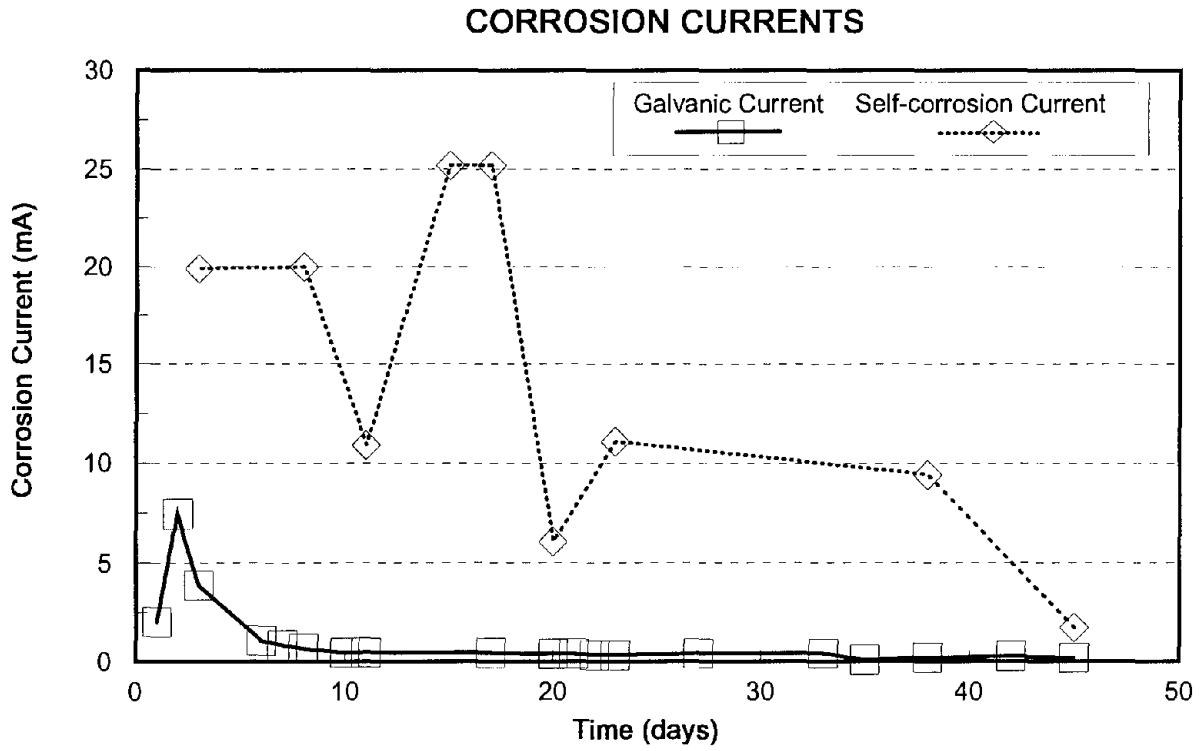


Figure 75. Galvanic, self-corrosion, and anode efficiency data for zinc-55% Al.

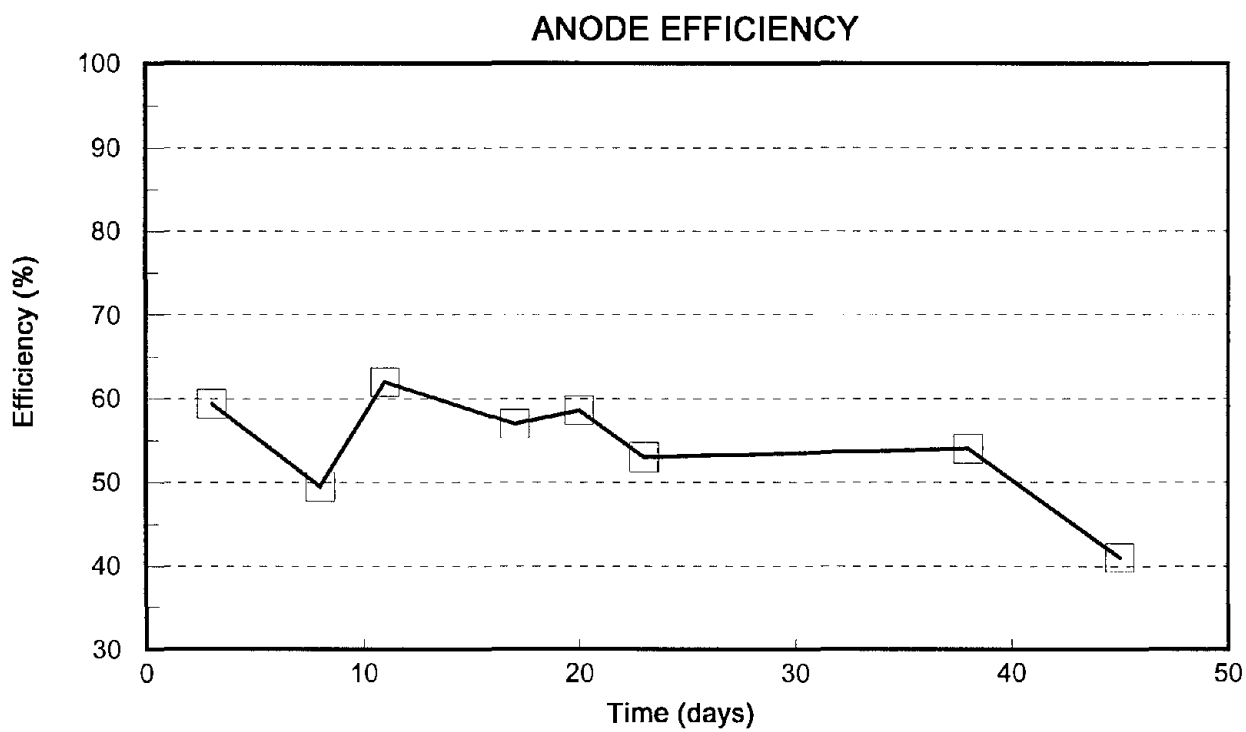
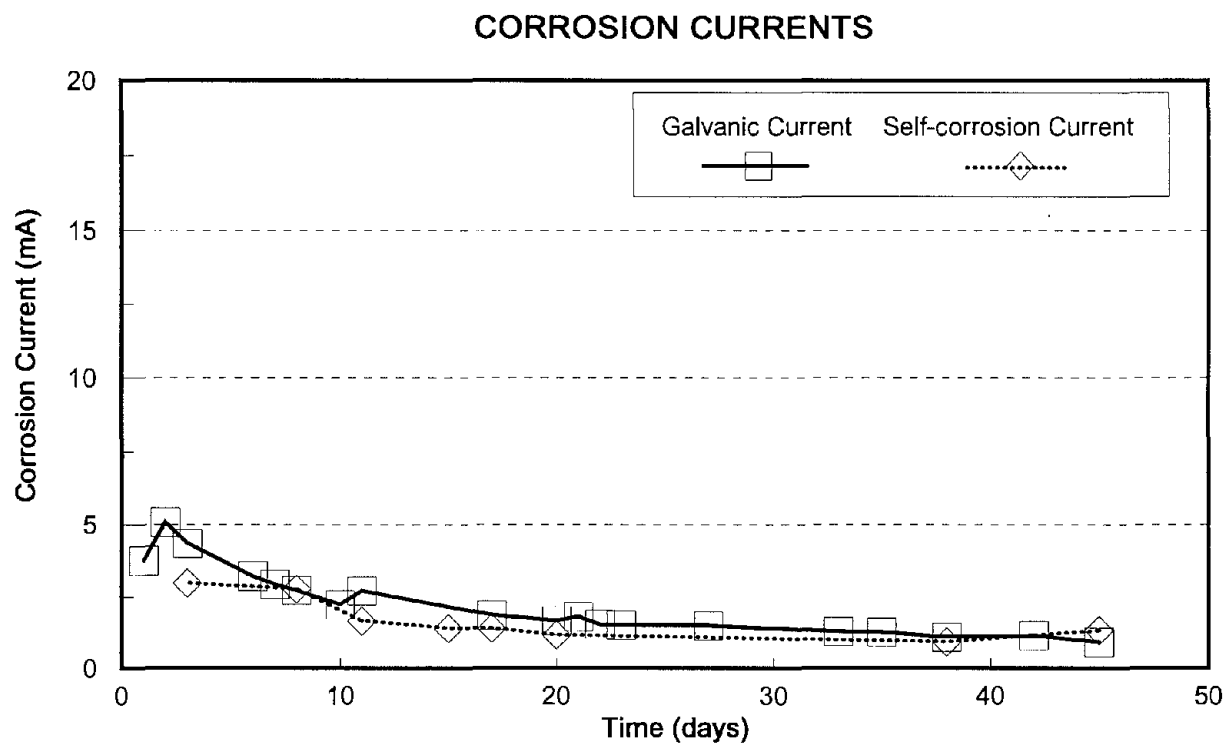


Figure 76. Galvanic, self-corrosion, and anode efficiency data for pure aluminum.

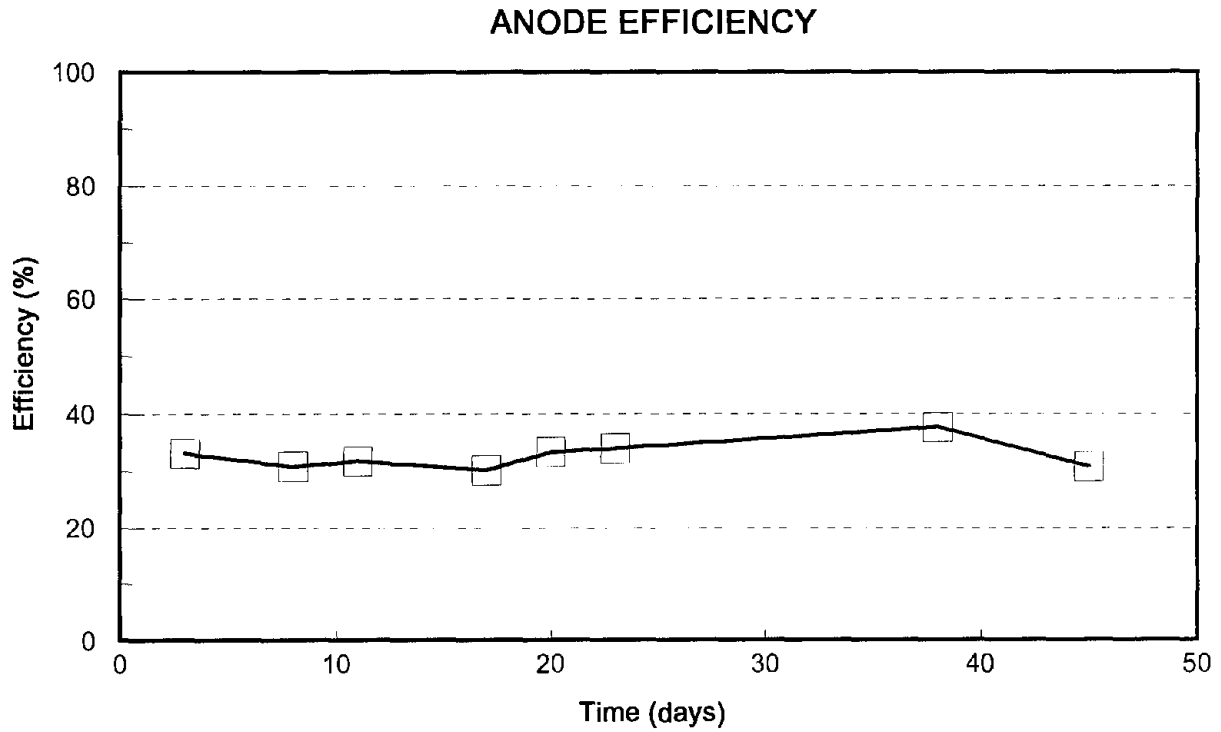
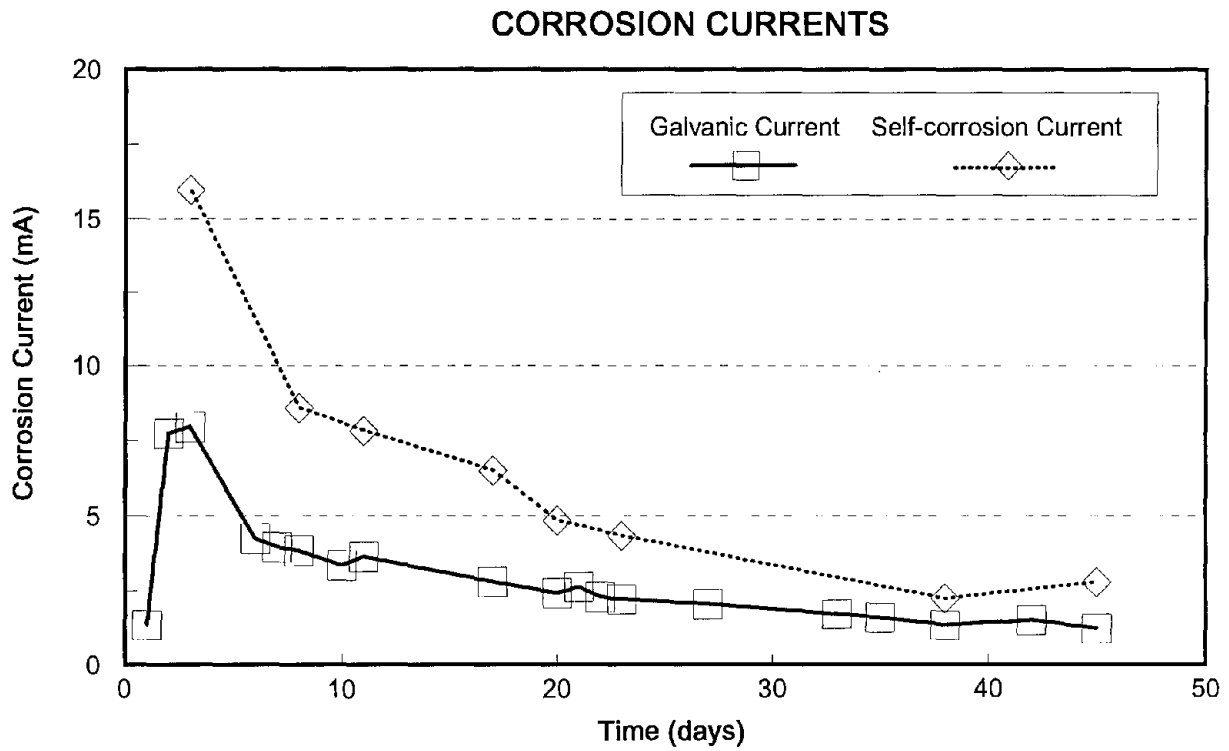


Figure 77. Galvanic, self-corrosion, and anode efficiency data for aluminum alloy 1.

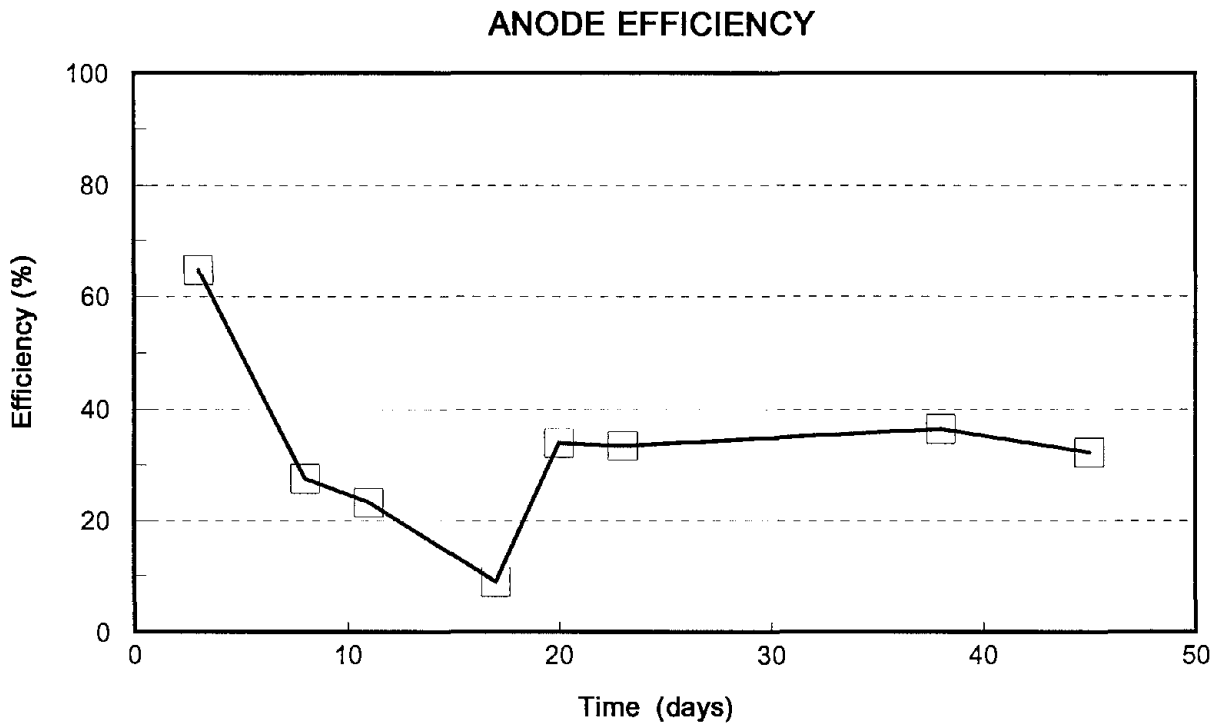
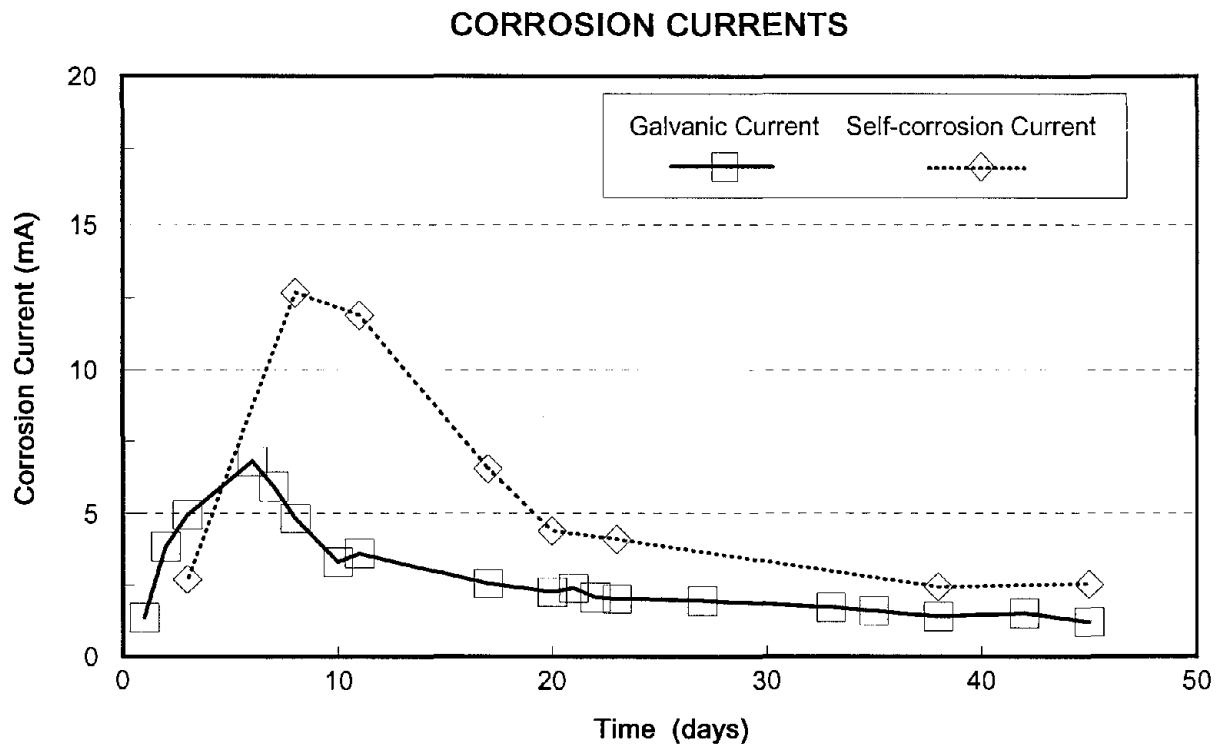


Figure 78. Galvanic, self-corrosion, and anode efficiency data for aluminum alloy 2.

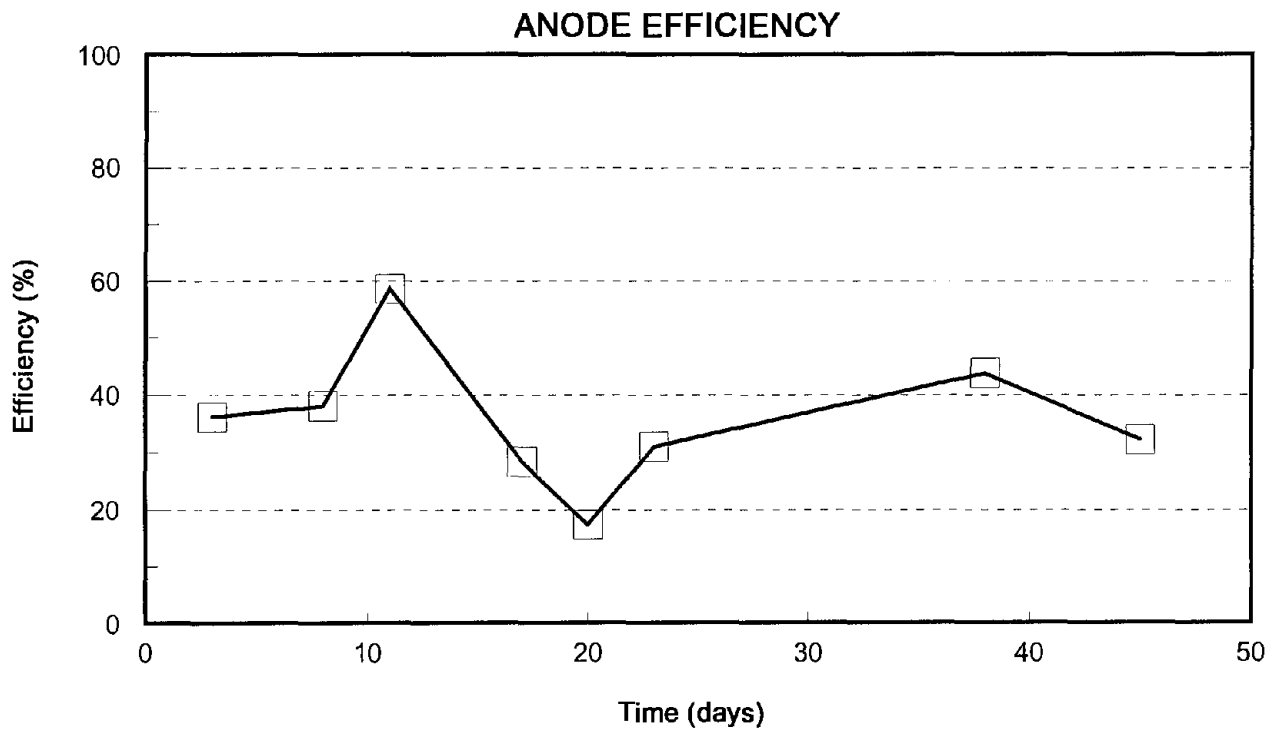
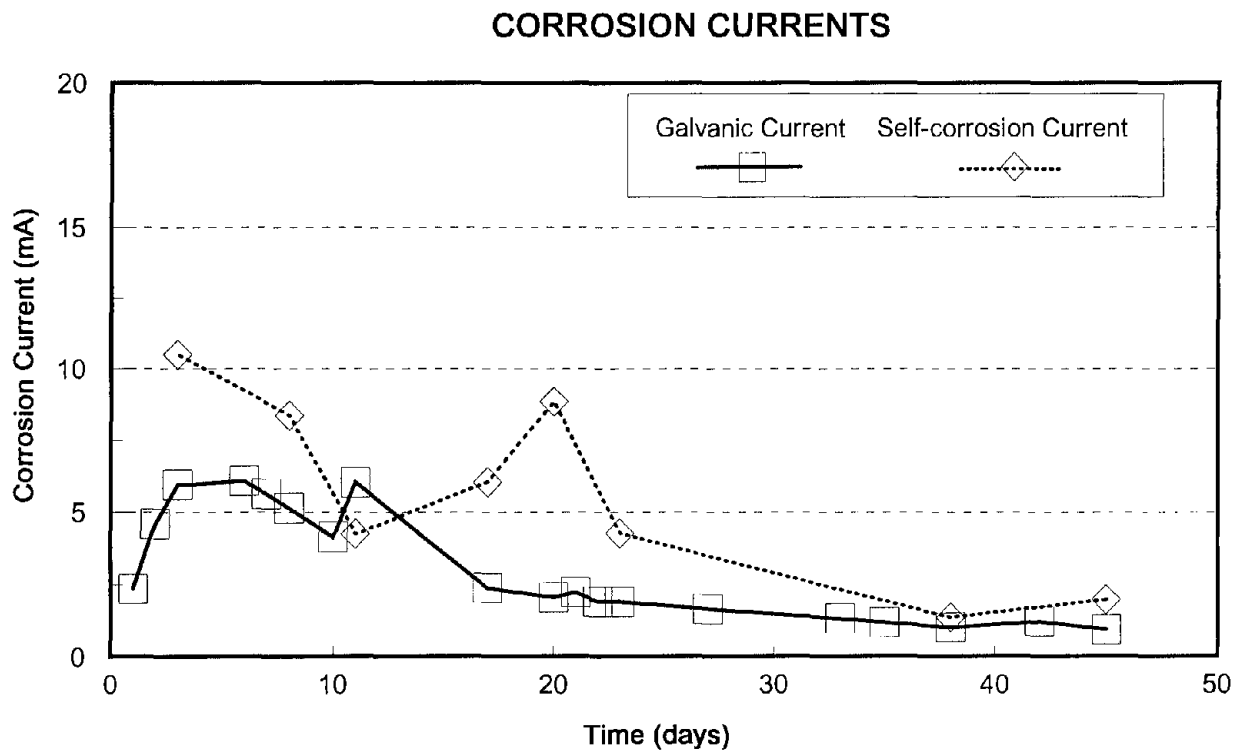


Figure 79. Galvanic, self-corrosion, and anode efficiency data for aluminum-5% Zn.

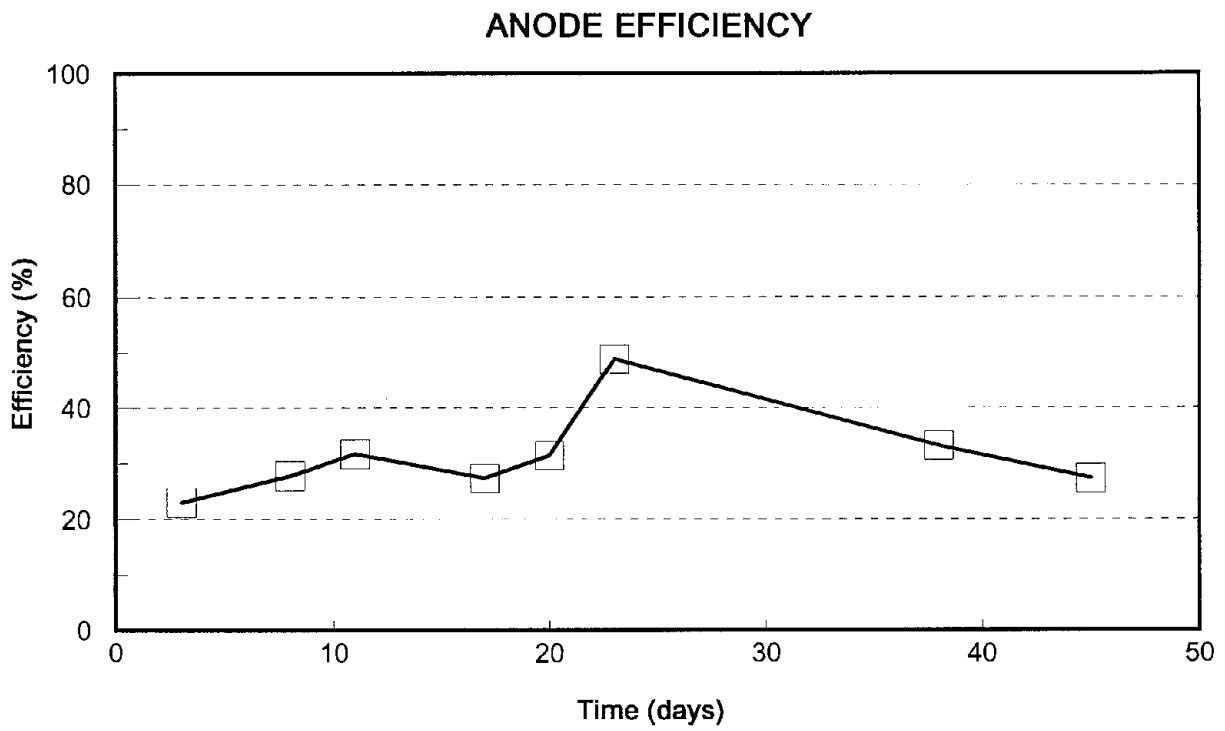
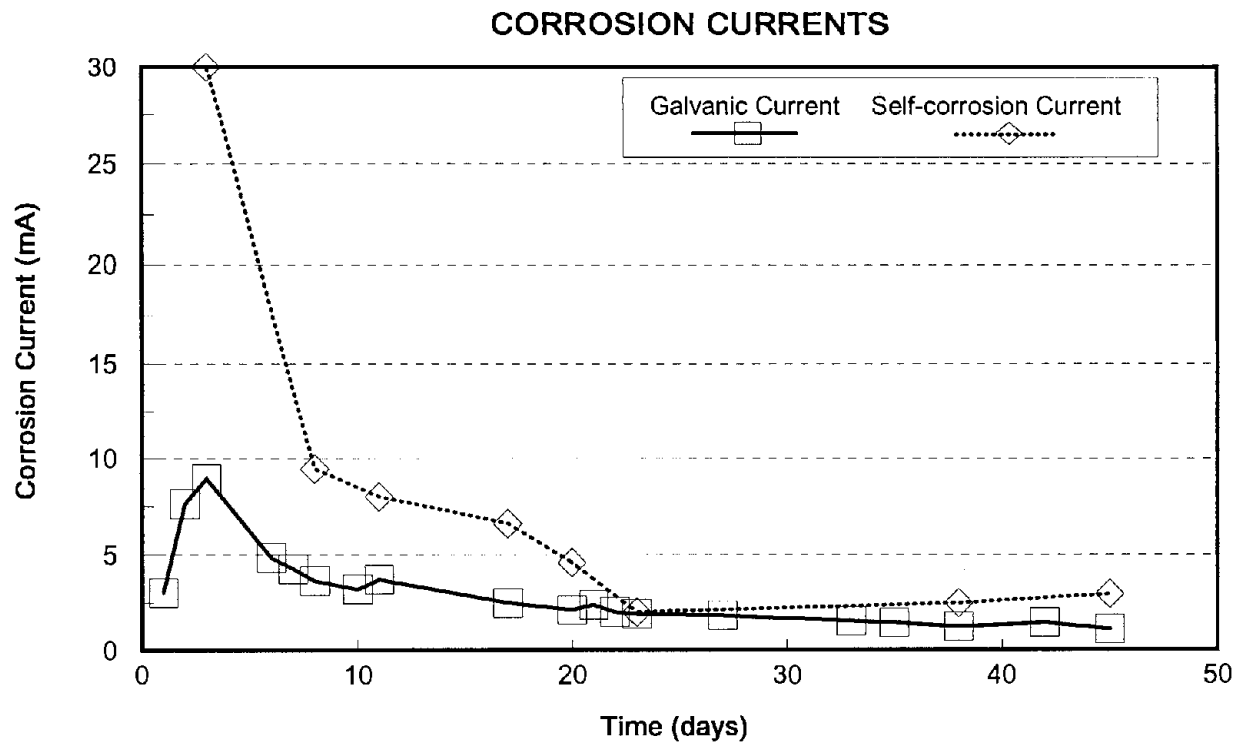


Figure 80. Galvanic, self-corrosion, and anode efficiency data for aluminum-10% Zn.

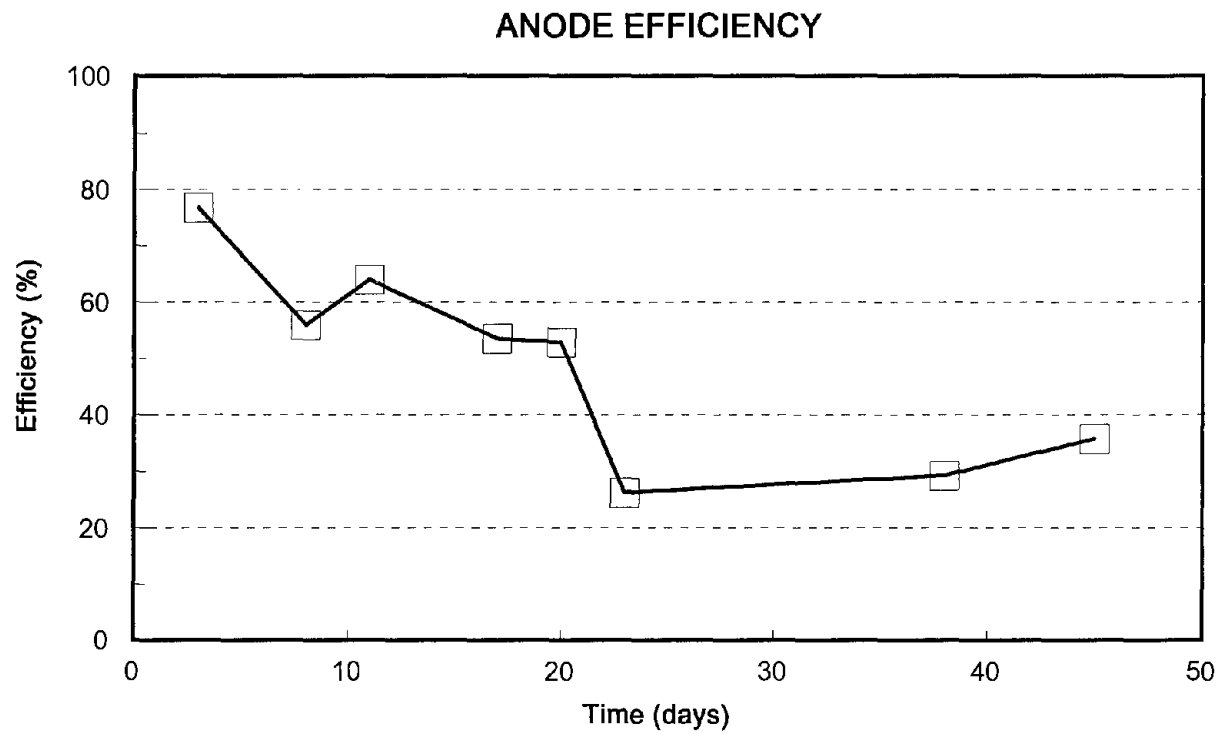
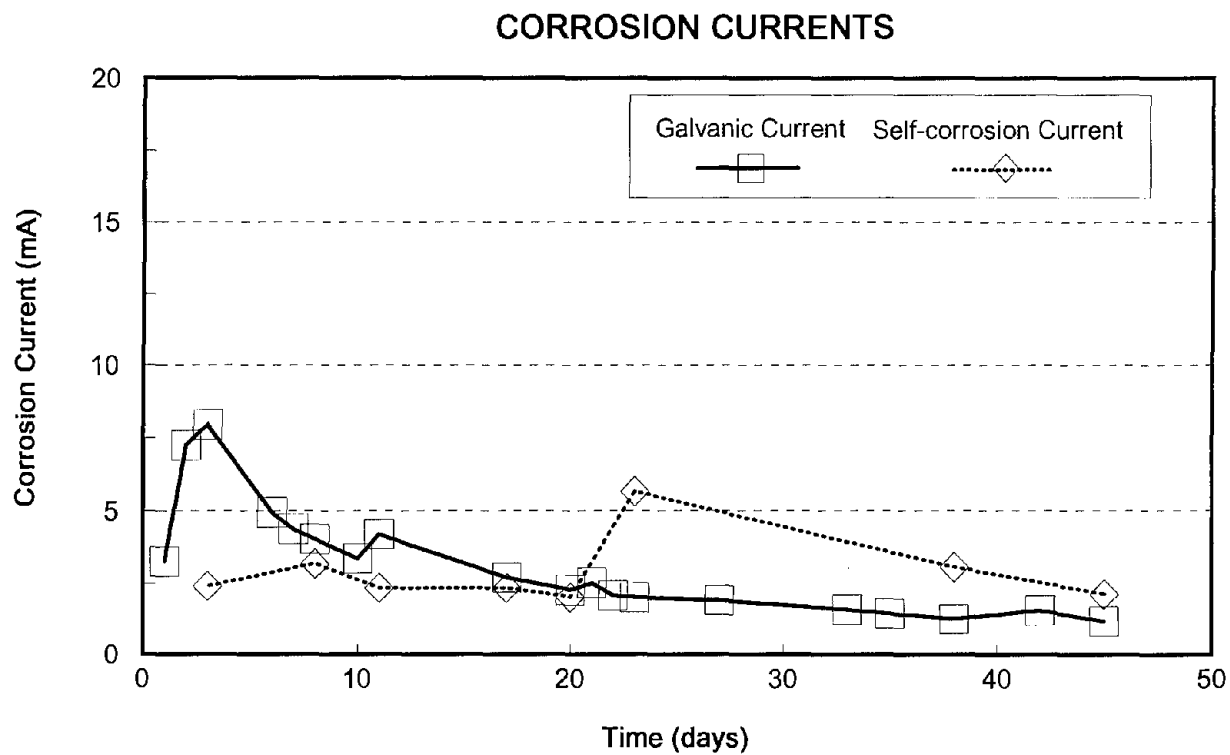


Figure 81. Galvanic, self-corrosion, and anode efficiency data for aluminum-1% Mg.

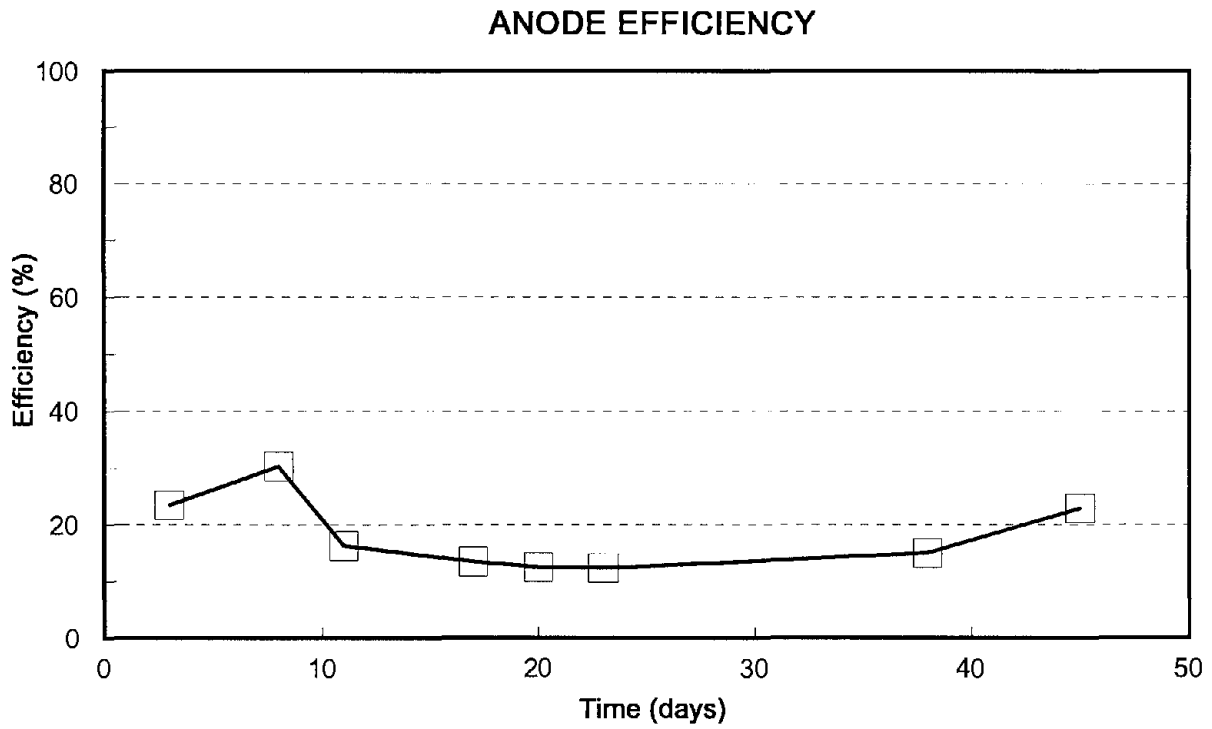
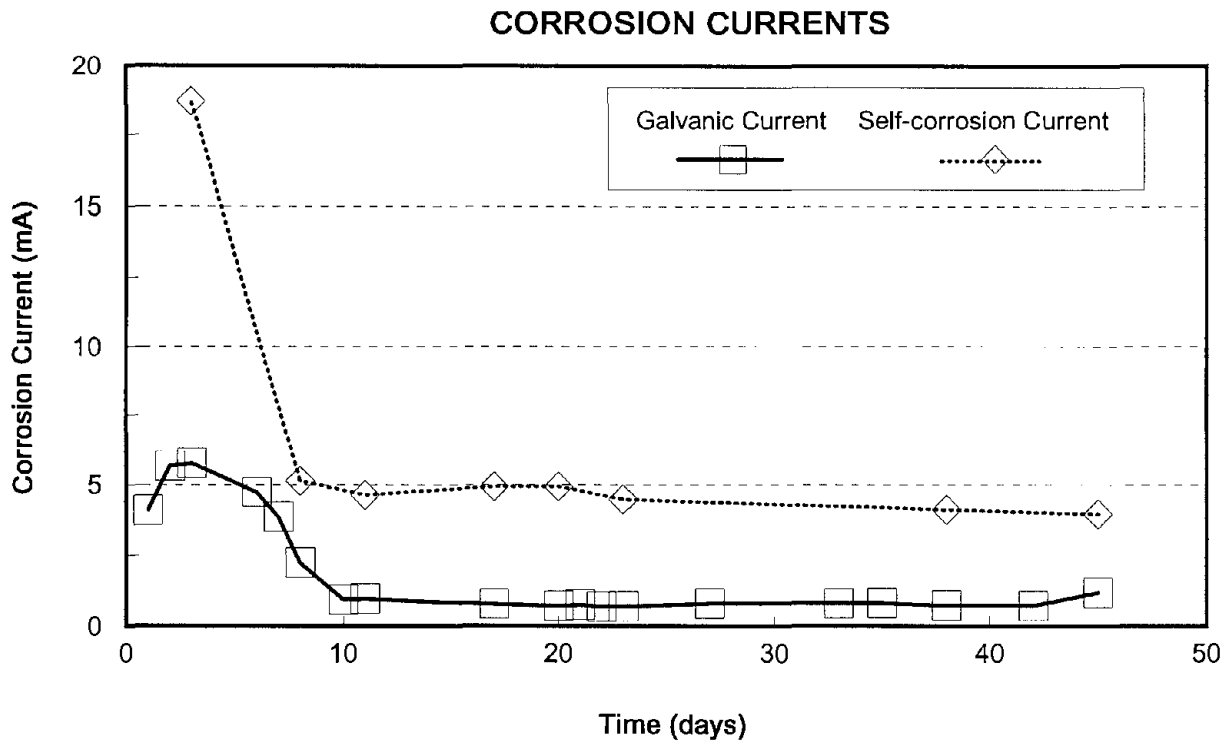


Figure 82. Galvanic, self-corrosion, and anode efficiency data for aluminum-10% Mg.

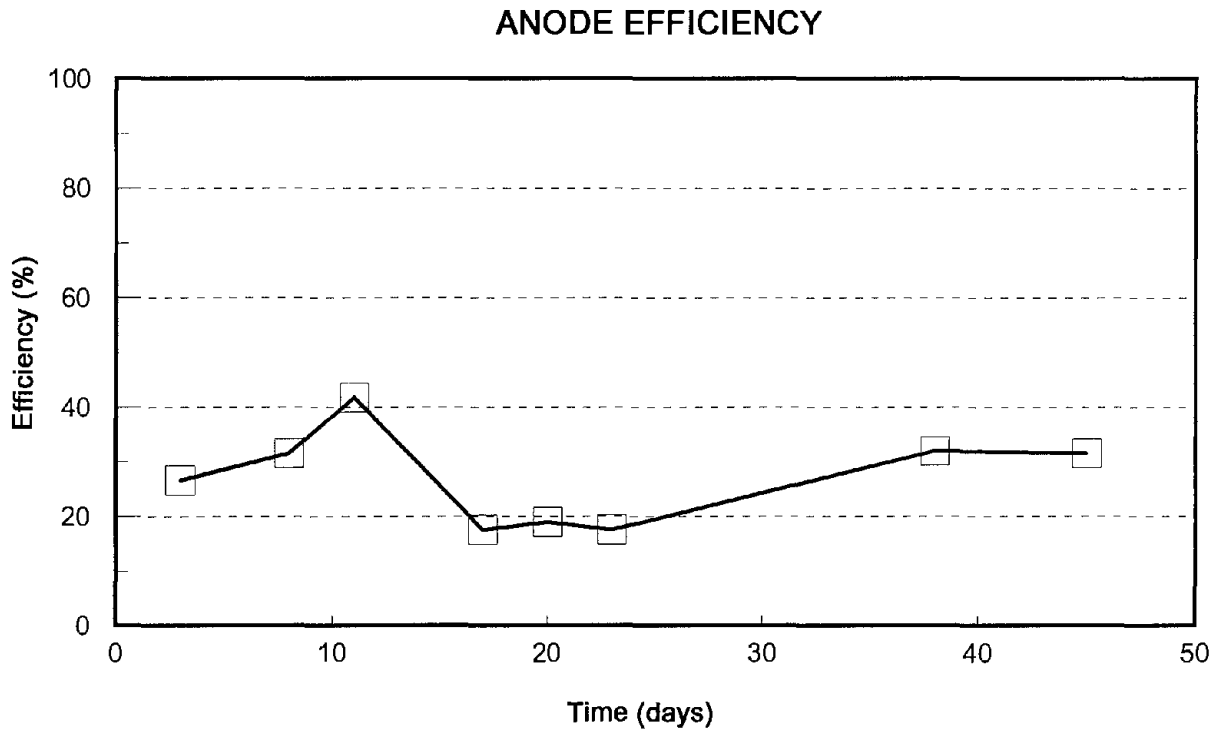
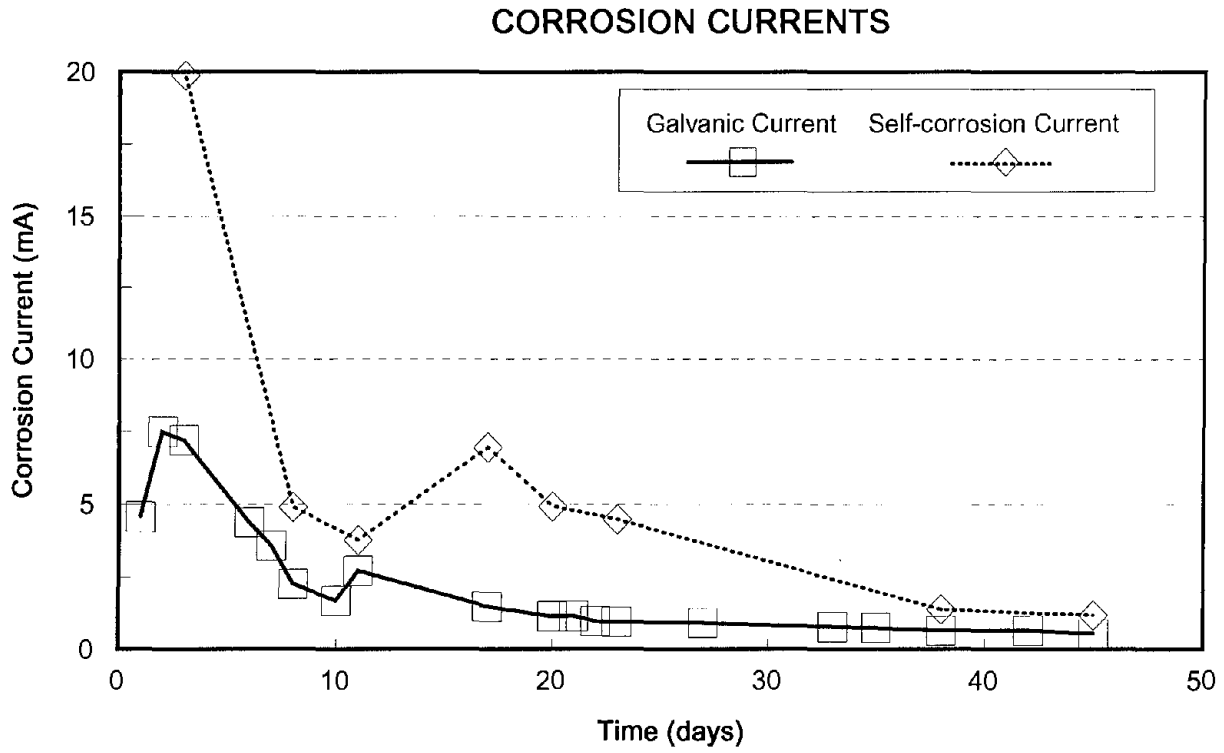


Figure 83. Galvanic, self-corrosion, and anode efficiency data for aluminum-5% Zn-3.5% Mg.

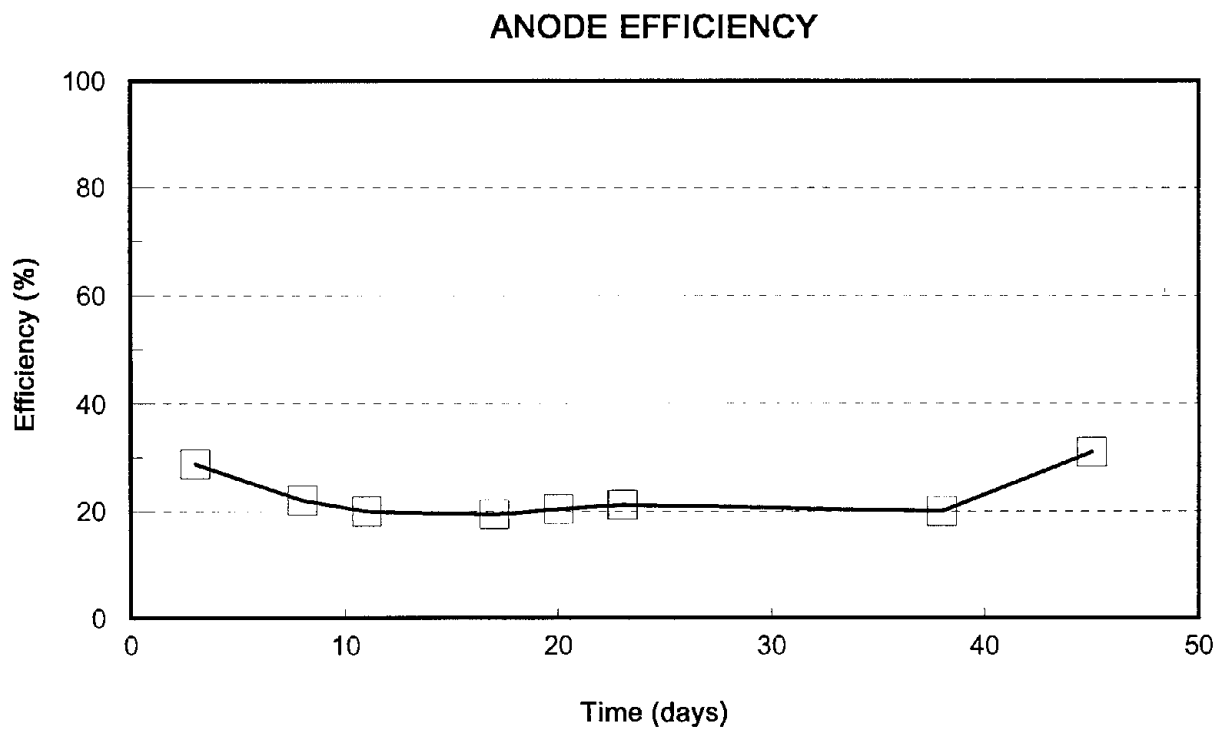
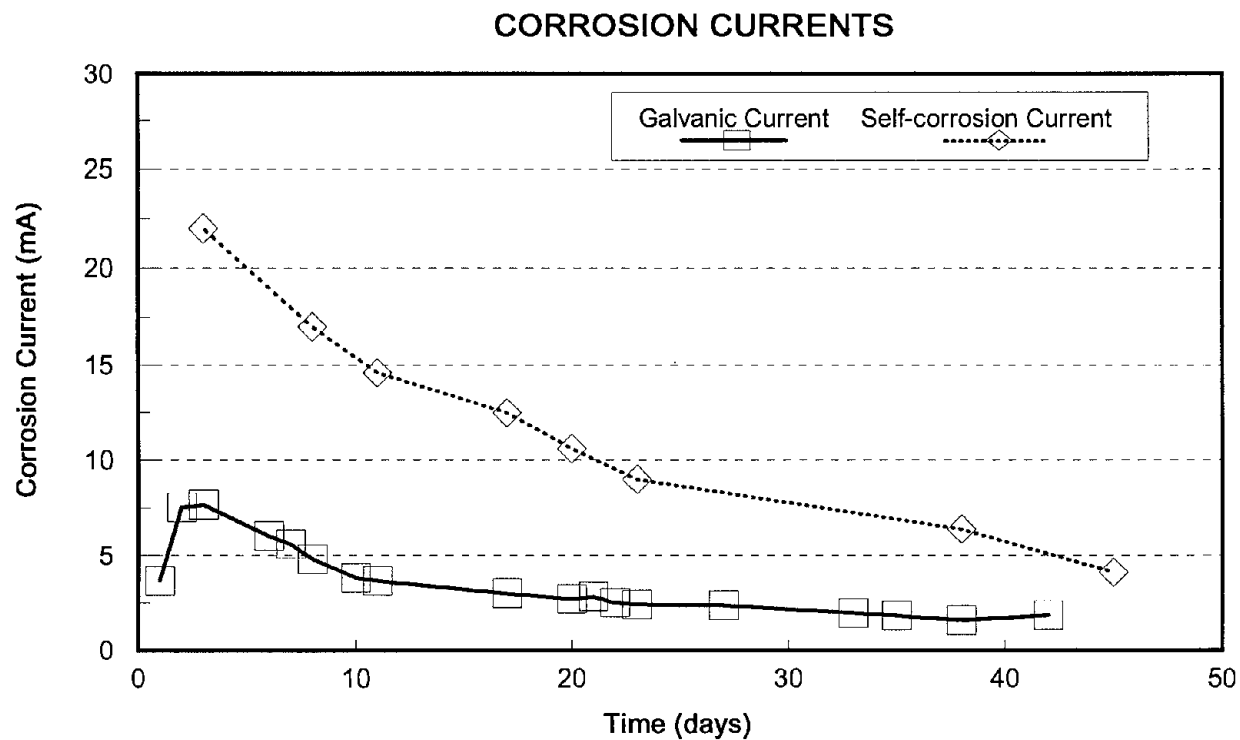


Figure 84. Galvanic, self-corrosion, and anode efficiency data for aluminum-5% Zn-0.1% Sn.

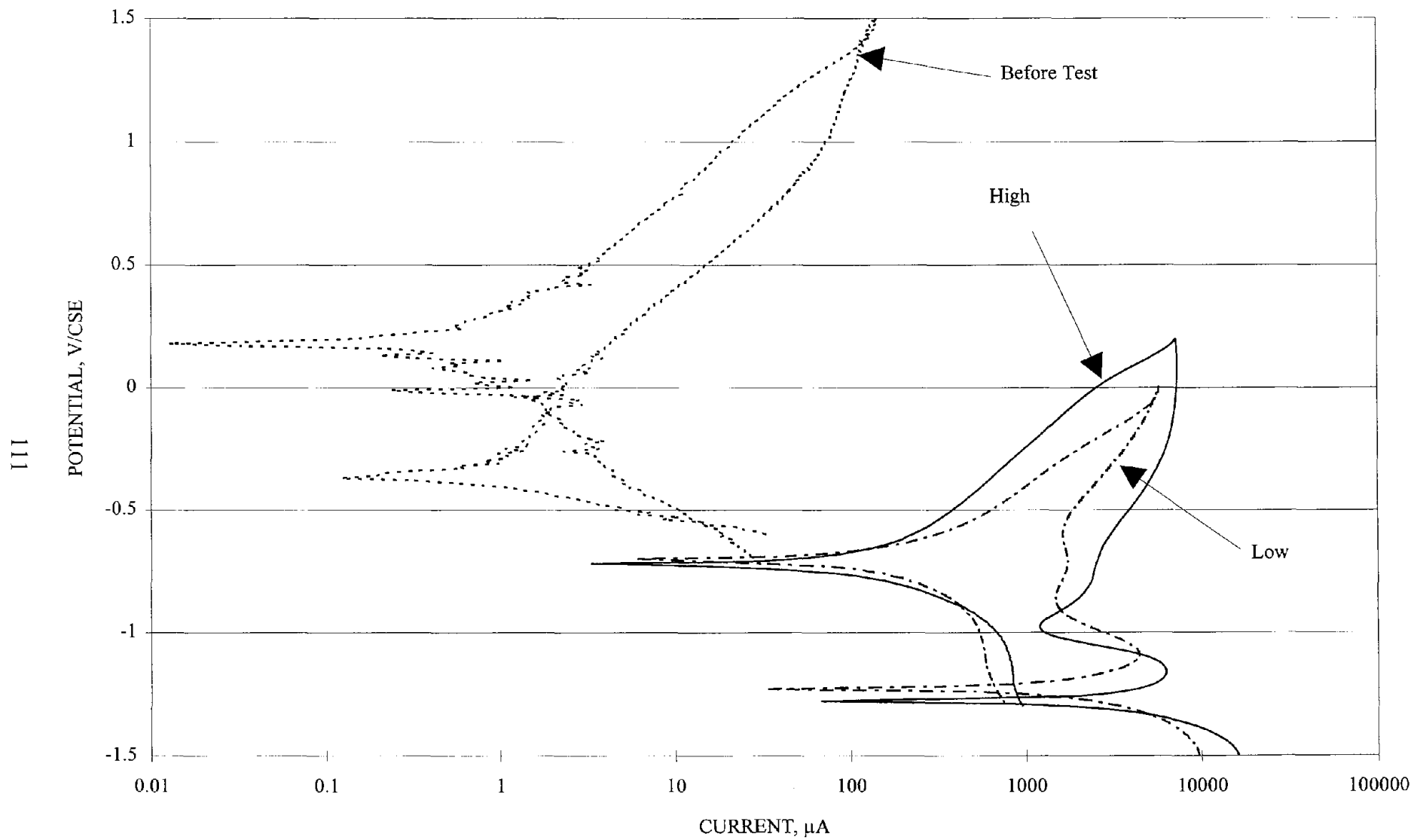


Figure 85. Cyclic polarization curves on pure zinc before galvanic coupling, at high current, and at low current (3800 ppm Cl).

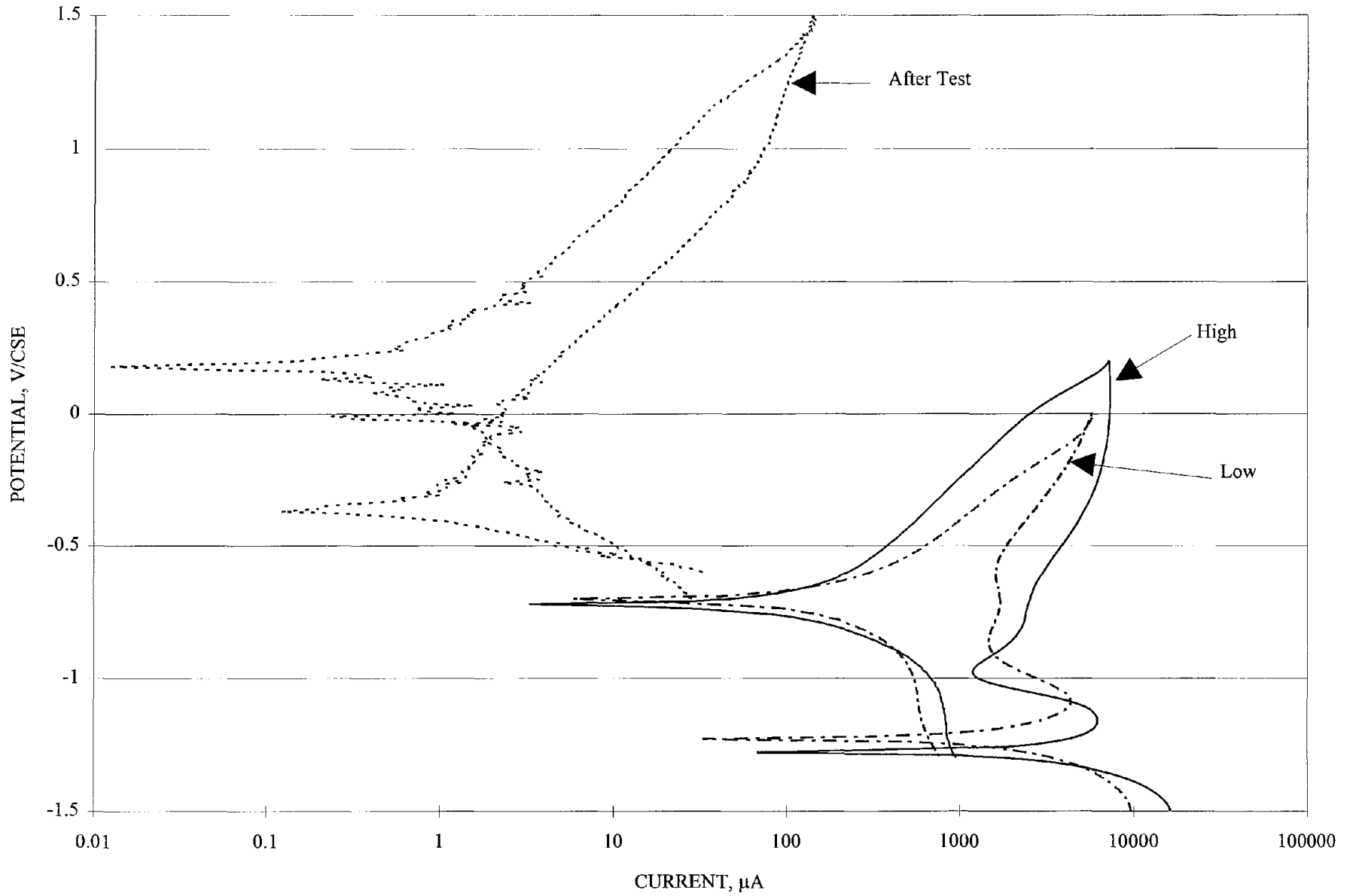


Figure 86. Cyclic polarization curves on pure zinc after galvanic coupling, at high current, and at low current (1300 ppm Cl).

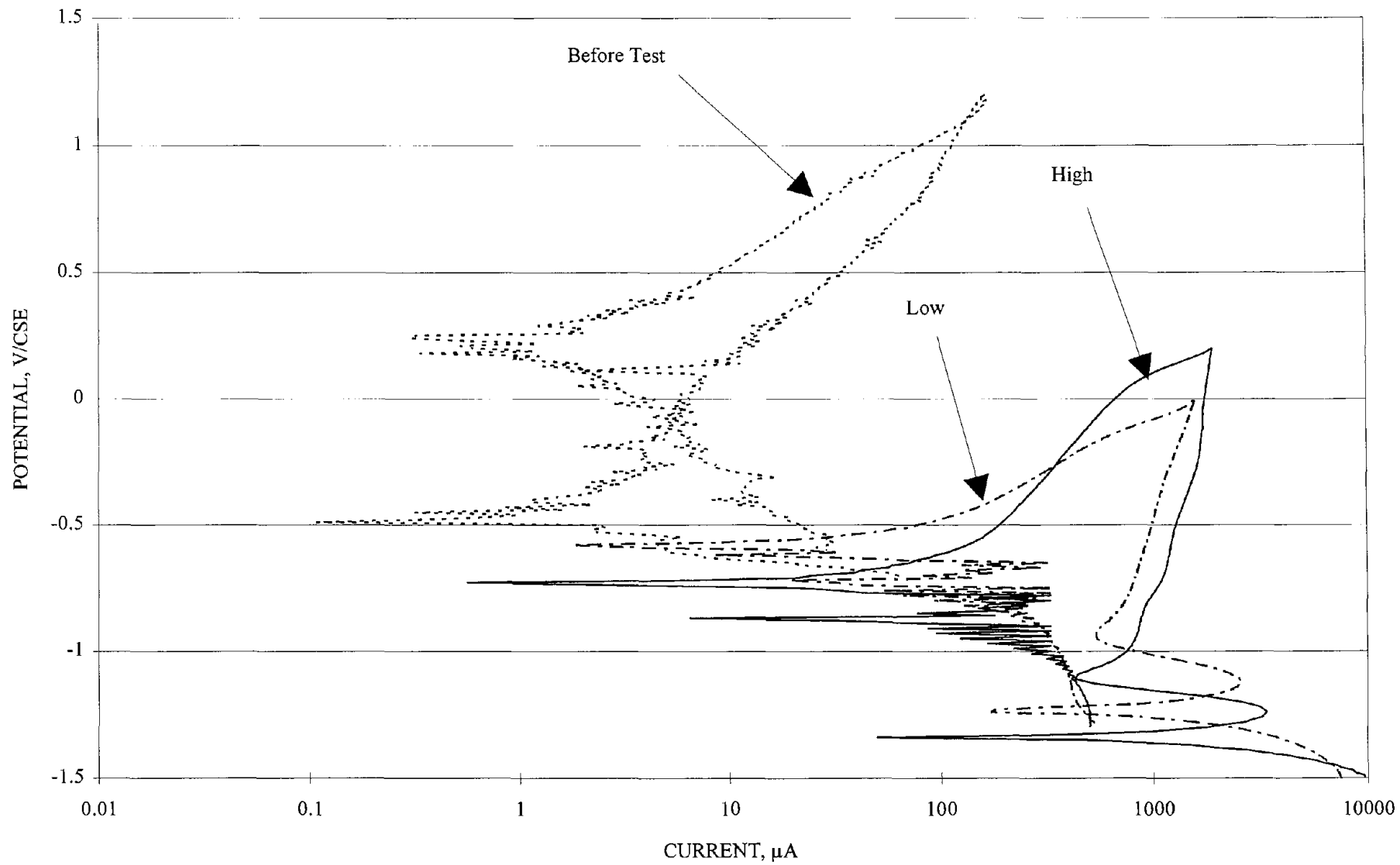


Figure 87. Cyclic polarization curves on zinc alloy before galvanic coupling, at high current, and at low current (3800 ppm Cl).

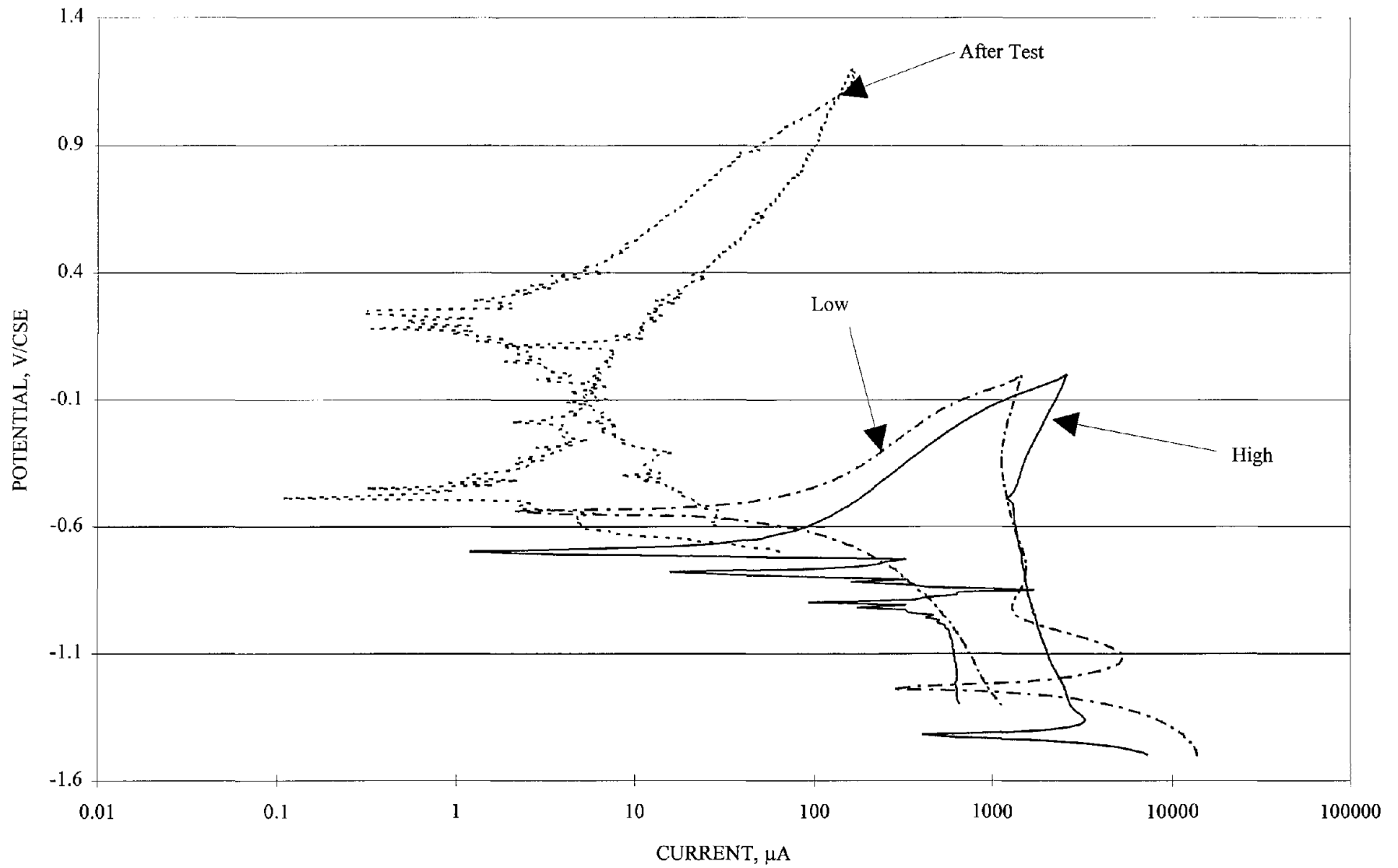


Figure 88. Cyclic polarization curves on zinc alloy after galvanic coupling, at high current, and at low current (1300 ppm Cl).

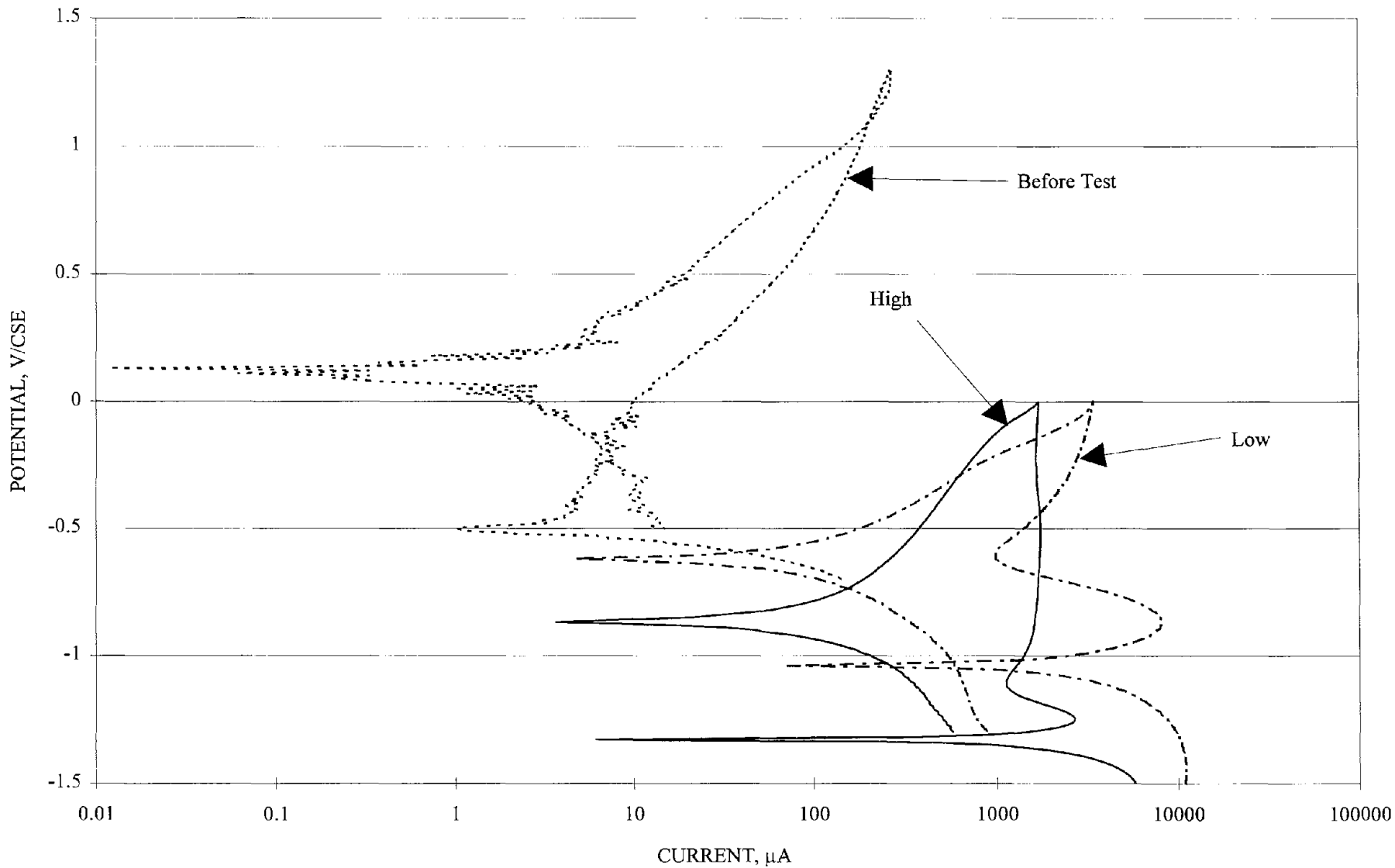


Figure 89. Cyclic polarization curves on zinc-5% Al alloy before galvanic coupling, at high current, and at low current (3800 ppm Cl).

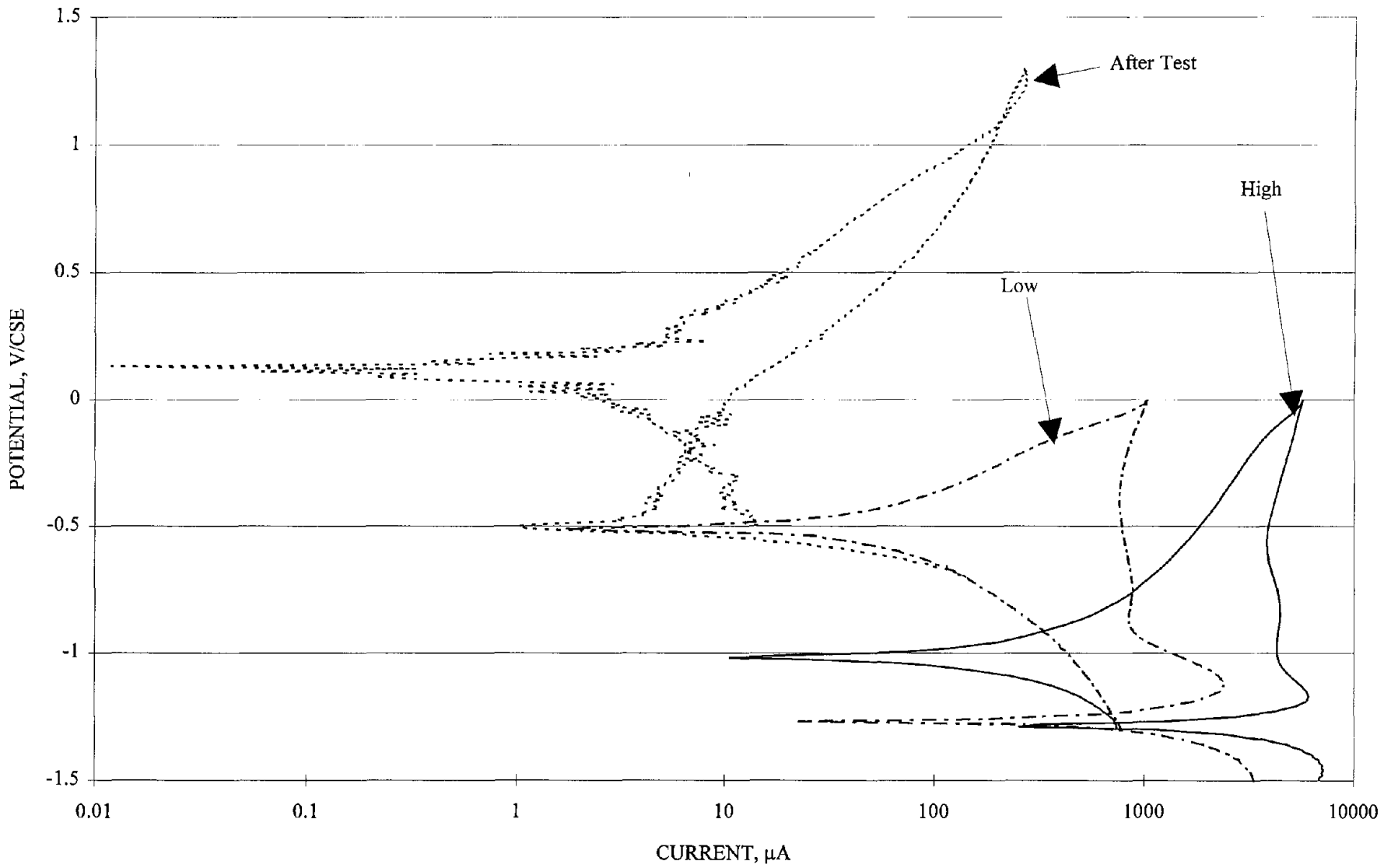


Figure 90. Cyclic polarization curves on zinc-5% Al alloy after galvanic coupling, at high current, and at low current (1300 ppm Cl).

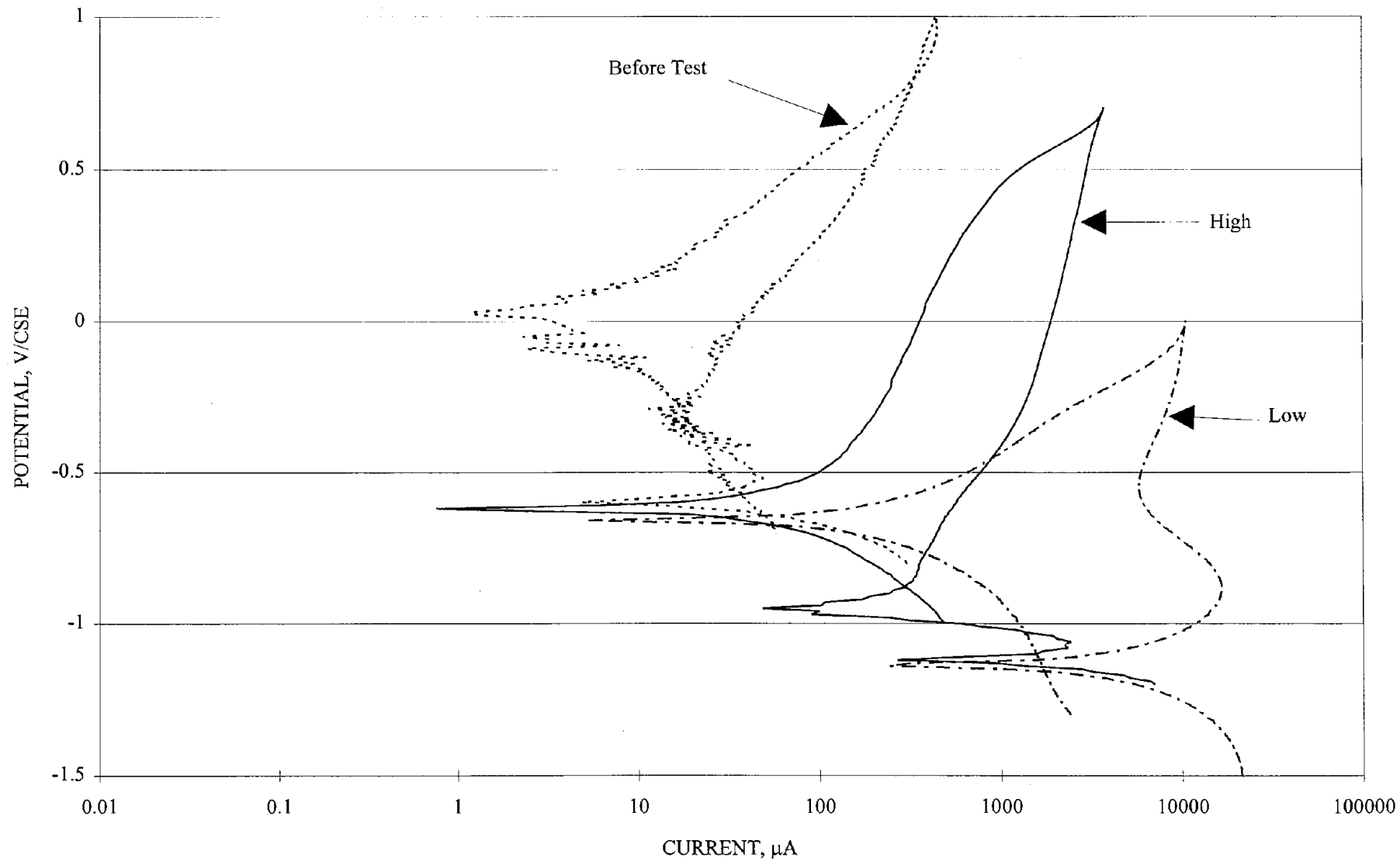


Figure 91. Cyclic polarization curves on zinc-15% Al alloy before galvanic coupling, at high current, and at low current (3800 ppm Cl).

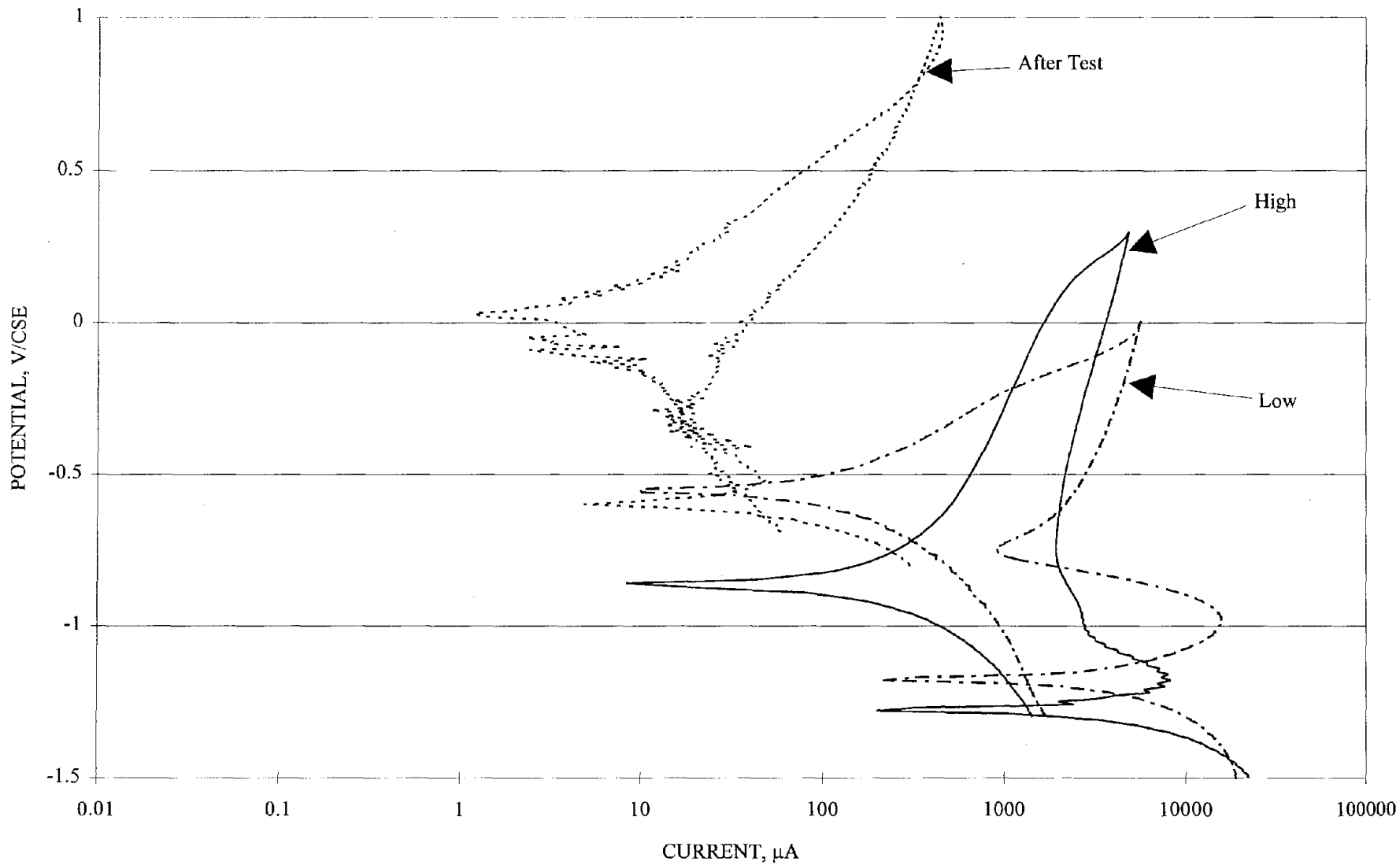


Figure 92. Cyclic polarization curves on zinc-15% Al alloy after galvanic coupling, at high current, and at low current (1300 ppm Cl).

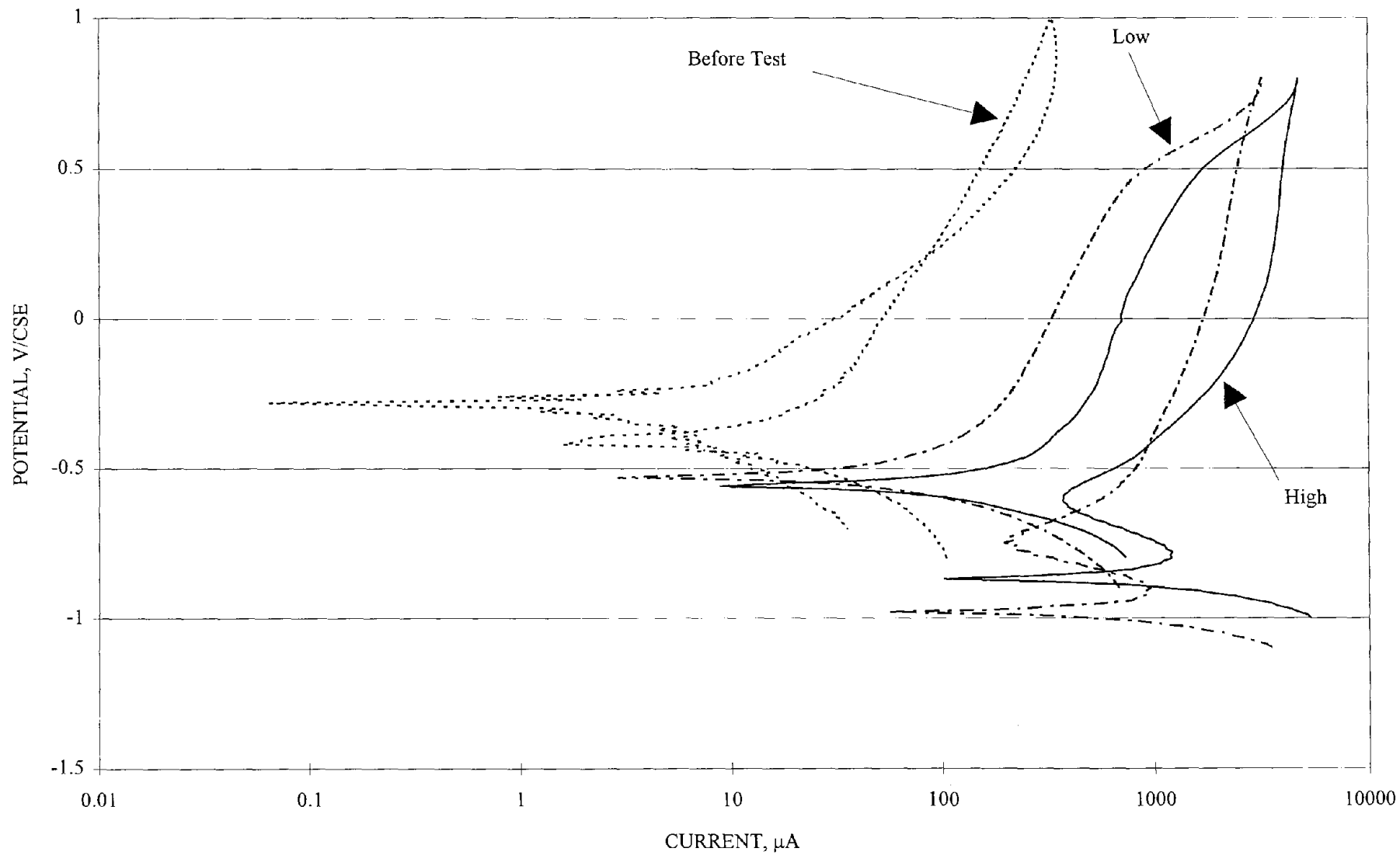


Figure 93. Cyclic polarization curves on zinc-55% Al alloy before galvanic coupling, at high current, and at low current (3800 ppm Cl).

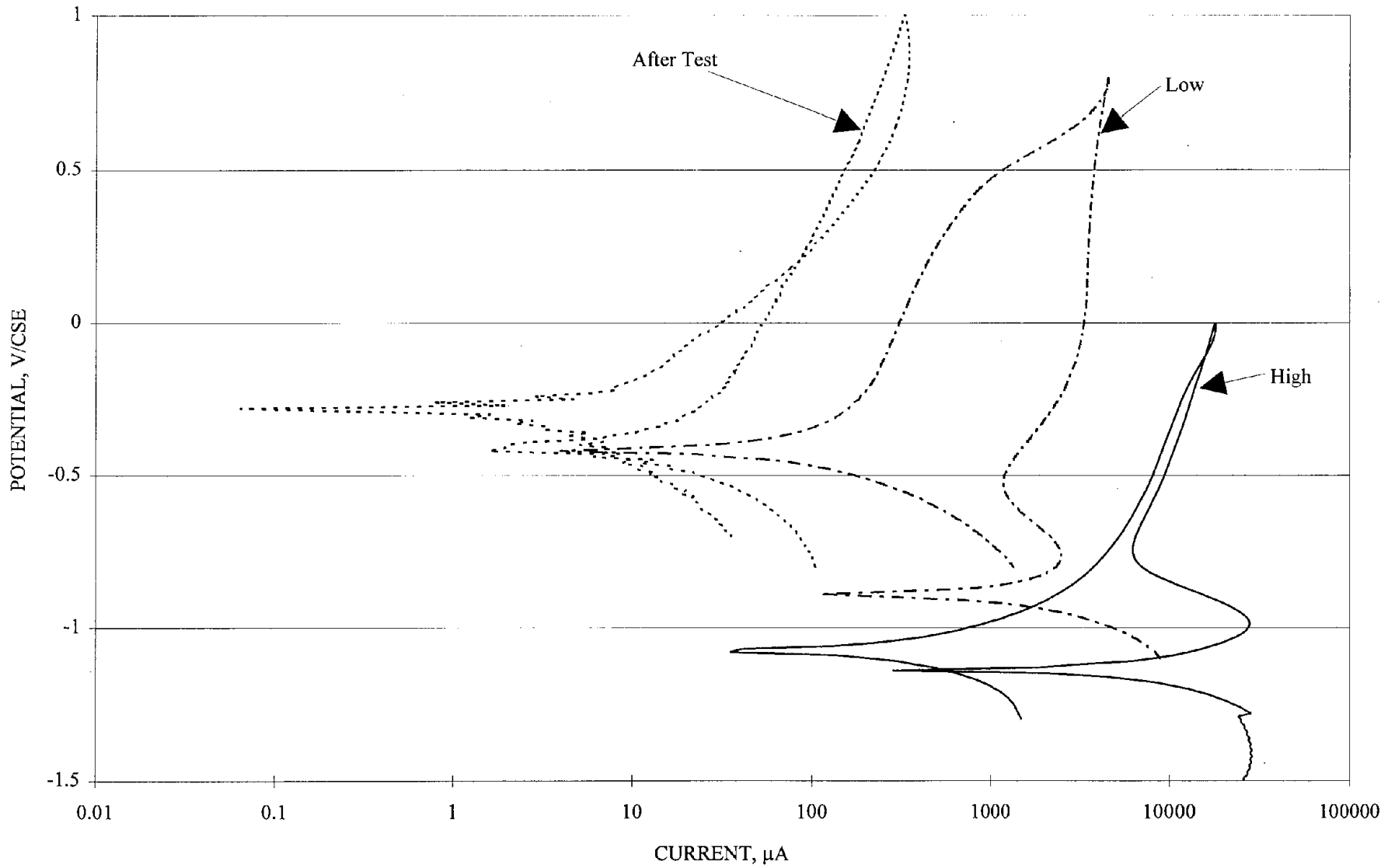


Figure 94. Cyclic polarization curves on zinc-55% Al alloy after galvanic coupling, at high current, and at low current (1300 ppm Cl).

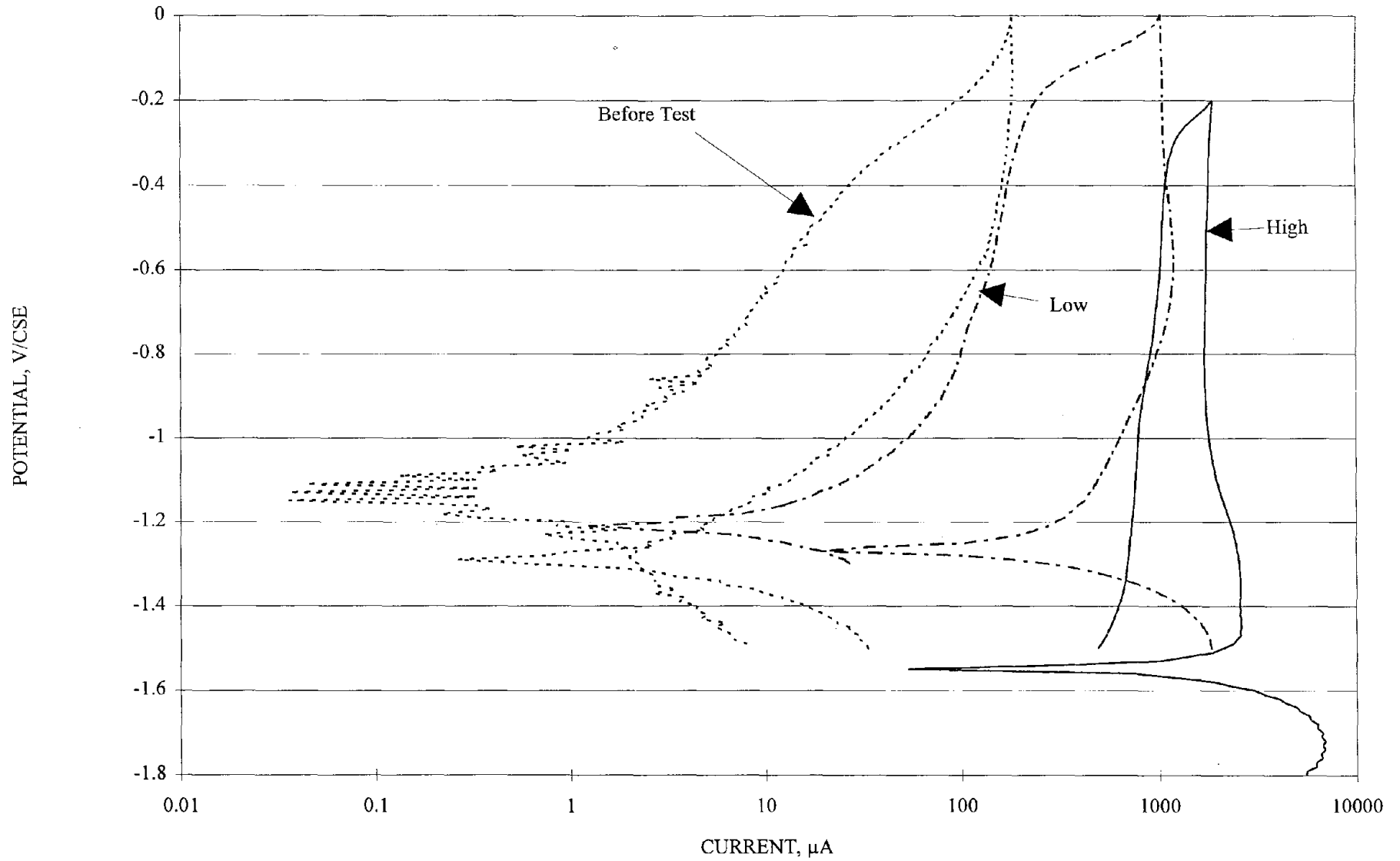


Figure 95. Cyclic polarization curves on pure aluminum before galvanic coupling, at high current, and at low current (3800 ppm Cl).

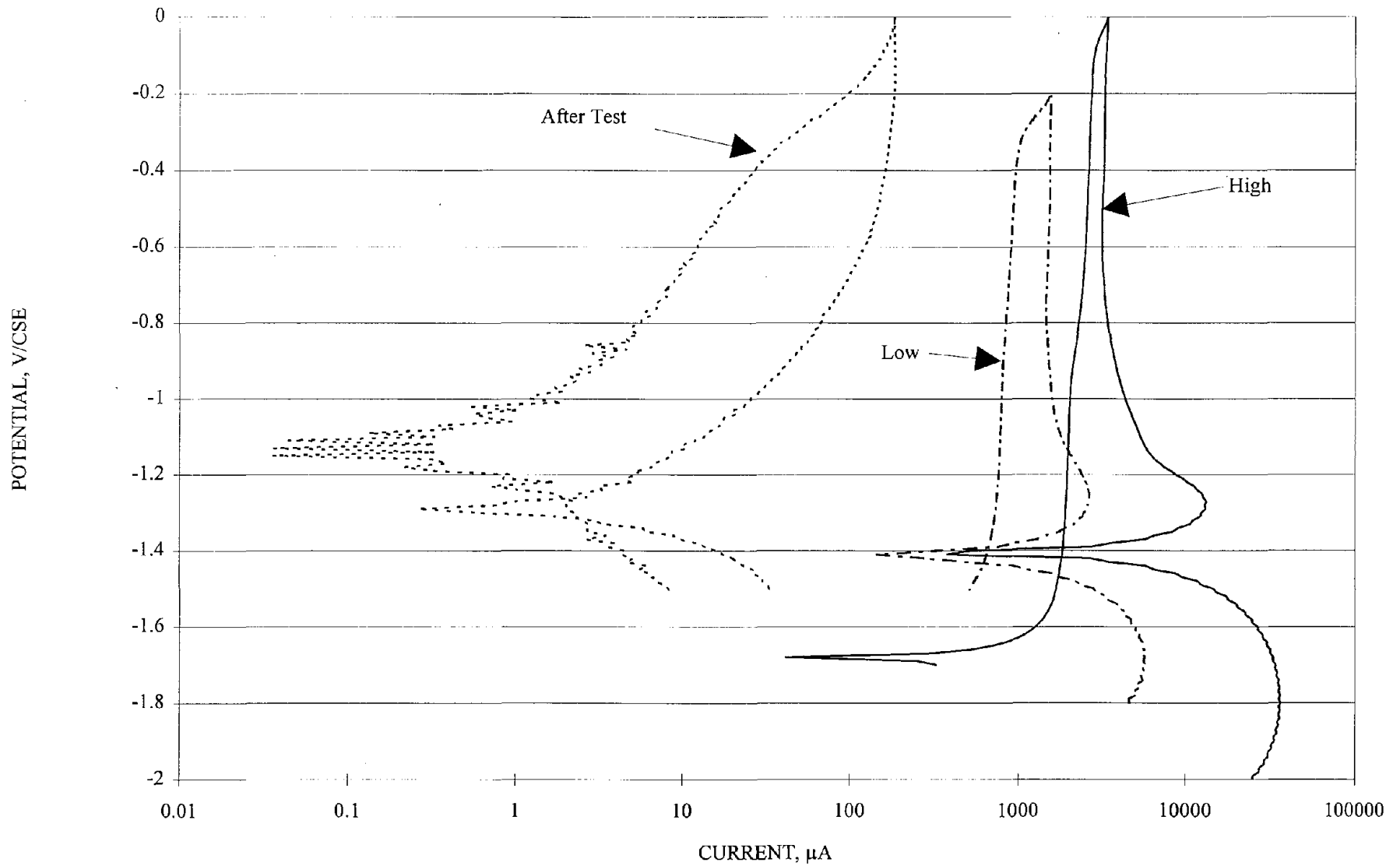


Figure 96. Cyclic polarization curves on pure aluminum after galvanic coupling, at high current, and at low current (1300 ppm Cl).

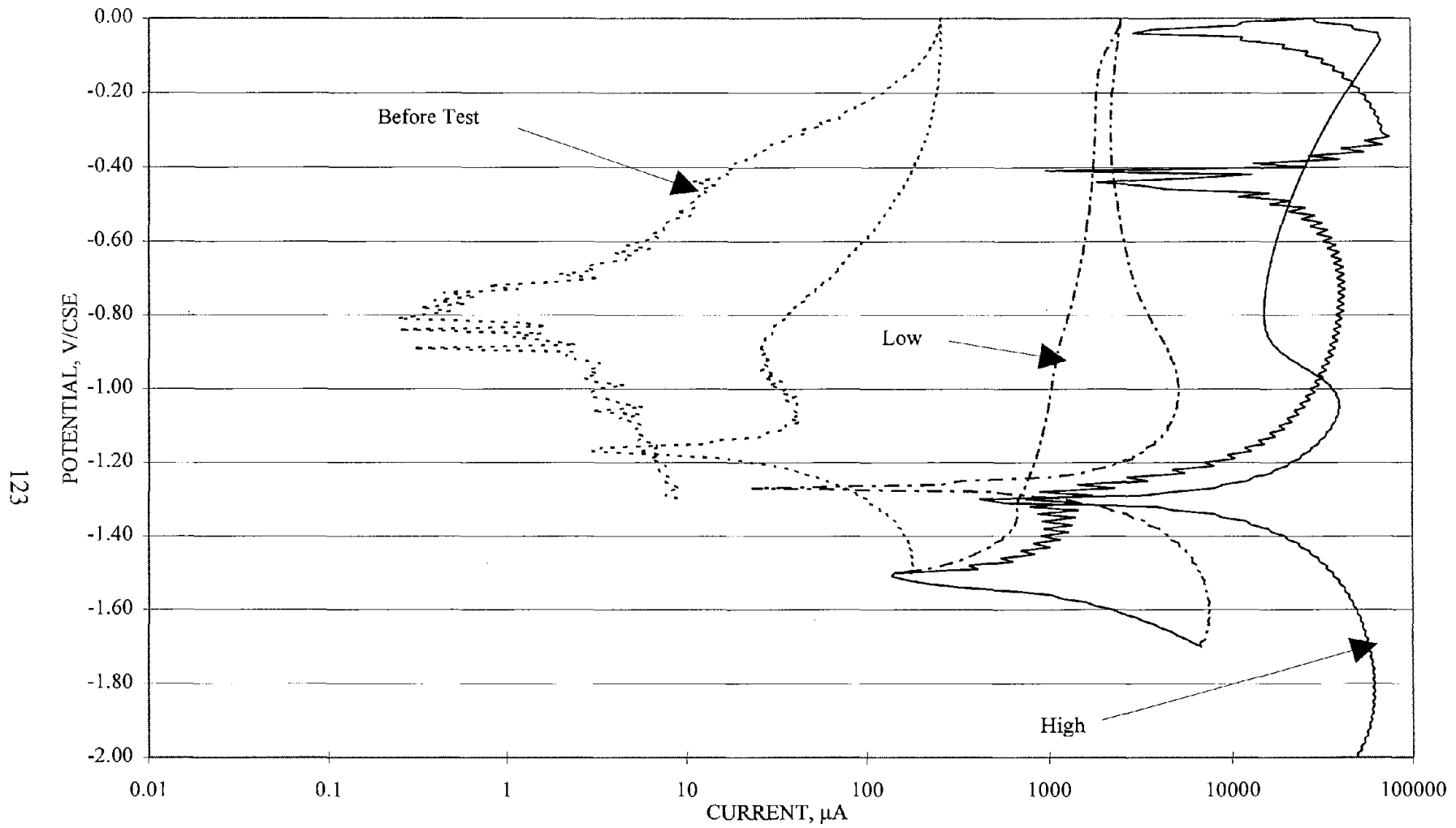


Figure 97. Cyclic polarization curves on aluminum alloy 1 before galvanic coupling, at high current, and at low current (3800 ppm Cl).

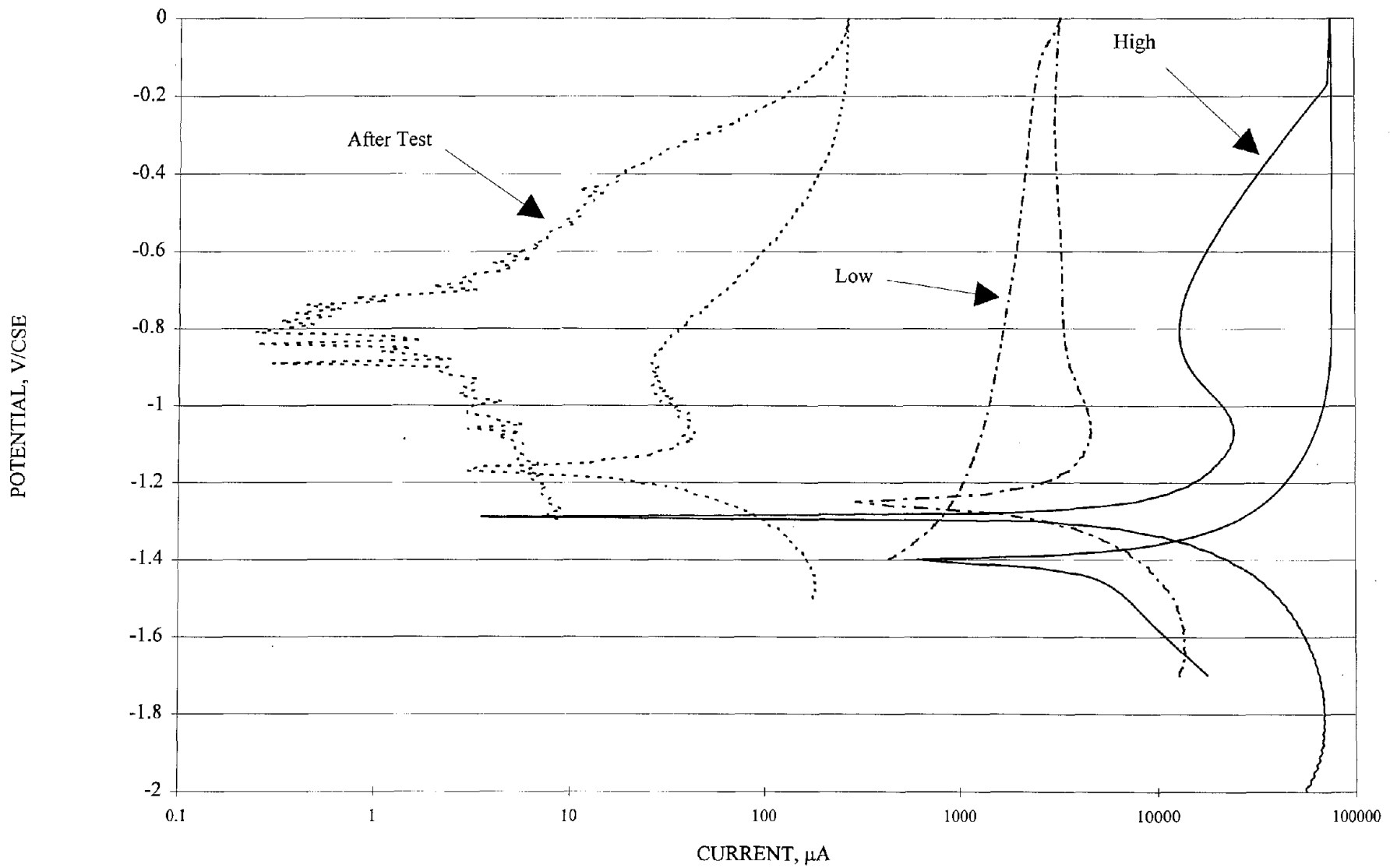


Figure 98. Cyclic polarization curves on aluminum alloy 1 after galvanic coupling, at high current, and at low current (1300 ppm Cl).

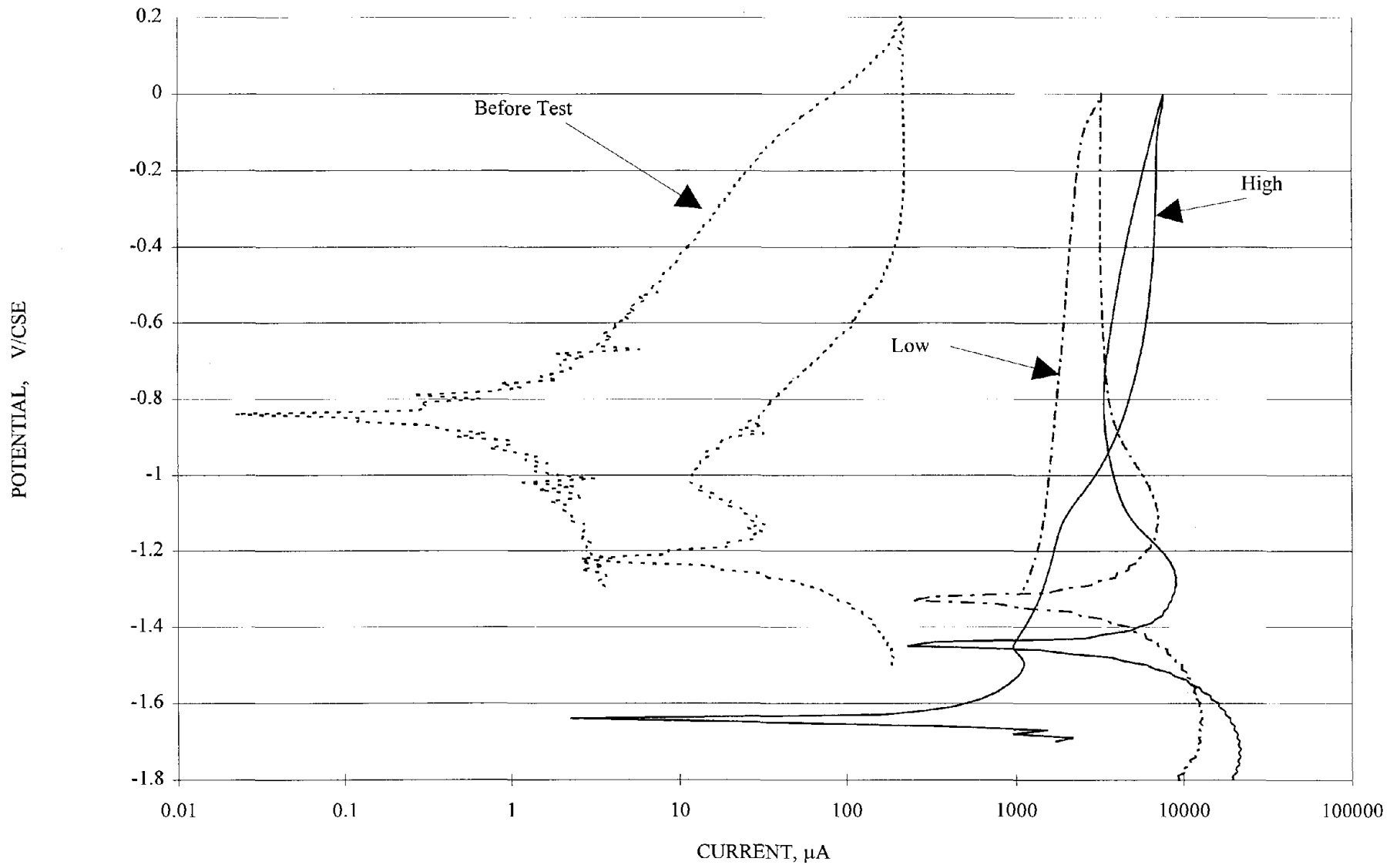


Figure 99. Cyclic polarization curves on aluminum alloy 2 before galvanic coupling, at high current, and at low current (3800 ppm Cl).

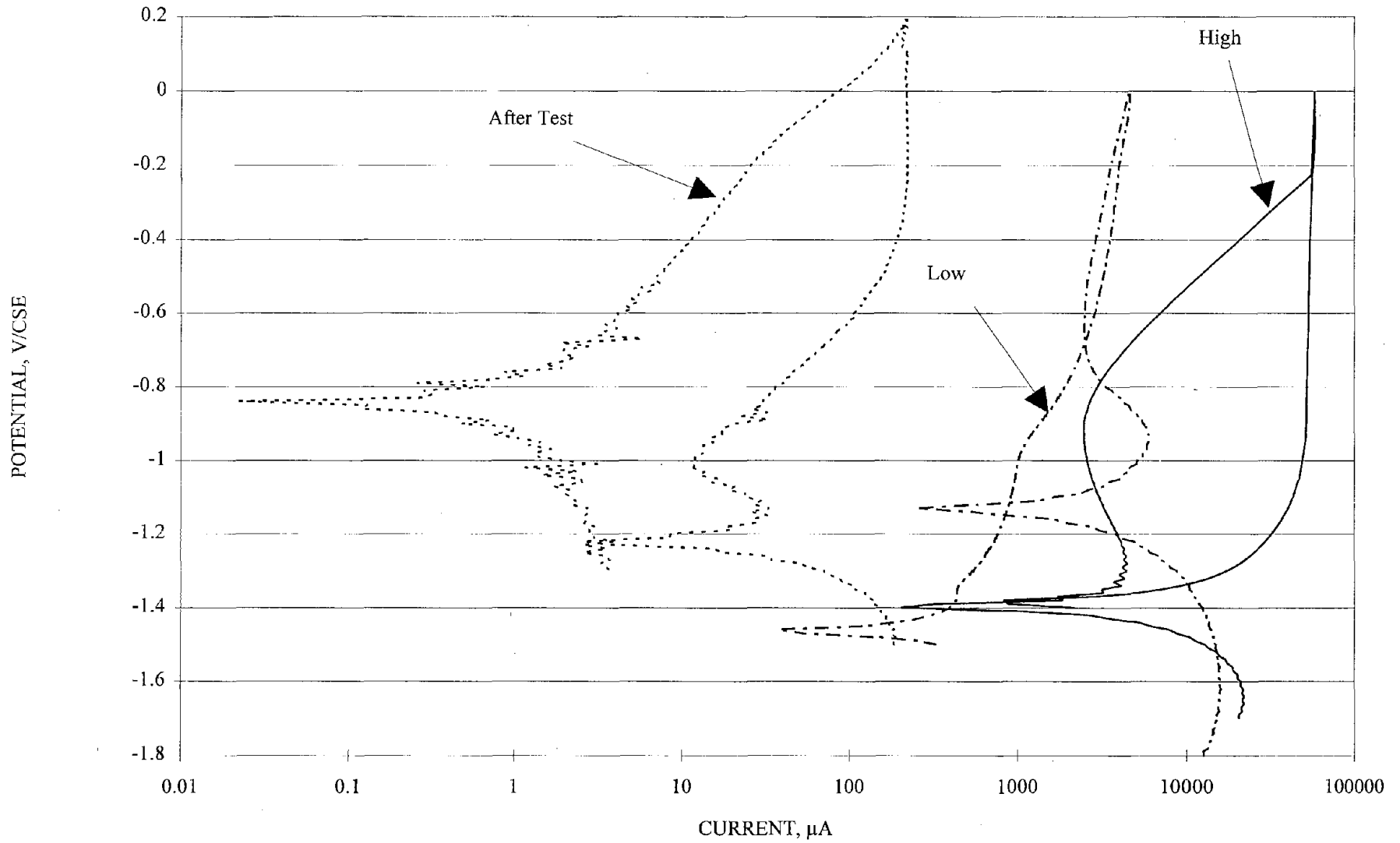


Figure 100. Cyclic polarization curves on aluminum alloy 2 after galvanic coupling, at high current, and at low current (1300 ppm Cl).

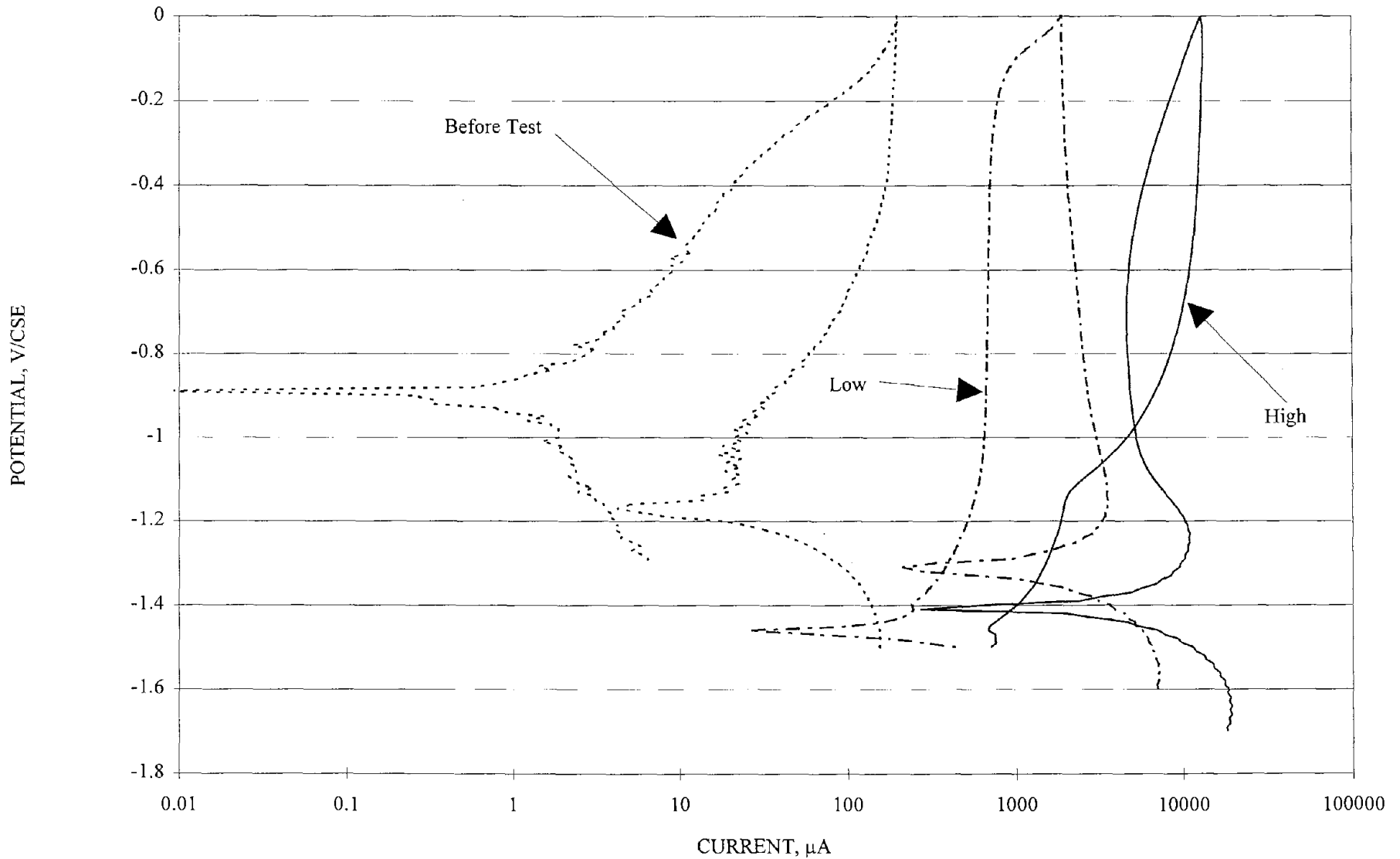


Figure 101. Cyclic polarization curves on aluminum-5% Zn alloy before galvanic coupling, at high current, and at low current (3800 ppm Cl).

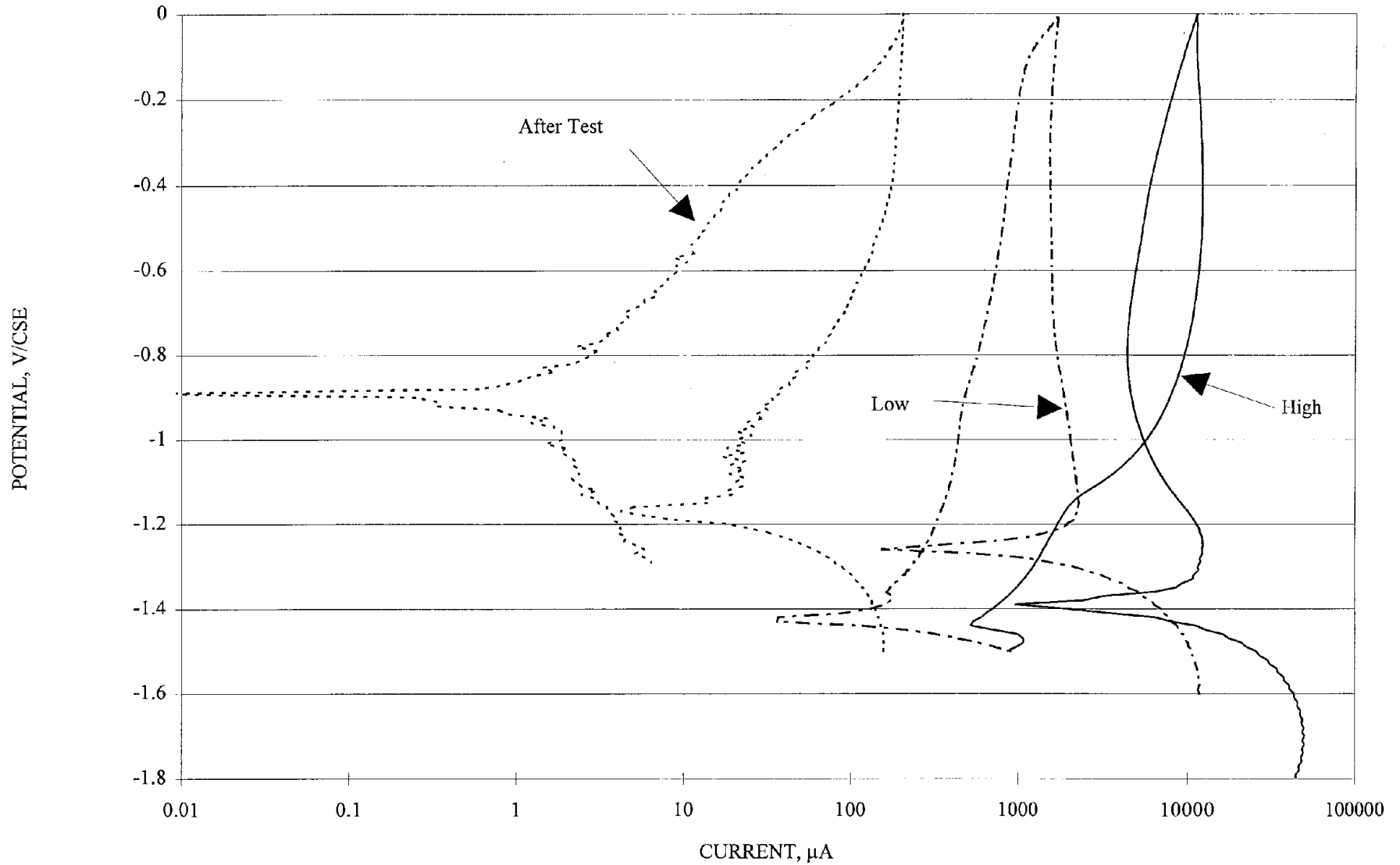


Figure 102. Cyclic polarization curves on aluminum-5% Zn alloy after galvanic coupling, at high current, and at low current (1300 ppm Cl).

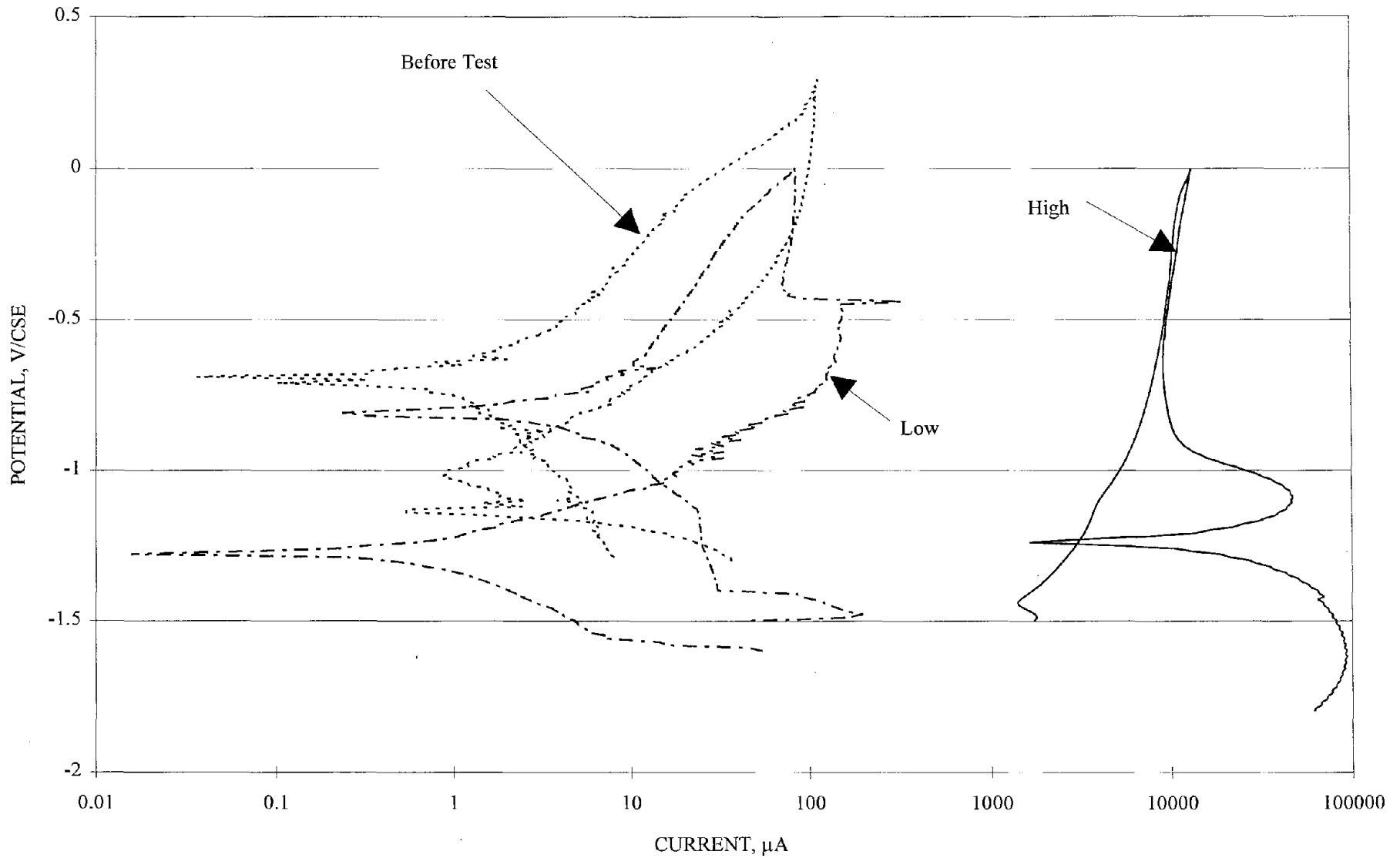


Figure 103. Cyclic polarization curves on aluminum-10% Zn alloy before galvanic coupling, at high current, and at low current (3800 ppm Cl).

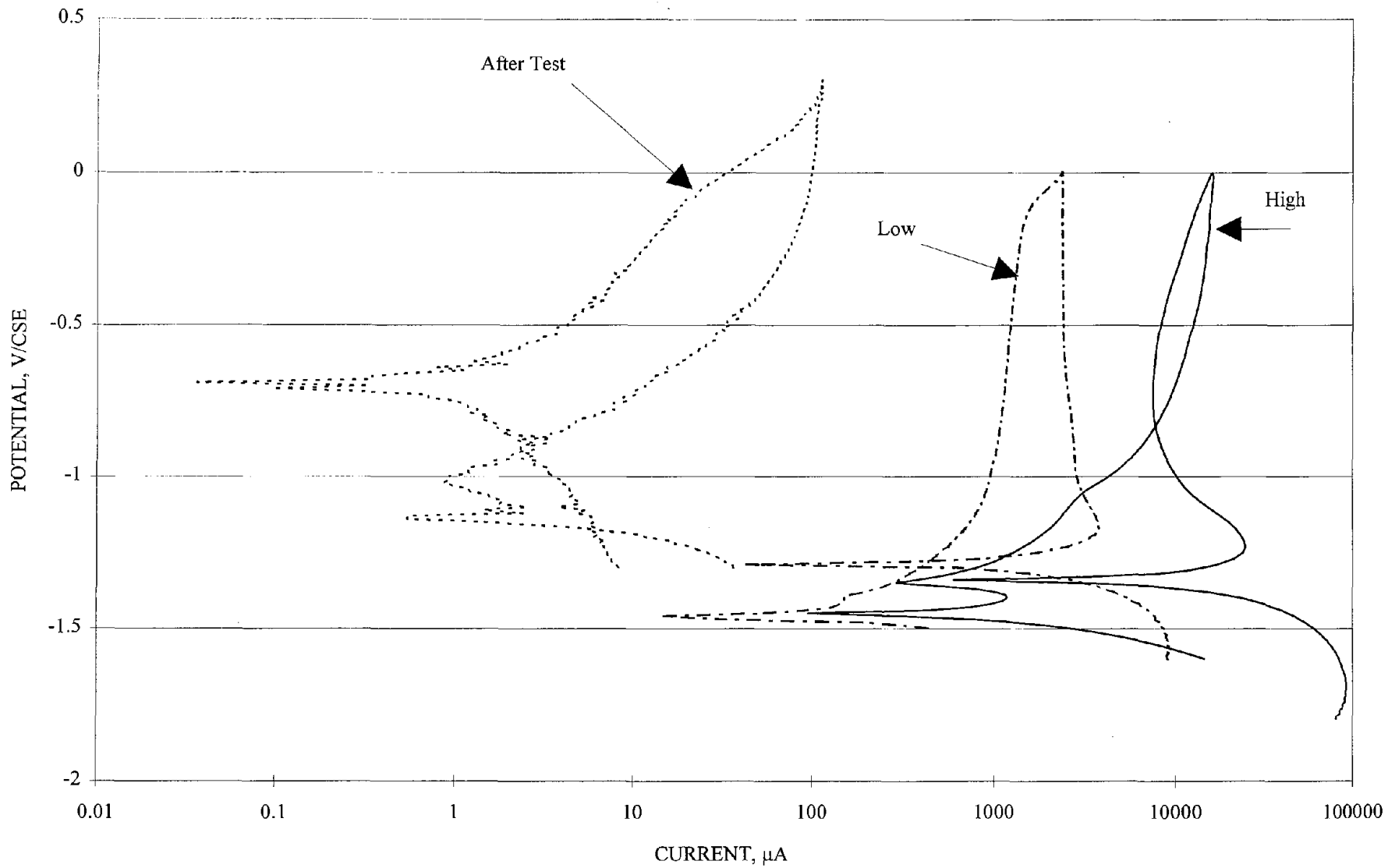


Figure 104. Cyclic polarization curves on aluminum-10% Zn alloy after galvanic coupling, at high current, and at low current (1300 ppm Cl).

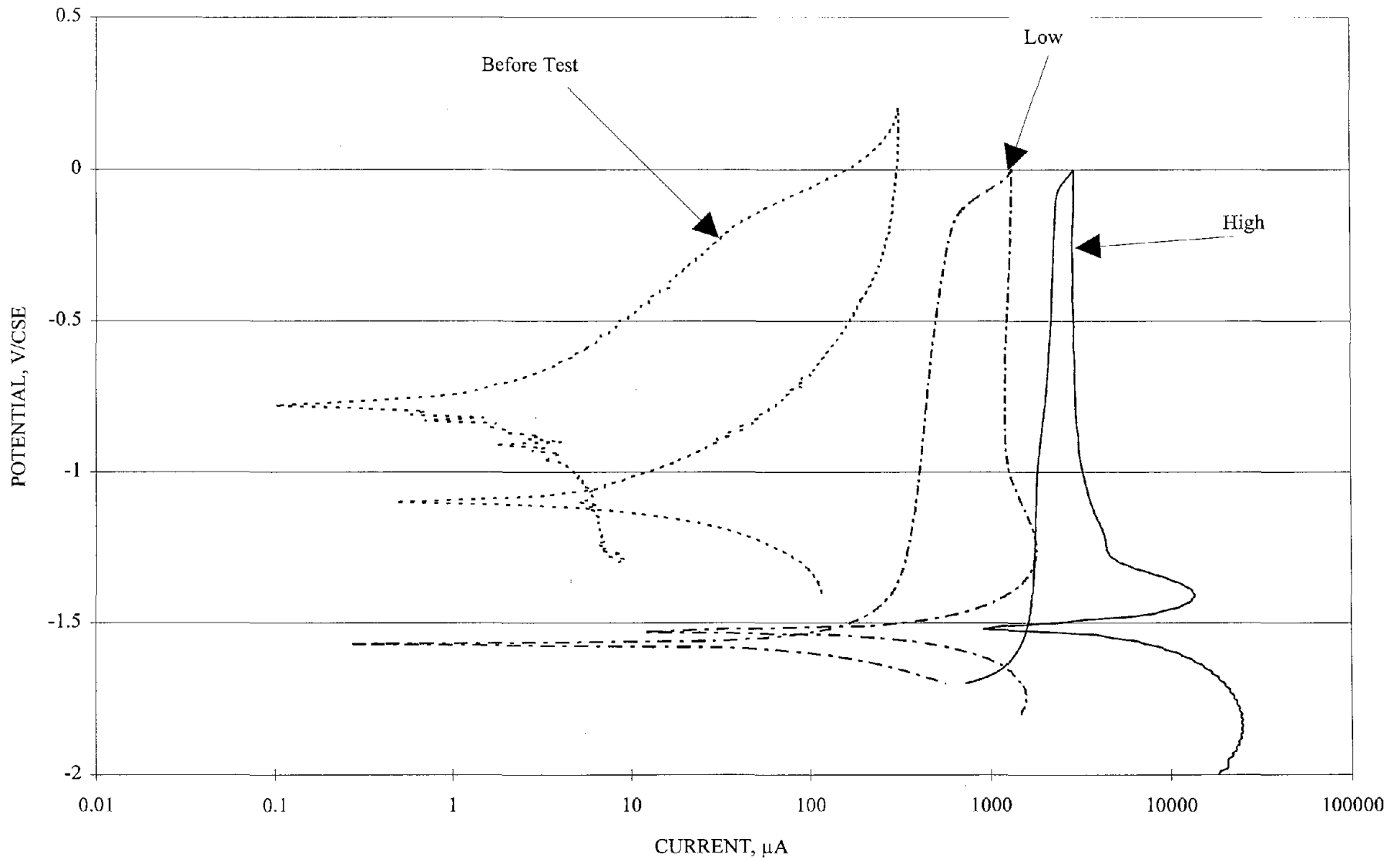


Figure 105. Cyclic polarization curves on aluminum-1% Mg alloy before galvanic coupling, at high current, and at low current (3800 ppm Cl).

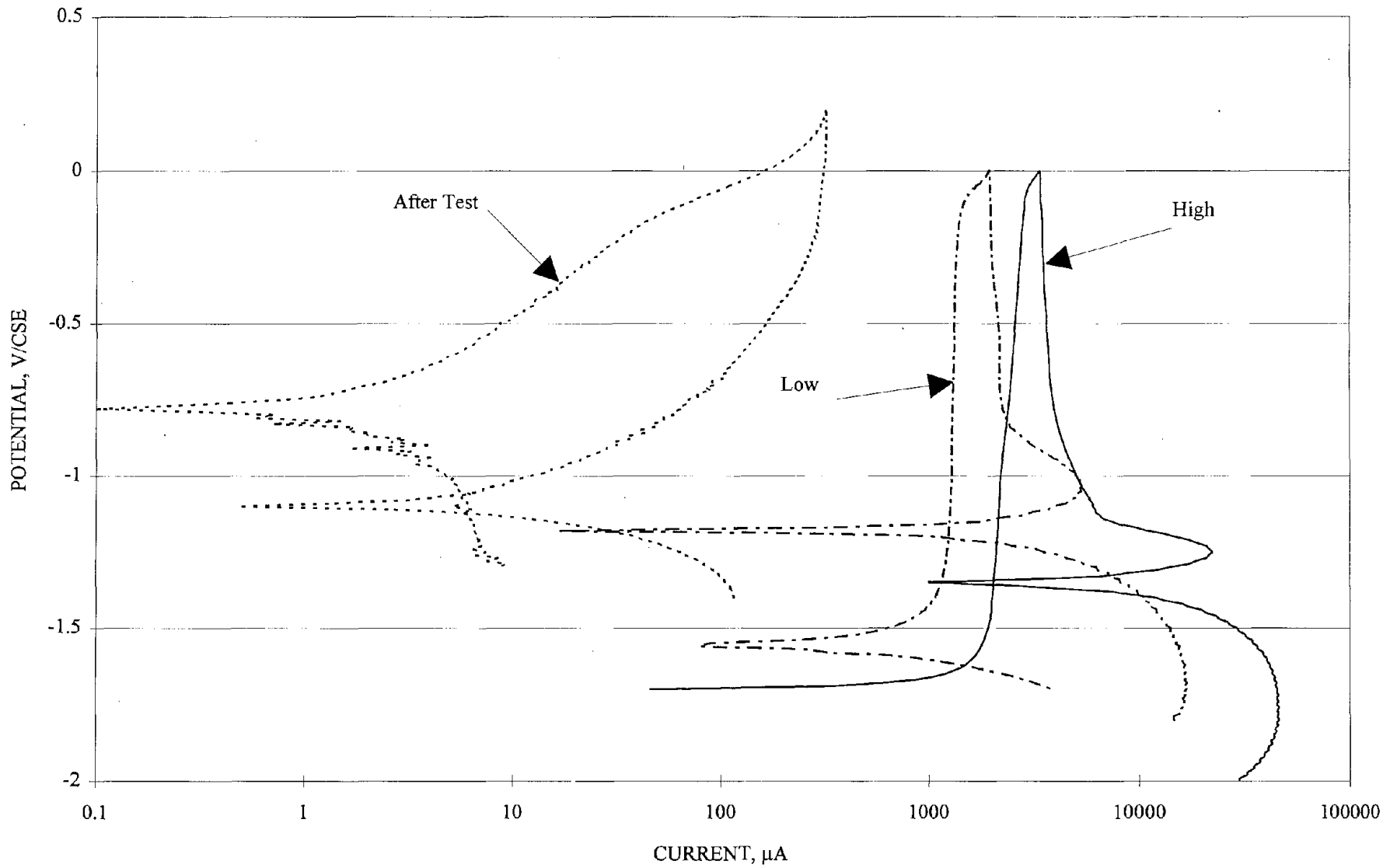


Figure 106. Cyclic polarization curves on aluminum-1% Mg alloy after galvanic coupling, at high current, and at low current (1300 ppm Cl).

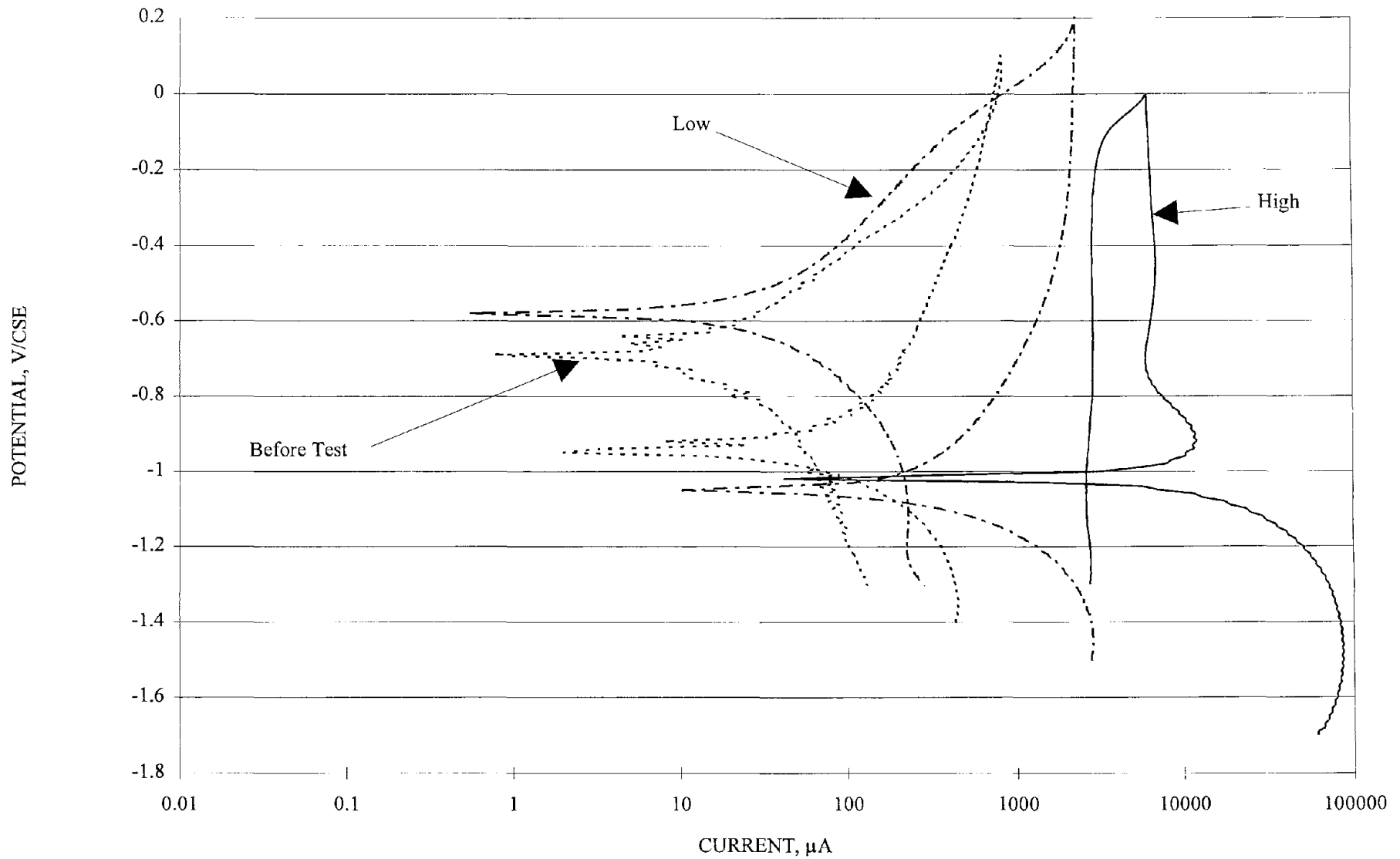


Figure 107. Cyclic polarization curves on aluminum-10% Mg alloy before galvanic coupling, at high current, and at low current (3800 ppm Cl).

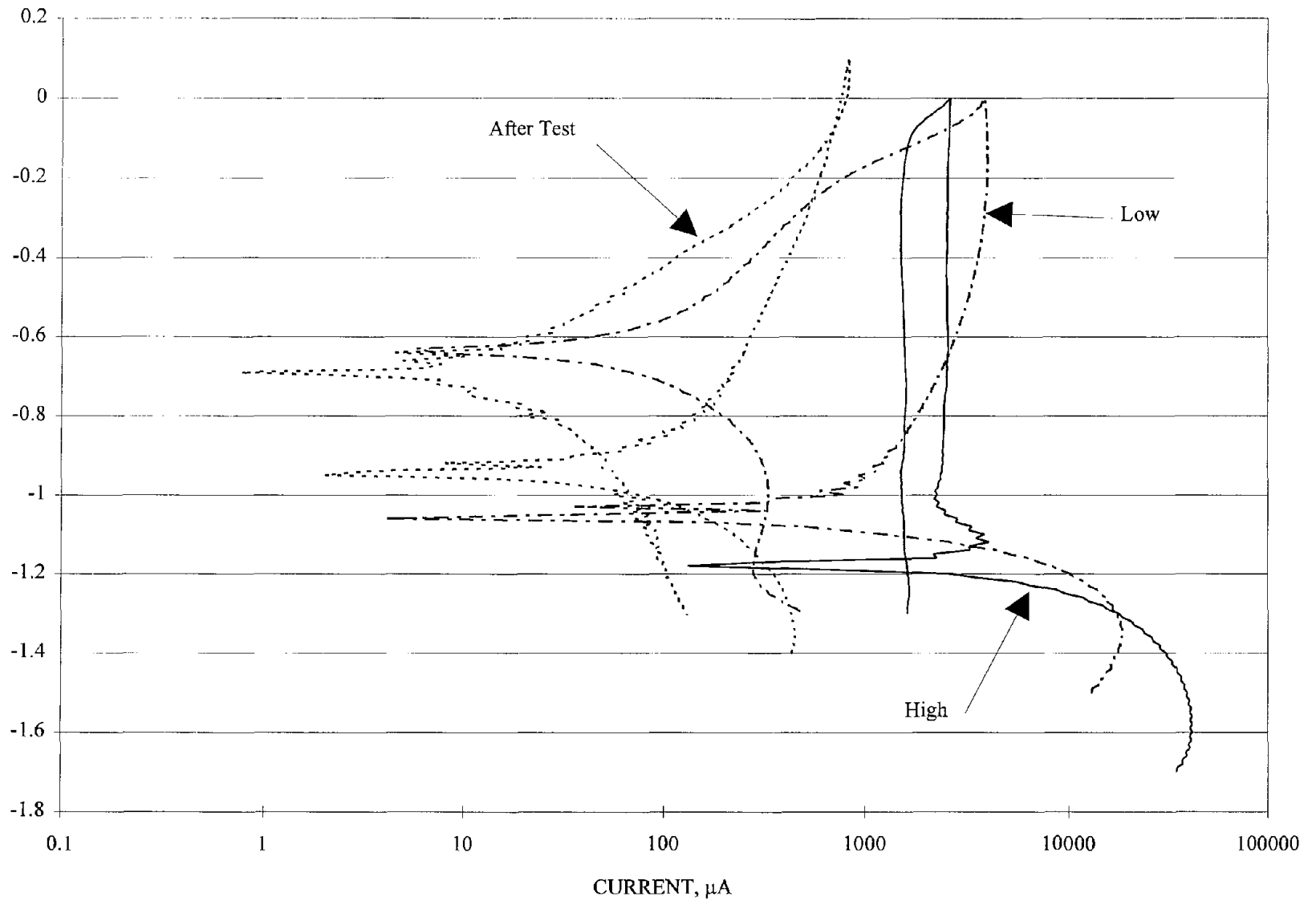


Figure 108. Cyclic polarization curves on aluminum-10% Mg alloy after galvanic coupling, at high current, and at low current (1300 ppm Cl).

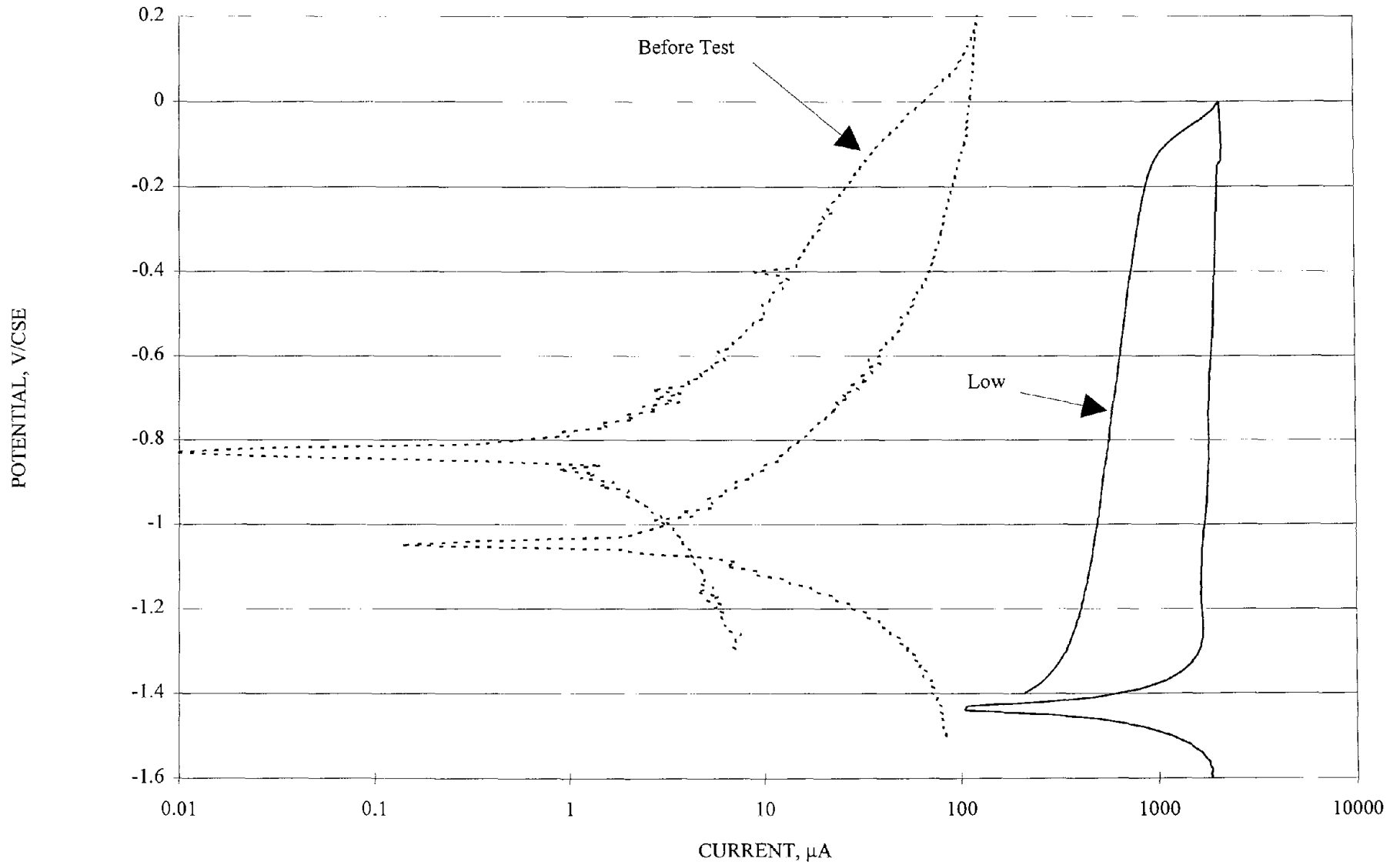


Figure 109. Cyclic polarization curves on aluminum-5% Zn-3.5% Mg alloy before galvanic coupling and at low current (3800 ppm Cl).

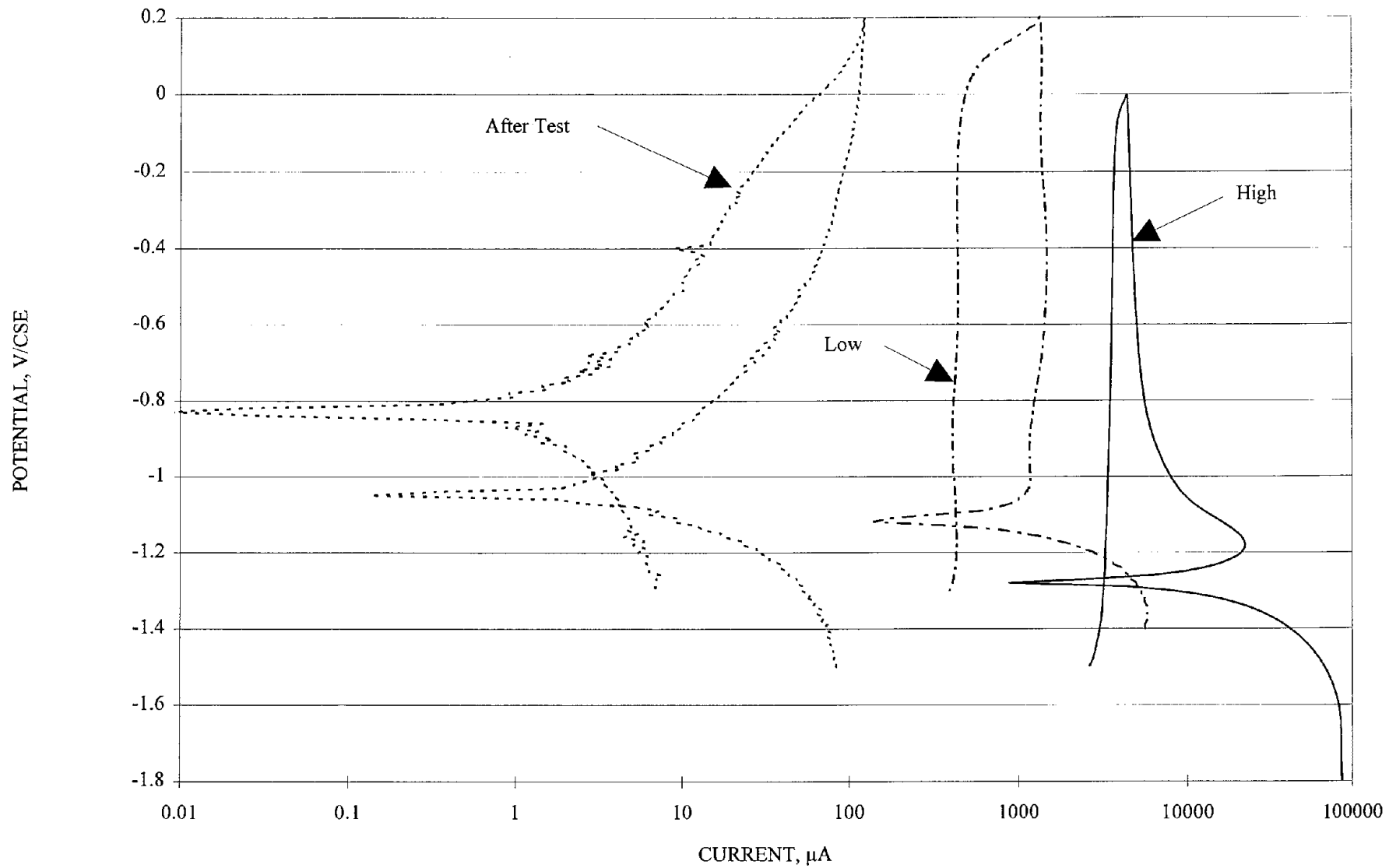


Figure 110. Cyclic polarization curves on aluminum-5% Zn-3.5% Mg alloy after galvanic coupling, at high current, and at low current (1300 ppm Cl).

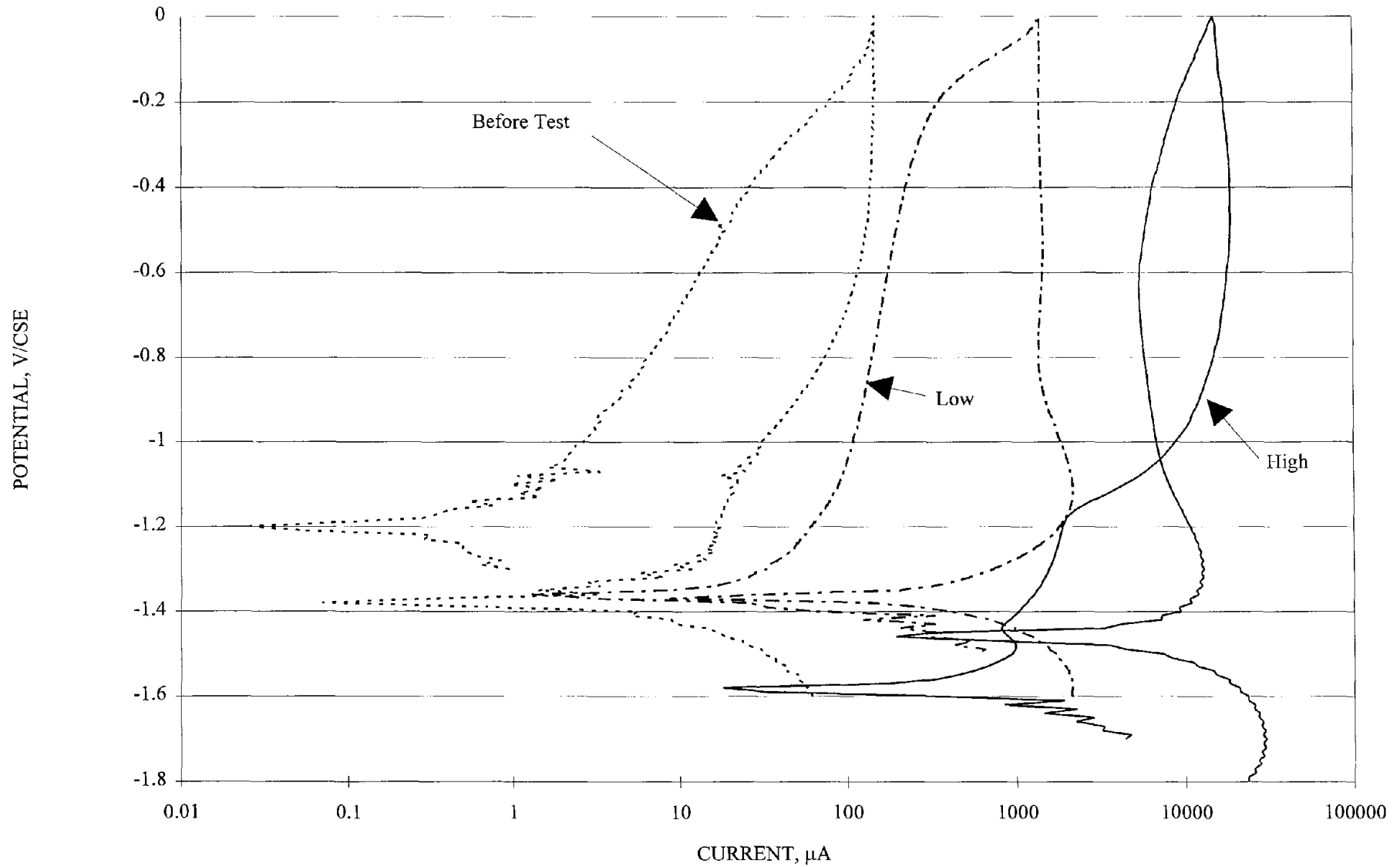


Figure 111. Cyclic polarization curves on aluminum-5% Zn-0.1% Sn alloy before galvanic coupling, at high current, and at low current (3800 ppm Cl).

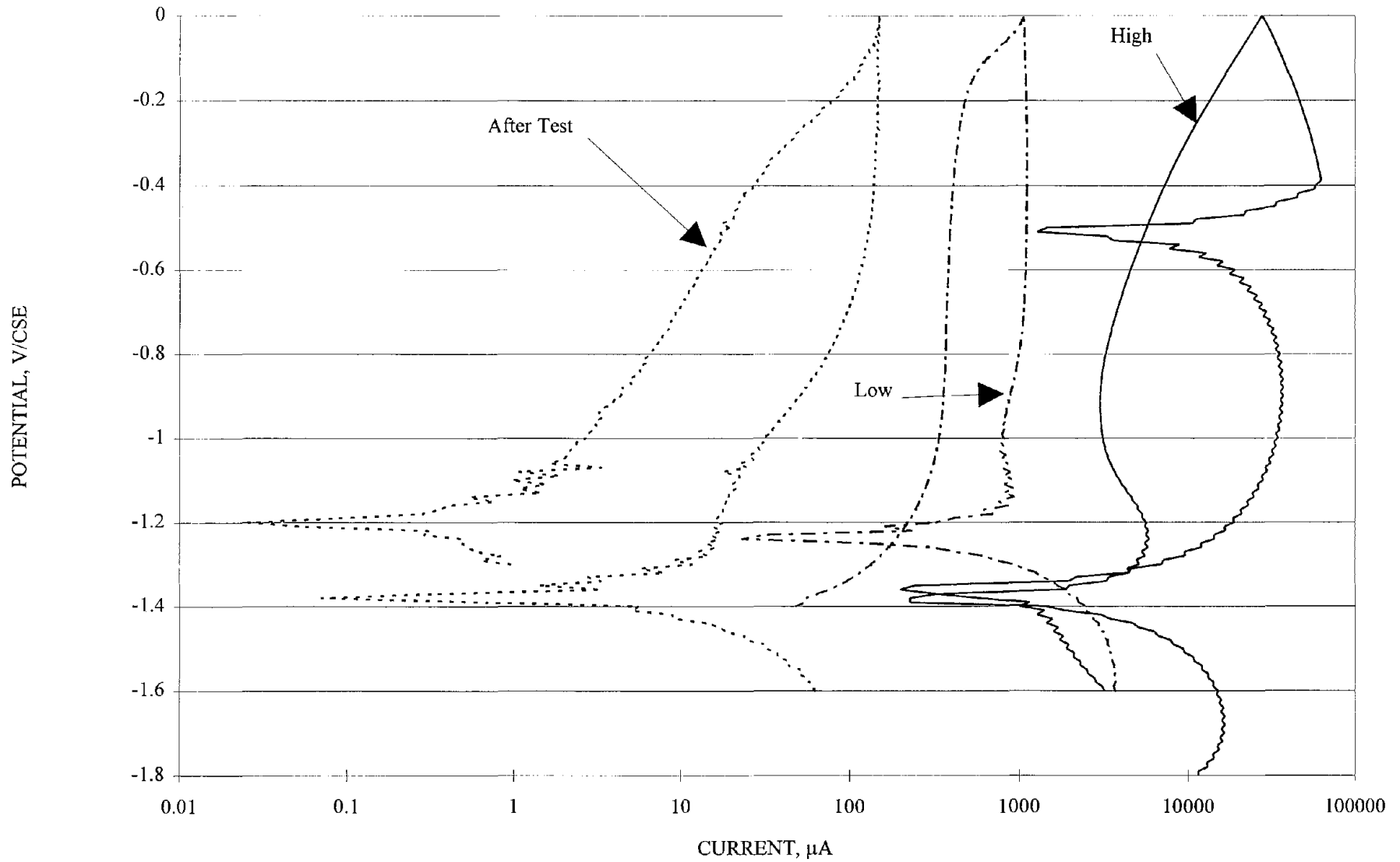


Figure 112. Cyclic polarization curves on aluminum-5% Zn-0.1% Sn alloy after galvanic coupling, at high current, and at low current (1300 ppm Cl).

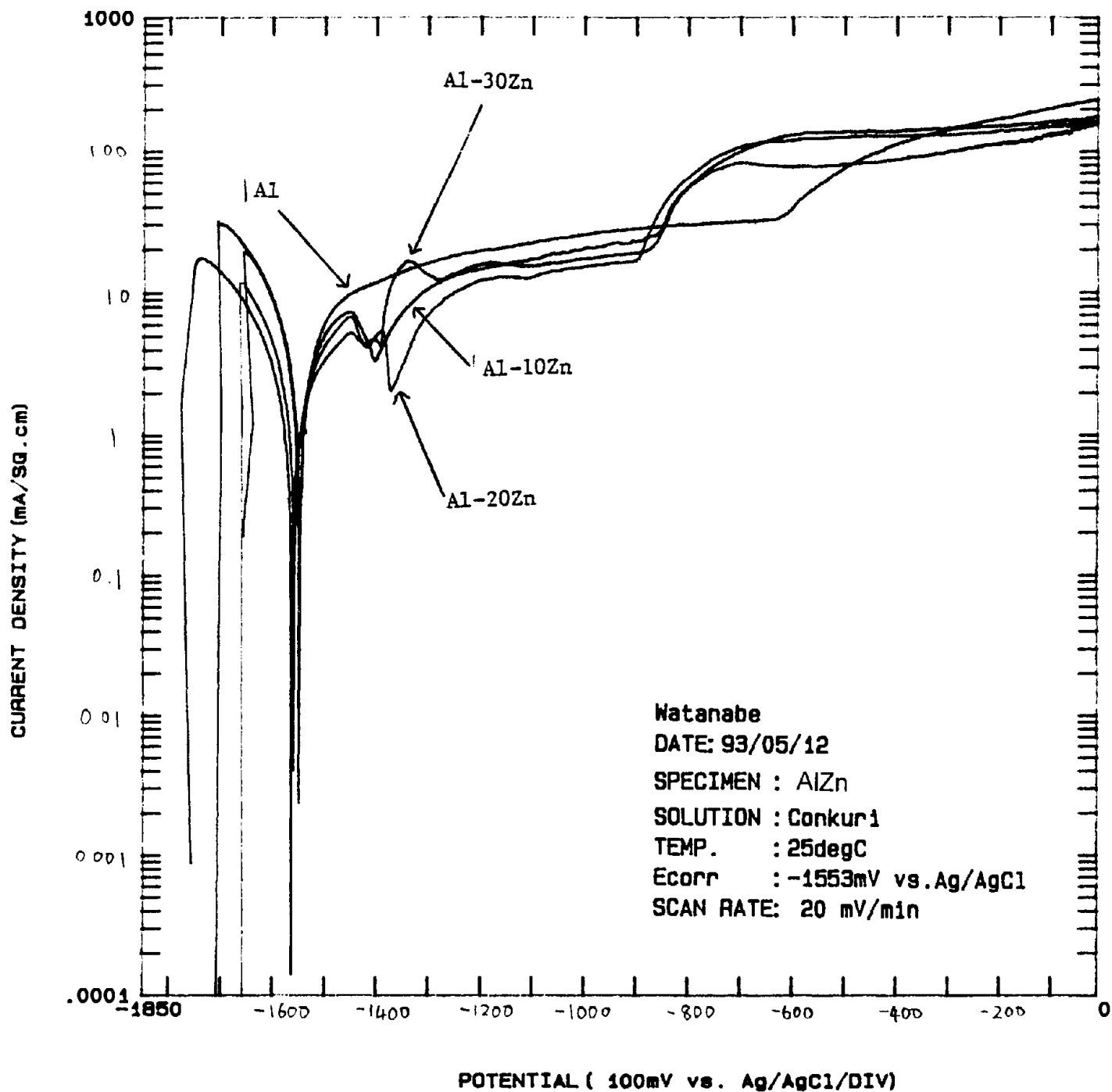


Figure 113. Anodic polarization of pure aluminum and aluminum-zinc alloys (10 to 30 percent zinc) in simulated porewater solution.

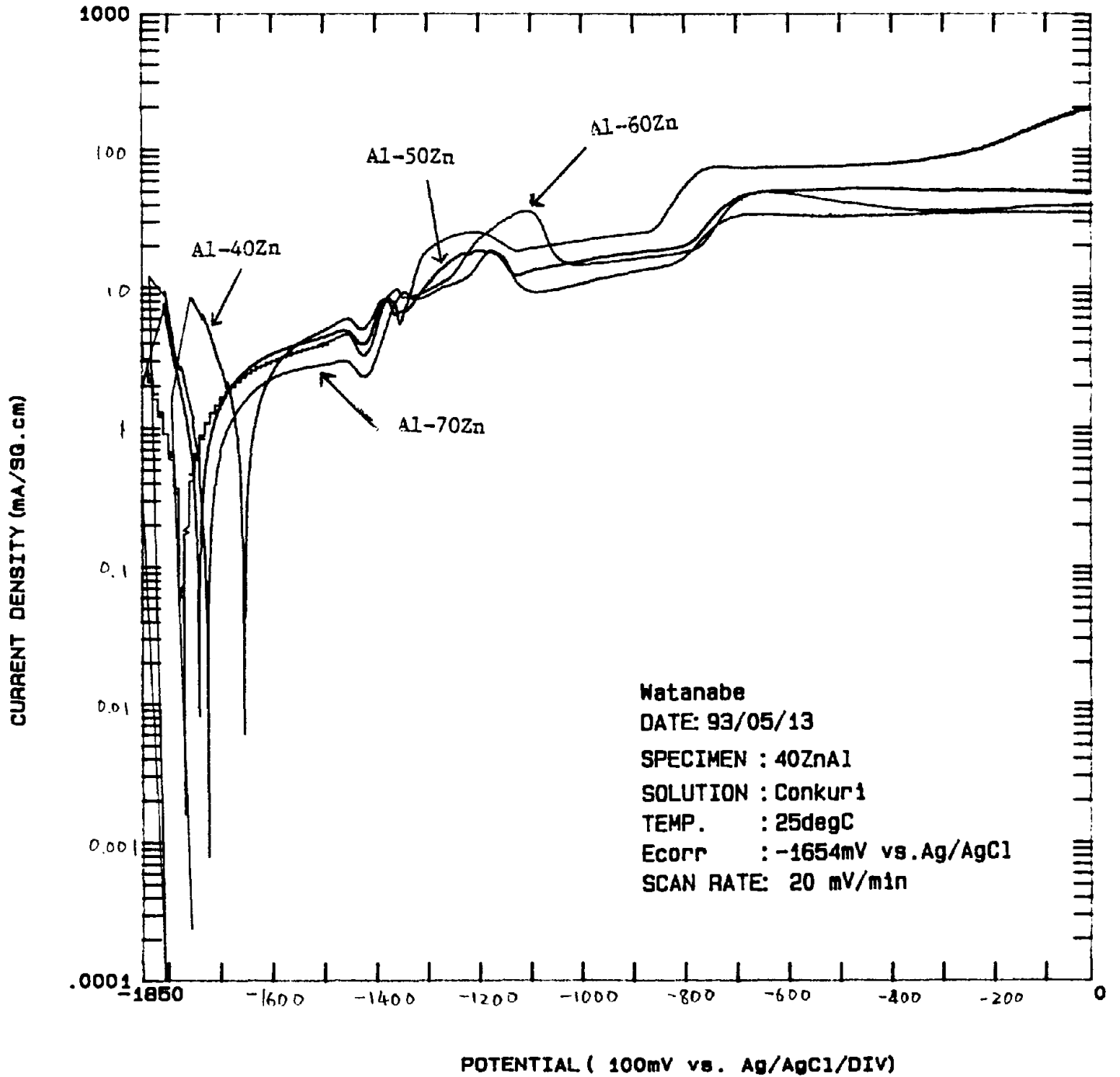


Figure 114. Anodic polarization of aluminum-zinc alloys (40 to 70 percent zinc) in simulated porewater solution.

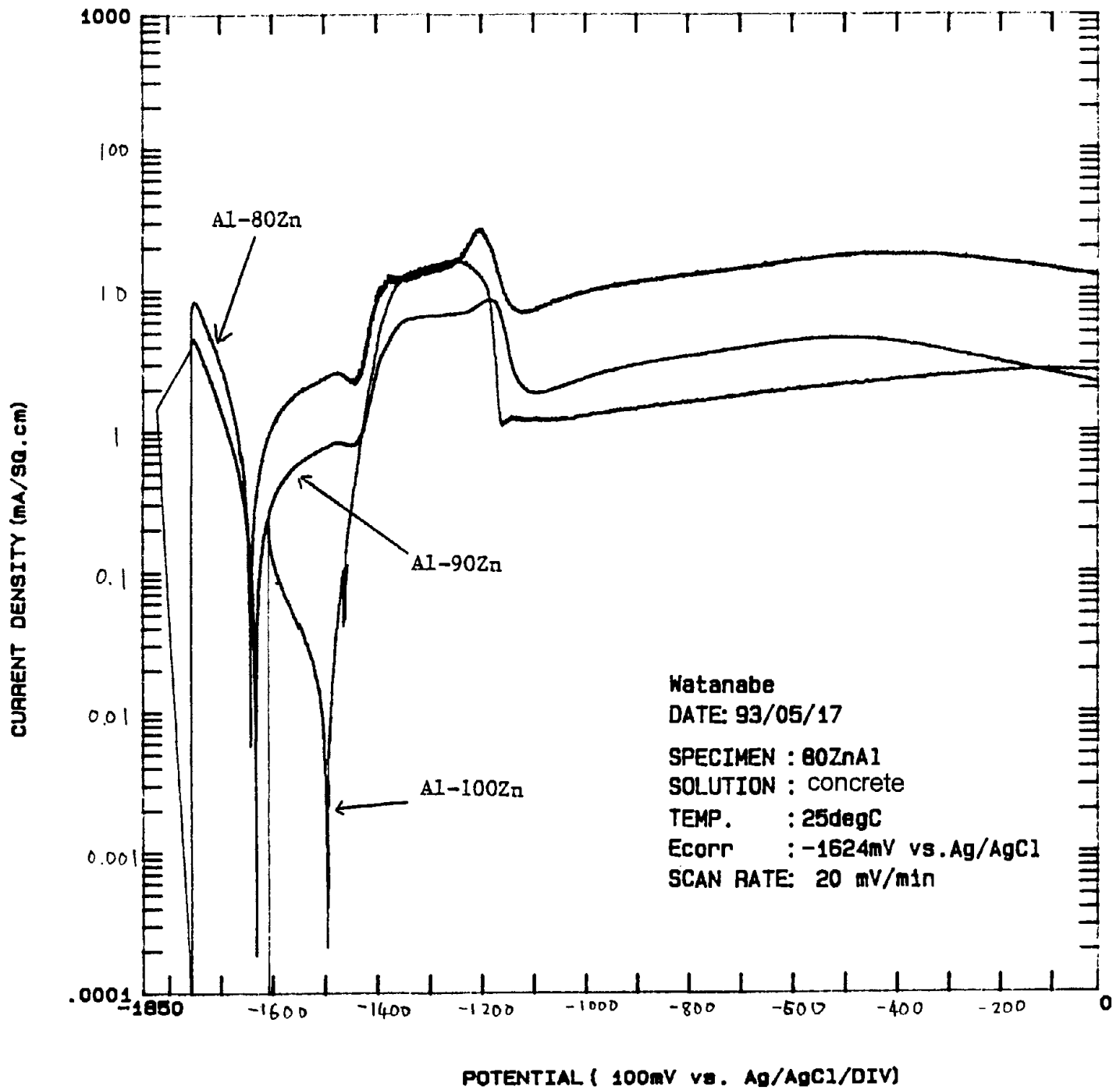


Figure 115. Anodic polarization of aluminum-zinc alloys (80 to 100 percent zinc) in simulated porewater solution.

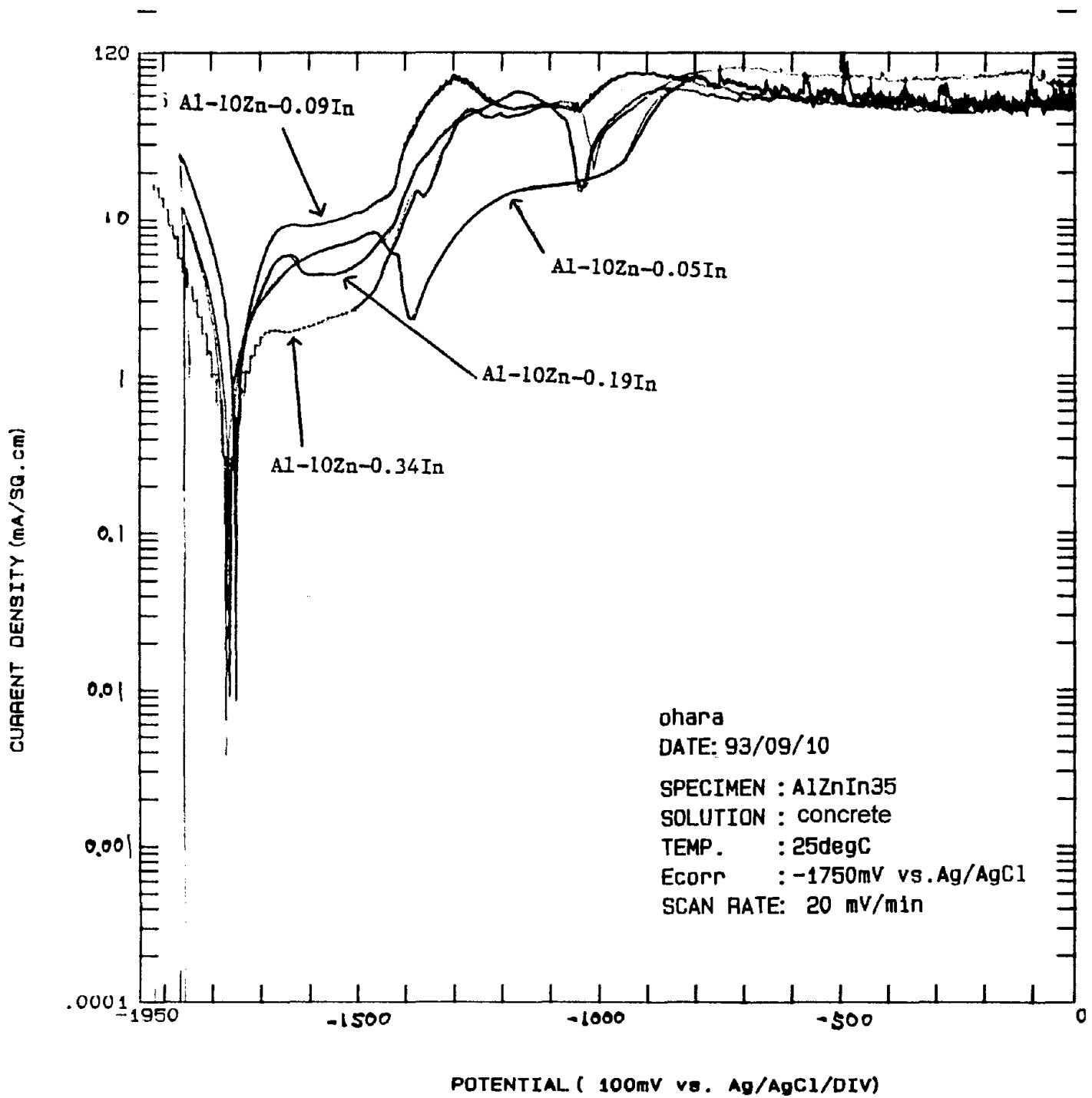


Figure 116. Anodic polarization of aluminum-10% zinc alloys vs. indium in simulated porewater solution.

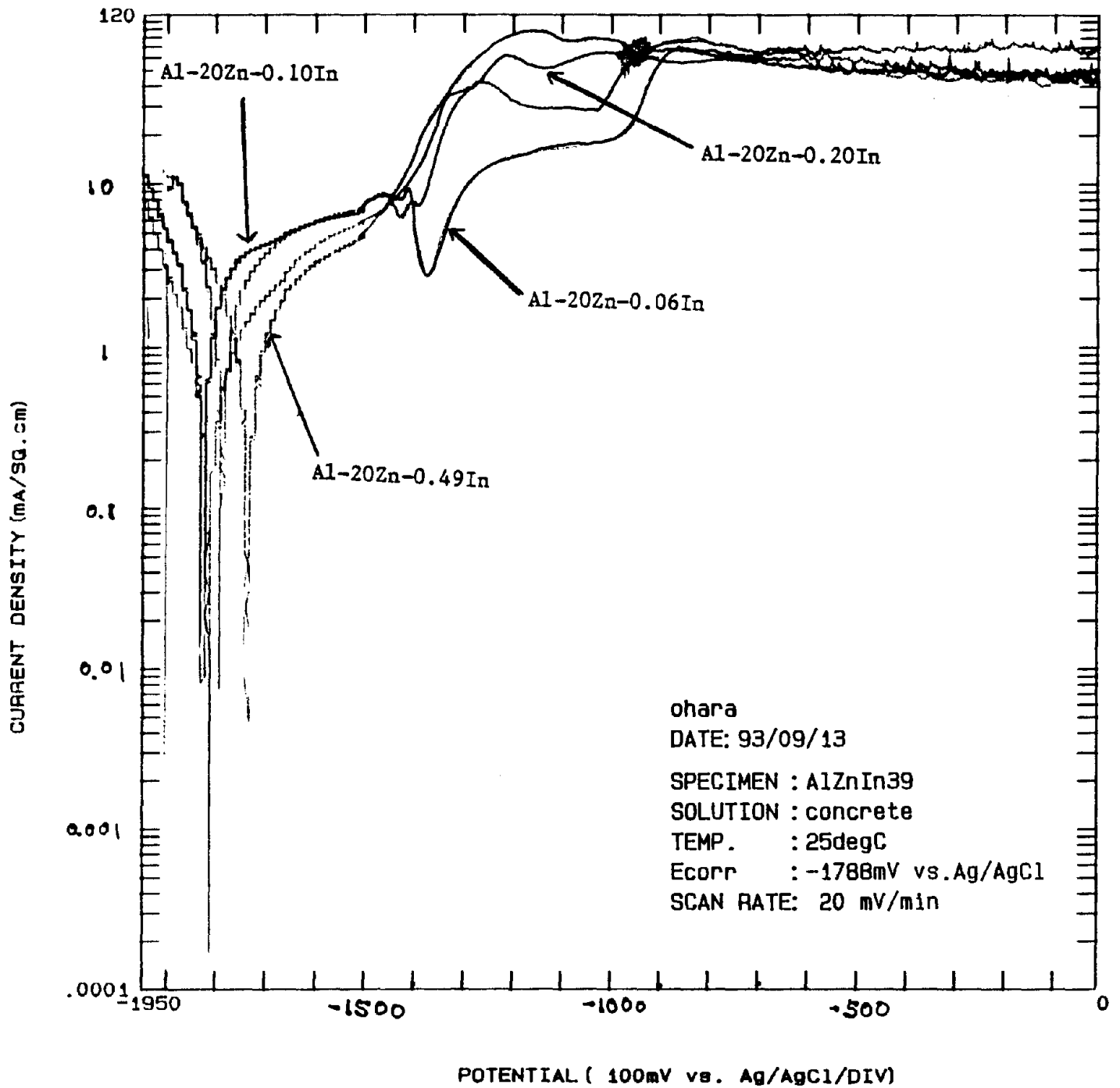


Figure 117. Anodic polarization of aluminum-20% zinc alloys vs. indium in simulated porewater solution.

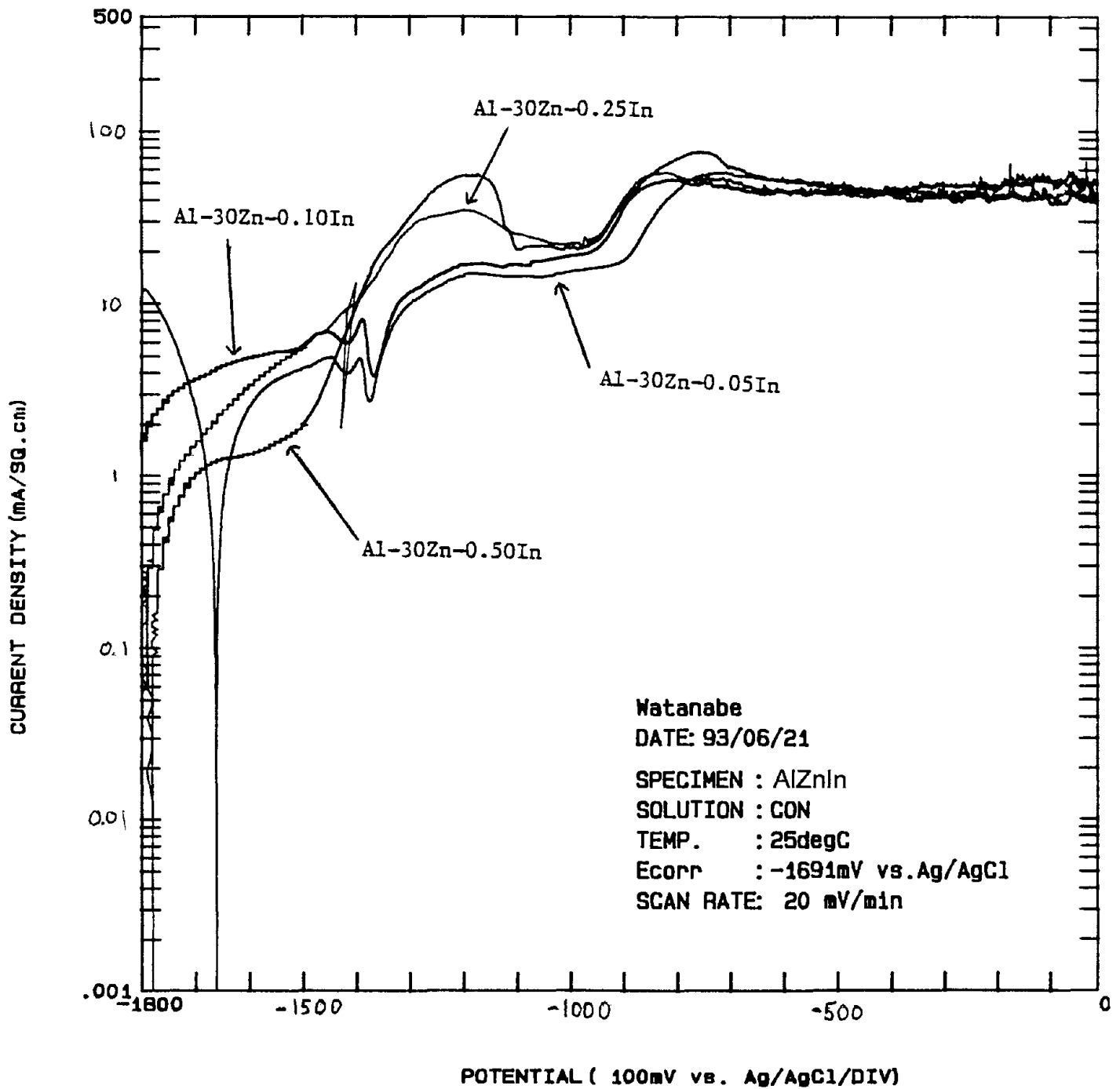


Figure 118. Anodic polarization of aluminum-30% zinc alloys vs. indium in simulated porewater solution.

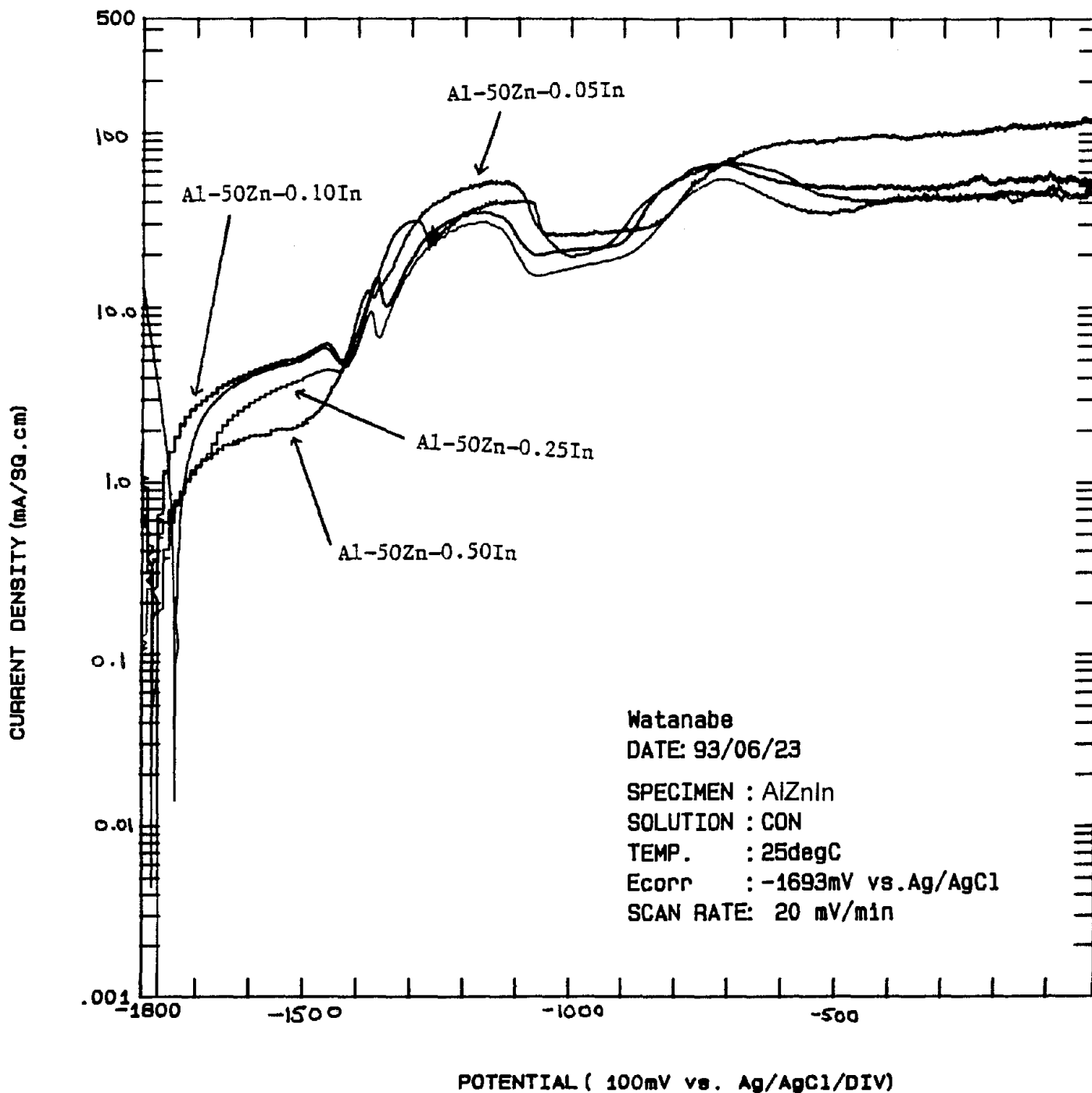


Figure 119. Anodic polarization of aluminum-50% zinc alloys vs. indium in simulated porewater solution.

REFERENCES

1. Federal Highway Administration, U.S. Memorandum, "Bridge Deck Deterioration: A 1981 Perspective," Office of Research, Washington, DC, Dec. 1981.
2. Federal Highway Administration, U.S. Memorandum, "FHWA Position on Cathodic Protection Systems Revisited," Office of the Administrator, Washington, DC, May 24, 1994.
3. W. Shreir, *Corrosion*, Volume 2, Newnes-Butterworths, Boston, 1976.
4. J.L. Saner, *Zinc Anodes to Control Bridge Deck Deterioration*, Illinois Department of Transportation, Report No. FHWA-IL-77-PR-69, December 1977.
5. D. Whiting and D. Stark, *Galvanic Cathodic Protection for Reinforced Concrete Bridge Decks - Field Evaluation*, NCHRP Report 234, June 1981.
6. J.A. Apostolos, "Cathodic Protection of Reinforced Concrete Using Metallized Coatings and Conductive Paints," *Transportation Research Record* 962, TRB, Washington, DC, 1984, pp. 22-29.
7. A.A. Sagues and R.G. Powers, "Sprayed Zinc Galvanic Anodes for Concrete Marine Bridge Substructures," Report No. SHRP-S-405, Strategic Highway Research Program, National Research Council, Washington, DC, 1994.
8. J.A. Apostolos, D.M. Parks, and R.A. Carello, "Cathodic Protection of Reinforced Concrete Using Metallized Zinc," *Materials Performance*, NACE, Houston, TX, Dec. 1987, pp. 22 - 28.
9. R.A. Carello, D.M. Parks and J.A. Apostolos, *Development, Testing and Field Application of Metallized Cathodic Protection Coatings on Reinforced Concrete Substructures*, Report No. FHWA/CA/TL-89/04, Caltrans, May 1989.
10. R.J. Kessler and R.G. Powers, "Zinc Metallizing for Galvanic Cathodic Protection of Steel Reinforced Concrete in a Marine Environment," *Corrosion/90*, Paper No. 324, NACE, Houston, TX, 1990.
11. M. Funahashi, K.F. Fong, and N.D. Burke, "Investigation of Rebar Corrosion in Partially Submerged Concrete," *Corrosion Forms & Control for Infrastructure*, STP 1137, American Society for Testing and Materials (ASTM), October 1992, pp. 232-245.
12. M. Funahashi and W.T. Young, "Investigation of E-Log I Tests and Cathodically Polarized Steel in Concrete," Paper No. 301, *Corrosion 94*, NACE, Houston, TX, 1994.

13. M. Takeda, N. Abe, and Y. Suzuki, "Corrosion Resistance and Physical Characteristics of 55% Al-Zn Alloy," Bousekikanri, Japan Association of Corrosion Control, Dec. 1992, pp. 441-449.
14. T.P. Cheng, J.T. Lee, K.L. Lin, and W.T. Tsai, "Electrochemical Behavior of Galvanized Al-Zn Coatings in Saturated Ca(OH)₂ Solution," *Corrosion*, NACE, June 1991, pp. 436-442.
15. T.C. Simpson, "Accelerated Corrosion Test for Aluminum-Zinc Alloy Coatings," *Corrosion*, NACE, July 1993, pp. 550-560.
16. D.R. Salinas and J.B. Bessone, "Electrochemical Behavior of Al-5% Zn-0.1% Sn Sacrificial Anode in Aggressive Media," *Corrosion*, Vol. 47, No. 9, NACE, September 1991, pp. 665-674.
17. J.W. Jang and I. Iwasaki, "Rebar Corrosion Under Simulated Concrete Conditions Using Galvanic Current Measurements," *Corrosion*, Vol. 47, No. 11, NACE, 1991, pp. 875-889.
18. M. Funahashi, "Cathodic Polarization Behavior of Anode and Cathode on Steel Embedded in Concrete," Paper No. 317, Corrosion/96, NACE, Houston, TX, 1996.
19. J.T. Reding and J.J. Newport, "Aluminum Anodes in Sea Water," *Materials Protection*, December 1966, pp. 15-18.
20. S.N. Smith and A.P. Goolsby, "A Consumer's Perspective of Aluminum Anode Quality Test Design," Paper 96552, Corrosion/96, NACE International, Houston, TX.
21. T. Sakano, K. Toda, and M. Hanada, "Tests on the Effects of Indium for High-Performance Aluminum Anodes," *Materials Protection*, December 1966, pp. 45-50.

Reproduced by NTIS

National Technical Information Service
Springfield, VA 22161

*This report was printed specifically for your order
from nearly 3 million titles available in our collection.*

For economy and efficiency, NTIS does not maintain stock of its vast collection of technical reports. Rather, most documents are printed for each order. Documents that are not in electronic format are reproduced from master archival copies and are the best possible reproductions available. If you have any questions concerning this document or any order you have placed with NTIS, please call our Customer Service Department at (703) 487-4660.

About NTIS

NTIS collects scientific, technical, engineering, and business related information — then organizes, maintains, and disseminates that information in a variety of formats — from microfiche to online services. The NTIS collection of nearly 3 million titles includes reports describing research conducted or sponsored by federal agencies and their contractors; statistical and business information; U.S. military publications; audiovisual products; computer software and electronic databases developed by federal agencies; training tools; and technical reports prepared by research organizations worldwide. Approximately 100,000 *new* titles are added and indexed into the NTIS collection annually.

For more information about NTIS products and services, call NTIS at (703) 487-4650 and request the free *NTIS Catalog of Products and Services*, PR-827LPG, or visit the NTIS Web site <http://www.ntis.gov>.

NTIS

*Your indispensable resource for government-sponsored
information—U.S. and worldwide*

NTIS does not permit return of items for credit or refund. A replacement will be provided if an error is made in filling your order, if the item was received in damaged condition, or if the item is defective.





U.S. DEPARTMENT OF COMMERCE
Technology Administration
National Technical Information Service
Springfield, VA 22161 (703) 487-4650
